Principles of Generalization for Sensorimotor Cerebellar Learning

Principes van Generalisatie voor Sensomotorisch Cerebellair Leren

Thesis

to obtain the degree of Doctor from the

Erasmus University Rotterdam

by command of the

rector magnificus

Prof.dr. A.L. Bredenoord

and in accordance with the decision of the Doctorate Board.

The public defence shall be held on

14th February 2023 at hrs 13:00

by

Francesca Romana Fiocchi

born in Rome, Italy.

Erasmus University Rotterdam

Doctoral Committee:

Promotor:	Prof.dr. C. I. de Zeeuw
Other members:	Prof.dr. G. Borst
	Prof.dr. D. Timmann
	Dr. A. Badura
Copromotors:	Dr. H.J. Boele
	Dr. D. Narain

Papá, Nonna (Ní!)

Table of Contents:

Preface

The central question of this Ph.D. dissertation is how sensorimotor integration is executed at the level of the cerebellum. How are external stimuli influencing motor learning? More specifically, after one behavior has been established in response to one stimulus, then will novel stimuli resembling the first one elicit the same responses? The name of this key learning mechanism is stimulus generalization and it has been an important focus of research in the fields of psychology and ethology. I applied the principles of classical conditioning using a cerebellar-related paradigm called Pavlovian eyeblink conditioning to study how sensorimotor learning in response to one specific stimulus would transfer when the properties of that stimulus are changed. As the only output of the cerebellar cortex, Purkinje cells are both involved in driving sensorimotor learning during Pavlovian eyeblink conditioning and are also responsible for orchestrating major events of development within cerebellar circuits. Their dysfunction or degeneration is the most common finding in animal models with an ataxic phenotype. Therefore, what happens to sensorimotor cerebellar-dependent learning during the development of these neurons? What are the origins of Purkinje cell dysfunction before ataxic symptoms manifest? Taken together, the findings reported in the current thesis contribute towards the scientific clarification of mechanisms underlying sensorimotor learning while taking developmental perspectives into consideration. Furthermore, it strives to provide the most optimal possible timeline for ataxic therapeutic interventions.

Francesca Romana Fiocchi

Chapter 1

Chapter 2

Stimulus generalization in mice during Pavlovian eyeblink conditioning

Francesca Romana Fiocchi[1], Stephanie Dijkhuizen[1], Sebastian S.K. Koekkoek[1], Chris I. De Zeeuw[1,2] and Henk-Jan Boele[1,3]

eNeuro, 2022

Affiliations:

(1) Department of Neuroscience, Erasmus MC, Rotterdam, The Netherlands

(2) Royal Dutch Academy of Arts & Science (KNAW), Netherlands Institute for Neuroscience, Amsterdam 1105 BA, The Netherlands

(3) Princeton Neuroscience Institute, Princeton, NJ 08540

Abstract

Here, we investigate stimulus generalization in a cerebellar learning paradigm, called eyeblink conditioning. Mice were conditioned to close their eyes in response to a 10 kHz tone by repeatedly pairing this tone with an air puff to the eye 250 ms after tone onset. After 10 consecutive days of training, when mice showed reliable conditioned eyelid responses to the 10 kHz tone, we started to expose them to tones with other frequencies, ranging from 2 to 20 kHz. We found that mice had a strong generalization gradient, whereby the probability and amplitude of conditioned eyelid responses gradually decreases depending on the dissimilarity with the 10 kHz tone. Tones with frequencies closest to 10 kHz evoked the most and largest conditioned eyelid responses and each step away from the 10 kHz tone resulted in fewer and smaller conditioned responses (CRs). In addition, we found that tones with lower frequencies resulted in CRs that peaked earlier after tone onset compared with those to tones with higher frequencies. Together, our data show prominent generalization patterns in cerebellar learning. Since the known function of cerebellum is rapidly expanding from pure motor control to domains that include cognition, reward-learning, fear-learning, social function, and even addiction, our data imply generalization controlled by cerebellum in all these domains.

Introduction

Given the advance of transgenics and optogenetics (Boyden, 2015; Deisseroth, 2011; Navabpour et al., 2020), mice have become increasingly a popular animal model to study mechanisms underlying cerebellar learning (Alba, 1994; Albergaria et al., 2018; Gao et al., 2016; Heiney, Wohl, et al., 2014; Kloth et al., 2015; Zhang et al., 2019). This also holds for Pavlovian eyeblink conditioning, a behavioral test that allows for wide variations in parameter space, including those of onset, duration and intensity of both conditional and unconditional stimuli (Alba, 1994; Chettih et al., 2011). Accordingly, experimental procedures for eyeblink conditioning in mice have been optimized over the last few years, evolving from EMG and MDMT to less invasive high-speed video recordings of the eyelids while

the mouse is walking on a treadmill system (Albergaria et al., 2018; De Zeeuw & Ten Brinke, 2015; Heiney, Wohl, et al., 2014; Koekkoek et al., 2002). Even so, some basic concepts of eyeblink conditioning, which have been studied quite extensively in humans and rabbits, have not yet been studied well in mice.

One of these concepts is called 'stimulus generalization'. Stimulus generalization is the phenomenon whereby a certain behavioral response is elicited by a stimulus other than the one that initially led to the acquisition of this specific response (Lashley & Wade, 1946; Pavlov, 1927; Razran, 1949). Stimulus generalization plays a crucial role in our daily life behavior. Think for instance about how we, as a pedestrian, will immediately respond to the sound of *any* car horn when we are about to cross a road. Indeed in neuroscience, stimulus generalization has probably been most extensively studied in the context of Pavlovian fear conditioning (Bang et al., 2008; Dymond et al., 2015; Hovland, 1937; Lissek et al., 2008; Meulders & Vlaeyen, 2013), showing that emotional and fight-or-flight responses can be easily triggered by stimuli other than the one used during acquisition training.

In the current study we employ Pavlovian eyeblink conditioning in mice to study the stimulus generalization of their responses that reflect *motor* memories. In the paradigm used in this study, mice were first trained to close their eyes in response to a tone with a frequency of 10 kHz, by repeatedly pairing this 10 kHz tone (conditional stimulus, CS) with a mild air puff to the eye (unconditional stimulus, US). After ten consecutive daily training sessions, which is sufficient for most mice to reliably show eyelid conditioned responses (CRs) to the 10 kHz tone, we suddenly introduced alternative tones with frequencies ranging between 2 to 8 kHz and 12 to 20 kHz. In contrast to the 10 kHz tone, these tones were never reinforced with the aversive air puff. In line with previous work (Dymond et al., 2015), we will use in this paper the term 'conditional stimulus or CS' to refer to the 10 kHz tone that was reinforced with the air puff US, and the term 'generalization stimulus (GS)' for the other tones, varying between 2 to 8 and 12 to 20 kHz, that were *never* reinforced with the air puff US. Thus, we set out to investigate to what extent eyeblink CRs are elicited by these GSs in mice that do show reliable CRs to the CS. The advantage of eyeblink conditioning is that it does not only permit robust variations in the stimulus parameters, but also that it reveals the CR probability as well as quantification of the size (or amplitude) and timing of the CRs. Eyeblink CRs are not simple reflexive blinks in response to the tone, but precisely timed responses, the amplitude of which increase gradually over the course of training (Boele et al., 2016). The adaptive timing of eyeblink CRs depends on the interval between CS and US onset: after conditioning the eye will be maximally closed just before the moment that the air puff (i.e., US) will be delivered. Thus, in this study we quantified CR probability, CR amplitude, and CR timing as a function of tone frequency, allowing us to investigate to what extent these different parameters are subject to the stimulus generalization principle.

Material and Methods

Subjects

We used 14 wild-type C57Bl/6 mice, seven of which were male and seven were female. Mice were between 11 and 16 weeks old at the start of the experiment. All mice were housed individually during the experiment with food and water ad libitum in a 12/12 h light/dark cycle. Experiments were performed during the light phase. All experiments were performed in accordance with the European Communities Council Directive. Protocols were reviewed and approved by the Erasmus Laboratory Animal Science Center (work protocol no. 15-273-138; project license no. AVD101002015273).

Auditory brainstem responses

Since C57Bl/6 mice are prone for developing hearing problems, we recorded prior to the start of eyeblink conditioning training the auditory brainstem responses (ABRs) to obtain hearing level thresholds. Mice were anesthetized with a ketamine/xylazine mixture at a dose of 100/10 mg/kg body weight, administered intraperitoneally (ketamine: Alfasan, Woerden, NL; xylazine: Sedazine®, AST Farma, Oudewater, NL). After this, they were placed in a sound- and light-attenuated box with the ears at a distance of 4 cm from a frontally placed loudspeaker. Needle electrodes were positioned subdermal at the base of both pinnae, the external part of the ear. The reference electrode was placed at the vertex, the upper surface of the head, and a ground electrode on the lower back. Stimuli were generated and presented by a RZb Multi I/O Processor (TuckerDavis Technologies) and BioSigRZ software. Responses were recorded using Medusa DA4PA, 4-dh Preamp device. Responses with amplitudes larger than 30 µV were considered as artefacts and therefore excluded from further analysis. Hearing level thresholds were measured at 4, 8, 16 and 32 kHz (Willott, 2006). Thresholds were defined as the lowest sound pressure level (SPL) at which a reproducible response (i.e., peak in the ABR trace) was still detectable. Since our main aim was to establish that mice could detect the tones used in our behavioral training paradigm and not to establish definite age and mouse species dependent absolute hearing thresholds, we performed our ABR recordings under anesthesia since it is technically less complicated. One should keep in mind, however, that ABR responses under ketamine/xylazine anesthesia, although it is a standard procedure in mice (Huang et al., 1995; Ingham et al., 2011; Willott, 2006), are generally weaker compared to those recorded in awake animals (van Looij et al., 2004). After the ABR recordings, which took about 20-30 minutes per animal, mice were injected with atipamezole (Antisedan®, Orion Pharam, Finland) (10 mg/kg body weight, administered intraperitoneal) for the reversal of xylazine.

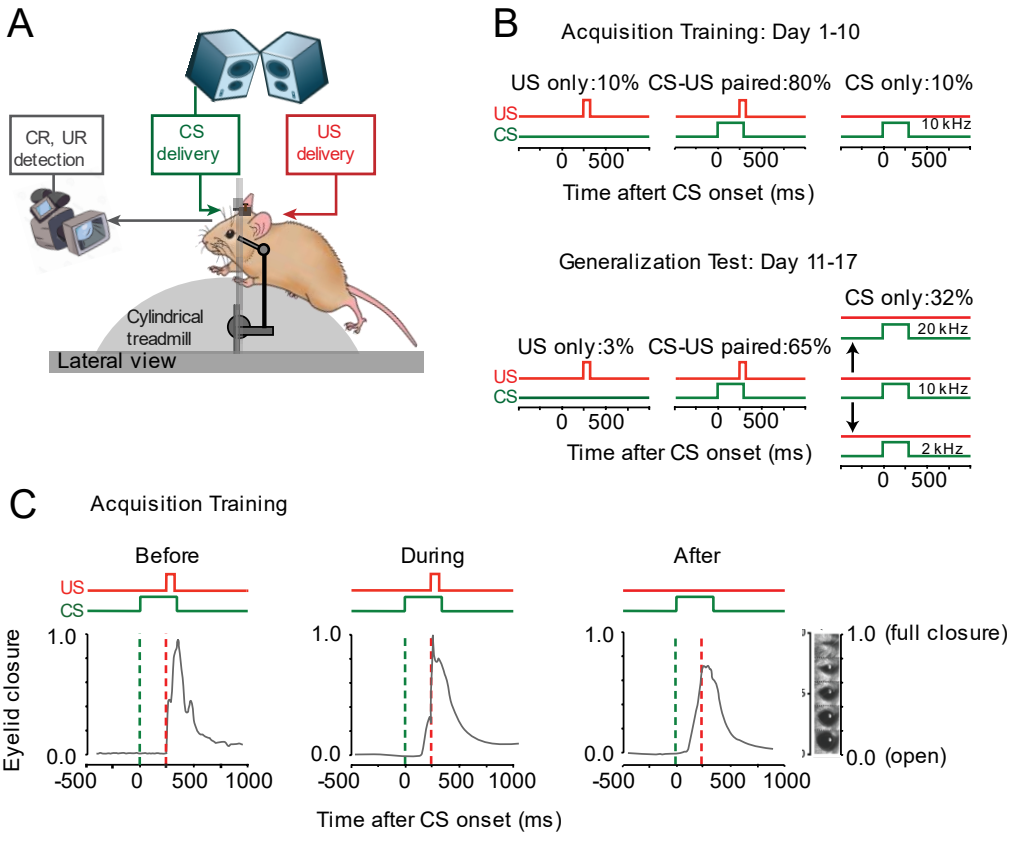

Figure 1. Eyeblink conditioning setup and experimental design. (**A**) Mice were placed in a light-isolating and sound-isolating chamber on a foam cylindrical treadmill that allowed them to walk freely with their heads fixed at a horizontal bar. The unconditioned stimulus, US (in red) consisted of a weak air puff to the left eye and the conditioned stimulus, CS (in green) consisted of a 10 kHz tone. Speakers were placed on both upper front corners of the chamber. Eyelid movements were recorded using a high-speed video camera system (300 fps). (**B**) Schematics of eyelid conditioning acquisition training and generalization test protocols. For each protocol the duration and the ratio of different trial types is presented at the top of the corresponding illustration. (**C**) Example eyeblink traces before, during, and after eyeblink conditioning. The CS (green) and US (red) onset and duration are shown at the top of each panel. Over the course of acquisition training, mice learn to close their eyes in response to the CS, which are called conditioned responses (CRs).

Surgery

After ABR recordings, mice had two days of recovery before they underwent surgery. Mice were anesthetized with 2% isoflurane (vaporizer for Isoflurane Anesthetic Model100 Vaporizer, Forane®, Surgivet) and body temperature was kept constant at ~37 degrees Celsius (DC Temperature controller, FHC). After fixation in a standard mouse stereotaxic alignment system (Stoelting) and under sterile conditions, the scalp was incised (~10 mm) to expose the skull. Membranous tissue was cleared and the bone was prepared with Optibond™ FL (All-in-one bonding agent Kerr®, Salerno, Italy). A small brass pedestal with a square magnet on top was attached to the skull with a dental composite (Charisma - Mitsui Chemical Group, Kulzer, Germany), using an xyz manipulator, allowing for fixation to a head bar at right angles during experiments. After surgery mice recovered under a heating lamp for at least 20 minutes, until they were fully awake. They were given post-operative analgesic (Rimadyl® Cattle, Cappelle a/d Ijssel, NL) on the following day. Mice had three days to fully recover, before eyeblink conditioning habituation training started.

Eyeblink conditioning apparatus

All behavioral experiments were conducted in custom built sound- and light- attenuating boxes. Mice were placed head-fixed on top of a cylindrical treadmill on which they were allowed to walk freely (Figure 1A) (Boele et al., 2018; Heiney et al., 2014). The treadmill consisted of a foam roller (diameter, ±15 cm; width, +/- 12 cm; Exervo, TeraNova EVA) with a horizontal metal rod through the axis that was connected with a ball bearing construction to two solid vertical metal poles. A horizontal messing bar was fixated to the same vertical poles at 3 to 5 cm above the treadmill. Mice were head-fixed to the bar with the use of a screw, allowing the magnet on top of the pedestal to perfectly dovetail another magnet with opposite polarity in the middle of the horizontal messing bar in the exact point of fixation, thereby ensuring easy fixation and perfect head stability (Figure 1A) (Boele et al., 2018; Chettih et al., 2011; Heiney et al., 2014). The CS was a 280 ms tone with a frequency of 10 kHz with a 25 ms ramp/decay time. The US consisted of a 30 ms duration mild corneal air puff, which was controlled by a VHS P/P solenoid valve (Lohm rate, 4750 Lohms; Internal volume, 30 µL, The Lee Company®, Westbrook, US) and delivered via a 27.5 mm gauge needle that was perpendicularly positioned at about 5 mm from the center of the left cornea. The back pressure on the solenoid valve was set at 30 psi. We used an interstimulus interval of 250 ms and an intertrial interval of 8-12 seconds. Eyelid movements were recorded using a high-speed video camera (333 fps, Basler® a cA640-750u m ID: 106748-15, Germany). Stimulus control and data acquisition were done with National Instruments hardware. All experiments were performed at approximately the same time of the day by the same experimenter.

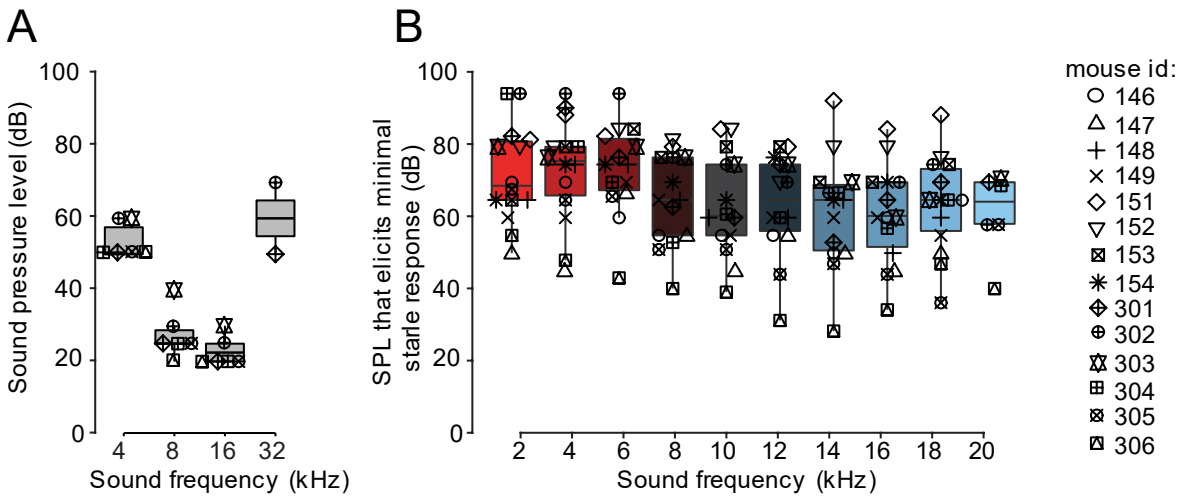

Figure 2. **Mouse ABRs and auditory eyelid startle responses to a range of sound frequencies and intensities.** (**A**) ABRs were measured at 4, 8, 16, and 32 kHz. Mice were most sensitive to sounds in the range of 8 and 16 kHz showing normal auditory thresholds. Each symbol represents one mouse. For the boxplot, the thick horizontal line is showing the median, the top edge of each box indicates the 25th percentile, bottom edge the 75th percentile, whisker lines extending above and below each box indicate the range of observations. (**B**) The SPLs that elicits minimal auditory eyelid startle response for different sound frequencies. This value was determined for each mouse carefully during 10 baseline sessions and used as CS or GS.

Eyeblink conditioning, habituation to eyeblink conditioning apparatus

Mice were head-fixed on the head bar and allowed to walk on the treadmill for 20–30 min/d for 2 d without any stimuli to get them acquainted with the eyeblink set-up.

Eyeblink conditioning, baseline measurements to find the proper tone threshold for each animal

After the two days of habituation, we measured the sensitivity of each mouse for the tone CS (10 kHz) and tone GSs (ranging from 2 to 8 and 12 to 20 kHz in steps of 2 kHz). Since the responsiveness of an individual mouse to auditory stimuli can slightly vary from day to day and since we were testing ten different tone frequencies and did not want to present too many trials during a baseline session, we repeated this measurement for ten consecutive days for each animal (30 minutes each day), until we found for each animal the proper sound pressure levels (SPL in dB) for each tone frequency (Figure 3A, 2B). Each baseline session consisted of 2 blocks of 10 tone-only trials and 1 US-only trial each, and thus had 2 tone-only trials of each tone frequency for each session.

As a behavioral readout for the tone sensitivity, we used the eyelid component of the auditory startle reflex (Boele et al., 2010). This startle response, sometimes referred to as alpha response, was quantified using the velocity signals (1st derivative of position signal) (Figure 3C). An eyelid response was considered as a startle response if there was a peak in the velocity signal between 30 to 80 ms after CS onset that was larger than 3 standard deviations of the 500 ms baseline period and larger than an arbitrary threshold set at 0.00025 (Figure 3B-D). We considered the potential effect of 'latent inhibition', which is the phenomenon whereby it takes longer to get conditioned to a familiar stimulus (i.e., a tone that one has heard many times) than to novel stimulus (i.e., a new tone). Therefore, all animals received the exact same number of CS-only trials during baseline, so that the novelty level of the tone was equal for all animals.

Eyeblink conditioning, acquisition training sessions

Mice were trained for 10 consecutive days (40 min/d). Each daily session was composed of 20 blocks of 12 trials each. Each block consisted of 1 US-only trial, 10 paired (CS-US with an interstimulus

interval, ISI of 250 ms) trials, and one CS-only trial (Fig. 1B,C). Trials were semi-randomly distributed, whereby a CS-only trial was always immediately preceded by at least two paired CS-US trials.

Eyeblink conditioning, generalization test sessions

The 10 days of acquisition training were followed by 7 generalization test sessions, during which the GSs were presented in addition to the CS. Each daily generalization test session was composed of 8 blocks of 31 trials each, including 20 paired CS-US trials, 1 US-only, and 10 tone (CS or GS) only trials (Figure 1B). Since the ratio of paired CS-US to CS/GS only trial changed significantly, we carefully checked day-by-day whether there was any extinction of eyeblink CRs. Since it is known that the probability of a CR is lower in a trial that is preceded by a trial wherein the tone was not reinforced (Najafi & Medina, 2020), in our experimental design a tone only trial (CS only or GS only) was always immediately preceded by two paired CS-US trials.

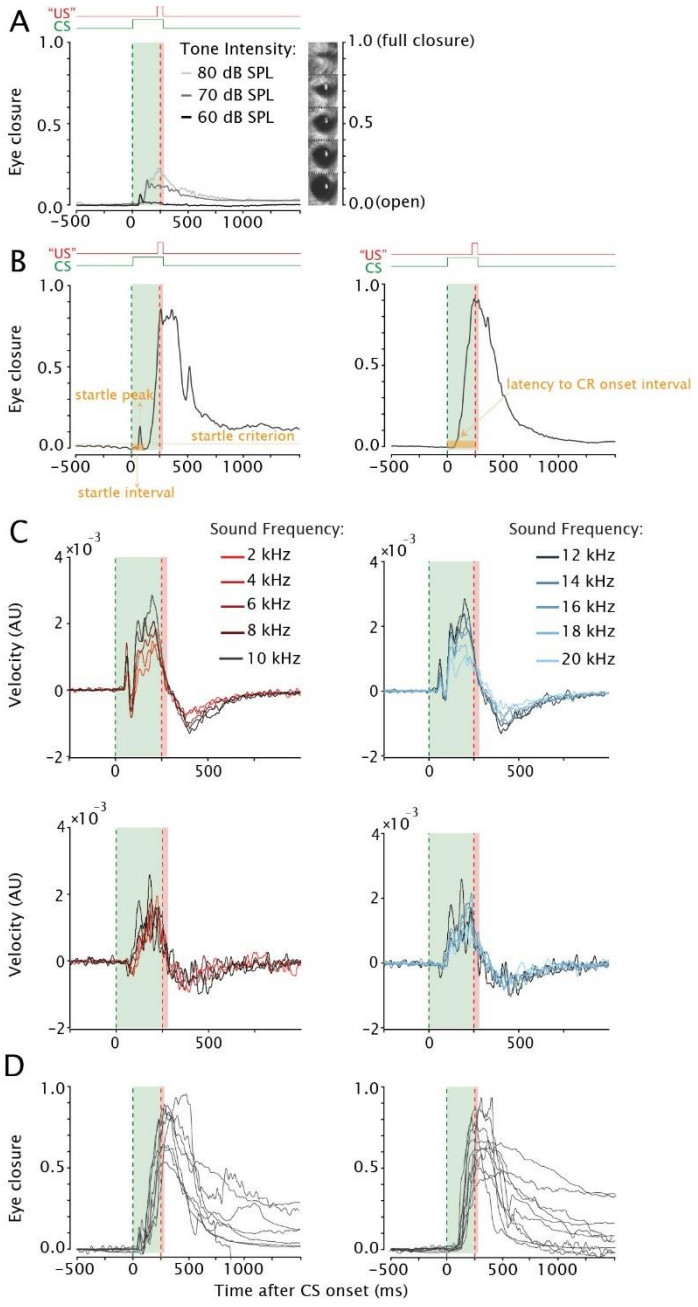

Figure 3. Mouse eyelid startle responses obscure CR onset. (**A**) Example eyelid responses to a 10 kHz tone in a naive unconditioned mouse presented at three different sound intensities: 60, 70, and 80 decibels (dB). In this example the 60 dB tone elicits just an a startle response, the 70 dB tone an a and b startle response, and the 80 an a and b startle and even a response that resembles a CR. For this mouse, a tone with a SPL of 60 dB would be a proper CS for training. (**B**) Example eyelid responses after training taken from the same animal. In the left panel, the a startle response obscures the CR onset. In the right panel, there is no startle response and consequently the latency to CR onset can be detected reliably. (**C**) Separation of startle and nonstartle trials was achieved by taking the first derivative of the eyelid position signal. In this velocity signal, the presence of a peak immediately after CS onset was the discriminator between startle (top panels) and nonstartle trials (bottom panels). Latency to CR onset was determined in nonstartle trials. For all other outcome measures, startle and nonstartle trials were combined. Similar to Figure 2, the blue gradient indicates GSs with frequencies higher than the 10 kHz CS and red gradient indicates GSs with frequencies lower than the 10 kHz CS. Each line is the averaged velocity signal of the eyeblink trace for one GS or CS frequency. For all panels, the green dashed line indicates CS onset, the red dashed line indicates expected US onset. The light green and red shadings indicate CS and US duration, respectively. Eyelid is fully open a 0 and fully closed at 1. The US is omitted in the CS-only trials. CS (tone), US (eye puff). (**D**) Eyelid responses separated by the presence of an a startle response. Left panel shows eyelid traces with a startle response, right panel shows traces without a startle response.

Eyeblink conditioning, data analysis

Individual eyeblink traces were analyzed with a custom-written MATLAB script (R2018a, Mathworks). First, the 2000 ms eyeblink traces were imported from the MySQL database into MATLAB. The trials were aligned at zero for the 500 ms pre-CS baselines. Trials with significant activity in the 500 ms pre-CS period (> 7-times the interquartile range) were regarded as invalid and disregarded for further analysis. The eyelid signal was min-max normalized so that a fully open eye corresponded with a value of 0 and a fully closed eye with a value of 1. This normalization was achieved by aligning the 500 ms pre-CS baselines of all traces and dividing each trace by the averaged UR value that was calculated over *all* eyelid traces in US only trials for one session. The normalized eyelid closure amplitude was expressed as fraction eyelid closure or FEC.

In our analysis we only included CS-only trials, since these trials show the full kinetic profile of the eyelid response. In valid normalized CS-only trials, eyelid responses were considered as a CR if the maximum amplitude was larger than 0.05 in the interval between 100-500 ms after CS onset and the presence of a positive slope in the 150 ms before the time point where the US would have been delivered (US is omitted in CS-only trials). For each session for each mouse, we calculated the percentage of trials in which a CR was present, which we will refer to as 'CR percentage'. In addition, we determined for each trial the maximum eyelid closure between 100 and 500 ms after CS onset, which we will refer to as 'Eye closure - all trials'. Similarly, we calculated the maximum eyelid closure between 100 and 500 ms after CS onset in trials wherein a CR was present based on the criteria described above, which we will refer to as 'Eye closure - CR trials'. CR adaptive timing was investigated by calculating the latency to the onset of the CR relative to CS onset, referred to as 'Latency to CR onset', and the latency to maximum eye closure relative to CS onset, referred to as 'Latency to CR peak'. Latency to CR onset and latency to CR peak were only calculated in trials wherein a CR was present. Latency to CR onset was only calculated for trials wherein no alpha startle response was present.

Statistical analysis was done using multilevel linear mixed-effects (LME) models in R Studio (code available upon request). LMEs have several major advantages over standard parametric and non-parametric tests (Aarts et al., 2014; Schielzeth et al., 2020), as they are more robust to violations of normality assumptions, which is often the case in biological data samples. Moreover, use of LME models are able to accommodate the nested structure of our data (i.e., trial nested within session, session nested within animal, animal nested within group). Finally, LME models are objectively better

at handling missing data points than repeated measures analysis of variance (ANOVA) models and do not require homoscedasticity as an inherent assumption. In our LME, we used session and tone frequency as fixed effects, and mouse as a random effect. Goodness of fit model comparison was determined by evaluating log likelihood ratio, BIC, and AIC values. The distribution of residuals was inspected visually by plotting the quantiles of standard normal versus standardized residuals (i.e., Q-Q plots). Correction for multiple comparisons was achieved, using false-discovery rate (FDR). Data were considered as statistically significant if the corrected p-value was smaller than 0.05.

Results

We used eyeblink conditioning to test stimulus generalization in mice that were conditioned using a 10 kHz tone. Before we started the eyeblink conditioning acquisition training, we carefully measured the sensitivity of each mouse to the specific tones used during the experiment.

Auditory brainstem and auditory startle responses

Some mouse strains, including the popular C57Bl/6 mouse strain, are susceptible to age-related hearing loss. On the other end, mice in general are anxious prey animals that are very sensitive to sounds and easily startle (Dent et al., 2018; King et al., 2015; Turner et al., 2005). To this end, we tested both auditory brainstem responses (ABRs) and auditory startle responses in the mice prior to the start of the training. ABRs were measured in mice at the age of 9 weeks after birth. We followed the standardized protocol during which clicks were presented at 4, 8, 16, and 32 kHz (Akil et al., 2016; Willott, 2006). At the lowest frequency of 4 kHz, a sound pressure level of 53 dB was needed to elicit a reliable ABR peak (Figure 2A). ABR peaks were elicited with the lowest sound pressure level of 23 dB at a frequency of 16 kHz. Our results are in line with previous work testing ABRs in various mouse strains, including C57Bl/6J, at roughly the same age range (Ison et al., 2007; Zheng et al., 1999). Since we found recognizable ABR peaks in the entire range of 4 to 32 kHz, and since our findings are in line with these previous reports in mice (Heffner & Heffner, 2007; Reynolds et al., 2010), we conclude that hearing was intact in our animals.

Next, we established for each mouse the auditory startle response threshold. One component of the auditory startle response is a quick, partial, eyelid closure with a latency to peak of ~ 50 ms. Sometimes this alpha startle is followed by a beta startle, or short-latency response (SLR), which has a latency to peak of ~100 ms, and these beta startles can easily mask and sometimes even mimic cerebellar CRs. For this reason, we carefully determined at each tone (CS and GS) frequency for each mouse the SPL that was just sufficient to elicit a very small alpha startle response, but absolutely no beta startle (Boele et al., 2010). The sound frequencies used ranged from 2 to 20 kHz in steps of 2 kHz; all stimuli had the same duration and ramp/decay pattern as those of the CS and GSs. Importantly, during the baseline measurement, these tones were never reinforced with an eye puff US. The baseline sessions were repeated for ten days, each day consisting of 20 trials, which was necessary to find a proper sound pressure level for each frequency and for each animal. To avoid the potentially differentiating effect of latent inhibition (Lubow, 1973; Lubow & Moore, 1959) between animals, all mice received the exact same amount of tone-only trials during the baseline session.

Responses to tone-only trials at different tone frequencies for the last baseline session revealed that there was considerable variation in sound sensitivity between mice (Figure 2B). However, response thresholds for different frequencies within each mouse looked quite uniform (Figure 2B). In line with the ABR measurements, and in agreement with previous work (Heffner & Heffner, 2007; Reynolds et al., 2010), we found that mice trended to be more sensitive, i.e., startled

more easily at higher tone frequencies (16-20 kHz) than at lower frequencies (2-6 kHz). For this reason, the GS at the higher frequencies were delivered at slightly lower sound pressure levels than those at the lower frequencies (Figure 2B). Once the proper sound pressure levels were established for each mouse for all tone frequencies, including the 10 kHz CS, these values were not changed anymore during the subsequent acquisition training sessions (day 1-10) and generalization test sessions (day 11-17).

Eyeblink conditioning - acquisition sessions (days 1– 10)

Eyeblink acquisition training started the day after the last baseline session. Mice were trained for ten consecutive days. Inspection of averaged traces showed that the size of eyelid responses to the CS gradually increased over the course of ten days acquisition training (Figure 4A). We quantified the CR percentage and found that three mice did not show a significant increase (Figure 4B, gray dashed lines). These three mice were therefore disregarded in any further analysis, since our main question focuses on stimulus generalization in animals that had learned the task properly. In the remaining 11 animals, we found a statistically significant main effect of session for the average CR percentage (Figure 4B; Table 1; $F(9,90)=10.85$, $p<.0001$, ANOVA on LME). Mice reached a stable CR percentage of about 65-70 around day 8 that did not further increase. We did not find an effect of sex on CR probability, male and female mice showed identical learning curves (Figure 9A; $F(9,1)=0.07$, $p=0.79$, ANOVA on LME). Further quantification of the eyelid response amplitudes, revealed that there was a statistically significant main effect of session for CR amplitude calculated over *all trials* (Figure 4C; Table 1; $F(9,2000)=16.56$, $p<.0001$, ANOVA on LME). Similar to CR percentage, there was no further increase after day 8. Based on the distribution of all eyelid responses (in Figure 4D session 8 to 10 pooled), we set an arbitrary cut-off at a FEC of 0.05 to distinguish between CRs (>=0.05) and non-CRs (<0.05). We calculated the CR amplitude over the *CR only trials* and found a similar main effect of session (Figure 4E; Table 1; $F(9,931)=8.14$, $p<.0001$, ANOVA on LME). (Also, see the distribution of FEC calculated over CR only trials from sessions 8 to 10 pooled in Figure 4F).

Finally, we looked in more detail at the adaptive timing of eyeblink CRs. As expected, the latency to CR peak showed a clear distribution centered around the onset of the expected US at 250 ms after CS onset (Figure 4G,H) that remained stable over ten acquisition sessions. We found no statistically significant effect of session for latency to CR peak (Figure 4G; Table 1, $F(9,931)=0.62$, $p=0.77$, ANOVA on LME). For the latency to CR onset, we could only use 272 out of 1018 CR trials, because of alpha startle response that obscured the CR onset (Figure 3D). Similar to latency to CR peak, we could not find an effect of session for latency to CR onset (Figure 4I,J; Table 1, $F(9,90)=1.47$, $p=0.17$; ANOVA on LME). Overall, we concluded that the majority of animals showed normal eyeblink conditioning in terms of CR percentage, CR amplitude, and CR timing.

Eyeblink conditioning - generalization test sessions (days 11–17)

After 10 d of acquisition training, we tested the stimulus generalization for seven consecutive days. During these generalization test sessions mice were subjected to GSs, with frequencies ranging from 2 to 8 and 12 to 20 kHz. Importantly, these GS were never reinforced with the air puff US. The GSs had the exact same duration of 280 ms and ramp/decay times of 25 ms as the 10 kHz CS. Since the generalization test sessions consisted of substantially more trials wherein the tone was not reinforced with an air puff US (see Materials and Methods), we carefully checked whether this would lead to any extinction of learned eyeblink CRs. We found no significant effect of session on CR percentage (Fig. 5A; $F(6,60) = 0.60$; $p = 0.73$, ANOVA on LME) and thus concluded that there was no extinction of

eyeblink CRs over the course of seven generalization test sessions. This allowed us to pool the data of all seven generalization test sessions to study the effect of GS tone frequency on CR percentage, CR amplitude, and CR timing using the exact same criteria that were used for analyzing the acquisition training data.

CR percentage

We found a significant main effect of tone frequency on CR percentage (Figs. 5B, 6A; Table 2; $F(9,726)=11.99$, $p<.0001$, ANOVA on LME) with a downward gradient for CR percentage in both directions, i.e., in the direction of frequencies higher and lower than the 10 kHz CS tone, although this gradient appeared less pronounced for the higher frequencies. For the 10 kHz tone, mice had a CR percentage of 67 (65), whereas for 2 and 20 kHz, we found percentages of 38 (66) and 55 (66), respectively (all values: mean 6 95% CI). Post hoc comparison revealed that GSs with frequencies of 12–16 kHz did not result in significantly different CR percentages compared with the CS, whereas GSs with frequencies between 2 and 8 and 18 and 20 kHz were statistically significant (Fig. 6A). We did not find an effect of sex on CR probability, male and female mice showed identical generalization curves (Fig. 9B; $F(9,1) = 0.45$, $p = 0.51$, ANOVA on LME). We conclude that the CR probability decreased as the GSs were more different from the trained CS and that this effect was stronger for lower frequencies than for higher frequencies.

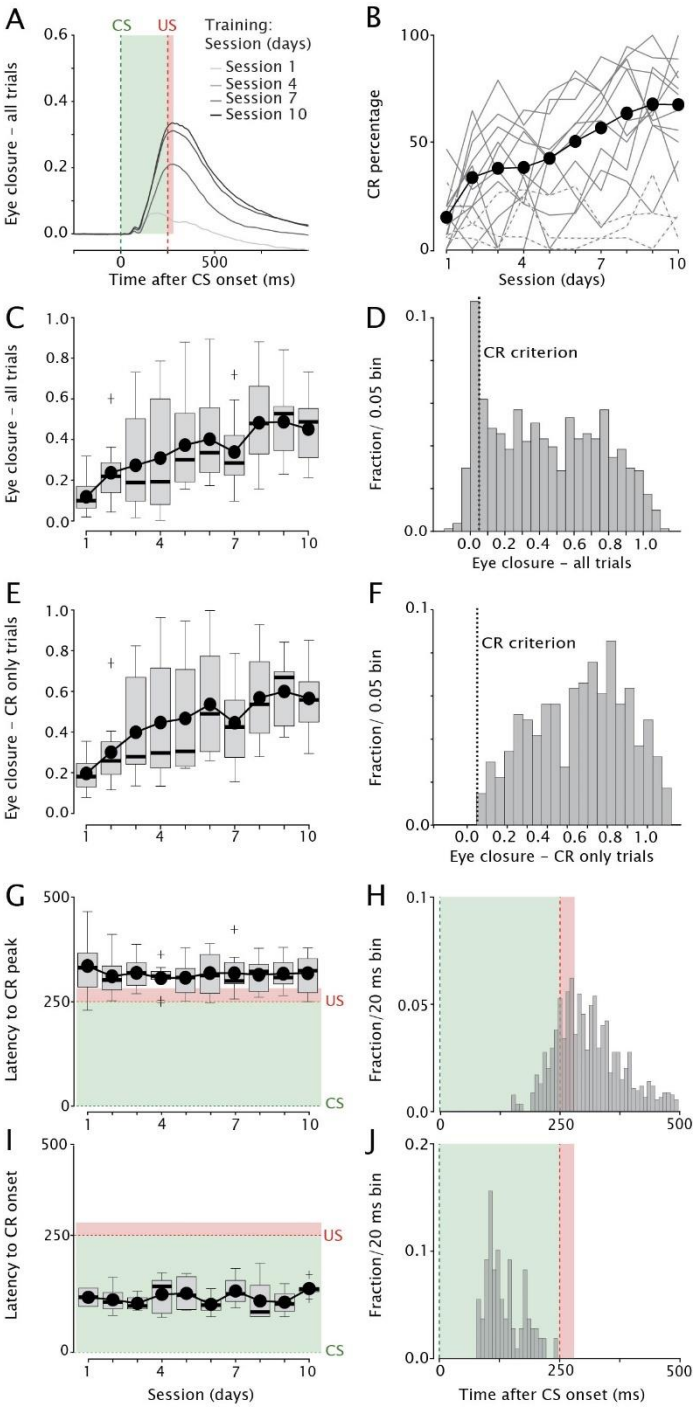

Figure 4. Mice acquire conditioned eyelid responses over the course of 10 consecutive training sessions. (**A**) Averaged eyeblink traces in CS-only trials during acquisition sessions 1, 4, 7, and 10 for the 11 mice that learned the task. The green dashed line indicates CS onset, the red dashed line indicates expected US onset. The light green and red shadings indicate CS and US duration, respectively. Eyelid is fully open at 0 and fully closed at 1. The US is omitted in the CS-only trials. (**B**) CR percentage as a function of acquisition training session. Each solid gray line represents a mouse that did learn the task (n =11), each dotted gray line represents an animal that did not learn the task, i.e., did not reach a CR percentage of .20 after 10 training days (n = 3). Black line with black filled dots indicates the mean of each session for the 11 animals that learn the task. (**C**) Eyelid closure amplitude over all trials plotted as a function of acquisition training session. The effect of session is statistically significant. For the boxplot, the thick horizontal line is showing the median, the top edge of each box indicates the 25th percentile, bottom edge the 75th percentile, whisker lines extending above and below each box indicate the range of observations, the plus symbols indicate outliers. The black line plot with filled black dots indicates the mean for each acquisition session. (**D**) Distribution of eyelid closure amplitude calculated over all trials

(acquisition sessions 8–10 pooled). Center of mass is around 0. For calculating the Eye closure – CR only trials, in panels in (**E–J**) we used a CR criterium of 0.05 indicated with the vertical dashed line. (**E**) Similar to (**C)** but now showing eyelid closure amplitude over CR only trials plotted as a function of acquisition training session. The effect of session is statistically significant. (**F**) Similar to (**D**) but now showing the distribution of eyelid closure amplitude calculated over CR only trials (acquisition sessions 8–10 pooled). (**G**) Latency to CR peak plotted as a function of training session. The green dashed line indicates CS onset, the red dashed line indicates US onset. The light green and red shadings indicate CS and US duration, respectively. There is no statistically significant effect of session. (**H**) Distribution of latency to CR peak for all trials (acquisition sessions 1–10 pooled). Note the adaptive timing of eyeblink CRs, whereby the CR peaks around the expected US (US is omitted in CS-only trials). (**I**) Similar to (**G**) but now showing latency to CR onset plotted as a function of training session. There is no statistically significant effect of session. (**J**) Similar to (**H**) but now showing the distribution of latency to CR onset for all sessions. For complete statistics for all panels, we refer to Table 1.

CR amplitude - all trials

When looking at all CS-only trials, we found a significant main effect of tone frequency (Fig. 5C,D; Table 2; F(9,4849)=44.34, p<.0001, ANOVA on LME), with a clear downward gradient in both directions, i.e., in the direction of frequencies higher and frequencies lower than the 10 kHz CS tone. Compared with CR percentage, the curves for both the CR amplitude calculated over all trials looked more symmetric. For the 10 kHz tone, mice had a CR amplitude calculated over all trials of 0.51 (60.04), whereas for 2 and 20 kHz they had amplitudes of 0.20 (60.04) and 0.29 (60.04), respectively (all values: mean 6 95% CI). Post hoc comparison revealed that GSs with frequencies close to the 10 kHz CS (12 kHz) did not result in significantly different CR amplitudes calculated over all trials, whereas GSs with frequencies equal or higher than 14 kHz or equal or lower than the 8 kHz CS were all significantly different (Fig. 6B; Table 3). When comparing the cumulative distributions of CR amplitudes calculated over all trials we found significant effects for all GS frequencies, except for the 12 kHz GS (Figs. 5E, 7A; for p-values, we refer to Table 4; all Kolmogorov–Smirnov test with correction for multiple comparison using FDR).

CR amplitude - CR only trials

We found a significant main effect of tone frequency for CR amplitude calculated over only trials with a CR (Figure 5F,G; Table 2; F(9,2692)=16.70, p<.0001, ANOVA on LME), with a downward gradient in both directions, i.e. in the direction of frequencies higher and frequencies lower than the 10 kHz CS tone. For the 10 kHz tone, mice had a CR amplitude calculated over CR trials of 0.63 (± 0.04), whereas for 2 and 20 kHz we found amplitudes of 0.42 (± 0.05) and 0.46 (± 0.05), respectively (all values mean ± 95% CI). Similar to CR amplitude calculated over *all* CS trials, we found that post hoc comparison revealed that GSs with frequencies close to the 10 kHz CS (12 kHz) did not result in significantly different CR amplitudes whereas GSs with frequencies equal or higher than 14 kHz or equal or lower than the 8 kHz CS were all significantly different (Figure 6C; Table 3). Interestingly, when comparing the cumulative distributions of CR amplitudes calculated over CR only trials, we found a pattern that looked slightly different from the one we found for CR amplitude calculated over all trials (Figure 5H). Although there was still a clear gradient, the range was narrower and GS frequencies of 6, 12 and 14 kHz did not result in statistically significant CR amplitudes (Figure 7B; for p values we refer to Table 4. All Kolmogorov-Smirnov test with correction for multiple comparisons using FDR). Previous work in rabbits showed a “binary choice phenomenon” (Khilkevich et al., 2018) whereby the probability of CRs gradually decreased on the degree of similarity between the GS and CS, but the amplitude of the CR remained constant. Since the CR threshold of 0.05 FEC is rather arbitrary, we also looked at higher CR thresholds of 0.10, 0.15, 0.20, 0.25, but could not establish a binary choice phenomenon (Figure 8A-D). Lastly, we established the threshold that would provide us with a binary choice, by step-wise

increasing the CR threshold. We found that a CR threshold of 0.45 was needed in order to get a non-significant effect of any of the tone frequencies (Figure 8E).

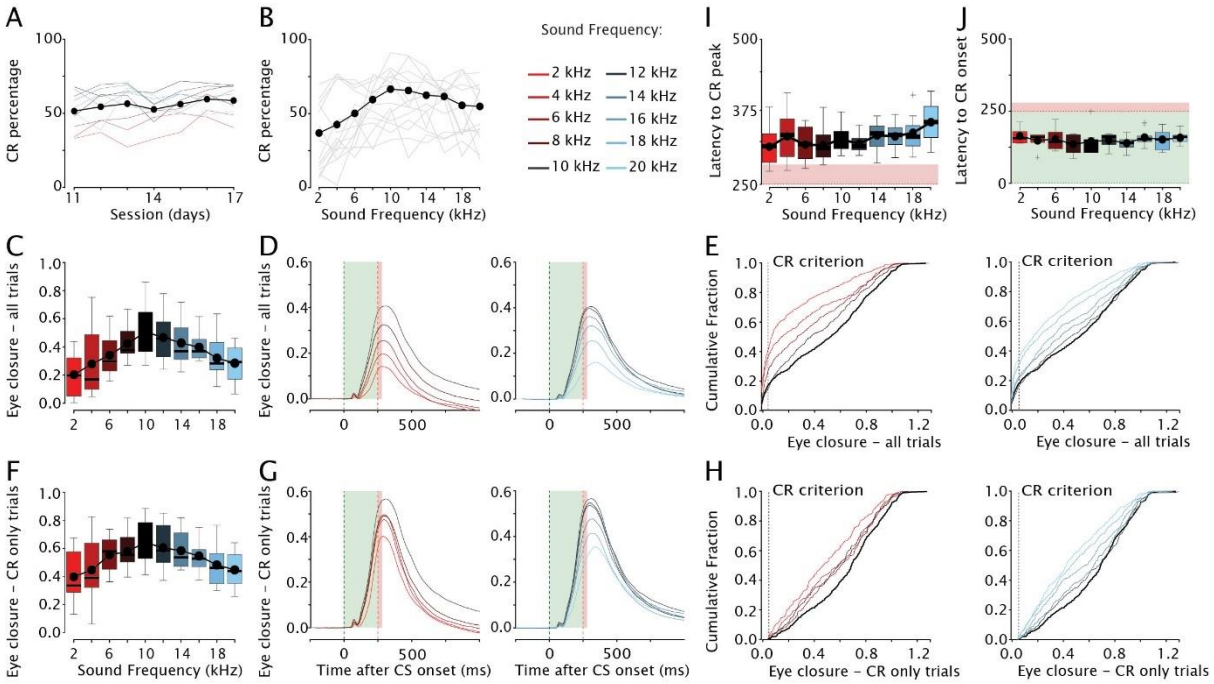

Figure 5. Generalization of conditioned eyelid responses in mice. (**A**) CR percentage as a function of generalization test session. Solid gray lines represent individual mice and the black line with black filled dots indicates the mean of each session. No effect was found for generalization session, indicating that there was no extinction of eyeblink CRs during the generalization test sessions. (**B**) CR percentage as a function of sound frequency. The 10 kHz tone is the CS, all other tone frequencies serve as GSs that are never reinforced with an air puff US. Solid gray lines represent individual mice, black line with black filled dots indicates the mean percentage CR for each GS. (**C**) Eyelid closure amplitude over all trials plotted as a function of sound frequency. For the boxplot, the thick horizontal line is showing the median, the top edge of each box indicates the 25th percentile, bottom edge the 75th percentile, whisker lines extending above and below each box indicate the range of observations, the plus symbols indicate outliers. The black line plot with filled black dots indicates the mean for each sound frequency used. For panels (**C–H**), the blue gradient indicates GSs with frequencies higher than the 10 kHz CS and red gradient indicates GSs with frequencies lower than the 10 kHz CS. (**D**) Averaged eyeblink traces in response to different sound frequencies. The green dashed line indicates CS onset, the red dashed line indicates expected US onset. The light green and red shadings indicate CS and US duration, respectively. Eyelid is fully open at 0 and fully closed at 1. The US is omitted in the CS-only trials. Note the symmetric generalization gradient. (**E**) Cumulative distribution function of eyelid closure calculated over all trials for the different sound frequencies. (**F**) Similar to (**C**) but now only for trials with a CR. (**G**) Similar to (**D**) but now for trials with a CR. (**H**) Similar to (**E**) but now for trials with a CR. (**I**) Effect of sound frequency on the latency to CR peak. Lower tones tend to elicit eyeblink CR that peak earlier than higher tones. (**J**) There was no effect of sound frequency on the latency to CR onset. For complete statistics, we refer to Table 2 and Table 3.

Latency to CR onset and peak Finally, we studied the effect of GS frequency on the timing of eyeblink CRs. As measures for CR timing, we looked at latency to CR onset and latency to CR peak. We found a significant main effect of tone frequency on latency to CR peak (Figs. 5I, 6D; Table 2; $F(9,2692)=5.56, p<.0001$, ANOVA on LME). Interestingly, we found a gradient whereby it appeared that the lowest frequencies resulted in CR peaks with the shortest latencies and the highest frequencies in CR peaks with the longest latencies. Post hoc comparison revealed that only the GS with the highest frequency (20 kHz) resulted in a significantly longer latency to CR peak compared with those to the 10

kHz CS. We thus conclude that tone frequency in mice has no effect on the latency to CR onset, but does have a mild effect on latency to CR peak. We found no significant main effect of tone frequency on latency to CR onset (Figs. 5J, 6E; Table 2; $F(9,322)=1.12$, $p=0.34$, ANOVA on LME). Regardless of CS or GS tone frequency, the latency to CR onset was around 150 ms after CS onset.

Discussion

We found that mice show a strong generalization of conditioned responses (CRs) in Pavlovian eyeblink conditioning using a tone as conditional stimulus. Both CR probability and CR amplitude decreased as the generalization stimuli (GSs) were more different from the conditional stimulus (CS). We also found a minor effect on the adaptive timing of eyeblink CRs whereby the tone lowest frequencies resulted in CR peaks with the shortest latencies and the highest frequencies in CR peaks with the longest latencies. No effect was found for latency to CR onset. Hence, our study provides a first investigation of stimulus generalization for eyeblink conditioning in mice using generalization stimuli (GSs) with tone frequencies higher *and* lower than the conditional stimulus (CS).

The cerebellum embodies more than two-thirds of all neurons in our brain and takes part to a large extent in the formation of procedural memories in motor behavior (De Zeeuw & Ten Brinke, 2015). Converging evidence highlights the role for cerebellum also in non-motor functions, such as social cognition (Van Overwalle et al., 2015), emotional processing (Schmahmann & Caplan, 2006), social behavior (Schmahmann & Sherman, 1998), addiction (Miquel et al., 2009; Moulton et al., 2014; Volkow et al., 2003), and fear learning (Lange et al., 2015; Maschke et al., 2003). Based on our finding that mice show a strong stimulus generalization in eyeblink conditioning, we expect that cerebellum is capable to regulate stimulus generalization both in motor and non-motor domains.

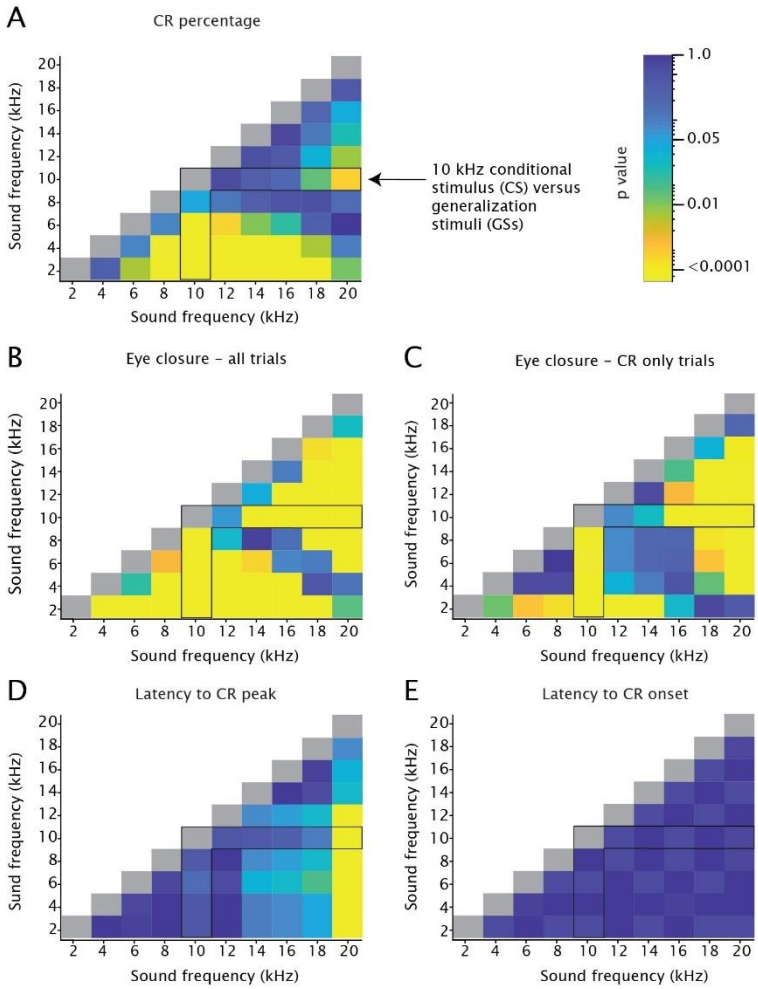

Figure 6. **Heatmaps showing adjusted p-values of all tone-tone comparisons for CR percentage, CR amplitude, and CR timing.** (**A**) Effect of tone frequency on CR percentage. The angular forked black box highlights the comparison between the 10 kHz CS and all the GSs. Note that the heatmap is on a logarithmic scale. All p-values were adjusted for multiple comparisons using FDR. Values correspond with those of Figure 5B. (**B**) Effect of tone frequency on eyelid closure calculated over all trials. Values correspond with those of Figure 5C. (**C**) Effect of tone frequency on eyelid closure calculated over CR only trials using a 0.05 criterium. Values correspond with those of Figure 5F. (**D**) Effect of tone frequency on latency to CR peak. Values correspond with those of Figure 5I. (**E**) Effect of tone frequency on latency to CR onset. Values correspond with those of Figure 5J. For complete statistics, we refer to Table 2 and Table 3.

Differential versus nondifferential training

Eyeblink conditioning can be performed according to a *non-differential* or *differential* protocol. During non-differential training, which is the paradigm we employed in our current study, subjects are trained with only one CS, for instance a 10 kHz tone, and tested with GSs after acquisition training is finished. During differential training, instead, subjects are trained with more than one CS, whereby one CS (CS+) is reinforced with a US and one or several other CSs are not reinforced at all (CS-). Since previous work has shown that these different eyeblink conditioning protocols have an effect on the stimulus generalization gradient (Hupka et al., 1969b; Moore & Mis, 1973), we will mainly compare our findings with previous studies using a non-differential protocol.

CR percentage

CR probability decreases with each incremental or decremental 2 kHz step away from the trained 10 kHz CS. Still, mice show CRs in a respectable amount of the trials at the upper and lower limits that we

tested in this study: where the 10 kHz CS evoked CRs in about 67% percent of the trials, the lower limit 2 kHz and upper limit 20 kHz probe CS evoked CRs in 38% and 55% of the trials, respectively. This gradient in CR probability was seen both at a mouse individual level as well as a group level (Figure 5B), indicating that the gradient was not simply a smoothing effect due to averaging data (Razran, 1949). Previous studies on stimulus generalization during non-differential eyeblink conditioning primarily looked at CR percentage (i.e., CR probability) (Table 5). Rabbits generally show a CR probability pattern that looks very similar to the one we observed in mice: the highest CR probability to the trained CS and progressive decrease in response probability to more distant GS frequencies (Garcia et al., 2003 Khilkevich et al., 2018; Moore, 1964; Moore & Mis, 1973; Siegel et al., 1968; Solomon & Moore, 1975). None of these studies, though, assessed GSs in both directions of the frequency spectrum, i.e., for tone frequencies higher *and* lower than the CS (Table 5). Interestingly, rabbits trained using a differential eyeblink conditioning protocol yielded a steeper CR gradient in stimulus generalization testing than those trained in a non-differential procedure (Liu, 1971; Moore, 1964).

CR amplitude

Similar to CR percentage, the amplitude of conditioned eyelid closure calculated across *all CS trials* shows a stepwise decrease when the difference between the trained CS and GS increases. Since CR probability and amplitude of eyelid closure show a strong covariation on a single session level, this is not a surprising result. Indeed, previous studies done in rabbits, show the same phenomenon for eyelid closure calculated over all trials. For instance, Garcia et al. (2003) and Ohyama et al. (2003) report that the *magnitude* (i.e., CR amplitude calculated over all CS trials) of eyeblink responses shows a progressive decrease with each incremental step in tone frequency away from the CS. In addition, Khilkevich et al. (2018), using electrical stimulation of mossy fibers as CS, similarly show that GSs with stimulation frequencies lower than the CS result in a lower CR amplitude.

Only a subset of previous studies also describes the amplitude of eyelid closure for only those trials wherein the animal shows a CR (Garcia et al., 2003; Kehoe et al., 1995; Khilkevich et al., 2018). Looking at this value in our study, using a 0.05 CR criterion, we again observed the same gradient with the highest CR amplitude to the trained CS and a progressive decrease in CR amplitude for each incremental or decremental 2 kHz step away from the CS. Although this gradient was less steep than for CR amplitude calculated over all trials, we could not establish the clear binary choice phenomenon reported by Khilkevich et al., 2018, whereby the probability of CRs gradually decreased on the degree of similarity between the GS and CS, but the amplitude of the CR remained constant. Since a FEC of 0.05 is an arbitrary CR threshold, we also looked at higher CR thresholds (Figure 8B-E), but could not establish the binary choice. The most parsimonious explanation for this discrepancy between our study and Khilkevich et al., 2018, is the difference in the eyelid motor plant between mice and rabbits. In mice, the main force driving eyeblink CRs comes from contraction of the orbicularis oculi muscle, while in rabbits (and humans) there is, in addition to the contraction of the orbicularis oculi muscle, a more pronounced role for a simultaneous relaxation of the levator palpebrae muscle (Ansari & Nadeem, 2016). This results in a different CR expression profiles, whereby conditioned rabbits show a clear bimodal (or better: zero-inflated) distribution of CR amplitudes (Garcia et al., 2003b; Khilkevich et al., 2018). For mice, this bimodal distribution is present, but clearly less obvious compared to the ones reported for rabbits (Albergaria et al., 2018; Kloth et al., 2015; ten Brinke et al., 2017) (Compare histograms in Figure 4D,F with those reported in Khilkevich et al., 2018 Figure 2A).

Another difference between our study and the Khilkevich et al., 2018 study, is the performance level of the animals at the end of training. Khilkevich et al. trained their rabbits "until both CR percentage was high (CR% > 90%) and CR amplitudes were robust and near the target amplitude" In practice, this meant that most rabbits were trained for ten sessions. In our experiment, mice reached maximum conditioning levels of about 70% CRs and CR amplitudes of about 0.5. These values for our mice did not further increase and remained stable after acquisition session 8. Thus, the Khilkevich (2018) rabbits were clearly performing better than our mice: the rabbits were overtrained, whereas in our mice there was theoretically still room for further improvement. This difference in performance level could also explain why Khilkevich et al., 2018 report a binary choice and we observe more a continuum of responses.

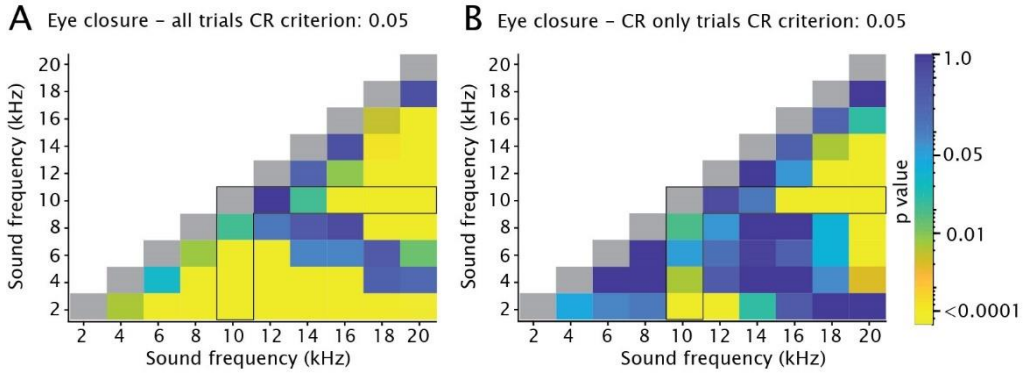

Figure 7. Heatmaps showing adjusted p-values of all tone-tone comparisons for cumulative CR amplitude. (**A**) Effect of tone frequency on cumulative CR amplitude calculated over all trials. Color indicates p-value. The angular forked black box highlights the comparison between the 10 kHz CS and all GSs. Note that the heatmap is on a logarithmic scale. All p-values were calculated using a Kolmogorov–Smirnov test on the cumulative distribution function (CDF). All p-values were adjusted for multiple comparisons using FDR. Values correspond with those of Figure 5E. (**B**) Similar to (**A**) but now for the effect of tone frequency on cumulative CR amplitude calculated over CR only trials using 0.05 criterium. Values correspond with those of Figure 5H. For complete statistics, we refer to Table 4.

CR timing

Most previous studies on stimulus generalization during eyeblink conditioning ignored the adaptive timing properties of eyelid CRs (Khilkevich et al., 2018; Liu, 1971; Moore, 1964; Moore & Mis, 1973; Siegel et al., 1968). Our data show that mice CRs peaked significantly later to GSs with higher frequencies compared to those with lower frequencies. These findings are in line with response patterns described by Garcia and colleagues (2003). Interestingly, when electrical stimulation of the forelimb, that had served as a CS, was suddenly switched from 50 kHz to a 100 kHz stimulus train, an opposite effect was reported: the latency to CR peak was shorter for the higher frequency stimulus (Svensson et al., 1997). We have no clear explanation for this effect of tone frequency on latency to CR peak. It may reflect processing of auditory information between the level of sensory organs (cochlea) and the cerebellar mossy fiber input system.

In mice, there is no effect of tone frequency on the latency to CR onset. This finding is in line with previous work in mice, showing that the latency to CR onset is rather unaffected by the duration of the CS (Chettih et al., 2011), which is another difference between eyeblink CRs in mice compared to other species (rabbits, humans, ferrets). Indeed, a trending (but not significant) increase in CR onset latency has been described for stimulus generalization in rabbits (Garcia et al., 2003).

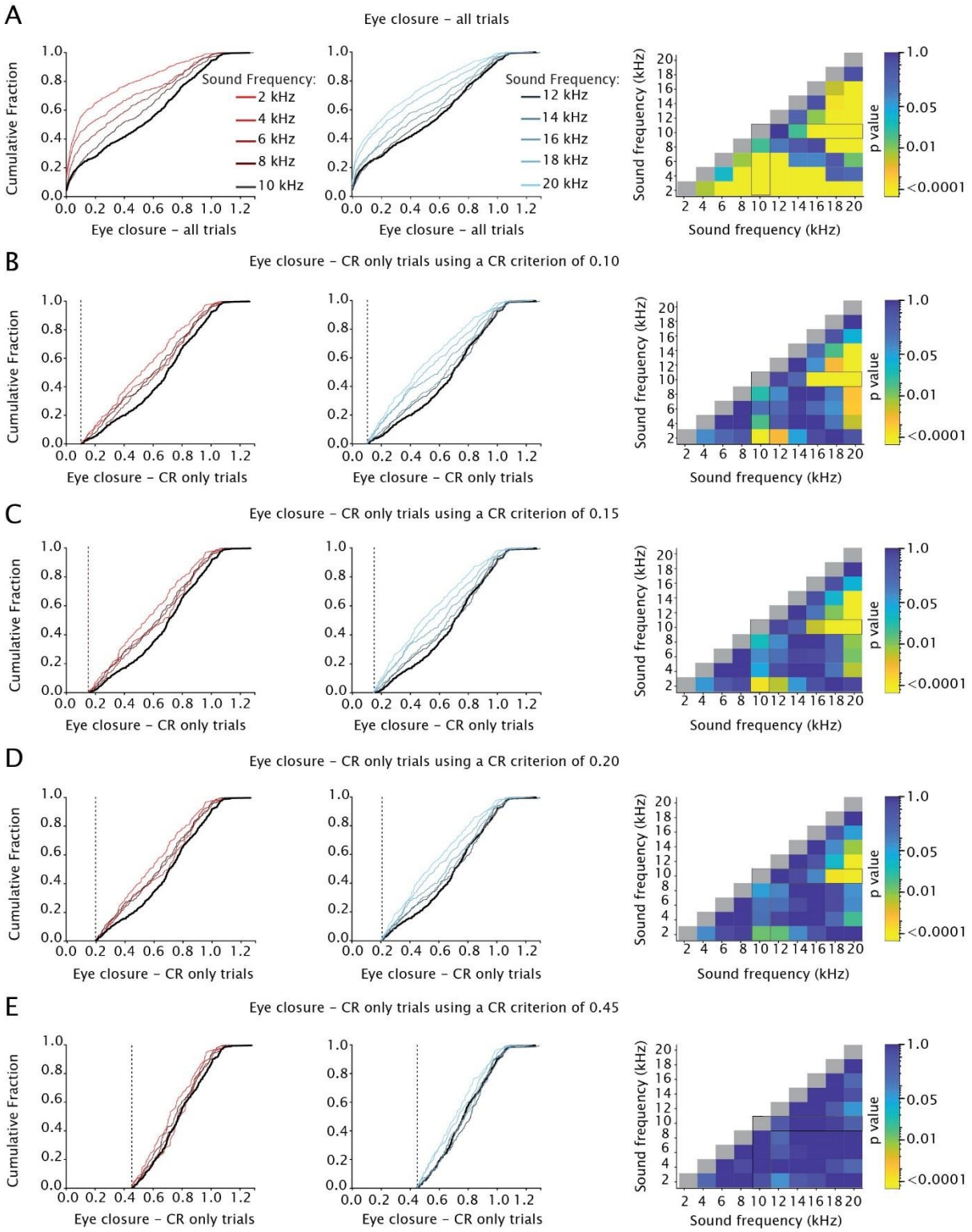

Figure 8. **Heatmaps showing adjusted p-values of all tone-tone comparisons for cumulative CR amplitude using different CR thresholds.** (**A**) Effect of sound frequency on cumulative CR amplitude calculated over all trials. Color indicates p-value. The angular forked black box highlights the comparison between the 10 kHz CS and all GSs. Note that the heatmap is on a logarithmic scale. All p-values were calculated using a Kolmogorov–Smirnov test on the cumulative distribution function (CDF). All p-values were adjusted for multiple comparisons using FDR. Similar to Figure 5, the blue gradient indicates GSs with frequencies higher than the 10 kHz CS and red gradient indicates GSs with frequencies lower than the 10 kHz CS. (**B–D**) Similar to (**A**) but now using a CR criteriums of 0.10, 0.15, and 0.20 FEC. (**E**) Similar to (**B–D**) but now using the lowest CR threshold whereby there is a nonsignificant effect of GS for all frequencies. In mice, this threshold appeared to be 0.45. Thus, a threshold

of 0.45 FEC was needed to get a binary response pattern, as reported previously (Khilkevich et al., 2018), whereby the probability of a CR gradually decreases depending on the similarity between CS and GS, but the amplitude of the CR remained constant. Note that this 0.45 is close to the split of the bimodal distributions shown in Figure 4D,F.

Latent inhibition

Three out of fourteen animals did not learn the task within the ten days of acquisition training, which is slightly higher compared to previous work by our group (Beekhof et al., 2021; Boele et al., 2018; de Oude et al., 2021; Grasselli et al., 2020). The difference between this study and previous work, is the amount of CS pre-exposure during the ten baseline sessions, which potentially leads to 'latent inhibition'. Latent inhibition is the phenomenon whereby it takes longer to get conditioned to a familiar stimulus than to novel stimulus. The pre-exposure to the CS (20 in total) and GS (20 in total for each frequency) during the ten baseline sessions could explain why these 3 animals did not learn the task. Although we made sure all animals received the exact same amount of CS-only and GS-only trials during the baseline sessions to keep the novelty level of the tone equal for all animals, it could be that the latent inhibition effect varies between animals.

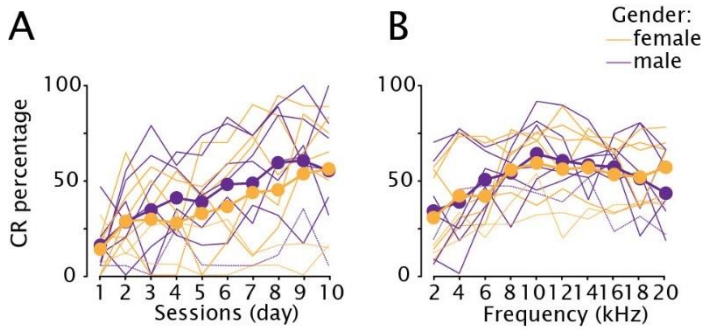

Figure 9. No effect of sex on acquisition and generalization of conditioned eyeblink responses. (**A**) CR percentage during acquisition sessions 1–10. Each colored line represents an individual mouse (yellow for females, purple for males). All animals are included (n = 14), also the ones that did not learn the task (n = 3) and are therefore excluded from the main statistical analysis of this paper. Thicker lines indicate the averages respectively for males and females including all the animals. (**B**) Generalization test sessions pooled together. Same color coding as in A. Here again, all animals are included in the averages.

Comparison between generalization curves from eyeblink conditioning and fear conditioning

Stimulus generalization has been studied previously using fear conditioning. However, to our knowledge, a complete assessment of conditioned fear responses as a function of a wide range of tone frequency is missing: all studies probed generalization of fear responses presenting only one or a few novel auditory cue(s) (see for instance: Shaban et al., 2006; Zhang et al., 2019). In addition, most fear conditioning studies use a differential paradigm during acquisition. For these two reasons combined, it is almost impossible to compare our eyeblink conditioning generalization curve with those using fear conditioning. It would be interesting to find out how US intensity affects the shape of the generalization curve. One could do so using eyeblink conditioning, using a stronger US, which is known to induce more fear (Boele et al., 2010) and leads to faster acquisition (Freeman et al., 1993; Kehoe & White, 2002; Passey, 1948; Smith, 1968; Spence et al., 1953 – see Boele et al., 2016). Based on work done on fear conditioning (Dunsmoor et al., 2009, 2017; Laxmi et al., 2003), we predict that a more aversive US leads to stronger generalization (i.e., a less steep gradient). In addition, the training paradigm (differential vs. non-differential training) has effects on the shape of the curve (Dunsmoor & LaBar, 2013).

Neural mechanisms

The study of stimulus generalization primarily comes from fields of ethology or experimental psychology and has been investigated with various experimental paradigms other than Pavlovian eyeblink conditioning, such as fear conditioning and operant conditioning. These investigations on stimulus generalization have been performed in many species including humans, goldfishes, rats and pigeons, and generally report a decreasing generalization gradient when moving away from the trained stimulus (Baron, 1973; Ghirlanda & Enquist, 2003b; Thomas & Mitchell, 1962), similar to what we found in Pavlovian eyeblink conditioning in mice. Interestingly, Guttman and Kalish (1956) showed that stimulus generalization does not originate from a failure in perceptual discrimination, but instead it is an active process. This principle probably also applies to cerebellar learning rules during eyeblink conditioning. Although early reports on stimulus generalization in eyeblink conditioning have shown that lesions of non-cerebellar structures, for instance hippocampus or cerebral cortex, affect eyeblink conditioning and stimulus generalization in eyeblink conditioning (Solomon & Moore, 1975), the leading idea now is that the essential eyeblink conditioning memory trace is formed in cerebellum (Freeman, 2015; Freeman & Steinmetz, 2011; Heiney et al., 2014; Mauk & Buonomano, 2004; Mauk & Donegan, 1997; Mccormick et al., 1981, 1981; McCormick et al., 1982; ten Brinke et al., 2015; Yeo & Hesslow, 1998). Purkinje cells in well-defined microzones in cerebellar cortex receive converging inputs from the mossy fiber – parallel fiber pathway, which transmits the CS, and the climbing fiber pathway, which transmits the US (De Zeeuw et al., 2021; De Zeeuw & Ten Brinke, 2015). Repeated pairing of CS and US leads to the acquisition of a simple spike pause in Purkinje cells in response to the CS (Jirenhed et al., 2017; Narain et al., 2018; Ohmae & Medina, 2015; ten Brinke et al., 2015). Although further research is needed, one could imagine that the higher and lower frequency tones are not equally represented in the parallel fiber beams and thereby contributing to the asymmetric distribution in the stimulus - response relation.

The simple spike pause in turn causes a temporary disinhibition of cerebellar nuclei neurons, which (indirectly) innervate the motor neurons that control the eyelid musculature (Halverson et al., 2015, 2018; Jirenhed et al., 2017; ten Brinke et al., 2017). In addition, mossy fiber and climbing fibers send of collaterals directly to the cerebellar nuclei. Our previous work has shown that the number of varicosities on these mossy fiber collaterals in the cerebellar nuclei increases quite robustly with eyeblink conditioning (Boele et al., 2013). Moreover, the number of these varicosities correlates positively with the amplitude of eyelid CRs, indicating that these mossy fibers are important for CR expression. Work by Ohyama and colleagues (2003) has shown that pharmaceutical disconnection of Purkinje cell inhibition from the cerebellar nuclei results in much smaller CRs to GSs, but that CRs to the trained CS remained largely the same in size, although the adaptive timing of these CRs was affected (Ohyama, 2003b). This suggests that mossy fiber collaterals form a CS-specific pathway from the pontine nuclei to the cerebellar nuclei. We hypothesize that cerebellar cortex and nuclei play synergistic roles in CR expression and timing. GSs that resemble the CS will result in a rather similar and strong neural representation in the parallel fiber input at the Purkinje cell, resulting in a rather similar simple spike pause. GSs that are more different instead, will result in a weaker representation, leading to a weaker Purkinje cell response.

Chapter 2- Supplementary Information

Table 1| Eyeblink conditioning outcome measures during acquisition training (session 1-10). All values represent mean ± 95% CI. The ANOVA on linear mixed-effect model (LME) shows the main effect of session. Abbreviations: CR, conditioned response.

Session	CR percentage	CR amp-all trials	CR amp-CR only trials	Latency to CR peak	Latency to CR onset
1	14 (± 8)	0.11 (± 0.05)	0.19 (± 0.06)	329.7 (± 51.1)	130.7 (± 276.3)
2	33 (± 12)	0.23 (± 0.10)	0.30 (± 0.12)	306.7 (± 31.6)	124.9 (± 41.5)
3	37 (± 16)	0.27 (± 0.16)	0.39 (± 0.19)	314.3 (± 28.4)	116.5 (± 31.8)
4	38 (± 13)	0.30 (± 0.19)	0.44 (± 0.21)	302.6 (± 22.7)	137.8 (± 56.7)
5	42 (± 15)	0.37 (± 0.15)	0.46 (± 0.20)	303.4 (± 28.0)	139.9 (± 44.8)
6	50 (± 15)	0.40 (± 0.15)	0.53 (± 0.17)	313.8 (± 30.9)	114.0 (± 23.7)
7	56 (± 16)	0.33 (± 0.12)	0.44 (± 0.13)	313.5 (± 28.2)	145.7 (± 61.8)
8	63 (± 17)	0.48 (± 0.15)	0.56 (± 0.14)	310.0 (± 24.2)	122.1 (± 95.8)
9	67 (± 14)	0.48 (± 0.11)	0.59 (± 0.10)	312.5 (± 24.6)	119.2 (± 37.1)
10	67 (± 14)	0.45 (± 0.11)	0.56 (± 0.10)	313.5 (± 29.2)	151.5 (± 19.5)
ANOVA on LME	$F(9,90)=10.85, p<.0001$	$F(9,2000)=16.56, p<.0001$	$F(9,931)=8.14, p<.0001$	$F(9,931)=0.62, p=0.77$	$F(9,90)=1.47, p=0.17$

Table 2| Eyeblink conditioning outcome measures during generalization test sessions (session 11-17). All values represent mean ± 95% CI. The ANOVA on linear mixed-effect model (LME) shows the main effect sound frequency. Post-hoc comparisons are shown in Figure 6 and Table 3 and 4. Abbreviations: CR, conditioned response.

Tone freq.	CR percentage	CR amp-all trials	CR amp-CR only trials	Latency to CR peak	Latency to CR onset
2 kHz	38 (± 6)	0.20 (± 0.04)	0.42 (± 0.05)	310.0 (± 13.9)	162.5 (± 15.0)
4 kHz	43 (± 7)	0.28 (± 0.06)	0.49 (± 0.07)	323.9 (± 15.7)	147.8 (± 17.9)
6 kHz	50 (± 6)	0.34 (± 0.05)	0.54 (± 0.05)	311.0 (± 9.10)	158.1 (± 21.4)
8 kHz	58 (± 6)	0.42 (± 0.04)	0.56 (± 0.04)	315.1 (± 9.79)	148.8 (± 23.3)
10 kHz	**67 (± 5)**	**0.51 (± 0.04)**	**0.63 (± 0.04)**	**320.1 (± 8.96)**	**145.3 (± 16.0)**
12 kHz	65 (± 5)	0.46 (± 0.04)	0.60 (± 0.04)	311.5 (± 9.72)	151.3 (± 18.9)
14 kHz	63 (± 5)	0.43 (± 0.04)	0.59 (± 0.04)	327.8 (± 10.3)	142.6 (± 13.1)
16 kHz	61 (± 4)	0.40 (± 0.03)	0.55 (± 0.04)	324.9 (± 11.8)	155.8 (± 13.4)
18 kHz	55 (± 6)	0.31 (± 0.04)	0.47 (± 0.05)	332.1 (± 12.5)	141.2 (± 16.0)
20 kHz	55 (± 6)	0.29 (± 0.04)	0.46 (± 0.05)	341.3 (± 13.6)	152.8 (± 13.3)
ANOVA on LME	F(9,726)=11.99,p<.0001	F(9,4849)=44.34,p<.0001	F(9,2692)=16.70,p<.0001	F(9,2692)=5.56,p<.0001	F(9,322)=1.12,p=0.34

Table 3| Post hoc comparison between the 10 kHz CS and all other GS frequencies for CR amplitude calculated over all trials and CR amplitude calculated over CR trials. All values represent FDR corrected post-hoc comparisons using an ANOVA on linear mixed-effect model. Abbreviations: CS, conditional stimulus; GS, generalization stimulus.

CS 10 kHz versus GS	2 kHz	4 kHz	6 kHz	8 kHz	12 kHz	14 kHz	16 kHz	18 kHz	20 kHz
CR amp - all trials	p<.0001	p<.0001	p<.0001	p<.0001	p=0.056	p<.0001	p<.0001	p<.0001	p<.0001
CR amp - CR only trials	p<.0001	p<.0001	p=0.0004	p=0.0002	p=0.076	p=0.021	p<.0001	p<.0001	p<.0001

Table 4| Post hoc comparison between the 10 kHz CS and all other GS frequencies for cumulative CR amplitude calculated over *all trials* and cumulative CR amplitude calculated over *CR only trials*. All values represent FDR corrected post-hoc comparisons using a two-sample Kolmogorov-Smirnov test on the cumulative distribution. Abbreviations: CS, conditional stimulus; GS, generalization stimulus.

CS 10 kHz versus GS	2 kHz	4 kHz	6 kHz	8 kHz	12 kHz	14 kHz	16 kHz	18 kHz	20 kHz
CR amp - all trials	p<.0001	p<.0001	p<.0001	p=0.0110	p=1.092	p=0.0105	p<.0001	p<.0001	p<.0001
CR amp - CR only trials	p<.0001	p=0.0032	p=0.0562	p=0.0095	p=0.621	p=0.1067	p<.0001	p<.0001	p<.0001

Table 5| Overview of previous studies on stimulus generalization and Pavlovian eyeblink conditioning studies. Note that none of these studies was done in mice.

Authors	Animals	CS type	US	CR	Methods	Analysis	Results	Training type	CS	Probe CSs
Siegel, 1968	rabbit	tone	4 mA shock	NM response	DC signal	(i)CR percentage single subject/average	CR decremental gradient	non differential	0.5 kHz75 dB	0.5, 1.2, 2.0, 3.0, 4.0 kHz dB
		tone							1.2 kHz 75 dB	0.5, 1.2, 2.0, 3.0, 4.0 kHz dB
		tone							2.0 kHz 75 dB	0.5, 1.2, 2.0, 3.0, 4.0 kHz dB
		tone							3.0 kHz 75 dB	0.5, 1.2, 2.0, 3.0, 4.0 kHz dB
		tone							4.0 kHz 75 dB	0.5, 1.2, 2.0, 3.0, 4.0 kHz dB
Hupka, 1969	rabbit	tone	2 mA shock	NM response	DC signal	(i) CR percentage average	CR decremental gradient steeper for the CS+ 0.4 kHz	differential	CS+ 0.4 kHz CS-1.6 kHz	0.4, 0.8, 1.6, 2.2, 2.8, 3.4, 4.0 kHz
		tone						differential	CS+ 1.6 kHz CS- 2.8 kHz	0.4, 0.8, 1.6, 2.2, 2.8, 3.4, 4.0 kHz
		tone						differential	CS+ 2.8 kHz CS- 4.0 kHz	0.4, 0.8, 1.6, 2.2, 2.8, 3.4, 4.0 kHz
		tone						differential	CS+ 1.6 kHz CS- 0.4 kHz	0.4, 0.8, 1.6, 2.2, 2.8, 3.4, 4.0 kHz
		tone						differential	CS+ 2.8 kHz CS- 1.6 kHz	0.4, 0.8, 1.6, 2.2, 2.8, 3.4, 4.0 kHz
		tone						differential	CS+ 4.0 kHz CS- 2.8 kHz	0.4, 0.8, 1.6, 2.2, 2.8, 3.4, 4.0 kHz
Swadlow and Schneider man, 1970	rabbit	electrical stimulat	5 mA shock	Eyelid response		(i)CR percentage average	CR decremental gradient for frequency + duration/intensity, but no frequency + TSE	non differential	LGN 1.5 sec trains (21 pps, 0.21 msec)	LGN-a 1.5 pulse trains (18 test param with change in frequency + TSE/pulse dur/ intensity)
Liu, 1971	rabbit	tone	2 mA shock	NM response	EMG	(i)CR percentage average	CR decremental gradient peak at probe CS (1.4 kHz 75 dB)	non differential	CS+ 2.4 kHz 75 dB CS+ 1.2 kHz 75 dB (C2*)	0.4, 0.8, 1.2, 1.6, 2.0 kHz 75 dB
		tone					CR decremental gradient steeper at CS+ in T-T and T-L than C1	non differential	1.2 kHz 75 dB (C1*)	0.4, 0.8, 1.2, 1.6, 2.0 kHz 75 dB
		tone						differential	CS+ 1.2 kHz 75 dB CS- 2.4 kHz 75 dB (T-T*)	0.4, 0.8, 1.2, 1.6, 2.0 kHz 75 dB

		tone/light						differential	CS+ 1.2 kHz 75 dB CS- light (T-L*)	0.4, 0.8, 1.2, 1.6, 2.0 kHz 75 dB
		tone					CR decremental gradient slope steeper along (F) than (I)	differential	CS+ 1.2 kHz 75 dB CS- 2.4 kHz 60 dB (I+F*)	0.4, 0.8, 1.2, 1.6, 2.0 kHz 75 dB 1.2 kHz 65, 70, 80, 85 dB
Moore, 1972	rabbit	tone	2 mA shock	Eyelid response	EMG	(i)CR percentage average	CR decremental steeper in T-T and T-L	non differential	1.2 kHz (T)	0.4, 0.8, 1.2, 1.6, 2.0 kHz
		tone						differential	CS+ 1.2 kHz CS- 2.4 kHz (T-T)	0.4, 0.8, 1.2, 1.6, 2.0 kHz
		tone/light						differential	CS+ 1.2 kHz CS- light (T-L)	0.4, 0.8, 1.2, 1.6, 2.0 kHz
Moore & Mis, 1973	rabbit	tone	2 mA shock	NM response	DC signal	(i)CR percentage average	CR percentage to CS-lower for differential training	non differential	0.9 kHz 75 dB	0.3, 0.6, 0.9, 1.2, 1.5, 1.8, 2.1 kHz 75 dB
		tone						non differential	0.9 kHz 95 dB	0.3, 0.6, 0.9, 1.2, 1.5, 1.8, 2.1 kHz 75 dB
		tone						non differential	1.5 kHz 75 dB	0.3, 0.6, 0.9, 1.2, 1.5, 1.8, 2.1 kHz 75 dB
		tone						non differential	1.5 kHz 95 dB	0.3, 0.6, 0.9, 1.2, 1.5, 1.8, 2.1 kHz 95 dB
		tone						differential	CS+ 1.5 kHz 75 dB CS- 0.9 kHz 75 dB	0.3, 0.6, 0.9, 1.2, 1.5, 1.8, 2.1 kHz 75 dB
		tone						differential	CS- 0.9 kHz 75 dB CS- 1.5 kHz 75 dB	0.3, 0.6, 0.9, 1.2, 1.5, 1.8, 2.1 kHz 75 dB
		tone						differential	CS+ 1.5 kHz 75 dB CS- 0.9 kHz 95 dB	0.3, 0.6, 0.9, 1.2, 1.5, 1.8, 2.1 kHz 95 dB
		tone						differential	CS+ 1.5 kHz 95 dB CS- 0.9 kHz 75 dB	0.3, 0.6, 0.9, 1.2, 1.5, 1.8, 2.1 kHz 95 dB
Solomon & Moore, 1975	rabbit	tone	2 mA shock	NM response	DC signal	(i)CR percentage average	(i) CR percentage gradient less steep for HP and CTX group	non differential	1.2 kHz 76 dB	0.4, 0.8, 1.2, 1.6, 2.0 kHz 76 dB
		tone						non differential	1.2 kHz 76 dB *(lesion HP)*	0.4, 0.8, 1.2, 1.6, 2.0 kHz 76 dB
		tone						non differential	1.2 kHz 76 dB *(lesion CTX)*	0.4, 0.8, 1.2, 1.6, 2.0 kHz 76 dB
Kehoe, 1995	rabbit	tone	2 mA shock	NM response	Photoelectric transducer	(i)CRpercentage/amplitude/onset average	(i)CR onset earlier in (A), (D) (ii)CR amplitude/percentage lower in (A) and (D) than (S)	non differential	0.5 kHz 55 dB	0.5-1.5(A*), 1.5-0.5(D*), 0.5 kHz(S*)

		tone						non differential	1.0 kHz 55 dB	0.5-1.5, 1.5-0.5, 1.0 kHz
		tone						non differential	1.5 kHz 55 dB	0.5-1.5, 1.5-0.5, 1.0 kHz
		tone					(i)CR onset earlier in (A), (D)	non differential	60 dB	60-90 dB, 90-60 dB, 60 dB
		tone						non differential	75 dB	60-90 dB, 90-60 dB, 75 dB
		tone						non differential	90 dB	60-90 dB, 90-60 dB, 90 dB
		tone					(i)CR decremental gradient likelihood/amplitude (ii) CR onset unchanged	non differential	50 ms	50, 400, 800, 1600 ms
		tone						non differential	400 ms	50, 400, 800, 1600 ms
		tone						non differential	800 ms	50, 400, 800, 1600 ms
Svennson, 1997	ferrets	electric stimulat	3 mA shock	Eyelid response	EMG	(i)CR onset/peaktime average	(i)CR onset/peaktime earlier	non differential	Left FL* 300 ms 50 Hz 1 mA	Left FL 300 ms 50 Hz 2 mA
		electric stimulat						non differential	MCP* 0.1 ms 50 Hz	MCP 0.1 ms 100 Hz
Garcia & Mauk, 2003	rabbit	tone	4 mA shock	(i)NM response (ii) eyelid response	(i) infrared LED (ii) photoelectric transucer	(i)CR percentage/amplitude/onset/peaktime average	(i)CR percentage/amplitude decremental gradient (ii)CR onset/peaktime increment	non differential	1.0 kHz 75 dB	1.0, 1.26, 1.59, 2.0, 2.52, 3.17, 4.0, 5.04 kHz 75 dB
Ohyama, 2003	rabbit	tone	0.8-2.5 mA shock	eyelid response	infrared LED	(i)CR/SLR percentage/ amplitude average	(i)SLR/CR decremental gradient (excl light) (ii)CR amplitude unchanged	non differential	1.0 kHz 85 dB	1.0, 1.85, 3.55, 6.1, 9.5 85 dB, light
		tone					*(I)SLR/CR amplitude decremental gradient*	*non differential*	*1.0 kHz 85 dB (PCX*) cerebellar cortex*	*1.0, 1.85, 3.55, 6.1, 9.5 85 dB, light*
		tone					(i)SLR/CR decremental gradient (excl light) (ii)CR amplitude unchanged	non differential	9.5 kHz 85 dB	1.0, 1.85, 3.55, 6.1, 9.5 85 dB, light
		tone					*(I)SLR/CR amplitude decremental gradient*	*non differential*	*1.0 kHz 85 dB (PCX) cerebellar cortex*	*1.0, 1.85, 3.55, 6.1, 9.5 85 dB, ligh*
		light					(i)SLR/CR light only	non differential	light	1.0, 1.85, 3.55, 6.1, 9.5 85 dB, light
Svennson, 2009	ferrets	electrical stimulat	3 mA shock	Eyelid response	EMG	(i) SS suppression single PCs	(i) SS* suppression earlier in PCs (ii) PCs fire freq unchanged	non differential	FL 0.5 kHz 300 ms 1mA pulse train	FL 0.5 kHz 300 ms 2mA pulse train

		electrical stimulat	CF 0.50 kHz 10 ms (x2)	Eyelid response	EMG	(i) SS suppression single PCs	(i)SS suppression earlier in PCs	non differential	MF* 0.5 kHz 400-800 ms pulse train	MF 1.0 kHz 400-800 ms pulse train
Khilkevich, 2018	rabbit	tone	1-3 mA shock	eyelid response	infrared LED	(i)CR percentage/amplitude average	(i) CR decremental gradient (ii) CR amplitude unchanged	non differential	1.0 kHz 75 dB 500 ms	1.0 kHz 75 dB 50, 100, 150, 200, 250, 300, 350, 400, 450 ms
		electrical stimulat						non differential	MF pulse train 100 Hz 100-150 mA	MF pulse train 90, 80, 70, 60, 50 Hz 100-150 mA
		electrical stimulat						non differential	MF pulse train 100 Hz 100-150 mA	MF (competing) pulse train 100 Hz 100-150 mA

Abbreviations	
C1	1 CS (tone/light)
C2	2 CSs (reinforced tone)
T	1 CS tone
T-T	Tone-Tone
T-L	Tone-Light
F+I	Frequency + intensity
A	Ascending tone
D	Descending tone
S	Steady tone
FL	Forelimb
MCP	Middle cerebellar peduncle
MF	Mossy Fibers
PCX	Picrotoxin
TSE	Total stimulus energy
LGN	Lateral geniculate nucleus
HP	Hippocampus
CTX	Cortex

Chapter 4

Differential spatiotemporal development of Purkinje cell populations and cerebellum-dependent sensorimotor behaviors

Gerrit C. Beekhof[1,4], Catarina Osório[1,4], Joshua J. White[1], Scott van Zoomeren[1], Hannah van der Stok[1], Billian Xiong[1], Ingo H.M.S. Nettersheim[1], Willem Ashwin Mak[1], Marit Runge[1], Francesca Romana Fiocchi[1], Henk-Jan Boele[1,2], Freek E. Hoebeek[1,3], Martijn Schonewille[1]*

Affiliations:

(1) Department of Neuroscience, Erasmus MC, Rotterdam, The Netherlands

(2) Princeton Neuroscience Institute, Princeton, NJ, USA

(3) Department for Developmental Origins of Disease, University Medical Center Utrecht Brain Center and Wilhelmina Children's Hospital, Utrecht, Netherlands

(4) These authors contributed equally for the work

eLife, 2021

Abstract

Distinct populations of Purkinje cells (PCs) with unique molecular and connectivity features are at the core of the modular organization of the cerebellum. Previously, we showed that firing activity of Purkinje cells differs between ZebrinII-positive (Z+) and -negative (Z−) cerebellar modules (Wu et al., 2019; Zhou et al., 2014). Here, we investigate the timing and extent of PC differentiation during development. We found that several features of PCs, including activity levels, dendritic arborisation, axonal shape and climbing fiber input, develop differentially between nodular and anterior PC populations. Although all PCs show a particularly rapid development in the second postnatal week, anterior PCs typically have a prolonged physiological and dendritic maturation. In line herewith, younger animals exhibit attenuated anterior-dependent eyeblink conditioning, but faster nodular-dependent compensatory eye movement adaptation. Our results indicate that specific cerebellar regions have unique developmental timelines which match with their related, specific forms of cerebellum-dependent behaviors.

Introduction

The parasagittal organization of the cerebellum is fundamental to confer specificity to the coordination and adaptation of behavior. This organization is based on cerebellar modules, that is, anatomical and functional units (Apps & Hawkes, 2009; Voogd, 1964; White & Sillitoe, 2013), known to control specific tasks such as limb and finger movement (Horn et al., 2010; S. J. Martin et al., 2000), compensatory eye movements (De Zeeuw & Yeo, 2005; Graham & Wylie, 2012; Sugihara, 2004; Voogd et al., 2012), and associative motor learning (Attwell et al., 2001; Hesslow & Ivarsson, 1994; Jirenhed et al., 2007; Mostofi et al., 2010; Raymond et al., 1996). Purkinje cells (PCs) from different modules not only express different levels of molecular markers (Apps & Hawkes, 2009; Cerminara et al., 2015), but also have different physiological properties (Xiao et al., 2014; Zhou et al., 2014), project to discrete

targets in cerebellar and vestibular nuclei (Garwicz & Ekerot, 1994; Sugihara et al., 2009), receive climbing fiber (CF) input from unique subnuclei of the inferior olive (Sugihara & Shinoda, 2004, 2007; Voogd & Ruigrok, 2004), are linked to specific muscle groups (Ruigrok, 2011; Ruigrok et al., 2008) and are differentially predisposed to degeneration in neurodegenerative mouse models (Sarna & Hawkes, 2003). Although the role of PCs in cerebellar circuitry and motor behavior has been explored extensively in the adult, the mechanisms underlying early circuitry formation and its impact in early motor function have not been systematically investigated. Understanding earlier circuitry formation is crucial to deciphering the relationship between functional zones and cerebellum-dependent behavior.

PCs are general orchestrators of cerebellar circuit development (Fleming & Chiang, 2015). For example, PCs contribute to the proliferation of granule cells through the release of Sonic Hedgehog (P. M. Lewis et al., 2004), as well as the parasagittal organization of afferents (Nunes et al., 1988) and interneurons (Sillitoe et al., 2008). Concurrent to influencing this variety of developmental processes, PCs undergo their own migration, monolayer organization and growth of their large planar dendritic trees and axonal arbors. Recent evidence suggests that transient disruptions in PC development can have lasting effects and influence the development of other brain areas (Badura et al., 2018; S. S.-H. Wang et al., 2014). However, there is still a great deal unknown about the normal developmental timeline of the cerebellar principal neuron, the Purkinje cell. The timing of the PC birth is related to its ultimate placement in the cerebellar cortex, with earlier born PCs settling generally more laterally than later born PCs (M. Hashimoto & Mikoshiba, 2003; Namba et al., 2011; Sillitoe et al., 2009). Additionally, a precise reorganization from embryonic clusters of PCs into the parasagittal stripes of the mature cerebellum is indicative of a very straightforward process from embryonic origins into mature modules (Fujita et al., 2012). Ultimately, the anatomical location of a PC has a large impact on its function within the circuit, correlates with its intrinsic properties and is developmentally determined.

Here, we sought to test the hypothesis that cellular and physiological differences in subpopulations of PCs in mice are established early in postnatal development and contribute to the formation of early cerebellar sensorimotor function. *In vivo* recordings revealed that by postnatal day (P) 12 it is possible to observe ZebrinII expression-related differences in firing rate of both simple (SSs) and complex spikes (CSs), and *in vitro* recordings in ZebrinII-positive (Z+) lobule X and ZebrinII-negative (Z–) lobule III confirmed that these differences are intrinsically driven as reported in the adult mouse and rat (Xiao et al., 2014; Zhou et al., 2014). Furthermore, we show that both PC populations also differ in their timeline of dendritic (from P18) and axonal (from P14) maturation. CF translocation appears to occur earlier in the nodular regions (by P7) further suggesting differences of developmental timelines between distinct cerebellar regions. Finally, we show that young animals (P21-P25), compared to adults, display more effective adaptation of compensatory eye movements, which is controlled by Z+ modules in the vestibulocerebellum (Sanchez et al., 2002; Zhou et al., 2014). In contrast, young animals show a reduction in their learning rate during eyeblink conditioning, which is linked to anterior Z– modules (Hesslow & Ivarsson, 1994; Mostofi et al., 2010), further supporting the emerging concept of differences in circuitry maturation in distinct cerebellar regions. Overall, this study shows for the first time that PC subpopulations' developmental timelines shape unique cerebellar circuitries that underlie different maturational profiles of specific cerebellar functions.

Material and Methods

Subjects

All animals in this study were handled and kept under conditions that respected the guidelines of the Dutch Ethical Committee for animal experiments and were in accordance with the Institutional Animal Care and Use Committee of Erasmus MC (IACUC Erasmus MC), the European and the Dutch National Legislation. All animals were maintained under standard, temperature controlled, laboratory conditions. Mice were kept on a 12:12 light/dark cycle and received water and food *ad libitum*. The following transgenic mouse lines were used in this study: *Slc1a64-EGFP*(*Tg(Slc1a6-EGFP)HD185Gsat/Mmucd*) (Gong et al., 2003), *Pcp2-cre*^{ERT2}(*Tg(Pcp2-creER*^{T2}*)17.8.ICS*) (Wu et al., 2019), and *Ai14* (*B6;129S6-Gt(ROSA*)26Sor$^{tm14(CAG-tdTomato)Hze}$/J) (Madisen et al., 2010). The following primer sequences were used for routine genotyping: *Slc1a6-EGFP* (5'-TTCCTGATTGCTGGAAAGATTCTGG−3'; 5'-AGTTCAGGGAAAGGCCATACCTTGG-3'; 5'-GGATCGGCCATTGAACAAGATGG-3'; 5'-AAGTTCATCTGCACCACCG-3'; 5'-TCCTTGAAGAAGATGGTGCG-3'),*Pcp2-cre*^{ERT2}(5'-CCATGGTGATACAAGGGACATCTTCC-3'; 5'-CATGTGAAATTGTGCTGCAGGCAGG-3'; 5'-GCTATGACTGGGCACAACAGACAATC-3'; 5'-CAAGGTGAGATGACAGGAGATCCTG-3'), and *Ai14*(5'-CTGTTCCTGTACGGCATGG-3'; 5'-CCGAAAATCTGTGGGAAGTC-3'; 5'-GGCATTAAAGCAGCGTATCC-3'; 5'-AAGGGAGCTGCAGTGGAGTA-3'). Both male and female mice were used in all experiments.

***In vivo* extracellular recordings and analysis**

The *in vivo* extracellular recordings were performed in a total of 161 mice with an age range from P12 to P269. We used either *Slc1a6-EGFP* (Dehnes et al., 1998) or C57BL/6J mice to record PCs. Briefly, mice were maintained under general anesthesia with isoflurane/O_2 (4% induction and 1–5–2% maintenance) while five holes were drilled using a high-speed diamond-tipped drill (Foredome, Bethel, CT, USA, RRID:SCR_021046). To obtain electrocorticogram (ECoG) signals, five pure silver ball-tipped electrodes (custom-made from 0.125 mm diameter silver wire; Advent research materials LTD, Eynsham, Oxford, United Kingdom, RRID:SCR_021045) were placed on the meningeal layer of the dura mater. Two silver electrodes were positioned bilateral above the primary cortex (M1, 1 mm rostral; 1 mm lateral; relative to Bregma), two were placed above the primary sensory cortex (S1, 1 mm caudal; 3.5 mm lateral; relative to Bregma), and one in the interparietal bone (1 mm caudal; 1 mm lateral; relative to Lambda). UV-sensitive composites, a layer of Optibond (Kerr, Bioggio, Switzerland) and Charisma Flow (Heraeus Kulzer, Hesse, Germany), were used to fix the silver electrodes and a pedestal in the mouse head. To obtain extracellular recordings a craniotomy was made in the occipital bone and temporarily closed with Kwik-Cast sealant (World Precision Instruments Inc, Sarasota, FL, USA, RRID:SCR_008593) to prevent cooling of the brain. In the end of the surgery, mice received 0.1–0.2 ml saline for hydration and 0.2 l O2/min. ECoG and extracellular recordings were sampled at 20 kHz (setup 1: Digidata 1322A, Molecular Devices LLC., Axon instruments, Sunnyvale, CA, USA, RRID:SCR_021041), amplified, and stored for offline analysis (CyberAmp and Multiclamp 700A, Molecular Devices, RRID:SCR_021040) or at 50 kHz (setup 2: ECoG: adapted MEA60, Multichannel system, Reutlingen, Germany, RRID:SCR_021039; extracellular: Multiclamp 700B amplifier, RRID:SCR_018455, with a Digidata 1440; Molecular Devices, RRID:SCR_021038). Single-unit recordings started two hours after the termination of isoflurane application, only when the ECoG looked normal for an active mouse in an alert status. We recorded using borosilicate glass pipettes (Harvard apparatus, Holliston, MA, USA, RRIDSCR_021037) with 0.5–1.0 µm tips and a resistance of 6–12 MΩ. Glass pipettes were filled with internal solution containing (in mM): 9 KCl, 3.48 $MgCl_2$, 4 NaCl, 120 K^+-Gluconate, 10 HEPES, 28.5 Sucrose, 4 Na_2ATP, 0.4 Na_3GTP in total pH 7.25–7.35, osmolarity 290–300 mOsmol/Kg (Sigma-Aldrich, Merck KGaA, Darmstadt, Germany, RRID:SCR_008988); and 1% biocytin or 0.5% Evans Blue. At the

recording location biocytin was released with iontophoresis with 1 s pulses of 4 µA for 3 min (custom-built device, Erasmus MC, Rotterdam, The Netherlands, RRID:SCR_002737) or Evans blue was injected with pressure. This procedure was done to identify the location of the recordings. In our analysis, we included only the cells that we could identify the recording location by the use of the injection spot. For spike analysis of the PCs, only cells with a recording length of at least 90 s were included in the study (duration: 214±160 s). All *in vivo* recordings were analyzed using a MATLAB (MathWorks, Natick, MA, USA, RRID:SCR_001622) code to detect spikes using threshold and principal component analysis (Aminov et al., 2012) and a custom build MATLAB code to analyze inter spike variables. The CV is the variation in inter-spike-intervals (ISI) during firing and was calculated by dividing the standard deviation by the mean of ISIs. The CV2 represents the variance on a spike-to-spike base, it is less sensitive for a single outlier and was calculated as 2*|ISIn + 1-ISIn| / (ISIn+ 1+ ISIn). The regularity index was calculated by extracting regular spike patterns, using a CV2 threshold of <0.2 for at least three consecutive spikes (S.-L. Shin et al., 2007). Adult>P60 PCs data set localized in the flocculus used in this study has also been used in a previous study (Zhou et al., 2014).

***In vitro* extracellular recordings and analysis**

The *in vitro* extracellular recordings were performed in a total of 49 mice with an age range from P3 to P378. We used either *Slc1a6-EGFP* (Dehnes et al., 1998; Gong et al., 2003) or C57BL/6J mice to record PCs. As previously described (Wu et al., 2019), the brain was quickly removed and placed in ice-cold slice solution (continuously carbogenated with 95% O_2 and 5% CO_2) containing the following (in mM): 240 Sucrose, 2.5 KCl, 1.25 NaH_2PO_4, 2 $MgSO_4$, 1 $CaCl_2$, 26 $NaHCO_3$, 10 D-glucose. Acute sagittal slices 250 µm thick of vermal cerebellar tissue were cut in ice-cold slicing solution using a vibratome (VT1000S, Leica Biosystems, Wetzlar, Germany, RRID:SCR_016495) with a ceramic blade (Campden Instruments Ltd, Manchester, United Kingdom, RRID:SCR_021036). Directly after slicing, the slices were transferred to a recovery bath and were incubated in oxygenated artificial cerebrospinal fluid (ACSF) and maintained at 34°C for one hour. The ACSF was continuously carbogenated with 95% O_2 and 5% CO_2 and consisted of (in mM): 124 NaCl, 5 KCl, 1.25 Na_2HPO_4, 2 $MgSO_4$, 2 $CaCl_2$, 26 $NaHCO_3$, 20 D-glucose. After incubation period, slices were transferred to room temperature. To record the individual slices, these were transferred to a recording chamber and maintained at 34 ± 1°C with a feedback temperature controller with heater (Scientifica, Uckfield, United Kingdom, RRID:SCR_021035) under continuous superfusion with the oxygenated ACSF.

For all the recordings, slices were bathed with ACSF supplemented with synaptic receptor blockers, NMDA receptor antagonist D-AP5 (50 µM, Hello Bio Ltd, Bristol, United Kingdom, RRID:SCR_021047), selective and competitive AMPA receptor antagonist NBQX (10 µM, Hello Bio Ltd, Bristol, United Kingdom, RRID:SCR_021047), non-competitive $GABA_A$ receptor antagonist and glycine receptor inhibitor Picrotoxin (100 µM, Hello Bio Ltd, Bristol, United Kingdom, RRID:SCR_021047). PCs were visualized with SliceScope Pro 3000, a CCD camera, a trinocular eyepiece (Scientifica, Uckfield, United Kingdom, RRID:SCR_021035) and ocular (Teledyne Qimaging, Surrey, Canada). Whole-cell and cell attached recordings were obtained using borosilicate pipettes (Harvard apparatus, Holliston, MA, USA RRIDSCR_021037) with a resistance of 4–6 MΩ, filled with internal solution containing (in mM): 9 KCl, 3.48 $MgCl_2$, 4 NaCl, 120 K^+-Gluconate, 10 HEPES, 28.5 Sucrose, 4 Na_2ATP, 0.4 Na_3GTP in total pH 7.25–7.35, osmolarity 290–300 mOsmol/Kg (Sigma-Aldrich, Merck KGaA, Darmstadt, Germany, RRID:SCR_008988). Cell-attached recordings were made with a seal of 30 MΩ to 2 GΩ and lasted for a minimum of 90 s up to 150 s. Recording pipettes were supplemented with 1 mg/ml biocytin to allow histological staining to identify PCs location. Cell-attached recordings were performed using an ECP-

10 amplifier (HEKA Electronics, Lambrecht, Germany, RRID:SCR_018399) and digitized at 20 kHz. Acquisition was done in Patchmaster (HEKA Electronics, Lambrecht, Germany, RRID:SCR000034) and ABF Utility (Synaptosoft, Fort Lee, NJ, USA, RRID:SCR_019222) was used to convert the Patchmaster files for analysis. Clampfit 10 (Molecular Devices, LLC, San Jose, USA, RRID:SCR_011323) was used to analyze spikes (Aminov et al., 2012) and a custom-build MATLAB code (MathWorks, Natick, MA, USA, RRID:SCR_001622) using inter spike properties was used to analyze spike variables (Shin et al., 2007).

Immunohistochemistry

For immunohistochemistry, mice were deeply anesthetized with sodium pentobarbital, perfused transcardially with sodium chloride solution (Baxter International Inc, Deerfield, IL, USA, #TKF7124, RRID:SCR_003974) followed by 4% paraformaldehyde (PFA) in 0.1M phosphate buffer (PB). The dissected brains were then post-fixed in 4% PFA for 2 hr at 4°C and then cryoprotected in 10% sucrose/0.1M PB (Sigma-Aldrich, #S-0389, RRID:SCR_008988) overnight at 4°C. Next day, the brains were embedded in 14% gelatin/30% sucrose/0.1M PB solution (gelatin: FujiFilm Wako Pure Chemical Corporation, Osaka, Japan, #077–03155, RRID:SCR_021034), fixed for 2 hr at room temperature and incubated overnight in 30% sucrose/0.1M PB solution.

For the *in vivo* electrophysiology, the injection spot was identified by the presence of biocytin or Evans blue. Briefly, brains were sectioned 40–100 µm thick in a coronal plane with a freezing microtome. Free-floating sections were rinsed with 0.1M PB and blocked for 2 hr in a solution of 0.5% Triton X-100/10% normal horse serum/0.1M PB at room temperature. With the exception of *Slc1a6-EGFP*-positive sections, all sections were incubated 4 days at 4°C in a solution of 0.5% Triton X-100/2% normal horse serum/0.1M PB with primary antibody against Aldolase C (1:1000, goat polyclonal, Santa Cruz Biotechnology, Dallas, TX, USA RRID:AB_2242641). After rinsing the sections with 0.1M PB, sections were incubated 2 hr at room temperature in a solution of 0.5% Triton X-100/2% normal horse serum/0.1M PB with secondary antibody Alexa Fluor 488-AffiniPure Donkey anti-goat (1:500, Jackson Immuno Research Labs, West Grove, PA, USA, RRID:AB_2340428) and Cy3-streptavidin (1:1000, Jackson Immuno Research Labs, RRID:AB_2337244). Finally, brain slices were incubated for 10 min with DAPI (Thermo Fisher Scientific, Waltham, MA, USA, RRID:AB_2629482) in 0.1M PB, rinsed with PB, mounted in slides in chrome alum (gelatin/chromate) and mounted with Mowiol (Polysciences Inc, Warrington, PA, USA, #17951).

To label recorded PCs, free-floating sagittal brain slices 250 µm thick obtained from *in vitro* electrophysiology recordings were fixed in 4% PFA/0.1M PB overnight at 4°C. Next, slices were permeabilized with 0.5% Triton X-100 in PB overnight at 4°C. The following day, brain slices were incubated with Cy3 Streptavidin for 1 hr at room temperature. Finally, brain slices were incubated for 10 min with DAPI in PB, rinsed with PB, mounted in slides in chrome alum (gelatin/chromate) and mounted with Mowiol.

Free-floating sagittal brain slices from P7, P14, P21, P35, and P60 C57BL/6J mice were permeabilized with 0.5% Triton X-100 in 0.1M PB for 1 hr at room temperature and blocked for 2 hr in a solution of 0.5% Triton X-100/10% normal horse serum/0.1M PB at room temperature. After, sections were incubated overnight at 4°C in a solution of 0.5% Triton X-100/2% normal horse serum/0.1M PB with primary antibody against Calbindin D-28k (1:10000, Swant, Marly, Switzerland, RRID:AB_2314070) and VGluT2 (1:2000, Millipore, RRID:SCR_008983). Next day, sections were rinsed in 0.1M PB and incubated at room temperature for 2 hr in a solution of 0.5% Triton X-100/2% normal horse serum/0.1M PB with secondary antibodies: Cy3-AffiniPure Donkey anti-Mouse (1:1000, Jackson Immuno Research Labs, RRID:AB_2340813) and Alexa Fluor 488-AffiniPure Donkey anti-Guinea Pig

(1:1000, Jackson Immuno Research Labs, RRID:AB_2340472). Finally, brain slices were incubated for 10 min with DAPI in 0.1M PB, rinsed with PB, mounted in slides in chrome alum (gelatin/chromate) and mounted with Mowiol.

To label axonal projections from *Pcp2-cre^{ERT2}; Ai14* mice brains were sectioned 150 µm thick in a coronal plane with a freezing microtome. Free-floating sections were rinsed with 0.1M PB and blocked for 2 hr in a solution of 0.5% Triton X-100/10% normal horse serum/0.1M PB at room temperature. Sections were then incubated overnight at 4°C in a solution of 0.5% Triton X-100/2% normal horse serum/0.1M PB with primary antibodies against Aldolase C (1:1000, goat polyclonal) and RFP (1:1000, Rockland). After rinsing the sections with 0.1M PB, sections were incubated 2 hr at room temperature in a solution of 0.5% Triton X-100/2% normal horse serum/0.1M PB with secondary antibodies Alexa Fluor 488-AffiniPure Donkey anti-goat (1:500, Jackson Immuno Research Labs, RRID:AB_2616594) and Cy3 AffiniPure Donkey anti-rabbit (1:500, Jackson Immuno Research Labs, RRID:AB_2307443). Finally, brain slices were incubated for 10 min with DAPI in 0.1M PB, rinsed with PB, mounted in slides in chrome alum (gelatin/chromate) and mounted with Mowiol.

Image acquisition and morphological analysis

Images were acquired at 8-bit depth and 1024 × 1024 pixel resolution with Axio Imager.M2 (Carl Zeiss Microscopy, LLC, USA, RRID:SCR_011876), LSM 700 (Carl Zeiss Microscopy, LLC, USA, RRID:SCR_017377) or a SP5/SP8 (Leica Microsystems, Wetzlar, Germany, SP5 RRID:SCR_020233, SP8 RRID:SCR_018169) confocal laser scanning microscope. For each experiment, images were acquired using the same laser power and detection filter settings.

To localize the injection site from *in vivo* recordings, wide-field fluorescent tile scan images were acquired with a 10X objective, 20% overlap and online-stitched. Only recorded neurons with an injection spot small enough to locate the cell to a lobule and its ZebrinII identity were analyzed, other PCs were discarded.

To image individual PCs, images were acquired with 10X/0.3 or 20X/0.8 objectives according with the cell size and with a z-interval of 1 µm. To quantify the dendritic arborization of biocytin-filled PC, the maximum projection of z-stack images of single cells were analyzed with the sholl analysis macro implemented in FIJI (ImageJ, RRID:SCR_002285) software. To quantify the area of a PC, the maximum projection of each image was thresholded in FIJI to fit the area of the cell and measured. Tile scan images of PCs and CFs from different lobules of the cerebellum were acquired with a 40X/1.3 (Magnification/Numerical Aperture) oil objective with a z-interval of 0.8 µm. For each age group, four sections were imaged (10 images per section) for each brain (three brains per age). For all the following quantifications, the maximum projection of the z-stack was used. Analysis of the VGluT2 synaptic puncta was performed in sagittal sections in regions of lobules I, II, III, IX, and X. Analysis of synapse densities was performed using the 'Analyze Particles' tool in FIJI software to quantify the number of VGluT2 puncta in a region of interest (ROI) and this number was then divided by the area (μm^2) of the ROI in the cerebellar cortex. The heights of ML and CFs were measured using three measurements per image. The ML height was measured as the distance from the edge of the PC soma to the apical edge of the ML and the CF height was measured as the distance from the from the edge of the PC soma to the apical edge of the last VGluT2 puncta. The CF extension was quantified as the ratio of the mean of CF height per the mean of ML height per image. Measurements for each mouse were averaged and the numbers computed from each group were pooled and averaged again to obtain the mean of all the measurements made. These analyses were done P7, P14, P21, P35, and P60 C57BL/6J mice and presented as percentages. Images of PC axon terminal arbors in the cerebellar

nuclei were acquired with a 20x objective with a z-interval of 1 µm. For each age group, sections were imaged for each brain (at least three brains per age). Isolated axon arbors were imaged and analyzed with the sholl analysis macro implemented in FIJI software. To quantify the area of a PC, the maximum projection of each image was thresholded in FIJI to fit the area of the cell and measured.

Compensatory eye movement recordings

Young (P21 on the first day of training) and adult (10–11 weeks old) C57BL/6J mice were used to perform compensatory eye movement recordings, which were described in detail previously (Schonewille et al., 2010). Briefly, to head restrain mice during the eye movement recordings a metal construct, *pedestal*, was placed on their skull under general anesthesia with isoflurane/O_2. After 3 days of recovery from the surgery, mice were head-fixed and placed in a mouse holder in the center of a turntable (diameter: 60 cm), surrounded by a cylindrical screen (diameter 63 cm) with a random-dotted pattern (*drum*). Compensatory eye movements [optokinetic reflex (OKR), visual vestibular ocular reflex in the light (VVOR) and dark (VOR)] were induced using a sinusoidal rotation of the drum in light (OKR), rotation of the table in the dark (VOR) or the rotation of the table in the light (VVOR) with an amplitude of 5° at 0.1–1 Hz. Motor performance in response to these stimulations was evaluated by calculating the gain (fitted eye velocity/fitted stimulus velocity) and phase (eye to stimulus difference in degrees) of the response.

To study motor learning, mice were subjected to a mismatch between visual and vestibular input to adapt the VOR. The VOR phase-reversal test was done during a period of 5 days, consisting of six 5-min training sessions every day with VOR recordings before, between, and after the training sessions. Between recording sessions, mice were kept in the dark to avoid unlearning of the adapted responses.

The first training day, in-phase stimulation of the visual (the drum) and vestibular stimuli (turntable) rotated in phase at 0.6 Hz and both with an amplitude of 5°, inducing a decrease of gain. In the following days, the drum amplitude was increased to 7.5° (day 2) and 10° (days 3, 4, and 5), while the amplitude of the turntable remained at 5°. This resulted in the reversal of the VOR direction, an inversion of the compensatory eye movement driven by vestibular input, moving the eye in the same direction as the head rotation instead of the normal compensatory opposite direction.

A CCD camera was fixed to the turntable in order to monitor the eyes of the mice. Eye movements were recorded with eye-tracking software (ETL-200, ISCAN systems, Burlington, NA, USA, RRID:SCR_021044). Eyes were illuminated during the experiments using two table-fixed infrared emitters (output 600 mW, dispersion angle 7°, peak wavelength 880 nm) and a third emitter, which produced the tracked corneal reflection, was mounted to the camera and aligned horizontally with the optical axis of the camera. Eye movements were calibrated by moving the camera left-right (peak-to-peak 20°) during periods that the eye did not move (Stahl, 2004). Gain and phase values of eye movements were calculated using custom-made MATLAB scripts, available at GitHub (GitHub, San Francisco, CA, USA, https://github.com/MSchonewille/iMove; copy archived at swh:1:rev:e0dda8be37519e58387c2b9702479625e66b54ec; Beekhof, 2021; Schonewille et al., 2010). Consolidation is the percentage of adaptive change that was still present after 23 hr in the dark and was calculated as 100%*(dxt0-dx+1 t0)/(dxt0-dxt30), with dxt0 as the value before training on the first day, dx+ 1t0 as the value before training on the next day and dxt30 as the last, final value on the first day.

Eyeblink conditioning

Young (P21, on the first day of training) and adult (10–11 weeks old) C57BL/6J mice were used to perform EBC behavioral tests as done previously (H. J. Boele et al., 2018). Briefly, a metal pedestal was placed on the mice skull under general anesthesia with isoflurane/O_2 in order to allow for head fixation during the EBC experiments. After 3 days of recovery, mice were head-fixed and placed on top of a foam cylindrical treadmill on which they were allowed to walk freely. Mice were habituated for 2 days (30 min per day) before beginning the conditioning sessions in a sound- and light-isolating chamber which houses the eye-blink set-up. No stimuli was delivered during habituation.

Eyelid movements were monitored under infrared illumination using a high-speed (3333 frames/s) monochrome video camera. To calculate the fraction of eyelid closure (FEC), a region of interest (ROI) was selected around the eye when this was fully open (including the pupil, iris and immediate surrounding fur). The grayscale values of the pixels in the ROI were converted to binary in such way that the pupil and iris had a value of 0 and the fur a value of 1. All pixels in the ROI were summed to calculate the area of fur in all frames. In the end, the raw pixels were normalized into FEC units (from 0 – fully open eye, to 1 – fully closed eye [Heiney et al., 2014]). After the habituation session the EBC test lasted 5 days. Each day there were two sessions, one in the morning and one in the afternoon spanned 6 hr. All experiments were performed at approximately the same time of day by the same experimenter. On the day of acquisition session 1, each animal first received 20 conditioned stimulus-only trials as a baseline measure, to establish that the conditioned stimulus did not elicit any reflexive eyelid closure. During each session, every animal received in total 200 paired conditioned stimulus-unconditioned stimulus trials, 20 unconditioned stimulus only trials, and 20 conditioned stimulus only trials. These trials were presented over 20 blocks, each block consisted of 1 unconditioned stimulus only trial, 10 paired conditioned stimulus-unconditioned stimulus trials, and 1 conditioned stimulus only trial. The interval between the onset of the conditioned stimulus and that of the unconditioned stimulus was set at 250 msec. The conditioned stimulus was a green LED light (conditioned stimulus duration 280 msec, LED diameter 5 mm) placed 10 cm in front of the mouse's head. The unconditioned stimulus was a weak air-puff applied to the eye (30 psi, 30 msec duration), which was controlled by a pressure injector and delivered via a needle perpendicularly positioned at 5 mm from the center of the left cornea.

Individual eyeblink traces were analyzed with a custom written script in MATLAB R2018a. Trials with significant activity in the 500 msec pre-conditioned stimulus period were regarded as invalid for further analysis. Valid trials were further normalized by aligning the 500 msec pre-conditioned stimulus baselines and calibrating the signal so that the size of a full blink was 1. In valid normalized trials, all eyelid movements larger than 0.05 and with a latency to CR onset between 50 and 250 msec, a latency to CR peak of 100–250 msec (relative to conditioned stimulus onset) and a positive slope in the 150 msec before unconditioned stimulus time were considered as conditioned responses (CRs).

Statistical analysis

Error bars in all graphs indicate mean ± SEM. For each experiment, the sample size and statistical tests used are summarized in Table Supplementary 1. Data was tested for normality with Shapiro–Wilk tests and for equal variances using the *F*-test. For normal distributed data, statistical significance was determined by the two-way ANOVA with multiple comparisons or mixed-effects test with repeated measures. If the data was not normally distributed, statistical significance was calculated using the Kruskal–Wallis test with multiple comparisons. The minimum level of significance accepted for all tests

was p<0.05. Statistical analyses were performed using GraphPad Prism (GraphPad Software, San Diego, CA, USA, RRID:SCR_002798).

Results

Developing Purkinje cells operate at different rates depending on their cerebellar location

Following our previous work (Zhou et al., 2014), we investigated when the differences between Z– and Z+ PC activity emerge during development. We first performed extracellular recordings *in vivo* in PCs of *Slc1a6-EGFP* or C57BL/6J awake mice (Figure 1A$_1$). *Slc1a6-EGFP* mice express enhanced green fluorescent protein (EGFP) under the *Slc1a6* promotor, an expression pattern that correlates with high levels of ZebrinII (aldolase C) (Gincel et al., 2007, p. 200; Gong et al., 2003). PCs were identified during the recording by the presence of SSs and CSs, while the consistent presence of a pause in SS following each CS (i.e. climbing fiber pause [CF pause]) confirmed that the recording was obtained from a single unit (De Zeeuw et al., 2011; Figure 1A$_2$-Figure 1—Figure Supplementary 1A$_1$). Additionally, it was confirmed that CSs cause a pause in SS activity as the interval between CSs and the following SS was longer than the interval between two SSs in virtually all recorded cells (Figure 1— Figure Supplementary 2A).

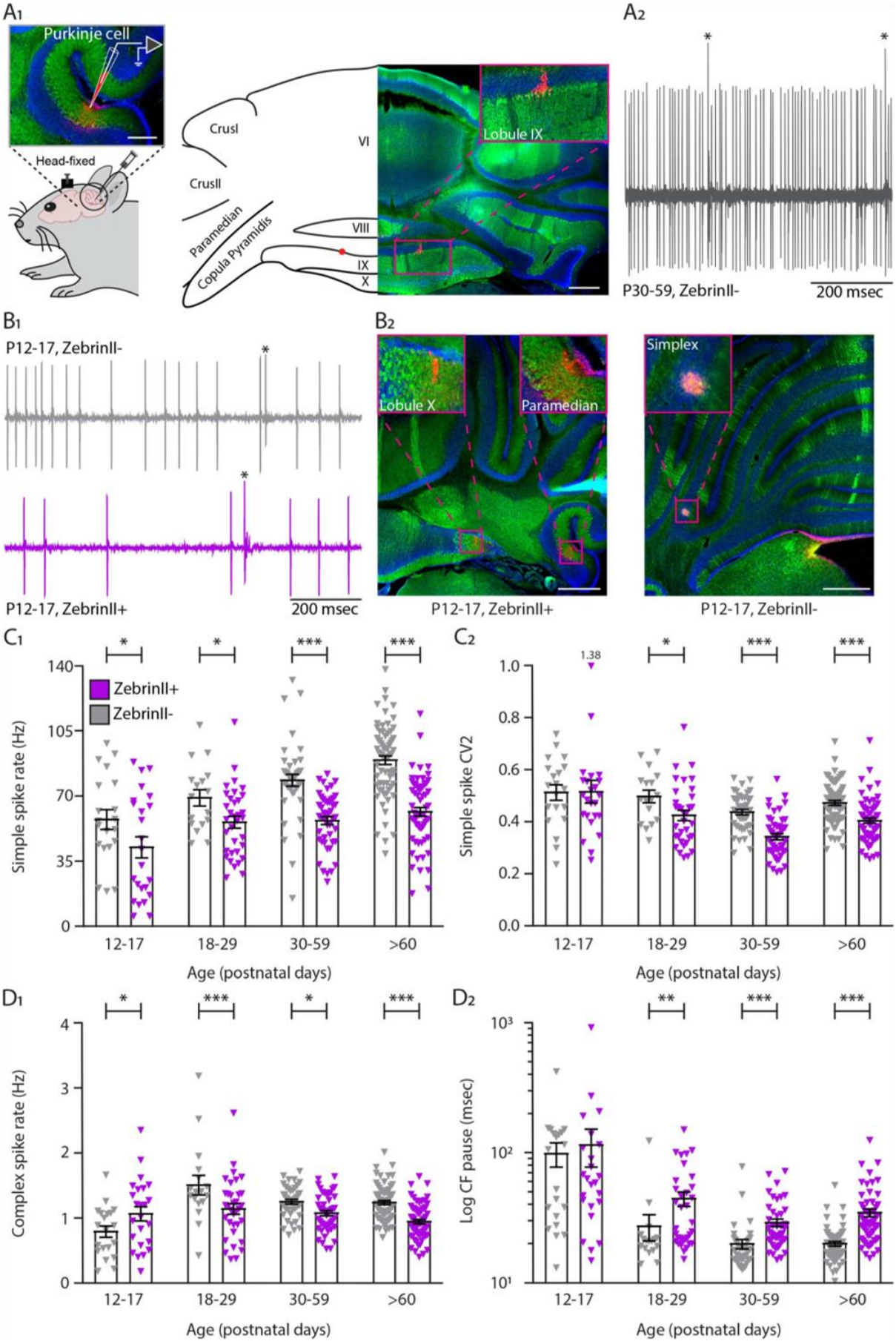
A1
Purkinje cell
Head-fixed
CrusI
CrusII
Paramedian
Copula Pyramidis
VI
VIII
IX
X
Lobule IX
A2
P30-59, ZebrinII-
200 msec
B1
P12-17, ZebrinII-
P12-17, ZebrinII+
200 msec
B2
Lobule X
Paramedian
Simplex
P12-17, ZebrinII+
P12-17, ZebrinII-
C1
ZebrinII+
ZebrinII-
Simple spike rate (Hz)
Age (postnatal days)
12-17
18-29
30-59
>60
C2
Simple spike CV2
1.38
D1
Complex spike rate (Hz)
D2
Log CF pause (msec)

Figure 1. Simple and complex spike activity develops differently between ZebrinII-related PC populations.
(**A_1**) Schematic illustration of single unit cerebellar extracellular recordings in PCs of awake head fixed mice (left). Schematic representation of a cerebellar coronal section and respective image showing lobules VI, VIII, IX and X, Crus I, Crus II, Paramedian and Copula Pyramidis. Cerebellar coronal section with PCs labelled with Aldolase C (green). Inset showing recording site marked with biocytin (red) in lobule IX (right). (**A_2**) Example trace of *in vivo* P30-59 Z− PC recording identified by its hallmark feature, the occurrence of complex spikes (asterisks) and simple spikes. (**B_1**) Example traces of Z− and Z+ PCs extracellular recordings at P12-17 with clearly distinguishable simple spikes and complex spikes (asterisks). (**B_2**) Photomicrographs of coronal sections with examples of Z+ (left) and Z– (right) P12-17 PCs in lobule X, Paramedian and Simplex, respectively. PCs are labelled with Aldolase C (green). Insets showing recording sites marked with biocytin (red) in lobule X, Paramedian (left) and Simplex (right). (**C_1**) PC simple spike firing rate, (**C_2**) coefficient of variation 2 for simple spikes, (**D_1**) complex spike firing rate and (**D_2**) CF pause recorded *in vivo* for Z– PCs (grey) and Z+ PCs (purple) in 4 age groups. Age groups: P12-17, P18-29, P30-59 and >P60. Error bars represent SEM., for values see Table Supplementary 1. * denotes $p<0.05$, ** $p<0.001$ and *** $p<0.0001$. Scale bars = (**A_1**) 100 µm (left), 500 µm (right), and (**B_2**) 500 µm.

PC recording locations were determined with biocytin or Evans blue, and their ZebrinII identity was determined histologically (Figure $1B_2$ -Figure 1— Figure Supplementary $1A_2$). Immunohistochemical and electrophysiological data were divided in four different age groups: an early postnatal group of P12-P17, a juvenile group from P18 to P29, an adolescent group from P30 to P59, and an adult group from P60. We observed that SS firing rate is significantly higher in Z− PCs when compared with the Z+ PCs in all age groups, starting from early postnatal ages (P12-P17, Z−: 57.3±5.3 Hz, Z+: 42.3 ± 5.7 Hz, $p=0.013$, see Table Supplementary 1 for additional age groups). Moreover, Z– PCs significantly increase their firing rate progressively from P12 until reaching their mature rate (P12-P17, Z– vs.>P60 Z–:$p<0.0001$) while Z+ PCs firing rate remained low and plateaued at P18, which is not significantly different from the rate at the mature stage (P18-P29 Z+ vs. Z+:>P60 Z+:$p=0.185$) (Figure $1B_1$,C_1, Figure 1— Figure Supplementary $1A_3$, Table Supplementary 1 for additional age groups). Although there is no difference in SS regularity, measured as coefficient of variation 2 (CV2), in the young P12-P17 group (CV2, Z–: 0.51±0.03, Z+: 0.51±0.04, $p=0.94$), there is a significant difference between Z– and Z+ PC regularity in the older groups. From P18 onwards, Z– PCs are more irregular than Z+ PCs (>P60, Z–: 0.47±0.01, Z+: 0.40±0.01, $p<0.001$) (Figure $1C_2$). Differences in the coefficient of variance (CV) between Z– and Z+ were only observed in the adult group (>P60, $p<0.0001$). Additionally, CV decreases from early postnatal onward in both groups (Table Supplementary 1); as PCs become mature the variation in inter-spike-intervals (ISI) is reduced compared to young PCs (Figure 1— Figure Supplementary $1B_1$). The gradual shift to more regular activity was confirmed by a decreasing regularity index of SSs as the age increases for both groups, with only a significant higher level in Z+ PCs at P30-P59 ($p=0.011$, Figure 1— Figure Supplementary $1B_2$, Table Supplementary 1).

Although recordings were grouped based on ZebrinII expression, the observed developmental timeline could potentially also correlate with other factors. To examine this, we further subdivided recordings based on lobular identity. In adult mice, PCs in anterior, largely Z–, lobules I to III have higher SS firing rates than those in the nodular, largely Z+, lobules IX and X (Figure 1 = Figure Supplementary $3A_1$. Table Supplementary 1). For PCs recorded at P30-59 the pattern is similar, suggesting that in the latter stages of development, PC SS activity is also coupled to ZebrinII identity (Figure 1 – Figure Supplementary $3A_2$, Table Supplementary 1). For the P18-P29 and P12-P17 groups the sample sizes are insufficient to draw strong conclusions (Figure 1— Figure Supplementary $3A_{3–4}$). Hence, we employed a second approach, comparing the development of SS activity in two Z– regions, anterior lobules I to V vs. Z– hemisphere, and two Z+ regions, nodulus vs. flocculus regions. Although the number of samples prohibits strong conclusions, the developmental pattern of SS firing rate in the

anterior and hemispheric region appears largely comparable, with significant increases toward adult levels, also after P12-P17 (Figure 1— Figure Supplementary 3 B1). The development of activity is similar between the nodulus and flocculus as well, and best described by a stepwise increase from P12-P17 to P18-P29, after which the levels remain stable (Figure 1— Figure Supplementary 3 B2). Thus, sample sizes hamper strong conclusions, as it is technically challenging to record PC activity *in vivo* without anesthesia, in for example P12-P17 mice. Finally, because some of the data set appear to be bimodal in this youngest group, we examined if at P12-P17 specifically there was any association between the PCs locations and their electrophysiological properties. Therefore, we mapped the location of P12-P17 PCs in the cerebellar cortex and their correspondent SS rate (Figure 1— Figure Supplementary 4A), CS rate (Figure 1— Figure Supplementary 4B), SS CV2 (Figure 1— Figure Supplementary 5A), and SS CV values (Figure 1— Figure Supplementary 5B). We find no evidence for bimodal distributions of data based on location of PCs.

Taken together, these results are in line with previous analyses in which we and others demonstrated the presence of differences across lobules in adult mice (Chopra et al., 2020; Xiao et al., 2014; Zhou et al., 2014). Our results suggest that differences in SS firing rate between Z– and Z+ PCs arise during development as early as P12 and the CS firing rate and CF pause settle at adult levels after the period of synapse elimination at P18. Overall, the firing rate of ZebrinII-identified PC populations differentiates from early postnatal ages, and reached a stable, adult level in Z+ PCs first.

Developing PCs of distinct cerebellar regions have different intrinsic activity

PCs are intrinsically active in the absence of excitatory and inhibitory synaptic inputs (De Zeeuw et al., 2011; Raman & Bean, 1999; Womack & Khodakhah, 2002). In our previous work, we found that the difference in PC SS firing rate recorded *in vivo* was primarily the result of intrinsic activity of PCs in the adult mouse (Zhou et al., 2014). Next, we asked what is the contribution of intrinsic activity to the activity of developing PCs and when during development the differences in intrinsic activity arise among different populations of PCs. To answer these questions, we performed *in vitro* electrophysiological recordings on sagittal cerebellar sections of P3 to adult mice to measure the intrinsic properties of PCs throughout cerebellar development (Figure 2- Figure Supplementary 1A).

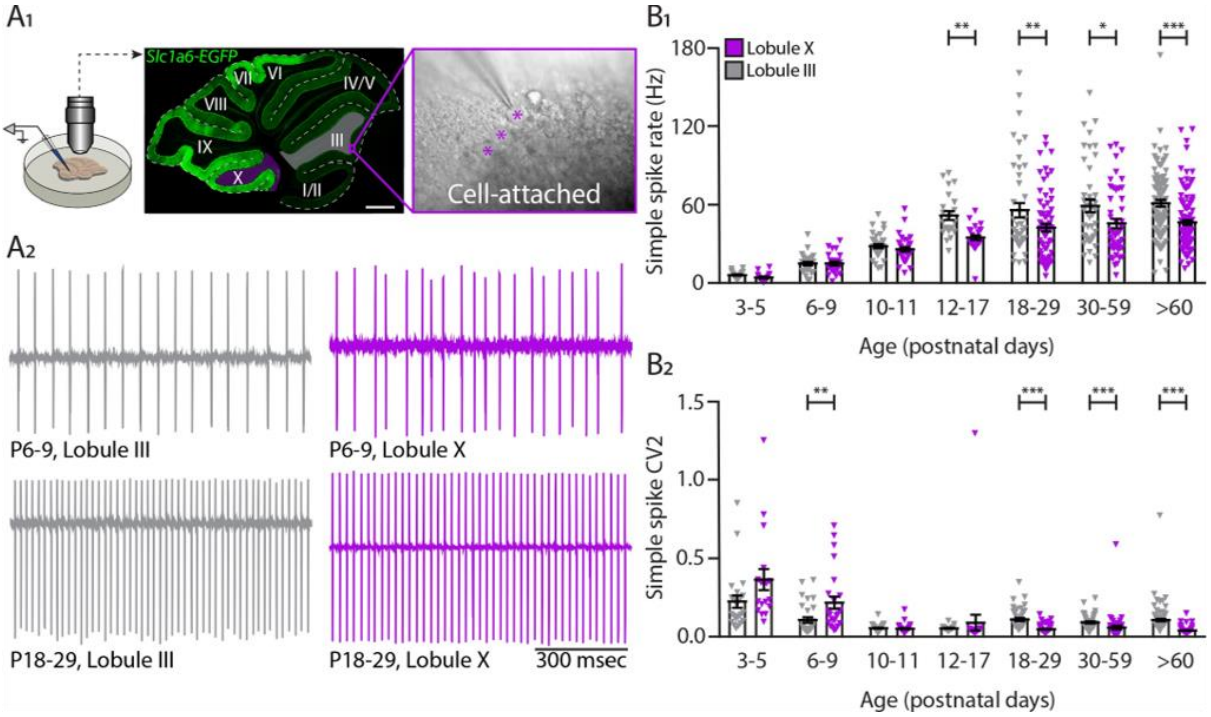

Figure 2. Intrinsic activity develops differently between lobule III and lobule X PC populations. (**A_1**) Cell-attached recordings *in vitro* in *EAAT4-eGFP* mice that express eGFP in PCs. Recordings of intrinsic PC activity were made in lobules III and X. PCs were identified by the size of the soma (asterisk) clearly visible in the PC layer. (**A_2**) Example traces of cell-attached recordings of lobule III and X PCs at P6-9 and P18-29. (**B_1**) PC intrinsic simple spike rate and (**B_2**) coefficient of variation 2 (CV2, see methods) recorded *in vitro* for lobule III PCs (grey) and lobule X PCs (purple) in 7 age groups. Age groups: P3-5, P6-9, P10-11, P12-17, P18-29, P30-59 and >P60. Error bars represent SEM., for values see Table Supplementary 1. * denotes p<0.05, ** p<0.001 and *** p<0.0001. Scale bar = (**A_1**) 500 µm.

Because ZebrinII parasagittal patterning is only complete around P12-P15 (Brochu et al., 1990; Lannoo et al., 1991) and ZebrinII labeling is ambiguous before P12, we focus our *in vitro* studies on lobules III and X (Brochu et al., 1990; Sugihara & Quy, 2007; Zhou et al., 2014; Figure 2A_1), which can be readily identified in the cerebellum at all ages, are oriented in such a way that it is possible to record from them in a single sagittal slice and have previously been demonstrated to be representative of the Z– and Z+ PC populations (Wu et al., 2019; Zhou et al., 2014). To remove the impact of synaptic inputs to PCs, we used blockers for NMDA, AMPA, $GABA_A$ and glycine receptors during the cell-attached recordings. For this experiment, we analyzed seven different age groups: P3-P5, P6-P9, P10-P11, P12-P17, P18-P29, P30-P59 and an adult group>P60. PC firing rate significantly increases from P3-P5 to P10-P11 (LIII p=0.0002; LX p=0.0007), but over these first days of development there were no differences in the firing rate between PCs of different cerebellar regions (Figure 2A_2,B_1-Figure 2— Figure Supplementary 2B, Table Supplementary 1). Starting from P12 to P17, similar to the *in vivo* data, we observed that the intrinsic activity of PCs located in lobule X is significantly different from those located in lobule III (LIII: 51.7±3.4 Hz; LX: 34.8±2.0 Hz, p=0.008, Figure 2B_1). After this key point during development, the differences in intrinsic firing rate in PCs from both cerebellar regions are maintained into adulthood (>P60, LIII: 61.2±2.5 Hz; LX: 46.3±1.9 Hz, p<0.0001). In contrast to the results *in vivo*, SS rate *in vitro* are both only significantly different from adult rates until P12-P17. However, the strongest increase in rate occurs later in lobule III PCs (P10-P11 to P12-P17:+23.5 Hz) than in those in lobule X (P6-P9 to P10-11:+11.1 Hz) (Table Supplementary 1). In line with the *in vivo* results (Figure 1B_2), there is a significant increase in irregularity in lobule III PCs from P18 when compared with lobule X PCs (CV2, LIII: 0.11±0.01; LX: 0.05±0.00, p<0.0001) and this is maintained into adulthood (>P60, CV2, LIII: 0.11±0.01; LX: 0.04±0.00, p<0.0001) (Figure 2B_2). These differences in CV2 are confirmed by lower CV and higher regularity index levels for lobule X PCs when compared with lobule III PCs from P18 to P29 onwards (P18-P29 CV, LIII: 0.14±0.01; LX: 0.10±0.01,p<0.007; P18-P29 regularity index, LIII: 0.016±0.002; LX: 0.060±0.004, p<0.0001) (Figure 2— Figure Supplementary 1$C_{1–2}$). Young PCs at P6-P9 exhibit a significantly higher CV and higher regularity index in lobule III PCs when compared with lobule X PCs, suggesting the potential presence of subtler differences in early development (Figure 2— Figure Supplementary 1$C_{1–2}$). All together, these data indicate that differences in SS firing rate at least in lobules III and X are indeed the result of differences of intrinsic activity of distinct PC subpopulations starting at P12-P17 and maintained into mature ages.

However, one cannot exclude the role of extrinsic input in PC SS rates. As observed in Figure 2—figure supplement 2, in both lobule III/Z– and lobule X/Z+ PCs, the firing rate *in vivo* was significantly higher than the firing rate *in vitro* (Figure 2— Figure Supplementary 2A_1). This difference is evident from P18-P29 onwards. However, there was a higher input component in the lobule III/Z– when compared with lobule X/Z+ PCs (Figure 2— Figure Supplementary 2A_2) contributing to the regional difference between the two subtypes of PCs.

Dendrite complexity is more pronounced in PCs in the anterior lobule III

Neuronal morphology is a key determinant of the functional properties of neurons. Several studies have shown that different cell types show a causal relationship between firing patterns and neuronal morphology such as dendritic structure (Mainen & Sejnowski, 1996; Vetter et al., 2001), dendritic size (Gollo et al., 2013), and branching points (Ferrante et al., 2013). Hence, we hypothesized that differences in activity between different cerebellar regions could suggest differences in PC morphology. To investigate this possibility, we analyzed dendritic arborization complexity in different PC subpopulations of adult mice and during development. PCs from lobules I/II/III and IX/X were filled with biocytin and stained with Cy3-streptavidin. We then performed sholl analysis (Ferreira et al., 2014) to quantify PC dendritic arbor complexity, maximum length from the cell soma and cell area. Concomitantly with the physiology data, we observed that from P6-P11 to P12-17 there is a rapid increase in dendritic complexity and area (Figure 3A) across all PCs. However, unlike in the physiological data there is no significant difference in dendritic complexity (P12-P17, LI-III: 336.1±31.7; LIX-X: 291.2±17.1, p=0.38, Figure 3B_1), maximum length (P12-P17, LI-III: 138.3±5.1 µm; LIX-X: 142.5±3.9 µm, p=0.74, Figure 3B_2), and area (P12-P17, LI-III: 5419±399 µm^2; LI-X: 6109±462 µm^2,p=0.46, Figure 3B_3) between PCs in anterior (lobules I/II/III) and nodular (lobules IX/X) regions at P12-P17. While dendritic arborization in lobules IX-X marginally changed after this time point, dendritic complexity significantly increased in lobules I-III from the third postnatal week (from P18) into adulthood: dendritic complexity (P60, LI-III: 663.1±23.8; LIX-X: 445.7±22.2, p<0.0001, Figure 3B_1), maximum length (P60, LI-III: 206.6±5.9 µm; LIX-X: 169.9±4.0 µm, p<0.0001, Figure 3B_2), and area (P60, LI-III: 10890±412 µm^2; LIX-X: 8520±377 µm^2, p<0.0001, Figure 3B_3). A difference in size and complexity in dendritic arborization of PC subpopulations can therefore be first observed at P18 (see Table Supplementary 1).

Because PC morphology can vary depending on their location in the same lobule during development (Nedelescu et al., 2018; Nedelescu & Abdelhack, 2013; Sudarov & Joyner, 2007), we investigated the location of each PC analyzed per age in the apex, base and sulcus of each lobule (Figure 3— Figure Supplementary 1A). There was not systematic bias in our sampling from apex, base or sulcus (Figure 3— Figure Supplementary 1B_1) at different developmental ages and between anterior and nodular lobules (Figure 3— Figure Supplementary 1B_2). Additionally, most of the cells collected for this analysis were located in lobule III and X (Figure 3— Figure Supplementary 1$C_{1–2}$) at different developmental ages.

Our data show that indeed the rapid period of maturation for PCs occurs between P9 to P12. The slow period of dendritic expansion however differs between PC populations. PCs located predominantly in lobule III grow larger and have more complex dendritic trees compared to PCs located predominantly in lobule X. These data also suggest that, in line with their firing rates, PCs in lobule X reach their dendritic maturity earlier than PCs from lobule III.

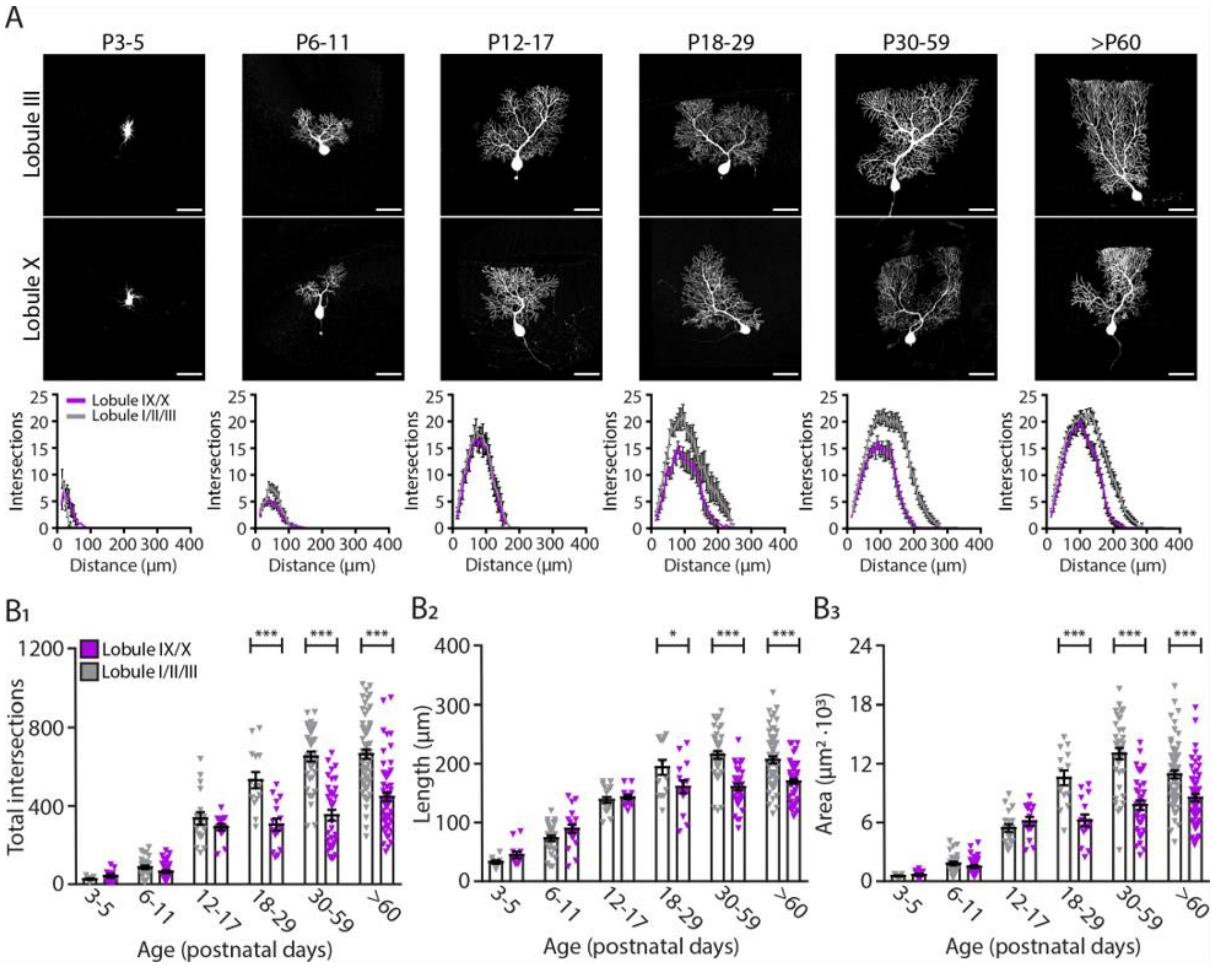

Figure 3. PCs located in the lobule III display a larger and elaborated dendritic tree. (**A**) Photomicrographs of PCs filled with biocytin in lobule III and X (top panel); and sholl analysis of PCs located in lobules I/II/III (grey) or IX/X (purple) in 6 age groups (lower panel). (**B_1**) Total number of intersections, (**B_2**) longest dendrite length and (**B_3**) PC area analysis for lobules I/II/III PCs (grey) and lobules IX/X PCs (purple) in 6 age groups. Age groups: P3-5, P6-11, P12-17, P18-29, P30-59 and >P60. Error bars represent SEM., for values see Table Supplementary 1. * denotes $p<0.05$, ** $p<0.001$ and *** $p<0.0001$. Scale bar = (**A**) 50 µm.

Translocation of climbing fibers occurs earlier in the nodular cerebellum

Both our physiological and morphological data suggest that PCs from the anterior lobule III, and Z– PCs recorded *in vivo*, reach mature levels later when compared to PCs from lobule X, or the Z+ population. Because CF and PC development are intertwined (Watanabe & Kano, 2011), we tested for potential differences between modules in CF development.

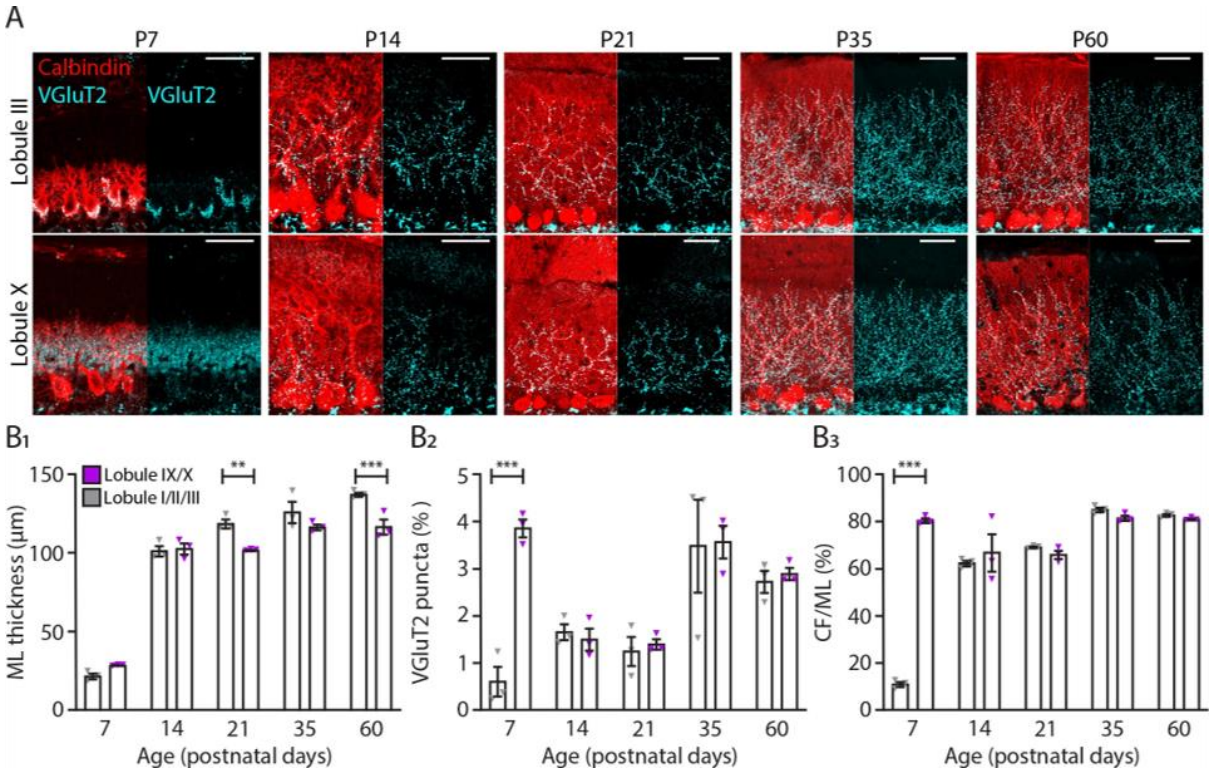

Figure 4. Translocation of climbing fibers occurs earlier in the nodular regions of the cerebellum. (**A**) Photomicrographs of lobule III and lobule X regions depicting climbing fiber (VGluT2 staining, cyan) and Purkinje cell (calbindin, red) development in five age groups. (**B_1**) Molecular layer (ML) thickness, (**B_2**) VGluT2 puncta per area of region of interest and (**B_3**) climbing fiber (CF) extension per ML thickness quantification for lobules I/II/III (gray) and lobules IX/X (purple) in five age groups. Age groups: P7, P14, P21, P35, and P60. Error bars represent SEM, for values see Table Supplementary 1. * denotes $p<0.05$, ** $p<0.001$, and *** $p<0.0001$. Scale bar = (**A**) 40 µm.

To characterize and compare CF development in lobules I-III and IX-X, we stained PCs with calbindin and CFs with VGluT2, which in the molecular layer labels CF terminals, at P7, P14, P21, P35, and P60 (Figure 4A). Remarkably, we found that at P7 there was a significant increase in VGluT2 puncta in lobules IX-X (P7, LI-III: 0.62 ± 0.31%; LIX-X: 3.87 ± 0.19%, $p<0.0001$, Figure $4B_2$) when compared with lobules I-III. As a result, at P7 the percentage of CF extension into the molecular layer (ML) was significantly increased in lobules IX-X (P7, LI-III: 11.1 ± 1.1%; LIX-X: 80.5 ± 1.0%, $p<0.0001$, Figure $4B_3$). These results suggest that CF translocation starts earlier in nodular lobules (Figure 4A). In anterior lobules, most of the VGluT2 puncta at P7 were still localized around the PC somata while in nodular lobules the CF terminals were predominantly targeting the younger dendritic arbors. From P7 to P14, there was a dramatic increase in ML thickness in both regions of the cerebellum (Figure $4B_1$) but the significant difference in VGluT2 puncta and CF terminals disappeared (VGluT2 puncta, P7: $p<0.0001$, P14: p=0.78; CF terminals, P7: $p<0.0001$, P14: $p=0.24$, Figure $4B_2$ and B_3). From P21 into adulthood, there was a significant increase in ML thickness in lobules I-III when compared with the nodular lobules (P60, LI-III: 137.5±1.3 µm; Lob IX-X: 116.9±4.9 µm, $p<0.001$, Figure $4B_1$). With the exception of an increase in VGluT2 puncta and CF terminals from P21 to P35 for both regions studied, no other differences were observed (Figure $4B_2$ and B_3; Table Supplementary 1). These results indicate that CF translocation into the PC dendrite starts earlier in nodular lobules when compared with anterior lobules I, II, and III pointing to another difference in the maturation of the cerebellar circuitries in different cerebellar regions.

PC axonal complexity increases during the second postnatal week

Our data demonstrate that intrinsic physiology of PCs as well as their input structure, the dendritic tree, develop differentially between anterior/Z– and nodular/Z+ populations as well as exhibiting a stark growth period beginning in the second half of the second postnatal week. We next asked whether the PC output structure, the axonal arbor, matches this developmental timeline. The PC axon is a large structure that targets specific cerebellar nuclei based on their location and ZebrinII identity (Sugihara et al., 2009). PC axons are present in the cerebellar nuclei as early as embryonic day (E) 15.5 in mice (Sillitoe et al., 2009) and E18 in rats (Eisenman et al., 1991). Targeting to the correct cerebellar subnuclei is also already in place at very early points in cerebellar development (Sillitoe et al., 2009). In culture, PC axons exhibit a multi-step developmental process (de Luca et al., 2009). However, the developmental process of PC axons *in vivo* is not known. Taking advantage of the *Pcp2-cre^{ERT2};Ai14* mouse model, we sparsely labeled PCs with red fluorescent protein (RFP) and searched for isolated axonal arbors within the cerebellar nuclei (Figure 5A). Labeling was optimal between P10 and P21, although it was sometimes possible to identify well-isolated axons at P7 as well. We therefore analyzed axon arbor morphology as a total group at P7, P10, P14, and P21, while comparisons between Z– and Z+ subnuclei were restricted to P10, P14 and P21 (Figure 5B). Labeled PCs were randomly distributed throughout the cerebellar cortex (Figure 5—figure supplement 1). We performed three-dimensional sholl analysis on single axon arbors with the first branching point as the center. This analysis revealed significant differences across age of PC axon arbor maximum length and complexity, as both parameters increase from P7 to P14 and then decrease at P21 (number of intersections, P7: 84.2±18.2; P10: 254.4±40.5; P14: 277.4±17.5; P21: 296.4±37.9, p=0.013; length, P7: 124.2±17.8 µm; P10: 212.7±24.4 µm; P14: 216.4±14.3 µm^2; P21: 225.2±16.1 µm^2, p=0.060, Figure 5C,E_1, E_2). Area taken up by the axon arbors, however, continued to increase with age (area, P7: 1.52±0.20 µm^2·10^3 P10: 1.47±0.25 µm^2·10^3; P14: 2.26±0.19 µm^2·10^3; P21: 3.07±0.29 µm^2·10^3, p<0.0001; Figure 5E_3). The primary source of the peak at P14 is driven by Z– axon arbors (Figure 5D_2). Sholl analysis revealed significant differences between Z– and Z+ axon arbors at P10, P14 and P21, with Z– axon arbors exhibiting a denser branching complexity than Z+ (P10: p=0.0457; P14: p=0.0017; P21: p=0.0388). Significant differences were found between Z– and Z+ groups for length and area but not number of intersections (intersections, p=0.252; length, p=0.0197; area, p=0.0257; Figure 5F_{1-3}). Taken together, our novel approach to analyze axon terminal development in cerebellar nuclei indicates that PC axons reach near mature shapes already early in development, with a peak in size around P14 and subtle differences between Z– and Z+ axons. Taken together, our novel approach to analyze axon terminal development in cerebellar nuclei indicates that PC axons reach near mature shapes already early in development, with a peak in size around P14 and subtle differences between Z– and Z+ axons.

Differential developmental timelines for the emergence of cerebellar-specific behaviors

Our data indicate that differentiation of cerebellar subpopulations can start early in development and suggest that different cerebellar regions have distinct developmental trajectories. To address if differences in cerebellar maturation have behavioral relevance, we aimed to study the performance of mice in cerebellum-dependent behavioral tasks that are directly linked to the PC subpopulations. The different developmental timeline of PC SS Activity was comparable between Z+ PCs in the flocculus and nodulus, as well as between Z– PCs in the hemispheres and anterior cerebellum (Figure 1— Figure Supplementary 3B). Based on these observations, we performed two cerebellum-dependent learning tests, vestibulo-ocular reflex (VOR) adaptation and eyeblink conditioning (EBC), linked to the Z+ flocculus and the Z− anterior and hemispheric cerebellar regions, respectively. To

facilitate the comparison, we determined the learning curves in juvenile mice directly after weaning (starting from P21) and for reference compared these curves to those of adult (10–11 weeks old) mice. The VOR ensures the stabilization of images on the retina via compensatory eye movement every time the vestibular system is activated (head movement).

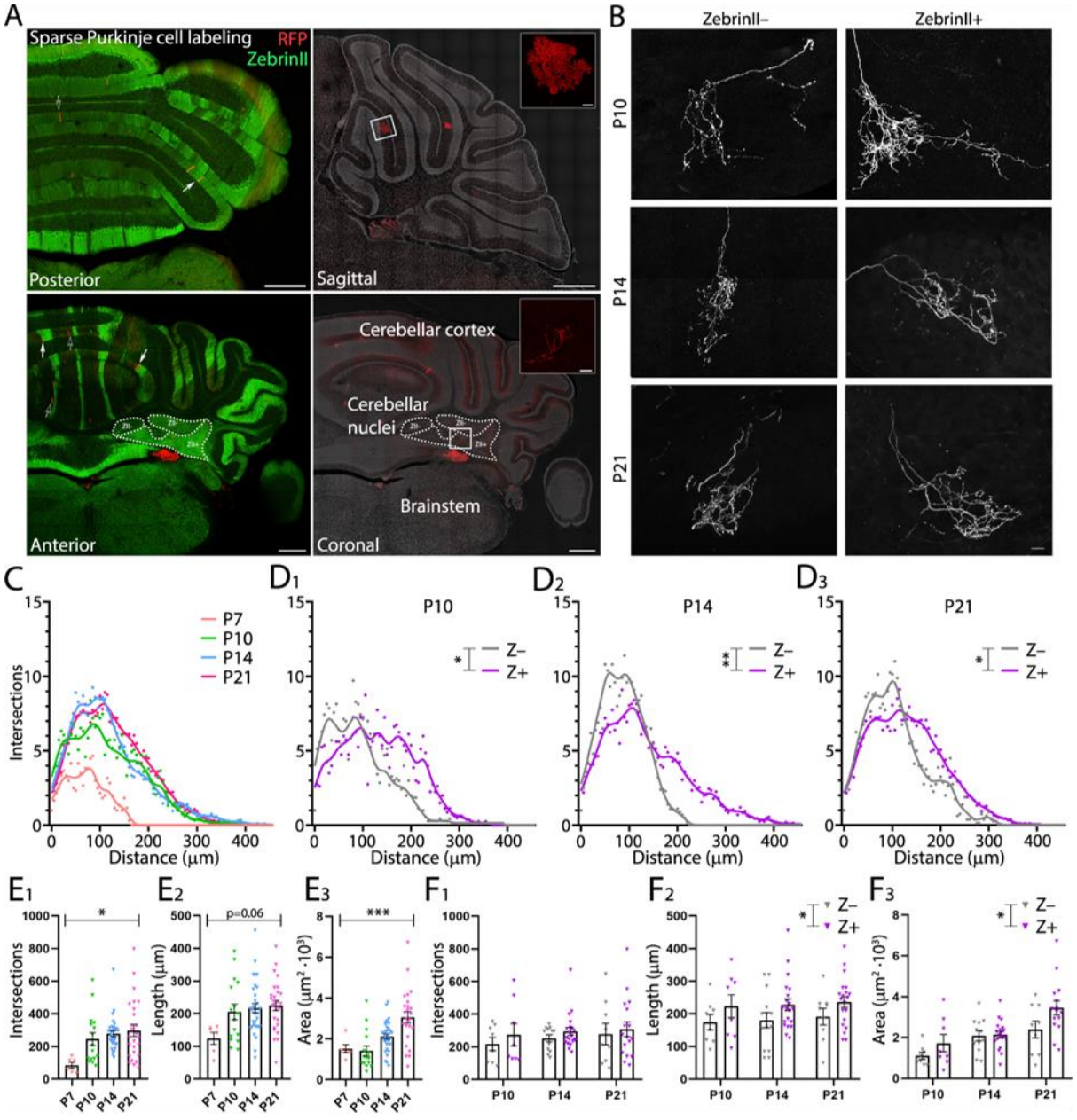

Figure 5. ZebrinII+ Purkinje cell axons are larger and less dense at all early postnatal ages. (**A**) Photomicrographs of cerebellar sections demonstrating sparse labeling of Purkinje cells. Left panels are stained with antibodies against ZebrinII as well as red fluorescent protein (RFP) to label Purkinje cells expressing RFP. Right panels are stained with DAPI and RFP to show examples of Purkinje cells and Purkinje cell axon arbors (top inset and bottom inset, respectively) in sagittal and coronal cerebellar sections (top and bottom right panels, respectively). (**B**) Photomicrographs of example ZebrinII– and ZebrinII+ axon arbors from P10, P14, and P21 mice. (**C**) Sholl analysis of all axon arbors at P7, P10, P14, and P21, average crosses are indicated with points and fitted with a smoothed line. (**D_{1-3}**) Sholl analyses of ZebrinII– and ZebrinII+ groups of axons at P10, P14, and P21, respectively. (**E_1**) Total number of intersections, (**E_2**) longest dendrite length and (**E_3**) axon arbor area analysis for all axons at different ages. (**F_1**) Total number of intersections, (**F_2**) longest dendrite length and (**F_3**) axon arbor

area analysis for ZebrinII– (gray) and ZebrinII+ axon arbors (purple) at P10, P14, and P21. Error bars represent SEM., for values see Table Supplementary 1. * denotes $p<0.05$, ** $p<0.001$, and *** $p<0.0001$. Scale bars = (**A**) 500 µm in large panels; 20 µm in top inset, 50 µm in bottom inset. (**B**) 20 µm.

VOR adaptation is the adjustment of compensatory eye movements based on a mismatch between vestibular and visual input, moving in the same or opposite direction (i.e. in or out of phase) (Ito, 1982; Nagao, 1989; Schonewille et al., 2010; Wulff et al., 2009). Moreover, compensatory eye movements are controlled by the flocculus, together with the nodulus forming the vestibulocerebellum, which is predominantly Z+ (Hawkes & Herrup, 1995; Sillitoe & Hawkes, 2002; Sugihara & Shinoda, 2004); Figure $6A_1$). In the EBC paradigm, a neutral sensory stimulus alone leads to a well-timed eyeblink after repeated pairing with a noxious stimulus which induces a reflexive eyelid closure (usually a mild air puff) (H. J. Boele, 2010; McCormick & Thompson, 1984; R. F. Thompson & Steinmetz, 2009). The cerebellar eyeblink regions putatively reside in the anterior cerebellum, in particular at the border of lobule IV-V to VI, and from the hemisphere lobule IV-V to simplex, a region that is largely ZebrinII-negative (Hawkes & Herrup, 1995; Heiney, Wohl, et al., 2014; Sillitoe & Hawkes, 2002; Sugihara & Shinoda, 2004); Figure $6B_1$).

We first tested if juvenile and adult animals differed in their basal optokinetic reflex (OKR; eye movements driven sole by visual input), vestibular-ocular reflex (VOR; eye movements driven sole by vestibular input in the dark) and visually enhanced VOR (VVOR, a combination of OKR and VOR in the light) (Figure 6— Figure Supplementary 1). We determined the gain (the ratio of eye movement to stimulus amplitude) and phase (timing of the response relative to input) of basal compensatory eye movements at different oscillation frequencies (0.1–1 Hz). Neither the OKR gain or phase differ significantly between age groups (OKR gain, young: 0.60±0.09; adult: 0.59±0.10, p=0.84; and OKR phase, young: −15.5±6.7; adult: −15.4±5.0, p=0.96, Figure 6— Figure Supplementary $1A_1$,B_1). In contrast, the VOR gain is significantly increased (VOR gain, young: 0.42±0.09; adult: 0.61±0.09, $p<0.0001$, Figure 6— Figure Supplementary $1A_2$) and the VOR phase decreased (VOR phase, young: 29.4±5.8; adult: 21.4±4.5, p=0.0024, Figure 6— Figure Supplementary $1B_2$) in adult mice when compared with juveniles. Moreover, while there are no differences in the VVOR phase (VVOR phase, young: 1.33±0.46; adult: 1.35±0.13, p=0.97, Figure 6— Figure Supplementary $1B_3$), there is a significant increase in the VVOR gain of juvenile animals compared with adults (VVOR gain, young: 0.89±0.01; adult: 0.96±0.01, p=0.009, Figure 6— Figure Supplementary $1A_3$).

Subsequently, we tested juvenile and adult mice on a phase-reversal VOR adaptation protocol. This test aimed to evaluate the ability of the animals to reverse the direction of their VOR, from the compensatory, normal direction, opposite to the head rotation, to moving in the same direction as the head (visual and vestibular stimulation in phase). Surprisingly, we observed that the training resulted in juvenile animals reversing their VOR phase, probed in the dark with only vestibular stimulation, faster with significantly lower gain values on the first 3 days and higher phase values on all days (VOR gain, days 1–3, all $p<0.01$ phase reversal, all $p<0.0001$, Figure $6A_2$ and Figure 6— Figure Supplementary 2A–B). Multiple factors can underlie such a robust difference in VOR adaptation, including differences in (a) starting point, (b) gaze parameters, (c) path and speed of adaptation and (d) consolidation. With respect to the starting point (a), both the baseline data and pre-training values of the VOR phase reversal indicate that the juvenile mice start the training with a lower gain and higher phase value, suggesting that a difference in starting point contributed to the overall difference in the curve. It should be noted though, that on day 2 adult mice start with gain values similar to those of juvenile mice on day 1, and still display a slower learning curve from that point onwards. To evaluate the potential role of gaze (b) (S.-L. Shin et al., 2014), we analyzed the eye movements during the

training sessions when visual and vestibular input are combined (Figure 6— Figure Supplementary 2D–E). Gain and phase values of juvenile are significantly closer to the optimal values based on the visual input, but the differences with adult mice are small relative to the differences observed in the VOR adaptation curves (S.-L. Shin et al., 2014). Presenting compensatory eye movement data in separate gain and phase plots impedes the possibility to examine the trajectory, or 'tactics', employed by the mice to complete the task. To visualize the path and speed of adaptation (c), we re-plotted gain and phase in a polar plot (Figure 6— Figure Supplementary 3A,B, respectively). Overall, eye movements of juvenile mice not only move faster from the pre-training position in the right top quadrant to the target gain and phase value left on the x-axis, but also follow a shorter path with lower gain values in the period that the phase increases, potentially indicating a different tactic for adaptation. Finally, we analyzed the consolidation of the adaptation (d) overnight, when animals were kept in the dark for 23 hr. We focused on consolidation of gain change from day 1 to day 2 and phase from day 2 to 3 and 3 to 4, to assure that there are sufficiently large adaptive changes in the comparisons. Consolidation is significantly larger in juvenile mice than in adult mice, for gain decrease (p=0.0005) and for phase increase (p=0.0006 and p=0.0069, respectively, Figure 6— Figure Supplementary 2C). Taken together, these data indicate that the difference in VOR adaptation between juvenile and adult mice depends on multiple factors. While correcting for starting points would remove some of the difference, particularly the difference in consolidation, linked to cerebellar functioning (Wulff et al., 2009), is very robust.

Next, mice were trained to associate a 250 msec LED light (conditioned stimulus) and a 30 msec air puff delivered to the mouse cornea (unconditioned stimulus) co-terminating with the conditioned stimulus, which triggers an unconditioned response (UR), an eyeblink reflex. After training, the conditioned stimulus alone evokes perfectly timed conditioned responses (CR, preventative eyelid closure) (Figure $6B_1$). Juvenile animals exhibit a significantly lower CR percentage after the first day of learning (juvenile: 20.4 ± 4.4%; adult: 30.9 ± 6.0%, p=0.027, Figure $6B_2$) when compared with the adult animals. Moreover, the amplitude of the eyelid closure in response to the conditioned stimulus (fraction eyelid closure) is reduced in juvenile animals (Figure 6— Figure Supplementary $4A_2$,C_1,C_2,C_3,C_4). The difference in CR percentage was not due to reduced eyelid closure abilities in juvenile mice because UR timing and onset is similar between the two groups (UR onset, young: 5.61±0.15; adult: 6.41±0.10, p=0.41; UR peak time, young: 67.2±1.0; adult: 69.0±1.0, p=0.55, Figure 6— Figure Supplementary $4A_1$,B_1,B_2).

Taken together, our data indicate that juvenile animals had an attenuated rate of EBC acquisition while the VOR adaptation was heightened in juvenile animals when compared with adult animals. This suggests different developmental timelines in distinct cerebellar regions underlie the emergency of cerebellar specific behaviors.

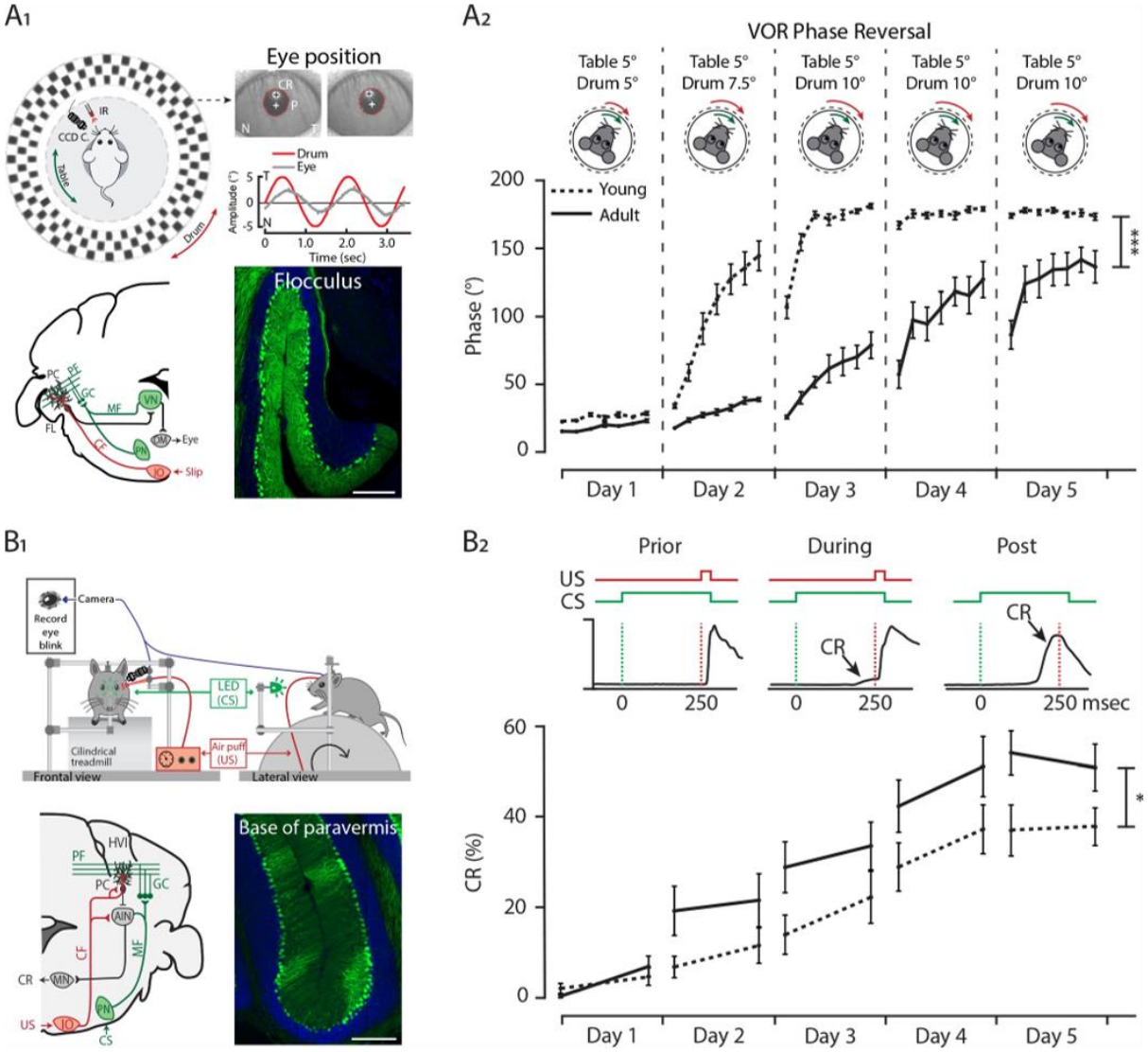

Figure 6. Differential development of cerebellar regions impacts the maturation of cerebellar-specific behaviors. (A_1) Schematic illustration of eye movement recording setup. Mice are head-fixed in the center of a turntable (green arrow) for vestibular stimulation and surrounded by a random dotted pattern *drum* (red arrow) for visual stimulation. A CCD camera was used for infrared (IR) video-tracking of the left eye (top left). Examples of nasal (N) and temporal (T) eye positions. Red circles=pupil fit; black cross=corneal reflection (CR); white cross=pupil (P) center. Example trace of eye position (gray) with drum position (red), during stimulation at an amplitude of 5° and frequency of 0.6 Hz (top right). Cerebellar circuitry controlling compensatory eye movements and their adaptation. Purkinje cells in the flocculus (FL) receive vestibular and visual input via the mossy fiber (MF) - parallel fiber (PF) system (green) and climbing fiber which influence eye movements via the vestibular nuclei (VN) and the oculomotor (OM) neurons. PN, pontine nuclei; GC, granule cell (bottom left). Photomicrograph of the flocculus a ZebrinII+ Purkinje cell predominant region; Purkinje cells labeled with Aldolase C (green) (bottom right). **(A_2)** Results of 5 days of vestibule-ocular reflex (VOR) phase reversal training, probed by recording VOR (in the dark before, between and after sessions) with mice kept in the dark in between experimental sessions in young (P21-25, dotted line) and adult (P70-90, full line) mice. **(B_1)** Schematic illustration of the eyeblink conditioning setup. Head-fixed mice on a freely moving treadmill, are presented a green LED light (conditioned stimulus, CS) followed several hundred milliseconds later by a weak air-puff on the eye (unconditioned stimulus, US). Eyelid movements were recorded with a camera (top). Cerebellar circuitry controlling eyeblink conditioning. Purkinje cells in the paravermal region around the primary fissure receive inputs carrying sensory information from for example the pontine nuclei (PN) through the mossy fiber-parallel fiber (MF-PF) pathway and the error signal from the inferior olive (IO) through the climbing fiber (CF). These Purkinje cells in turn influence eyelid muscles via the anterior interposed nucleus (AIN) and motor nuclei (MN) (bottom left). Photomicrograph of the base of paravermis a ZebrinII– Purkinje cell predominant region; Purkinje cells labeled with Aldolase C (green) (bottom right). **(B_2)** As a result of repeated conditioned stimulus (CS)-

unconditioned stimulus (US) pairings, mice will eventually learn to close their eye in response to the conditioned stimulus (CS), which is called the conditioned response (CR) (top). Percentage of conditioned response (CR%) in young (dotted line) and adult (full line) mice during 5 days of training (bottom). Error bars represent SEM., for values see Table Supplementary 1. * denotes $p<0.05$, ** $p<0.001$, and *** $p<0.0001$. Scale bars = (A) 200 µm.

Discussion

While the variety of sensorimotor and cognitive functions controlled by the cerebellum and its intricate architecture have been widely studied in adult animals, the development of its regional differences in physiology, morphology and connectivity is more enigmatic. Identification of developmental milestones in different cerebellar regions is essential for deciphering the emergence of functional cerebellar circuits. In this study, we uncover that different subpopulations of PCs acquire unique morphological and physiological features during distinct developmental timelines, such that PCs of the posterior cerebellum, particularly lobule X, reach their adult stage prior to PCs of the anterior, in e.g. lobule III, cerebellum (Figure 7). In line with this observation, we found a relative underperformance of juvenile mice in the EBC, linked to anterior cerebellar regions (Figure $6B_2$).

Distinct developmental trajectories of specific cerebellar circuitries

PCs are generated in the ventricular zone at the base of the fourth ventricle (Hoshino et al., 2005; Morales & Hatten, 2006; Yamada et al., 2014). Cerebellar compartmentalization has been shown to correlate with PCs birth dates: early-born (E10-E11.5) will become adult Z+ PCs and late-born (E11.5-E13) will become adult Z– PCs (M. Hashimoto & Mikoshiba, 2003; Larouche & Hawkes, 2006; Namba et al., 2011). Thus, there is a strong relationship between embryonic compartments and adult zonal patterning associated with the modular organization of the olivo-cortico-nuclear circuit (Brochu et al., 1990; Pijpers & Ruigrok, 2006; Sugihara & Shinoda, 2004, 2007; Voogd, 2003; Voogd & Ruigrok, 2004). The maturation of the zonal phenotype is only complete around P12-P15, based on the molecular markers ZebrinII (Brochu et al., 1990; Lannoo et al., 1991) or PLCβ4 (76).

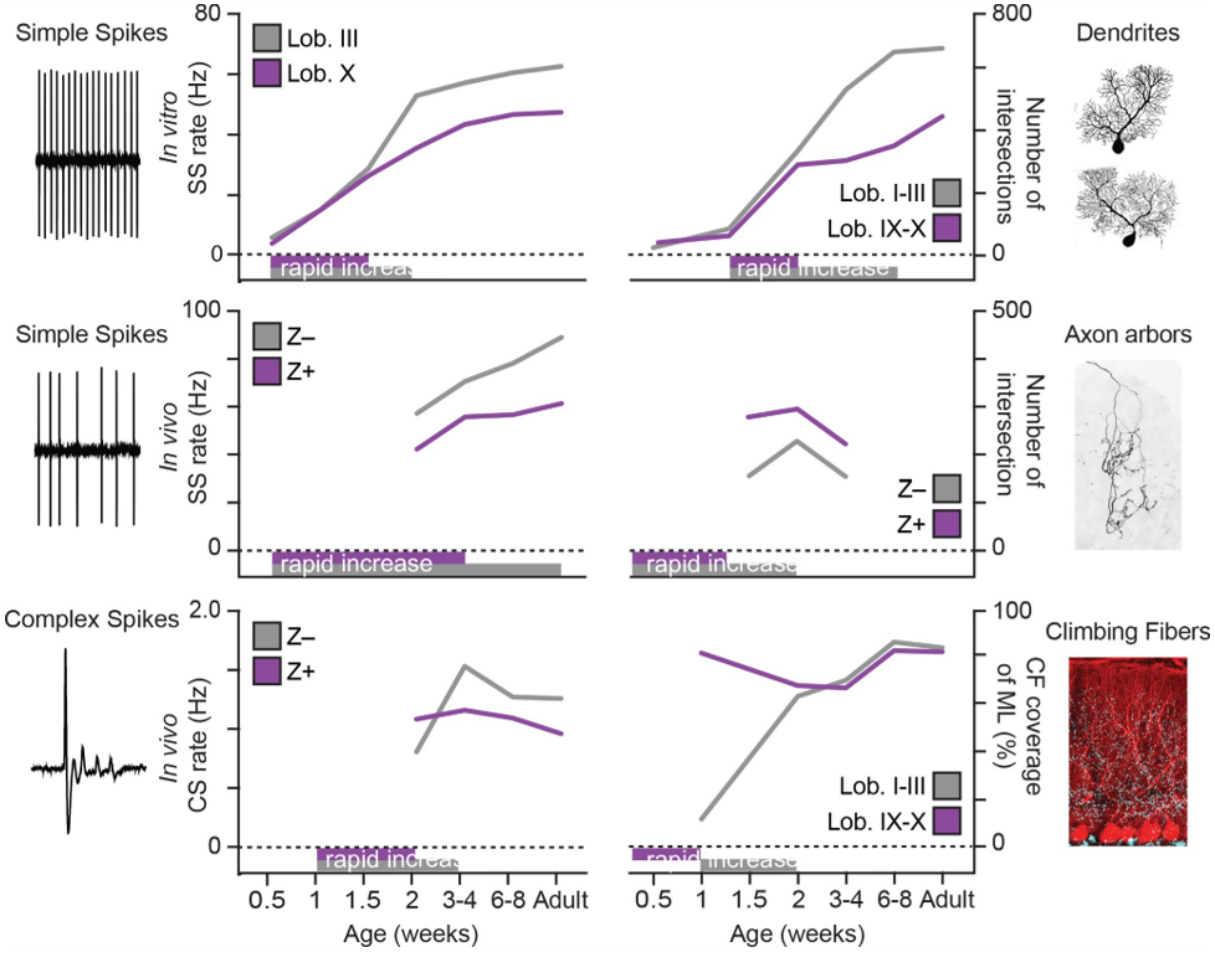
Simple Spikes
In vitro SS rate (Hz)
80
0
Lob. III
Lob. X
rapid increase
800
0
Number of intersections
Lob. I-III
Lob. IX-X
rapid increase
Dendrites
Simple Spikes
In vivo SS rate (Hz)
100
0
Z–
Z+
rapid increase
500
0
Number of intersection
Z–
Z+
rapid increase
Axon arbors
Complex Spikes
In vivo CS rate (Hz)
2.0
0
Z–
Z+
rapid increase
100
0
CF coverage of ML (%)
Lob. I-III
Lob. IX-X
rapid increase
Climbing Fibers
0.5 1 1.5 2 3-4 6-8 Adult
Age (weeks)
0.5 1 1.5 2 3-4 6-8 Adult
Age (weeks)

Figure 7. Summary of developmental timelines of Purkinje cell activity and morphology. Left, selected features for physiological activity, represented by simple spike firing rate *in vitro*, simple spike rate *in vivo* and complex spike rate *in vivo*. Below the graphs periods of rapid development are indicated, either based on our data or by extrapolation when first recorded levels are already high, see e.g. simple spike rate *in vivo*. Right, selected morphological features, represented by dendritic shape, axonal shape (both as total number of intersections) and climbing fibers (as % of climbing occupation of molecular layer). Note that, although not all data points are available and extrapolation is required, the general trend emerging is that of rapid development in the second postnatal week (P7 to P14) and that Lobule III/ZebrinII– PCs typical complete rapid development later. Z– = ZebrinII negative, Z+ = ZebrinII positive, SS=simple spike, CS=complex spike.

Although this patterned organization of heterogeneity is a unique feature of the cerebellum, its impact on early cerebellar circuitry assembly was unknown. In our studies, developmental electrophysiological and morphological analyses revealed that lobule X/Z+ PCs reached adult stable properties earlier than anterior lobule III/Z– PCs (Figure 7), particularly when it comes to simple and complex spike activity, as well as dendritic morphology. This suggests that the configuration of mature PCs follows directly from their development, which is a consequence of their birthdate. *In vivo* recordings followed by post-mortem analysis allowed us to group PC acquired throughout the cerebellum into Z+ and Z– subpopulations. Signs of ZebrinII-related differentiation in the electrophysiological properties, similar to those observed in firing rate of SS in the adult mouse *in vivo* (Zhou et al., 2014), could already be detected in the end at the second postnatal week from P12 (Figure $1C_1$). When examined across lobules, rather than in direct relation to ZebrinII, the slower development appears most obvious in lobules I-II, III, VI-VII and the Z− PCs in the hemispheres, while particularly lobule X and the flocculus appear to reach adult levels at P18-P29 (Figure 1— Figure Supplementary 3A–B), but prohibit us from making conclusive statements. As also found in adult mice based in *in vitro* recording from lobules III and X (Wu et al., 2019; Zhou et al., 2014), the difference at P12-P19 is, at least in part, caused by differences in intrinsic activity (Figure $2B_1$). We focus our *in vitro* studies of intrinsic activity on lobule III in the anterior vermis and lobule X in the nodular vermis (Brochu et al., 1990; Sugihara & Shinoda, 2007; Zhou et al., 2014; Figure $2A_1$), as these regions can be readily identified in the cerebellum at all ages, are oriented in such a way that it is possible to record from them in a single sagittal slice and have previously been demonstrated to be representative of the Z– and Z+ PC populations (Wu et al., 2019; Zhou et al., 2014). Z+ PCs demonstrate early maturation of their physiological properties by reaching a SS activity level *in vivo* at P18 that is not significantly different from that in adulthood. Contrarily, in PCs from anterior regions of the cerebellum the activity continues to gradually increase until adulthood (Figure 1— Figure Supplementary 3). Similarly, CS activity, which results exclusively from the activity of neurons in the inferior olive, also showed reduced activity of Z+ PCs compared with Z– PC CSs from P18-P27 (Figure $1D_1$). Overall, physiological differences in two populations of PCs are first detected at the end of the second postnatal week and result from intrinsic differences combined with an input component (Figure 2— Figure Supplementary 2).

Previous reports have shown that, in rats, changes in physiological properties during development match the time course of dendritic growth, without differentiating subtypes (McKay & Turner, 2005). Indeed, we observed a marked dendritic growth around the second and third week in the mouse. Starting from P18, PCs of the anterior lobule III continue to grow and develop a larger dendritic area and more elaborated dendritic tree when compared with the nodular lobule X PCs. Similar to our physiology data, PCs in the nodular lobule X region appear to reach their adult stage at P18, although a smaller growth is still present from the adolescent to adult stage. This suggests that in some populations of PCs their maturation is not only linked with their location in the cerebellum

(Altman, 1972), but also coupled to their physiological development. The development of cerebellar circuits is not solely dependent on an intrinsic genetic code that regulates cell autonomous early activity and early morphologic features. During development, different types of afferents target specific regions of the cerebellum rearranging its circuitry. In particular, mossy fiber (C. l. Armstrong et al., 2009; Ji & Hawkes, 1995, p. 1; Sotelo & Wassef, 1991) and CF (Chédotal et al., 1997; Sotelo & Chédotal, 2005; Voogd & Ruigrok, 1997) afferents terminate into parasagittal domains that align with the ZebrinII domains. CF development has been carefully described (K. Hashimoto et al., 2009; Kano et al., 2018; Watanabe & Kano, 2011).

Our results revealed a unique temporal development of the functional differentiation of the CF synapses. Concomitantly with early maturation of the nodular lobule X described previously also CF translocation occurs earlier in this cerebellar region (Figure 4). Additionally, CS activity *in vivo* shows that differences between Z– and Z+ PCs are evident by P12 but in the juvenile age group (P18-P29) they resemble the direction observed at adult mature stages. This period, P12-P18, is known to be the late phase of CF elimination (Kano et al., 2018). Although PCs during development are innervated by multiple CFs (K. Hashimoto et al., 2009; K. Hashimoto & Kano, 2005), the CS rate has never been found to be higher during development than in adulthood (Arancillo et al., 2015; Kawamura et al., 2013; Sokoloff et al., 2015), and we verify that here for both Z+ and Z– populations. Our data also reveal that CF pause duration is normalized after the period of synapse elimination at P18 (Figure $1D_2$). Initial dendritic outgrowth is known to be independent of input signals (Alvarado-Mallart & Sotelo, 1982, p.; Dusart et al., 1997; Sotelo & Arsenio-Nunes, 1976). However, CFs are necessary to complete PC dendritic growth and synapse maturation (Sotelo, 2004; Sotelo & Arsenio-Nunes, 1976).

Moreover, positional cues from PCs are necessary for the correct CF-PC connection (Chédotal et al., 1997). When during development these molecules are expressed in diverse PCs subtypes could partially explain specific levels of CF maturation. During the second postnatal week features substantial changes in PC axon arbors as well. Complexity and length both significantly increase between P7 and P10 and P14. However, between P14 and P21, morphological pruning appears to take place (Figure 5). PC axons in culture also feature a multi-step development, first extending neurites and then switching to an arborizing phase (de Luca et al., 2009). However, this development had not been examined *in vivo*. PC axons in the adult feature differences between subnuclei of the cerebellar nuclei (Sugihara et al., 2009). While axons within the dentate nucleus exhibit very compact arbors, axons within the medial nucleus are not dense. We were able to detect signatures of this inter-nuclear difference in the developing mouse cerebellum. However, the intra-nuclear differences are subtle in the development of Z– and Z+ axon arbors. The differences between the subpopulations appear to be set early on and growth takes place within that difference already existing.

Developmental patterning of SS and CS rates *in vivo*, as well as that of the axonal projection features, were analyzed across the populations of Z– and Z+ PCs. SS activity *in vitro*, dendritic development and CF innervation were taken from virtually exclusively Z– anterior and Z+ nodular lobules, because ZebrinII is not expressed at the earlier time points tested for these parameters and the need for coronal slicing hinders analyzing multiple time points. The possibility that some of the observed differences are related to lobules or transverse zones cannot be excluded (C. L. Armstrong et al., 2001; C. l. Armstrong et al., 2009; Hawkes & Eisenman, 1997), particularly for the morphological changes. However, this selection of lobules is commonly used for comparisons Kim et al., 2012) and have consistently been confirmed with targeted recordings (Wu et al., 2019; Zhou et al., 2014). Differentiation in the translocation of input(s) further supports the concept that cerebellar circuitries

develop at specific and precise timelines that correlate with the subtype of PC and their physical location.

Spatiotemporal aspects of gene expression patterns and developmental trajectories

There are several lines of evidence that support the concept of spatial regulation of the cerebellum. In mammals, the cerebellar cortex is divided rostrocaudally into four transverse zones (anterior, central, posterior, and nodular) and mediolaterally into parasagittal stripes (C. L. Armstrong et al., 2000; C. L. Armstrong & Hawkes, 2000; Hawkes & Eisenman, 1997; Ozol et al., 1999). Both transverse and parasagittal compartments can be distinguished by gene expression. Analyses of the *meander tail* (Ross et al., 1990) and *lurcher* (Tano et al., 1992) mutant mice have revealed a genetic compartmental boundary between nodular and anterior lobules. Consistent with this notion, a recent single-cell RNA-sequencing study has shown gene expression correlated or anti-correlated with the ZebrinII pattern (Rodriques et al., 2019). A second spatial gene expression pattern was identified related to the vestibulocerebellar region (lobules IX and X), in which genes are exclusively expressed within or outside this region (Rodriques et al., 2019). But what is the developmental profile of these spatial expression differences, and what drives the differentiation?

Studies suggest that specification of PC subpopulations (both transversal and parasagittal subtypes of PCs) is regulated by cell autonomous mechanisms, more so than activity or afferent dependent, starting from the birth of the PCs (Chung et al., 2008; M. Hashimoto & Mikoshiba, 2003; Larouche & Hawkes, 2006; Namba et al., 2011) Hashimoto and Mikoshiba, 2003 PC birthdating experiments revealed that, in contrast with the expression of the markers available at the time, the eight clusters of PCs the authors identified embryonically were unchanged until adulthood. Although ZebrinII is a 'late-onset' parasagittal marker, others, such as neurogranin (Larouche et al., 2006), were shown to be expressed from E14.5 in a pattern that was maintained until P20. While *Slc1a6* expression is similar to that of ZebrinII in adult mice, its mRNA can already by detected from embryonic ages and immunohistochemical analysis supports a patterned, selective expression in the caudal cerebellum from embryonic day 18 (Yamada et al., 1997). Additionally, PLCβ4 expression is restricted to the Z– cells and its expression also begins just before birth. The PLCβ4-positive clusters in the neonate are complementary with the Z– neurons (Marzban et al., 2007). With the use of mouse genetics (Sillitoe et al., 2009) or adenovirus tracing (Namba et al., 2011) it was possible to verify that the birth date-related PCs correlated with the zonal pattern of ZebrinII.

Finally, it is known that the nodulus (vermal lobule X) and the flocculus are distinct divisions of the cerebellum at an early age (Fujita et al., 2012). Our electrophysiological data add to this notion that differences in physiological properties result from intrinsic properties of PCs (Figure 2) early in development. Intrinsic activity could be observed as early as P3 and differences between PC subpopulations become apparent starting from P12. Moreover, we observed that the influence of extrinsic inputs, the net effect of excitatory and inhibitory inputs, is relatively small in the second week, but starts to drive activity at P18. While this influence remains relatively stable in nodular lobule X/Z+ PCs, the net driving effect of extrinsic inputs increases over time for anterior lobule III/Z– PCs until the cells reach their full maturation in the adult (Figure 2— Figure Supplementary 2). It should be noted, however, that the methods we employed do not allow us to determine the individual contributions of each input, except that of the CFs, and that this maturation could also be the result of a shift in the balance between excitation and inhibition (Jelitai et al., 2016).

While the precise molecular mechanism underlying these differences is not well-defined, several lines of evidence suggest gene expression differences in subtypes of PCs may explain this phenomenon. For

instance, Z– PCs have a higher expression of TRPC3 (44) and its ablation decreases their firing rate to make them more similar to the firing rate of Z+ PCs with behavioral consequences. Additionally, the TRPC3 channel molecular cascade includes proteins expressed in parasagittal bands such as mGluR1b (Mateos et al., 2000)(, IP3R1 (Furutama et al., 2010), PLCβ3/4 (Sarna et al., 2006), and PKCδ (Barmack et al., 2000). Recently, specific ATPases and potassium channels were identified in Z– PCs that can also contribute to explain intrinsic differences (Rodriques et al., 2019). The physiology and morphology of PCs have striking interaction effects. As described previously (Bradley & Berry, 1979; McKay & Turner, 2005), from the second postnatal week PCs develop their characteristic dendritic tree coupled with functional transitions (Dusart & Flamant, 2012). Our data show for the first time that coupled with their electrophysiological properties, nodular lobule X PCs reach maturity of their dendritic tree faster than anterior lobule III PCs (Figure 3).

During the second postnatal week of development also the complexity of the PC axonal arbor increases significantly (Figure 5). Corticonuclear topography is related with the topography of the olivocerebellar pathway (Sugihara et al., 2009; Sugihara & Shinoda, 2007), in that Z+ PCs typically project to the lateral/caudoventral cerebellar nuclei while Z– neurons typically project to the medial/rostrodorsal parts of the cerebellar nuclei. In adult rats, PC axon arbors have been shown to vary morphologically based on their location within the cerebellar nuclei with more Z+ subnuclei containing denser, more complex PC axonal arbors (Sugihara et al., 2009). Our data shows for the first time the existence of a similar pattern of distinct morphology of PC axons in the different subnuclei during development (Figure 5). Although neuronal subtypes of the related vestibular nuclei have been identified (M. Shin et al., 2011), neither the subtypes in the cerebellar nuclei nor the pattern of PC to cerebellar nuclei neuron projections have been comprehensively studied. Linking the projection pattern of Z+ and Z– PCs to genetically identified neuronal subpopulations of each cerebellar nuclei is a crucial future step in understanding the development and functioning of the olivocerebellar circuit.

Differential ontogeny of cerebellar-sensorimotor functions

Unique timelines in the maturation of cerebellar microcircuitries sparked the hypothesis that correlated behaviors are impacted and have distinct developmental profiles as well. Although the list of cerebellum-related behaviors is long, only few tasks have been directly linked to specific, restricted cerebellar regions. The difference in developmental timeline of PC SS activity, which directly influences downstream targets, is comparable between flocculus and nodulus, as well as between Z– PCs in the hemispheres and anterior cerebellum (Figure 1— Figure Supplementary 3B). Therefore, we examined VOR adaptation and EBC as proxies for Z+ and Z− cerebellar module-related behaviors, respectively. VOR adaptation and EBC are regulated by different modules in the cerebellum: VOR adaptation is controlled by the flocculus of the vestibulocerebellum, which is a Z+ region (Fujita et al., 2014; Ito, 2002; Lisberger, 1988; Sugihara & Quy, 2007; Zhou et al., 2014), and EBC is controlled by the hemispheric lobule VI, which is predominantly a Z– region (H. J. Boele, 2010; Heiney, Wohl, et al., 2014; Hesslow, 1994, 1994c; Mostofi et al., 2010; R. F. Thompson & Steinmetz, 2009).

Our data show that different elements of the nodular Z+ circuitry mature, that is reach their adult levels at the juvenile (P21) stage, earlier than anterior Z– circuitries and hence we hypothesize that this differentiation would manifest itself in the ability to perform related learning tasks. We found that young animals, compared to adult mice, start with a similar OKR baseline similar, but a lower VOR baseline (Figure 6— Figure Supplementary 1). A similar attenuation of VOR gain, but more specifically for lower to midrange frequencies, was observed previously, while we were not able to replicate the higher OKR gain at 1.0 Hz visual stimulation observed in that work (Faulstich et al., 2004).

Taken together, both studies suggest a delayed maturation of the VOR with a potential compensatory role for an 'overactive' OKR system. As OKR gain is attenuated by loss or dysfunctional cerebellar input, the VOR gain typically increases in those conditions (Schonewille et al., 2010; Van Alphen & De Zeeuw, 2002) and hence these results argue against any impairments due to incomplete development of the floccular region. When challenged with a learning paradigm, the VOR phase reversal, the younger animals adapted faster than adult animals. These results support our hypothesis that the flocculus circuitry at P21 is functional and suggests that it even allows for faster learning, a form of immature hyperplasticity, comparable to known forms of enhanced neural plasticity in development (Cai et al., 2014; Hensch & Bilimoria, 2012; Wiesel & Hubel, 1965). Additionally, when comparing the simple spike rate development in the flocculus with the nodular regions of the cerebellum (Figure 6— Figure Supplementary $3B_2$), even with limited data points, data suggests that by P18-29 these PCs have reached their adult firing rate stage. In contrast, younger animals have a poorer performance in the CR of the EBC paradigm compared to adult animals. Functional I aturity of the eyeblink response has been suggested to be due to immaturity of the afferent pathway when using an auditory cue (Nicholson and Freeman, 2000). However, the fact that we use a visual cue and compare the results with visual stimulus-driven OKR and VOR adaptation, argue against the role of an immature afferent pathway, while the presence of normal URs rejects the premise that an inability to blink is the cause. At P21 the firing rate of anterior Z– PCs in the eyeblink region (Figure 1— Figure Supplementary $3A_3$,B_1), is reduced when compared to adult counterparts (Figure 1— Figure Supplementary $3A_4$,B_1), which can likely contribute to the impaired CR in young animals (ten Brinke et al., 2015; Wu et al., 2019).

Evidence suggests that Z– and Z+ PCs utilize different forms of synaptic plasticity, but there is still no consensus on which plasticity mechanisms underlie VOR adaptation and EBC. Long-term depression (LTD) was the first type of synaptic plasticity implicated in cerebellar motor learning (Ito, 2000). LTD has been suggested to participate in the EBC response (Freeman, 2015; Grasselli & Hansel, 2014) and this form of plasticity is known to occur on Z– lobule III PCs while in Z+ lobule X PCs is not detected (Paukert et al., 2010; Wadiche & Jahr, 2005). Interestingly, blocking TRPC3 function eliminates LTD plasticity (S. J. Kim, 2013) and, we recently showed that, TRPC3 loss-of-function in mice showed an impaired EBC response (Wu et al., 2019), but normal VOR adaptation. LTD can be readily induced in the anterior regions of juvenile PCs (S. J. Kim, 2013) and LTD-deficient mice do not have impaired EBC, arguing against a central role for LTD in the EBC impairment in juvenile mice. Intrinsic excitability is increased after EBC (Schreurs et al., 1998; Titley et al., 2020) and deletion of calcium-activated potassium channel SK2 ablated this plasticity of intrinsic excitability (intrinsic plasticity) and resulted in impaired EBC, but enhanced VOR adaptation (Grasselli et al., 2020), a phenotype that is in line with the juvenile phenotype (Hesslow, 1994). Thus, a lack of ability to reach higher levels of excitability by young anterior Z– PCs could explain the lower performance in the P21 animals.

The latter example suggests that the temporal difference in the emergence of cerebellum-sensorimotor behaviors (Figure 6), could result from a distinct cell-autonomous excitability regulation in distinct PCs populations. Future studies will have to determine the precise parameters for induction of the difference forms of plasticity in each region, and their respective timelines.

Overall, this study highlights the heterogeneity within the cerebellum during development. Key parameters such as CF input, dendritic and axonal shape and intrinsic firing rate reach mature levels at different moments in postnatal development, depending on the subtype of PC and the regional location. The evolutionary advantage to have distinct developmental timelines in different cerebellar regions is likely to be related with their function. Increasing evidence has shown that in

addition to sensorimotor processing the cerebellum has a role in cognitive functions (Ito, 2008; White & Sillitoe, 2013) and early cerebellar dysfunction has been implicated in neurodevelopmental disorders (Kern, 2002; P. Martin & Albers, 1995; S. S.-H. Wang et al., 2014). Recently, a comprehensive study has shown that the diverse motor and non-motor functions of the cerebellar vermis are mediated by different groups of fastigial output neurons with specific connections. The authors identified two major classes of fastigial glutamatergic projection neurons: small neurons innervated by Z+ PCs, projecting to circuits associated with sensory processing, motor preparation and behavioral, cognitive, affective and arousal responses to novel or unexpected events, while large neurons innervated by Z– PCs connect with circuits associated with control of motor and autonomic functions (Fujita et al., 2020). Thus, uncovering the mechanisms underlying early circuitry formation in the developing cerebellum is imperative to understand the basis of cerebellum circuitry and associated disorders. Additional experiments are necessary to clarify developmental stages of other elements of cerebellar circuits such as mossy fiber or interneurons. Nevertheless, our results demonstrate that the emergence of cerebellar sensorimotor functions are tightly coupled with distinctive PC properties.

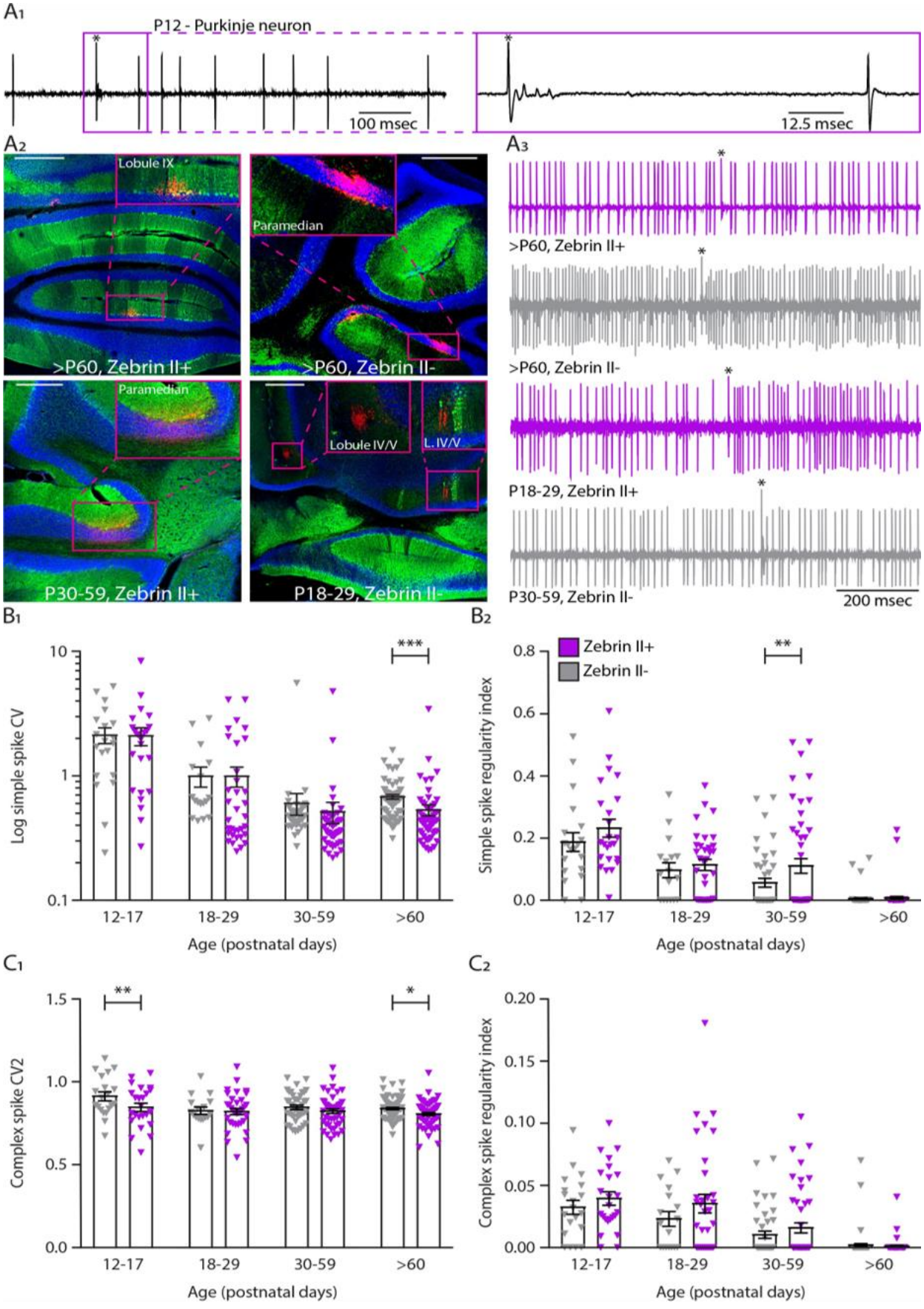
A1
P12 - Purkinje neuron
100 msec
12.5 msec
A2
Lobule IX
Paramedian
>P60, Zebrin II+
>P60, Zebrin II-
Paramedian
Lobule IV/V
L. IV/V
P30-59, Zebrin II+
P18-29, Zebrin II-
A3
>P60, Zebrin II+
>P60, Zebrin II-
P18-29, Zebrin II+
P30-59, Zebrin II-
200 msec
B1
Log simple spike CV
10
1
0.1
***
12-17
18-29
30-59
>60
Age (postnatal days)
B2
Zebrin II+
Zebrin II-
Simple spike regularity index
0.8
0.6
0.4
0.2
0.0
**
12-17
18-29
30-59
>60
Age (postnatal days)
C1
Complex spike CV2
1.5
1.0
0.5
0.0
**
*
12-17
18-29
30-59
>60
Age (postnatal days)
C2
Complex spike regularity index
0.20
0.15
0.10
0.05
0.00
12-17
18-29
30-59
>60
Age (postnatal days)

Figure Supplementary 1.1. I*n vivo* extracellular recordings of simple and complex spike activity in different ZebrinII-related Purkinje cell populations during development. (**A**$_1$) Example trace of a young P12 Purkinje cell recording identified by its hallmark feature, the occurrence of complex spikes (asterisk) and simple spikes (left). Inset depicting the complex spike (asterisk) following a climbing fiber pause with clear visible spikelets (right). (**A**$_2$) Photomicrographs of coronal sections with examples of P18-29 ZebrinII–, P30-59 ZebrinII+, >P60 ZebrinII+, and ZebrinII– Purkinje cells labeled with Aldolase C (green). Insets showing recording sites marked with biocytin (red) in lobules IX IV/V and Paramedian. (**A**$_3$) Example traces of ZebrinII– and ZebrinII+ Purkinje cells extracellular recordings at >P60 ZebrinII+ an ZebrinII–, P18-29 ZebrinII+, and P30-59 ZebrinII– with clearly distinguishable simple spikes and complex spikes (asterisks). (**B**$_1$) Purkinje cell coefficient of variation (CV) for simple spikes, (**B**$_2$) regularity index for simple spikes, (**C**$_1$) coefficient of variation 2 (CV2) for complex spikes and (**C**$_2$) regularity index for complex spikes recorded *in vivo* for ZebrinII– Purkinje cells (gray) and ZebrinII+ Purkinje cells (purple) in four age groups. Age groups: P12-17, P18-29, P30-59, and >P60. Error bars represent SEM., for values see Table Supplementary 1. * denotes $p<0.05$, ** $p<0.001$ and *** $p<0.0001$. Scale bars = (**A**$_2$) 500 µm (top left, top right, bottom right) and 250 µm (bottom left).

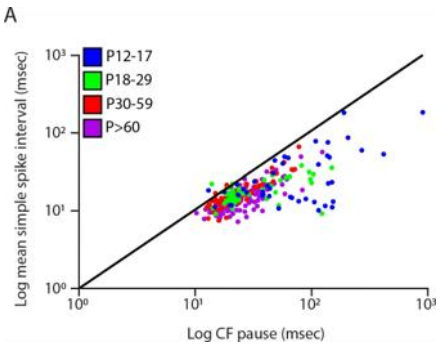

Figure Supplementary 1.2. Climbing fiber pause is longer than inter-simple spike-interval in the majority of the recorded cells. (**A**) Scatterplot of the log mean simple spike-interval versus the log climbing fiber (CF) pause of all cells recorded in four age groups (blue: P12-17; green: P18-29; red: P30-59 and purple: P>60). The diagonal black line represents the reference line where the climbing fiber pause is equally long as the simple spike-interval.

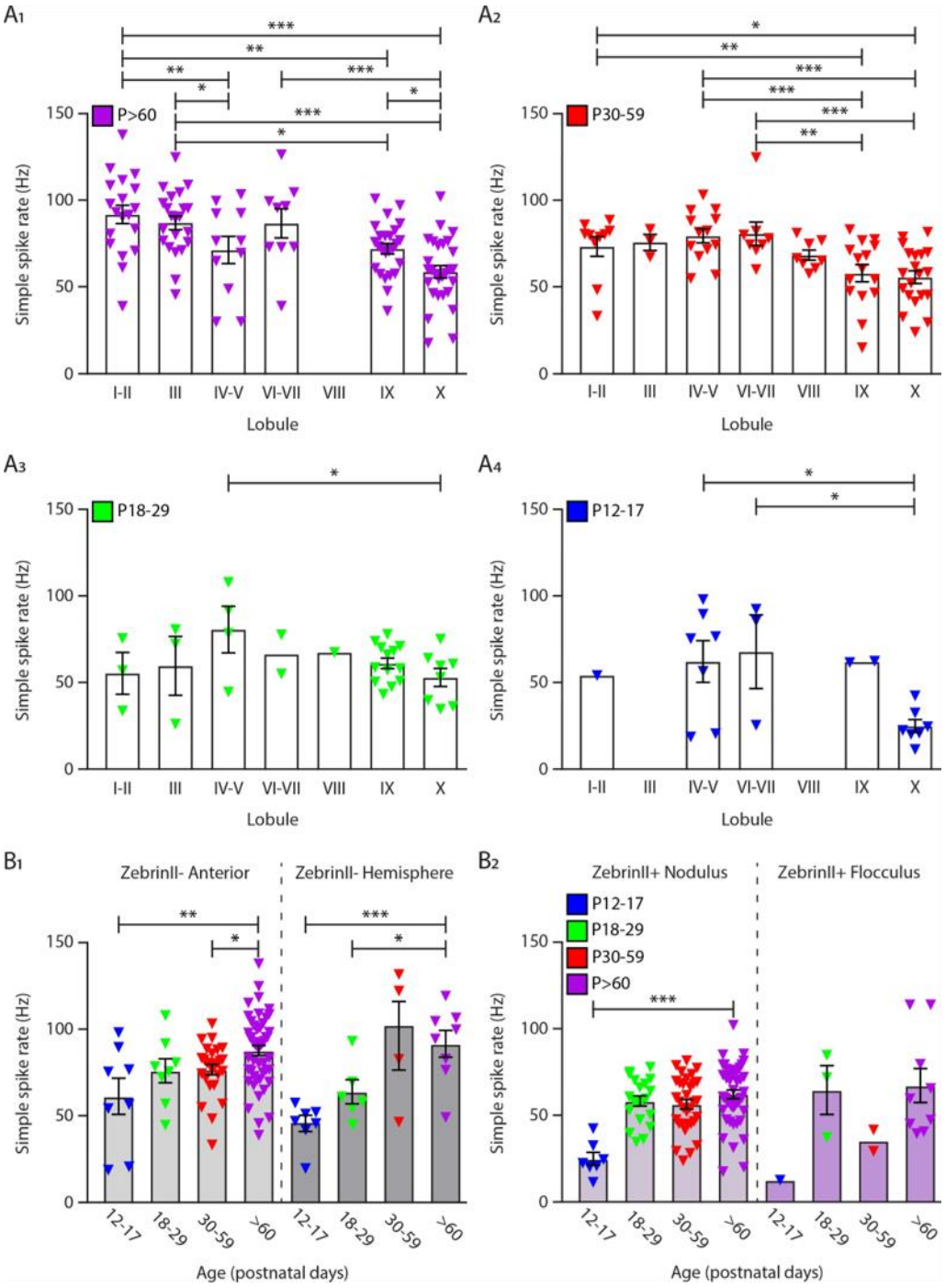

Figure Supplementary 1.3. ***In vivo*** **extracellular recordings of simple spike activity distributed by lobules and cerebellar regions during development.** Purkinje cell simple spike firing rate *in vivo* for Purkinje cells in all lobules at (**A_1**) >P60, (**A_2**) P30-59, (**A_3**) P18-29 and (**A_4**) P12-17. Purkinje cell simple spike firing rate *in vivo* for (**B_1**) ZebrinII– Purkinje cells in lobules I to V and ZebrinII– Purkinje cells in the hemispheres and for (**B_2**) ZebrinII+ Purkinje cells in the nodulus and ZebrinII+ Purkinje cells in the floculus in four age groups. Error bars represent SEM., for values see Table Supplementary 1. * denotes $p<0.05$, ** $p<0.001$, and *** $p<0.0001$.

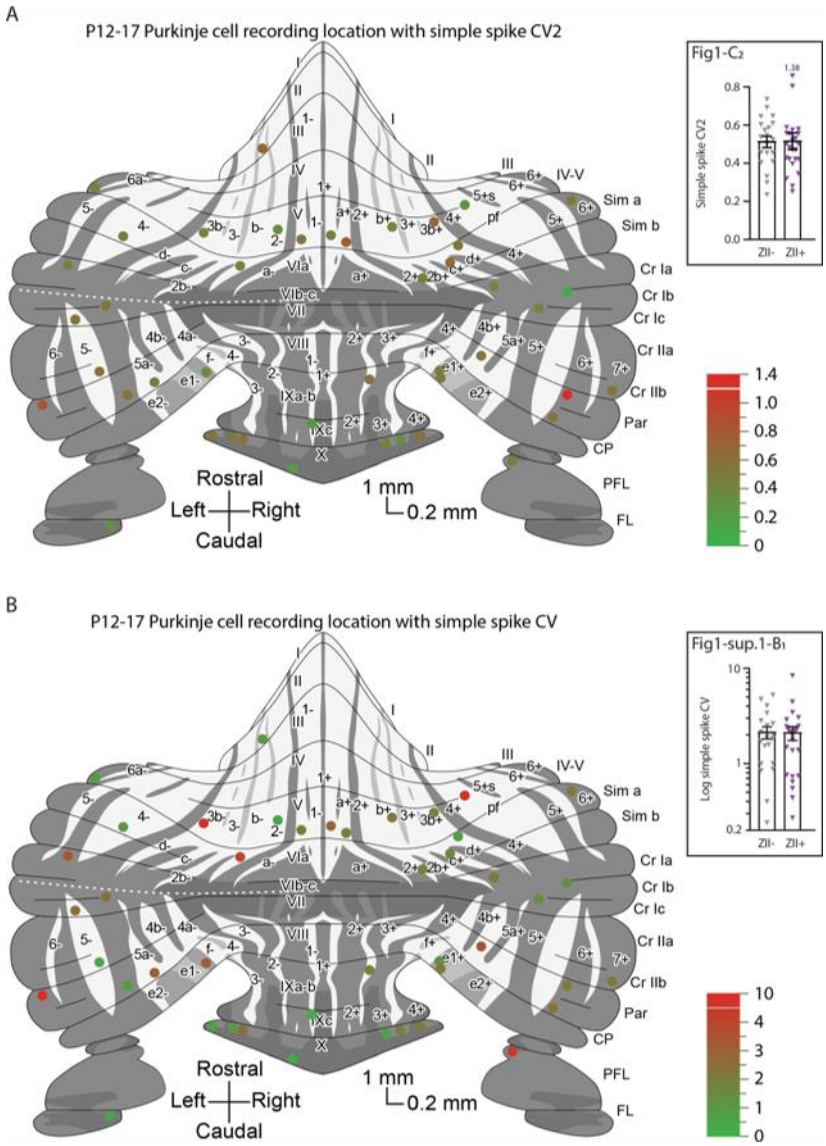

Figure Supplementary 1.4. Overview with color-coded simple spike and complex spike rate for all identified ZebrinII– and ZebrinII+ Purkinje cells. (**A**) P12-P17 Purkinje cell recording location with simple spike rate and (**B**) P12-P17 Purkinje cell recording location with complex spike rate.

© 2007, John Wiley & Sons. The schematic drawing in panels A and B is redrawn from Figure 3 from Sugihara and Quy, 2007b, with permission from John Wiley & Sons, Inc. It is not covered by the CC-BY 4.0 licence and further reproduction of this panel would need permission from the copyright holder.

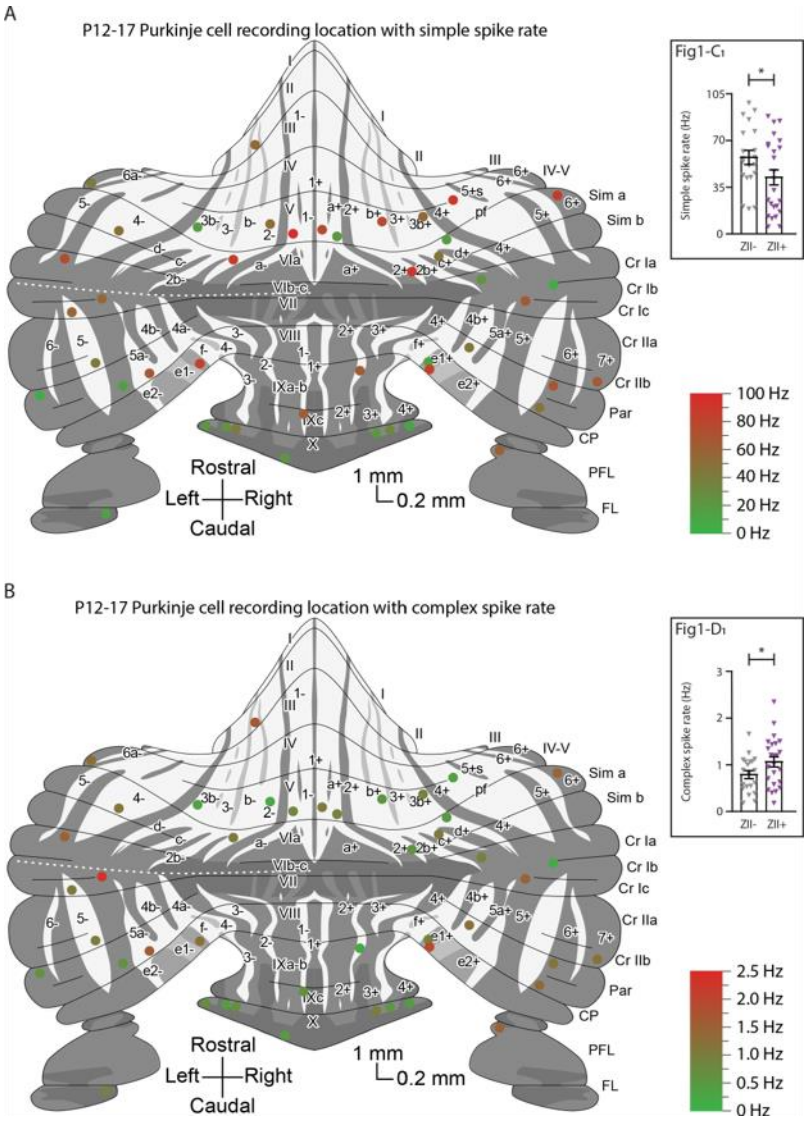

Figure Supplementary 1.5. Overview with color-coded simple spike coefficient of variation 2 (CV2) and coefficient of variation (CV) for all identified ZebrinII– and ZebrinII+ cells. (**A**) P12-P17 Purkinje cell recording location with simple spike coefficient of variation (CV2) and (**B**) P12-P17 Purkinje cell recording location with simple spike coefficient of variation (CV).

© 2007, John Wiley & Sons. The schematic drawing in panels A and B is redrawn from Figure 3 from Sugihara and Quy, 2007b with permission from John Wiley & Sons, Inc. It is not covered by the CC-BY 4.0 licence and further reproduction of this panel would need permission from the copyright holder.

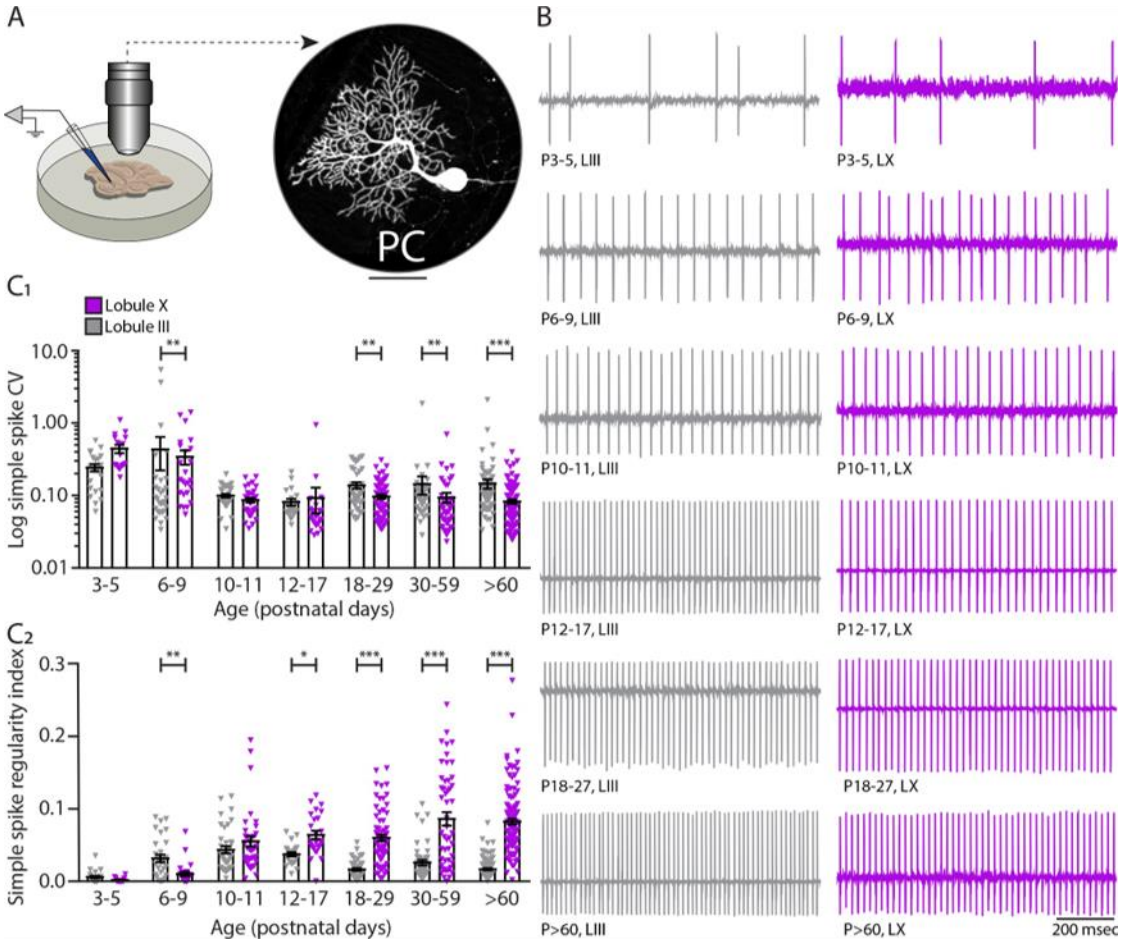

Figure Supplementary 2.1 ***In vitro*** **cell-attached recordings of intrinsic activity in different Purkinje cell populations during development.** (**A**) Schematic of cell-attached recordings *in vitro* in lobules III and X (left) and example of a Purkinje cell filled with biocytin and stained afterwards (right). (**B**) Example traces of cell-attached recordings of lobule III and X Purkinje cells at different developmental ages. (**C_1**) Purkinje cell coefficient of variation (CV) and (**C_2**) regularity index recorded *in vitro* for lobule III Purkinje cells (gray) and lobule X Purkinje cells (purple) in seven age groups. Age groups: P3-5, P6-9, P10-11, P12-17, P18-29, P30-59, and>P60. Error bars represent SEM., for values see Table Supplementary 1. * denotes $p<0.05$, ** $p<0.001$, and *** $p<0.0001$. Scale bar = (**A**) 50 µm.

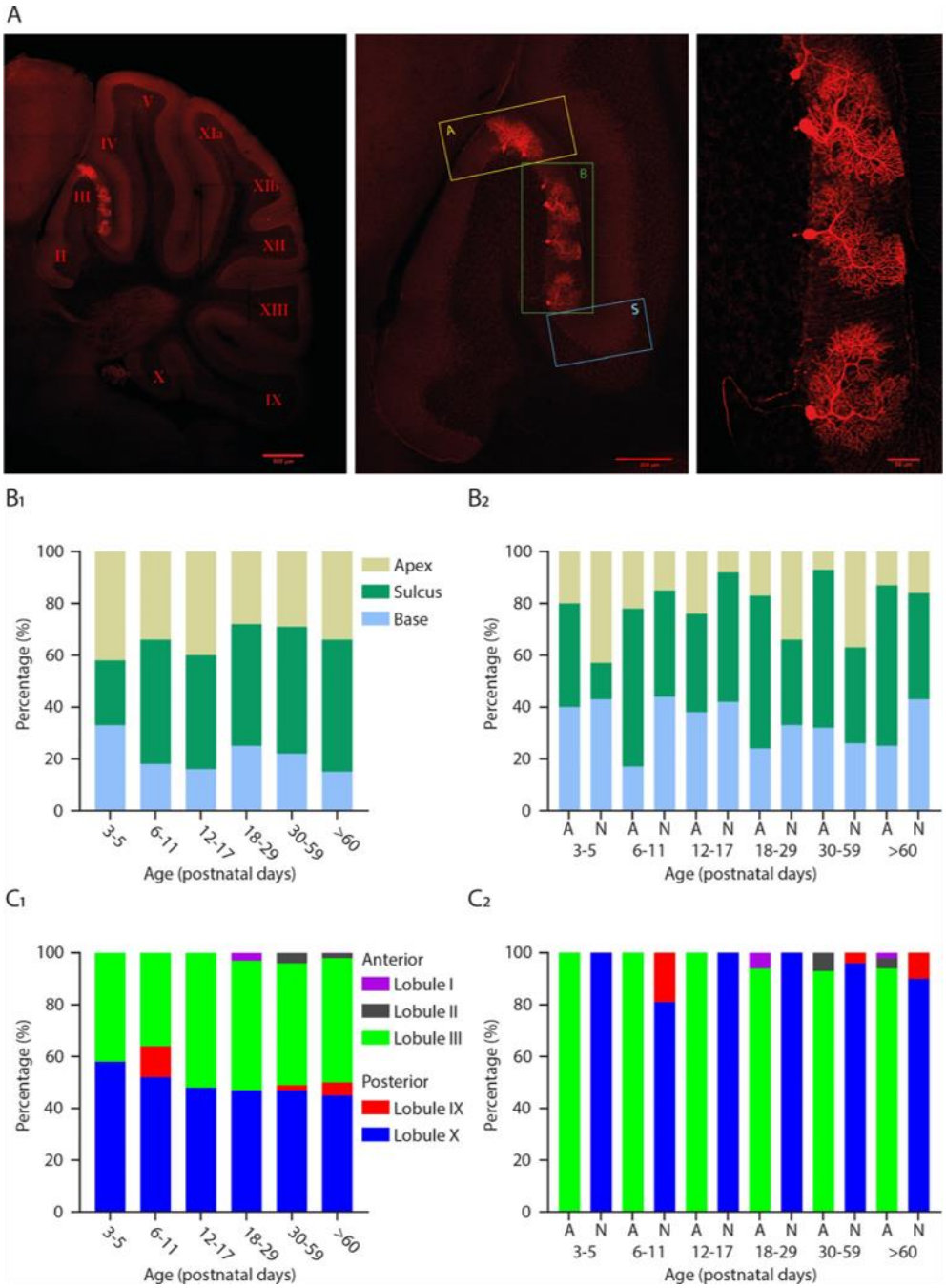

Figure Supplementary 3.1. Purkinje cell location in the cerebellum within each lobule. (**A**) Photomicrographs of Purkinje cells filled with biocytin in lobule III; regions within lobule III (A=apex; B=base; S=sulcus), Scale bar=500, 200 and 50 µm. (**B_1**) Percentage of Purkinje cells localized in the apex, sulcus or base at different developmental ages and (**B_2**) percentage of Purkinje cells localized in the apex, sulcus or base at different developmental ages between A (anterior) and N (nodular) lobules. (**C_1**) Percentage of Purkinje cells localized in anterior lobules I, II, and III and nodular lobules IX and X at different developmental ages and (**C_2**) percentage of Purkinje cells localized in lobules I, II, and III and lobules IX and X at different developmental ages between A (anterior) and N (nodular) lobules.

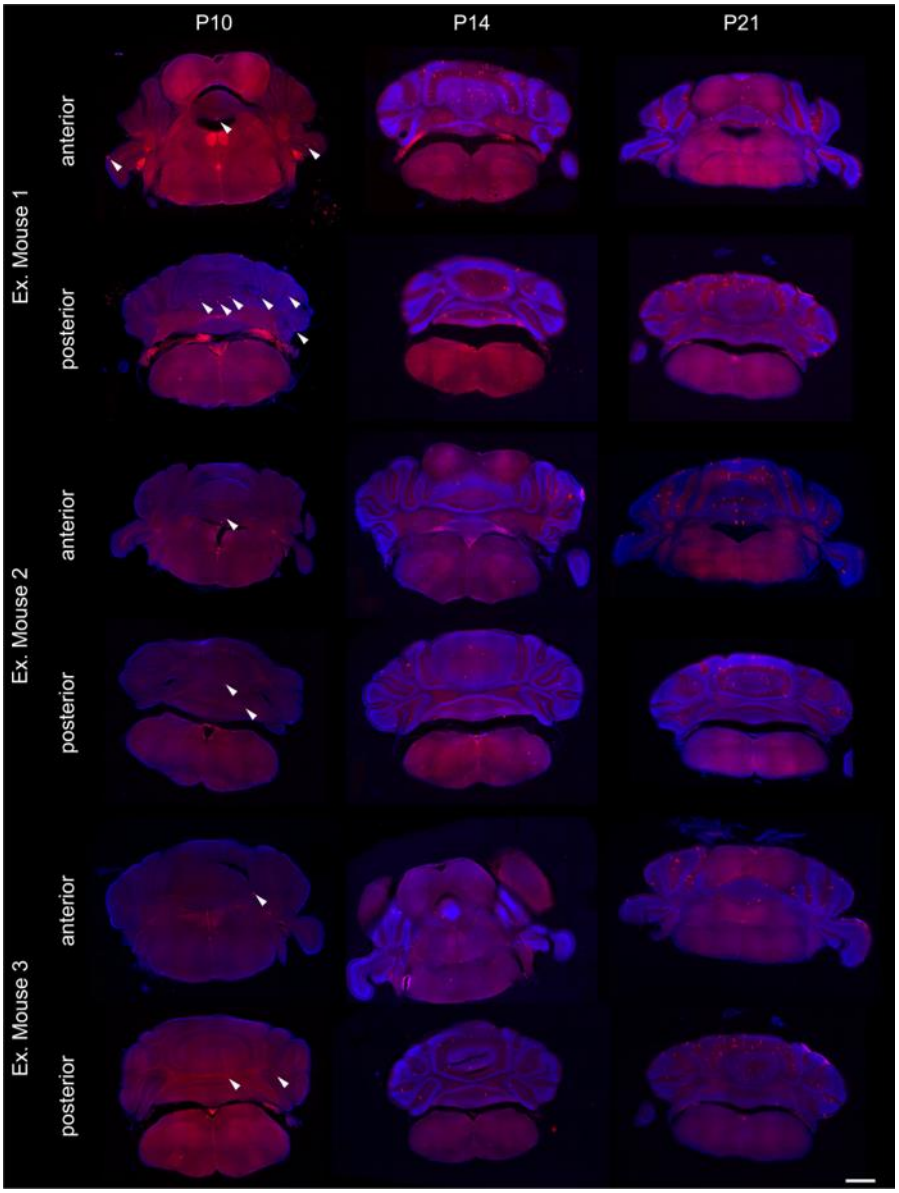

Figure Supplementary 5.1. Random distribution of labeled Purkinje cells for axon analysis. Sparsely labeled Purkinje cells are randomly distributed throughout the cerebellar cortex at P10, P14, and P21 as exemplified by three representative mice at each age. Purkinje cells are labeled with red fluorescent protein (RFP, red) and the structure of the sections are visible with DAPI (blue). A representative coronal section from the anterior and posterior cerebellum are shown for each mouse. White arrowheads indicate Purkinje cells at P10 when dendrites are not as developed. Purkinje cells in coronal sections are visible as planar lines at P14 and P21. Scale bar=1 mm.

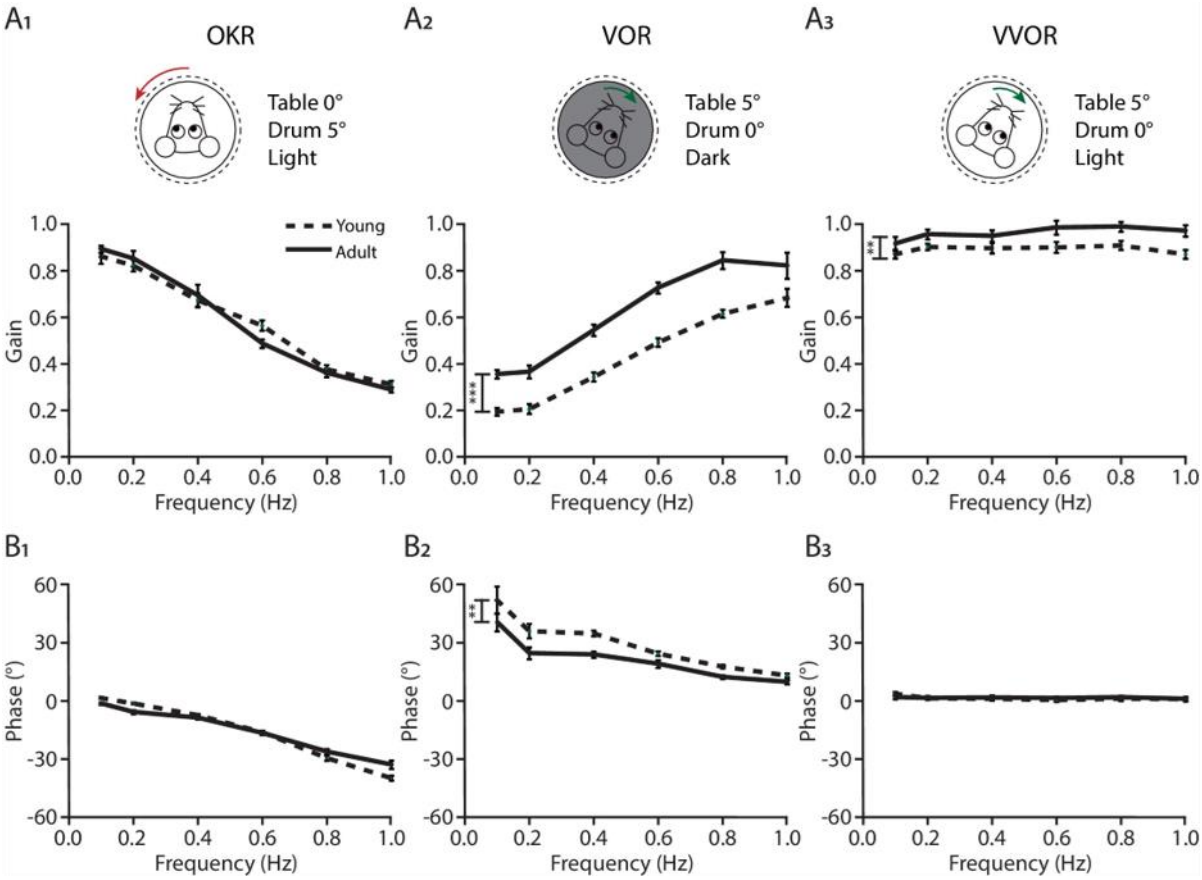

Figure Supplementary 6.1. Compensatory eye movements in young and adult mice. Gain (top) and phase (bottom) of baseline performance of compensatory eye movements: (**A_1 and B_1**) the optokinetic reflex (OKR), (**A_2 and B_2**) the vestibulo-ocular reflex (VOR) and (**A_3 and B_3**) the visually enhanced VOR (VVOR) in young (dotted line) and adult (full line) mice. Error bars represent SEM., for values see Table Supplementary 1. * denotes $p<0.05$, ** $p<0.001$ and *** $p<0.0001$.

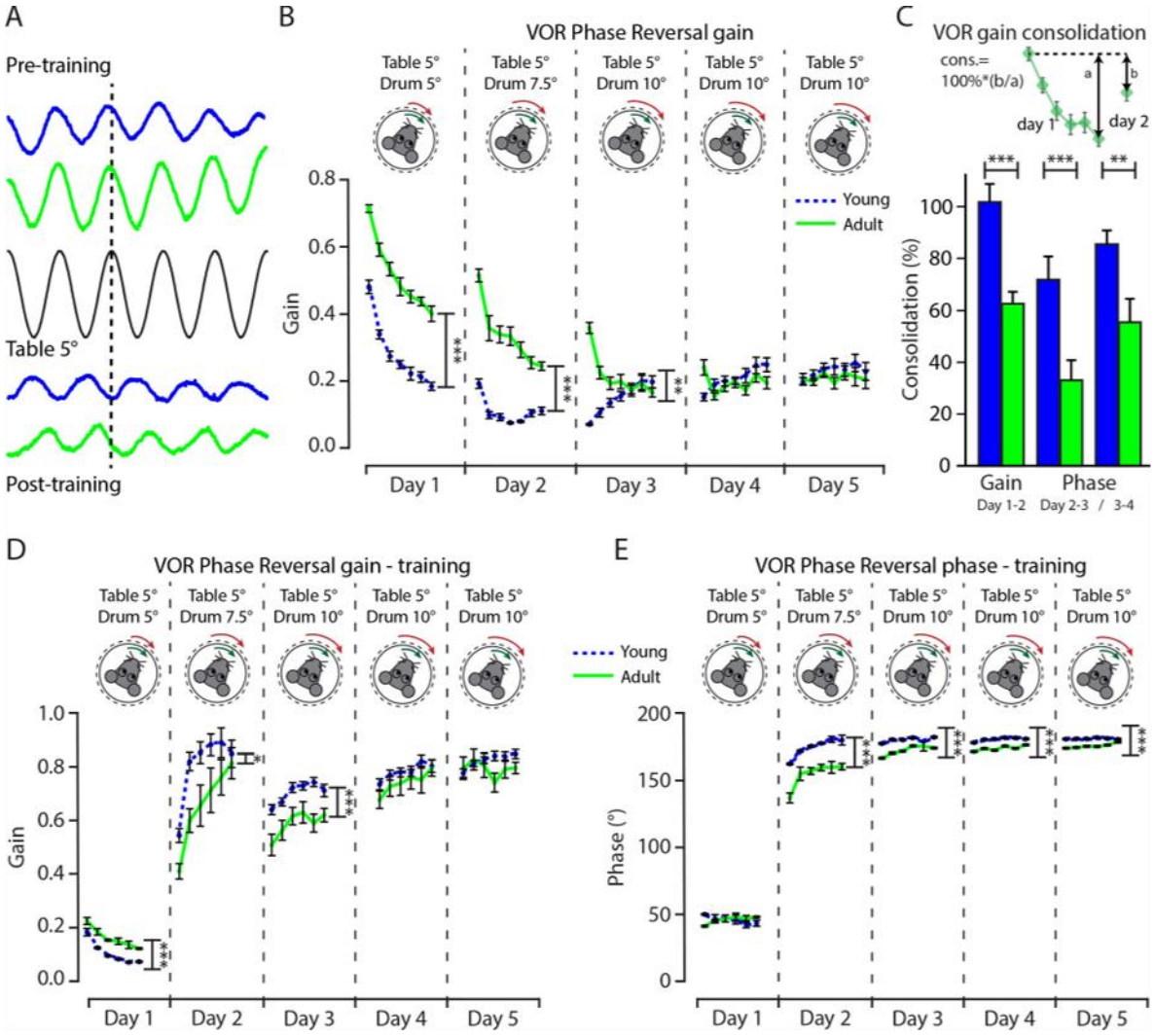

Figure Supplementary 6.2. Vestibulo-ocular reflex phase reversal gain, overnight consolidation, and gaze during training differ between juvenile and adult mice. (**A**) Example trace of eye movement position in young (blue) and adult (green) mice before and after training in relation with the table position (black) at an amplitude of 5°. (**B**) Gain of 5 days of vestibulo-ocular reflex (VOR) phase reversal, probed by recording VOR (in the dark before, between, and after sessions) with mice kept in the dark in between experimental sessions, in young (dotted line blue) and adult (full line green) mice. (**C**) Illustration of VOR gain consolidation analysis and the percentage of consolidation between young (blue) and adult (green) mice at days 1-2, 2–3, and 3–4. (**D**) Gain and (**E**) phase of 5 days of VOR phase reversal training, in young (dotted line blue) and adult (full line green) mice. Error bars represent SEM., for values see Table Supplementary 1. * denotes $p<0.05$, ** $p<0.001$, and *** $p<0.0001$.

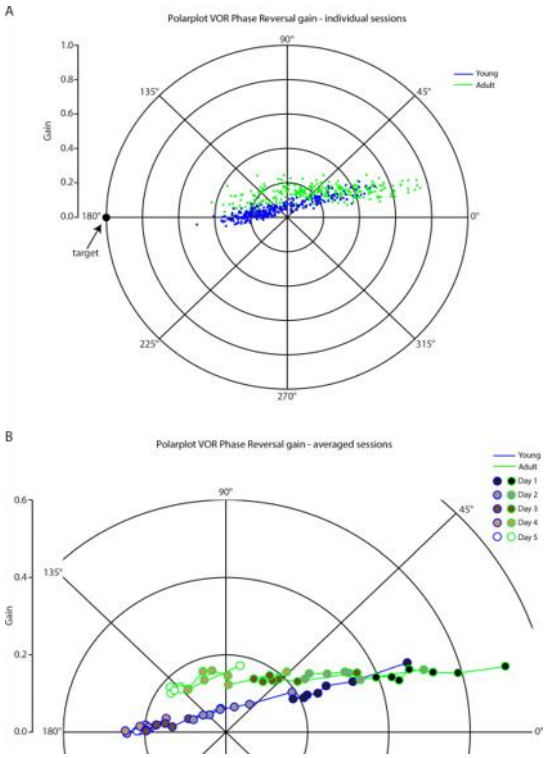

Figure Supplementary 6.3. Polar plot for vestibulo-ocular reflex phase reversal gain. Vestibulo-ocular reflex (VOR) phase reversal gain in (**A**) individual sessions and (**B**) averaged sessions per 5 days in young (blue) and adult (green) mice.

Table Supplementary 1

Related Figure	Test applied	Groups	*p*-value	Descriptive values	Number of cells / mice
Figure1 C_1 Simple spike rate (*in vivo*)	Two-way ANOVA multiple comparisons	P12-P17 Z– vs P12-P17 Z+	0.013	57.3 ± 5.3 Hz vs 42.3 ± 5.7 Hz	20 cells vs 24 cells from 24 mice
		P18-P29 Z– vs P18-P29 Z+	0.026	69.0 ± 4.4 Hz vs 55.9 ± 3.2 Hz	17 cells vs 34 cells from 25 mice
		P30-P59 Z– vs P30-P59 Z+	<0.0001	78.4 ± 3.2 Hz vs 56.7 ± 2.2 Hz	43 cells vs 47 cells from 48 mice
		>P60 Z– vs >P60 Z+	<0.0001	89.2 ± 2.3 Hz vs 61.5 ± 2.4 Hz	70 cells vs 62 cells from 64 mice
		>P60 Z– vs P12-17 Z–	<0.0001	89.2 ± 2.3 Hz vs 57.3 ± 5.3 Hz	70 cells vs 20 cells from 51 mice
		>P60 Z– vs P18-29 Z–	0.0002	89.2 ± 2.3 Hz vs 69.0 ± 4.4 Hz	70 cells vs 17 cells from 53 mice
		>P60 Z– vs P30-P59 Z–	0.0049	89.2 ± 2.3 Hz vs 78.4 ± 3.2 Hz	70 cells vs 43 cells from 72 mice
		>P60 Z+ vs P12-17 Z+	<0.0001	61.5 ± 2.4 Hz vs 42.3 ± 5.7 Hz	62 cells vs 24 cells from 59 mice
		>P60 Z+ vs P18-29 Z+	0.19	61.5 ± 2.4 Hz vs 55.9 ± 3.2 Hz	62 cells vs 34 cells from 59 mice
		>P60 Z+ vs P30-P59 +	0.22	61.5 ± 2.4 Hz vs 56.8 ± 2.2 Hz	62 cells vs 47 cells from 68 mice
Figure1 C_2 Simple spike CV2 (*in vivo*)	Two-way ANOVA multiple comparisons	P12-P17 Z– vs P12-P17 Z+	0.940	0.51 ± 0.03 vs 0.51 ± 0.04	20 cells vs 24 cells from 24 mice
		P18-P29 Z– vs P18-P29 Z+	0.020	0.50 ± 0.02 vs 0.42 ± 0.02	17 cells vs 34 cells from 25 mice
		P30-P59 Z– vs P30-P59 Z+	<0.0001	0.44 ± 0.01 vs 0.34 ± 0.01	43 cells vs 47 cells from 48 mice
		>P60 Z– vs >P60 Z+	<0.001	0.47 ± 0.01 vs 0.40 ± 0.01	70 cells vs 62 cells from 64 mice
Figure1 D_1 Complex spike rate (*in vivo*)	Two-way ANOVA multiple comparisons	P12-P17 Z– vs P12-P17 Z+	0.011	0.79 ± 0.09 Hz vs 1.06 ± 0.11 Hz	20 cells vs 24 cells from 24 mice
		P18-P29 Z– vs P18-P29 Z+	<0.001	1.50 ± 0.15 Hz vs 1.14 ± 0.08 Hz	17 cells vs 34 cells from 25 mice
		P30-P59 Z– vs P30-P59 Z+	0.019	1.25 ± 0.04 Hz vs 1.07 ± 0.04 Hz	43 cells vs 47 cells from 48 mice
		>P60 Z– vs >P60 Z+	<0.0001	1.24 ± 0.03 Hz vs 0.94 ± 0.04 Hz	70 cells vs 62 cells from 64 mice

		>P60 Z– vs P12-17 Z–	<0.0001	1.24 ± 0.03 Hz vs 0.79 ± 0.09 Hz	70 cells vs 20 cells from 51 mice
		>P60 Z– vs P18-29 Z–	0.005	1.24 ± 0.03 Hz vs 1.50 ± 0.16 Hz	70 cells vs 17 cells from 53 mice
		>P60 Z– vs P30-P59 Z–	0.86	1.24 ± 0.03 Hz vs 1.25 ± 0.04 Hz	70 cells vs 43 cells from 72 mice
		>P60 Z+ vs P12-17 Z+	0.16	0.94 ± 0.04 Hz vs 1.06 ± 0.11 Hz	62 cells vs 24 cells from 59 mice
		>P60 Z+ vs P18-29 Z+	0.010	0.94 ± 0.04 Hz vs 1.14 ± 0.08 Hz	62 cells vs 34 cells from 59 mice
		>P60 Z+ vs P30-P59 +	0.06	0.94 ± 0.04 Hz vs 1.07 ± 0.04 Hz	62 cells vs 47 cells from 68 mice
Figure1 D_2 Climbing fiber pause (*in vivo*)	Kruskal-Wallis test multiple comparisons	P12-P17 Z– vs P12-P17 Z+	0.940	81.1 ± 12.7 msec vs 79.6 ± 13.8 msec	20 cells vs 24 cells from 24 mice
		P18-P29 Z– vs P18-P29 Z+	0.007	27.2 ± 6.1 msec vs 44.3 ± 5.6 msec	17 cells vs 34 cells from 25 mice
		P30-P59 Z– vs P30-P59 Z+	<0.0001	19.9 ± 1.6 msec vs 28.9 ± 1.9 msec	43 cells vs 47 cells from 48 mice
		>P60 Z– vs >P60 Z+	<0.0001	20.0 ± 0.8 msec vs 34.5 ± 2.4 msec	70 cells vs 62 cells from 64 mice

Related Figure	**Test applied**	**Groups**	***p*-value**	**Descriptive values**	**Number of cells / mice**
Figure2 B_1 Simple spike rate (*in vitro*)	Two-way ANOVA multiple comparisons	P3-P5 LIII vs P3-P5 LX	0.78	6.0 ± 0.5 Hz vs 4.1 ± 0.8 Hz	23 cells vs 18 cells from 3 mice
		P6-P9 LIII vs P6-P9 LX	0.99	14.9 ± 1.3 Hz vs 14.8 ± 1.6 Hz	30 cells vs 25 cells from 6 mice
		P10-P11 LIII vs P10-P11 LX	0.65	28.2 ± 1.5 Hz vs 25.9 ± 1.6 Hz	37 cells vs 36 cells from 3 mice
		P12-P17 LIII vs P12-P17 LX	0.008	51.7 ± 3.4 Hz vs 34.8 ± 2.0 Hz	23 cells vs 25 cells from 4 mice
		P18-P29 LIII vs P18-P29 LX	0.002	55.8 ± 5.6 Hz vs 42.4 ± 2.9 Hz	43 cells vs 73 cells from 9 mice
		P30-P59 LIII vs P30-P59 LX	0.003	59.1 ± 4.8 Hz vs 45.6 ± 3.6 Hz	44 cells vs 50 cells from 7 mice
		>P60 LIII vs >P60 LX	<0.0001	61.2 ± 2.5 Hz vs 46.3 ± 1.9 Hz	102 cells vs 121 cells from 17 mice
		P3-P5 LIII vs P10-P11 LIII	0.0002	6.0 ± 0.5 Hz vs 28.2 ± 1.5 Hz	23 cells vs 37 cells from 6 mice

		P3-P5 LX vs P10-P11 LX	0.0007	4.1 ± 0.8 Hz vs 25.9 ± 1.6 Hz	18 cells vs 36 cells from 6 mice
		>P60 Z– vs P3-5 Z–	<0.0001	61.2 ± 2.5 Hz vs 6.0 ± 0.5 Hz	102 cells vs 23 cells from 20 mice
		>P60 Z– vs P6-9 Z–	<0.0001	61.2 ± 2.5 Hz vs 14.9 ± 1.3 Hz	102 cells vs 30 cells from 23 mice
		>P60 Z– vs P10-11 Z–	<0.0001	61.2 ± 2.5 Hz vs 28.2 ± 1.5 Hz	102 cells vs 37 cells from 20 mice
		>P60 Z– vs P12-17 Z–	0.05	61.2 ± 2.5 Hz vs 51.7 ± 3.4 Hz	102 cells vs 23 cells from 21 mice
		>P60 Z– vs P18-29 Z–	0.17	61.2 ± 2.5 Hz vs 55.8 ± 5.6 Hz	102 cells vs 43 cells from 26 mice
		>P60 Z– vs P30-P59 Z–	0.59	61.2 ± 2.5 Hz vs 59.1 ± 4.8 Hz	102 cells vs 44 cells from 24 mice
		>P60 Z+ vs P3-5 Z+	<0.0001	46.3 ± 1.9 Hz vs 4.1 ± 0.8 Hz	121 cells vs 18 cells from 20 mice
		>P60 Z+ vs P6-9 Z+	<0.0001	46.3 ± 1.9 Hz vs 14.8 ± 1.6 Hz	121 cells vs 25 cells from 23 mice
		>P60 Z+ vs P10-11 Z+	<0.0001	46.3 ± 1.9 Hz vs 25.9 ± 1.6 Hz	121 cells vs 36 cells from 20 mice
		>P60 Z+ vs P12-17 Z+	0.014	46.3 ± 1.9 Hz vs 34.8 ± 2.0 Hz	121 cells vs 25 cells from 21 mice
		>P60 Z+ vs P18-29 Z+	0.22	46.3 ± 1.9 Hz vs 42.4 ± 2.9 Hz	121 cells vs 73 cells from 26 mice
		>P60 Z+ vs P30-P59 +	0.85	46.3 ± 1.9 Hz vs 45.6 ± 3.6 Hz	121 cells vs 50 cells from 24 mice
Figure2 B_2 Simple spike CV2 (*in vitro*)	Kruskal-Wallis test multiple comparisons	P3-P5 LIII vs P3-P5 LX	0.36	0.22 ± 0.04 vs 0.37 ± 0.07	23 cells vs 18 cells from 3 mice
		P6-P9 LIII vs P6-P9 LX	0.002	0.11 ± 0.02 vs 0.22 ± 0.04	30 cells vs 25 cells from 6 mice
		P10-P11 LIII vs P10-P11 LX	0.43	0.05 ± 0.00 vs 0.05 ± 0.00	37 cells vs 36 cells from 3 mice
		P12-P17 LIII vs P12-P17 LX	0.07	0.05 ± 0.00 vs 0.09 ± 0.05	23 cells vs 25 cells from 4 mice
		P18-P29 LIII vs P18-P29 LX	<0.0001	0.11 ± 0.01 vs 0.05 ± 0.00	43 cells vs 73 cells from 9 mice
		P30-P59 LIII vs P30-P59 LX	<0.0001	0.09 ± 0.01 vs 0.06 ± 0.01	44 cells vs 50 cells from 7 mice
		>P60 LIII vs >P60 LX	<0.0001	0.11 ± 0.01 vs 0.04 ± 0.00	102 cells vs 121 cells from 17 mice

Related Figure	Test applied	Groups	*p*-value	Descriptive values	Number of cells / mice
Figure3 B_1 Dendritic intersections (sholl)	Two-way ANOVA multiple comparisons	P3-P5 LI-III vs P3-P5 LIX-X	0.79	26.2 ± 4.0 vs 42.77 ± 9.1	9 cells vs 12 cells from 3 mice
		P6-P11 LI-III vs P6-P11 LIX-X	0.52	86.8 ± 9.2 vs 64.1 ± 7.3	28 cells vs 38 cells from 9 mice
		P12-P17 LI-III vs P12-P17 LIX-X	0.38	336.1 ± 31.7 vs 291.2 ± 17.1	18 cells vs 14 cells from 4 mice
		P18-P29 LI-III vs P18-P29 LIX-X	<0.0001	530.9 ± 41.6 vs 304.5 ± 31.3	14 cells vs 15 cells from 9 mice
		P30-P59 LI-III vs P30-P59 LIX-X	<0.0001	651.3 ± 25.4 vs 351.6 ± 28.1	38 cells vs 35 cells from 7 mice
		>P60 LI-III vs >P60 LIX-X	<0.0001	663.1 ± 23.8 vs 445.7 ± 22.2	61 cells vs 59 cells from 17 mice
		>P60 LI-III vs P3-5 LI-III	<0.0001	663.1 ± 23.8 vs 26.2 ± 4.0	61 cells vs 9 cells from 33 mice
		>P60 LI-III vs P6-11 LI-III	<0.0001	663.1 ± 23.8 vs 86.8 ± 9.2	61 cells vs 28 cells from 38 mice
		>P60 LI-III vs P12-17 LI-III	<0.0001	663.1 ± 23.8 vs 336.1 ± 31.7	61 cells vs 18 cells from 34 mice
		>P60 LI-III vs P18-29 LI-III	0.002	663.1 ± 23.8 vs 531.0 ± 41.6	61 cells vs 14 cells from 33 mice
		>P60 LI-III vs P30-P59 LI-III	0.68	663.1 ± 23.8 vs 651.3 ± 25.4	61 cells vs 38 cells from 43 mice
		->P60 LIX-X vs P3-5 LIX-X	<0.0001	445.7 ± 22.2 vs 42.7 ± 9.1	59 cells vs 12 cells from 31 mice
		>P60 LIX-X vs P6-11 LIX-X	<0.0001	445.7 ± 22.2 vs 64.1 ± 7.3	59 cells vs 38 cells from 36 mice
		>P60 LIX-X vs P12-17 LIX-X	0.0003	445.7 ± 22.2 vs 291.2 ± 17.1	59 cells vs 14 cells from 29 mice
		>P60 LIX-X vs P18-29 LIX-X	0.0007	445.7 ± 22.2 vs 304.5 ± 31.3	59 cells vs 15 cells from 32 mice
		>P60 LIX-X vs P30-P59 LIX-X	0.002	445.7 ± 22.2 vs 351.6 ± 28.1	59 cells vs 35 cells from 40 mice
Figure3 B_2	Two-way ANOVA multiple comparisons	P3-P5 LI-III vs P3-P5 LIX-X	0.45	32.8 ± 2.9 µm vs 44.6 ± 5.5 µm	9 cells vs 12 cells from 3 mice
		P6-P11 LI-III vs P6-P11 LIX-X	0.12	73.0 ± 4.8 µm vs 89.3 ± 7.0 µm	28 cells vs 38 cells from 9 mice

Dendritic length from soma		P12-P17 LI-III vs P12-P17 LIX-X	0.74	138.3 ± 5.1 µm vs 142.5 ± 3.9 µm	18 cells vs 14 cells from 4 mice
		P18-P29 LI-III vs P18-P29 LIX-X	0.012	193.9 ± 12.8 µm vs 160.7 ± 11.0 µm	14 cells vs 15 cells from 9 mice
		P30-P59 LI-III vs P30-P59 LIX-X	<0.0001	215.1 ± 6.7 µm vs 160.3 ± 5.7 µm	38 cells vs 35 cells from 7 mice
		>P60 LI-III vs >P60 LIX-X	<0.0001	206.6 ± 5.9 µm vs 169.9 ± 4.0 µm	61 cells vs 59 cells from 17 mice
Figure3 B_3 Dendritic area size	Two-way ANOVA multiple comparisons	P3-P5 LI-III vs P3-P5 LIX-X	0.92	536 ± 45 μm^2 vs 648.8 ± 102 μm^2	9 cells vs 12 cells from 3 mice
		P6-P11 LI-III vs P6-P11 LIX-X	0.62	1807 ± 187 μm^2 vs 1489 ± 139 μm^2	28 cells vs 38 cells from 9 mice
		P12-P17 LI-III vs P12-P17 LIX-X	0.46	5419 ± 399 μm^2 vs 6109 ± 462 μm^2	18 cells vs 14 cells from 4 mice
		P18-P29 LI-III vs P18-P29 LIX-X	<0.0001	10541 ± 761 μm^2 vs 6200 ± 603 μm^2	14 cells vs 15 cells from 9 mice
		P30-P59 LI-III vs P30-P59 LIX-X	<0.0001	13011 ± 583 μm^2 vs 7763 ± 499 μm^2	38 cells vs 35 cells from 7 mice
		>P60 LI-III vs >P60 LIX-X	<0.0001	10890 ± 412 μm^2 vs 8520 ± 377 μm^2	61 cells vs 59 cells from 17 mice
Figure4 B_1 Molecular layer thickness	Two-way ANOVA multiple comparisons	P7 LI-III vs P7 LIX-X	0.16	21.8 ± 1.8 µm vs 28.6 ± 0.2 µm	3 mice
		P14 LI-III vs P14 LIX-X	0.78	101.5 ± 3.3 µm vs 102.9 ± 3.6 µm	3 mice
		P21 LI-III vs P21 LIX-X	0.002	118.9 ± 2.9 µm vs 101.8 ± 0.3 µm	3 mice
		P35 LI-III vs P35 LIX-X	0.05	126.3 ± 6.8 µm vs 116.7 ± 1.8 µm	3 mice
		P60 LI-III vs P60 LIX-X	<0.001	137.5 ± 1.3 µm vs 116.9 ± 4.9 µm	3 mice

Related Figure	**Test applied**	**Groups**	***p*-value**	**Descriptive values**	**Number of cells / mice**
Figure4 B_2 Molecular layer VGluT2 puncta	Two-way ANOVA multiple comparisons	P7 LI-III vs P7 LIX-X	<0.0001	0.62 ± 0.31 % vs 3.87 ± 0.19 %	3 mice
		P14 LI-III vs P14 LIX-X	0.78	1.67 ± 0.17 % vs 1.51 ± 0.23 %	3 mice
		P21 LI-III vs P21 LIX-X	0.79	1.26 ± 0.31 % vs 1.41 ± 0.11 %	3 mice

		P35 LI-III vs P35 LIX-X	0.88	3.50 ± 0.98 % vs 3.58 ± 0.35 %	3 mice
		P60 LI-III vs P60 LIX-X	0.76	2.74 ± 0.23 % vs 2.91 ± 0.13 %	3 mice
Figure4 B_3 Climbing fiber coverage of molecular layer	Two-way ANOVA multiple comparisons	P7 LI-III vs P7 LIX-X	<0.0001	11.1 ± 1.1 % vs 80.5 ± 1.0 %	3 mice
		P14 LI-III vs P14 LIX-X	0.24	62.4 ± 1.1 % vs 66.9 ± 7.8 %	3 mice
		P21 LI-III vs P21 LIX-X	0.41	69.1 ± 0.3 % vs 66.0 ± 1.7 %	3 mice
		P35 LI-III vs P35 LIX-X	0.36	85.1 ± 1.0 % vs 81.5 ± 1.1 %	3 mice
		P60 LI-III vs P60 LIX-X	0.66	82.7 ± 0.6 % vs 81.0 ± 0.4 %	3 mice
		P60 LI-III vs P7 LI-III	<0.0001	82.7 ± 0.6 % vs 11.1 ± 1.1 %	3 mice vs 3 mice
		P60 LI-III vs P14 LI-III	<0.0001	82.7 ± 0.6 % vs 62.4 ± 1.1 %	3 mice vs 3 mice
		P60 LI-III vs P21 LI-III	0.002	82.7 ± 0.6 % vs 69.1 ± 0.3 %	3 mice vs 3 mice
		P60 LI-III vs P35 LI-III	0.54	82.7 ± 0.6 % vs 85.1 ± 1.0 %	3 mice vs 3 mice
		P60 LIX-X vs P7 LIX-X	0.89	81.0 ± 0.4 % vs 80.5 ± 1.0 %	3 mice vs 3 mice
		P60 LIX-X vs P14 LIX-X	0.002	81.0 ± 0.4 % vs 66.9 ± 7.8 %	3 mice vs 3 mice
		P60 LIX-X vs P21 LIX-X	0.001	81.0 ± 0.4 % vs 66.0 ± 1.7 %	3 mice vs 3 mice
		P60 LIX-X vs P35 LIX-X	0.90	81.0 ± 0.4 % vs 81.5 ± 1.1 %	3 mice vs 3 mice
Figure5 D_1 Axonal intersections (sholl) P10	Two-way ANOVA multiple comparisons	P10 Z– vs P10 Z+	0.045	233.0 ± 42.4 vs 273.25 ± 68.5	7 axons vs 8 axons from 8 mice
Figure5 D_2	Two-way ANOVA multiple comparisons	P14 Z– vs P14 Z+	0.001	246.3 ± 22.8 vs 293.1 ± 24.6	11 axons vs 20 axons from 10 mice

Axonal intersections (sholl) P14					
Figure5 D_3 Axonal intersections (sholl) P21	Two-way ANOVA multiple comparisons	P21 Z– vs P21 Z+	0.038	274.2 ± 73.5 vs 306.6 ± 42.5	8 axons vs 18 axons from 7 mice
Figure5 E_1 Axonal intersections (sholl)	One-way ANOVA multiple comparisons	P7, P10, P14, P21	0.013	84.2 ± 18.2, 254.4 ± 40.5, 277.4 ± 17.5, 296.4 ± 37.9	6, 15, 31, 26 axons from 29 mice
Related Figure	**Test applied**	**Groups**	***p*-value**	**Descriptive values**	**Number of cells / mice**
Figure5 E_2 Axonal length from first intersection	One-way ANOVA multiple comparisons	P7, P10, P14, P21	0.060	124.2 ± 17.8 µm, 212.6 ± 24.3 µm, 216.4 ± 14.3 µm, 225.2 ± 16.1 µm	6, 15, 31, 26 axons from 29 mice
Figure5 E_3 Axonal area size	One-way ANOVA multiple comparisons	P7, P10, P14, P21	<0.0001	1.52 ± 0.20 $\mu m^2 \cdot 10^3$, 1.46 ± 0.24 $\mu m^2 \cdot 10^3$, 2.26 ± 0.19 $\mu m^2 \cdot 10^3$, 3.07 ± 0.29 $\mu m^2 \cdot 10^3$	6, 15, 31, 26 axons from 29 mice
Figure5 F_1 Axonal intersections (sholl)	Two-way ANOVA multiple comparisons	Interaction effect Z– vs Z+	0.25		
		P10 Z– vs P10 Z+	0.97	233.0 ± 42.4 vs 273.25 ± 68.5	7 axons vs 8 axons from 8 mice
		P14 Z– vs P14 Z+	0.97	246.3 ± 22.8 vs 293.1 ± 24.6	11 axons vs 20 axons from 10 mice
		P21 Z– vs P21 Z+	0.99	274.2 ± 73.5 vs 306.6 ± 42.5	8 axons vs 18 axons from 7 mice

		P21 Z– vs P10 Z–	0.96	274.2 ± 73.5 vs 233.0 ± 42.4	8 axons vs 7 axons from 41 mice
		P21 Z– vs P14 Z–	>0.99	274.2 ± 73.5 vs 246.3 ± 22.8	8 axons vs 11 axons from 57 mice
		P21 Z+ vs P10 Z+	>0.99	306.6 ± 42.5 vs 273.25 ± 68.5	18 axons vs 8 axons from 41 mice
		P21 Z+ vs P14 Z+	>0.99	306.6 ± 42.5 vs 293.1 ± 24.6	18 axons vs 20 axons from 57 mice
Figure5 F_2 Axonal length from first intersection	Two-way ANOVA multiple comparisons	Interaction effect Z– vs Z+	0.019		
		P10 Z– vs P10 Z+	0.83	200.7 ± 35.4 μm^2 vs 223.1 ± 35.3 μm^2	7 axons vs 8 axons from 8 mice
		P14 Z– vs P14 Z+	0.54	197.3 ± 25.7 μm^2 vs 227.7 ± 18.1 μm^2	11 axons vs 20 axons from 10 mice
		P21 Z– vs P21 Z+	0.74	188.1 ± 28.7 μm^2 vs 241.1 ± 17.7 μm^2	8 axons vs 18 axons from 7 mice
Figure5 F_3 Axonal area size	Two-way ANOVA multiple comparisons	Interaction effect Z– vs Z+	0.025		
		P10 Z– vs P10 Z+	0.82	1.17 ± 0.18 $\mu m^2 \cdot 10^3$ vs 1.73 ± 0.42 $\mu m^2 \cdot 10^3$	7 axons vs 8 axons from 8 mice
		P14 Z– vs P14 Z+	>0.99	2.14 ± 0.26 $\mu m^2 \cdot 10^3$ vs 2.37 ± 0.28 $\mu m^2 \cdot 10^3$	11 axons vs 20 axons from 10 mice
		P21 Z– vs P21 Z+	0.14	2.36 ± 0.46 $\mu m^2 \cdot 10^3$ vs 3.39 ± 0.33 $\mu m^2 \cdot 10^3$	8 axons vs 18 axons from 7 mice
Figure6 A_2 VOR phase reversal	Mixed-effects repeated measures	Young vs Adult day1	<0.0001	25.7 ± 0.9 ° vs 18.7 ± 1.1 °	16 mice vs 11 mice
		Young vs Adult day2	<0.0001	100.4 ± 15.7 ° vs 29.6 ± 2.9 °	
		Young vs Adult day3	<0.0001	162.9 ± 9.9 ° vs 56.4 ± 7.0 °	
		Young vs Adult day4	<0.0001	174.8 ± 1.5 ° vs 102.3 ± 8.7 °	
		Young vs Adult day5	<0.0001	175.9 ± 0.7 ° vs 126.4 ± 7.0 °	
Figure 6 B_2 Eyeblink conditioned response	Mixed-effects repeated measures	Young vs Adult	0.027	20.4 ± 4.4 % vs 30.9 ± 6.0 %	18 mice vs 13 mice

Related Figure	Test applied	Groups	*p*-value	Descriptive values	Number of cells / mice
Figure 7 Simple spike rate *(in vitro)*	Two-way ANOVA multiple comparisons	>P60 Z– vs P3-5 Z–	<0.0001	61.2 ± 2.5 Hz vs 6.0 ± 0.5 Hz	102 cells vs 23 cells from 20 mice
		>P60 Z– vs P6-9 Z–	<0.0001	61.2 ± 2.5 Hz vs 14.9 ± 1.3 Hz	102 cells vs 30 cells from 23 mice
		>P60 Z– vs P10-11 Z–	<0.0001	61.2 ± 2.5 Hz vs 28.2 ± 1.5 Hz	102 cells vs 37 cells from 20 mice
		>P60 Z– vs P12-17 Z–	0.05	61.2 ± 2.5 Hz vs 51.7 ± 3.4 Hz	102 cells vs 23 cells from 21 mice
		>P60 Z– vs P18-29 Z–	0.17	61.2 ± 2.5 Hz vs 55.8 ± 5.6 Hz	102 cells vs 43 cells from 26 mice
		>P60 Z– vs P30-P59 Z–	0.59	61.2 ± 2.5 Hz vs 59.1 ± 4.8 Hz	102 cells vs 44 cells from 24 mice
		>P60 Z+ vs P3-5 Z+	<0.0001	46.3 ± 1.9 Hz vs 4.1 ± 0.8 Hz	121 cells vs 18 cells from 20 mice
		>P60 Z+ vs P6-9 Z+	<0.0001	46.3 ± 1.9 Hz vs 14.8 ± 1.6 Hz	121 cells vs 25 cells from 23 mice
		>P60 Z+ vs P10-11 Z+	<0.0001	46.3 ± 1.9 Hz vs 25.9 ± 1.6 Hz	121 cells vs 36 cells from 20 mice
		>P60 Z+ vs P12-17 Z+	0.014	46.3 ± 1.9 Hz vs 34.8 ± 2.0 Hz	121 cells vs 25 cells from 21 mice
		>P60 Z+ vs P18-29 Z+	0.22	46.3 ± 1.9 Hz vs 42.4 ± 2.9 Hz	121 cells vs 73 cells from 26 mice
		>P60 Z+ vs P30-P59 +	0.85	46.3 ± 1.9 Hz vs 45.6 ± 3.6 Hz	121 cells vs 50 cells from 24 mice
Figure 7 Simple spike rate *(in vivo)*	Two-way ANOVA multiple comparisons	>P60 Z– vs P12-17 Z–	<0.0001	89.2 ± 2.3 Hz vs 57.3 ± 5.3 Hz	70 cells vs 20 cells from 51 mice
		>P60 Z– vs P18-29 Z–	0.0002	89.2 ± 2.3 Hz vs 69.0 ± 4.4 Hz	70 cells vs 17 cells from 53 mice
		>P60 Z– vs P30-P59 Z–	0.0049	89.2 ± 2.3 Hz vs 78.4 ± 3.2 Hz	70 cells vs 43 cells from 72 mice
		>P60 Z+ vs P12-17 Z+	<0.0001	61.5 ± 2.4 Hz vs 42.3 ± 5.7 Hz	62 cells vs 24 cells from 59 mice
		>P60 Z+ vs P18-29 Z+	0.19	61.5 ± 2.4 Hz vs 55.9 ± 3.2 Hz	62 cells vs 34 cells from 59 mice
		>P60 Z+ vs P30-P59 +	0.22	61.5 ± 2.4 Hz vs 56.8 ± 2.2 Hz	62 cells vs 47 cells from 68 mice

Figure 7 Complex spike rate *(in vivo)*	Two-way ANOVA multiple comparisons	>P60 Z– vs P12-17 Z–	<0.0001	1.24 ± 0.03 Hz vs 0.79 ± 0.09 Hz	70 cells vs 20 cells from 51 mice
		>P60 Z– vs P18-29 Z–	0.005	1.24 ± 0.03 Hz vs 1.50 ± 0.16 Hz	70 cells vs 17 cells from 53 mice
		>P60 Z– vs P30-P59 Z–	0.86	1.24 ± 0.03 Hz vs 1.25 ± 0.04 Hz	70 cells vs 43 cells from 72 mice
		>P60 Z+ vs P12-17 Z+	0.16	0.94 ± 0.04 Hz vs 1.06 ± 0.11 Hz	62 cells vs 24 cells from 59 mice
		>P60 Z+ vs P18-29 Z+	0.010	0.94 ± 0.04 Hz vs 1.14 ± 0.08 Hz	62 cells vs 34 cells from 59 mice
		>P60 Z+ vs P30-P59 +	0.06	0.94 ± 0.04 Hz vs 1.07 ± 0.04 Hz	62 cells vs 47 cells from 68 mice
Figure 7 Dendritic intersections (sholl)	Two-way ANOVA multiple comparisons	>P60 LI-III vs P3-5 LI-III	<0.0001	663.1 ± 23.8 vs 26.2 ± 4.0	61 cells vs 9 cells from 33 mice
		>P60 LI-III vs P6-11 LI-III	<0.0001	663.1 ± 23.8 vs 86.8 ± 9.2	61 cells vs 28 cells from 38 mice
		>P60 LI-III vs P12-17 LI-III	<0.0001	663.1 ± 23.8 vs 336.1 ± 31.7	61 cells vs 18 cells from 34 mice
		>P60 LI-III vs P18-29 LI-III	0.002	663.1 ± 23.8 vs 531.0 ± 41.6	61 cells vs 14 cells from 33 mice
		>P60 LI-III vs P30-P59 LI-III	0.68	663.1 ± 23.8 vs 651.3 ± 25.4	61 cells vs 38 cells from 43 mice
		->P60 LIX-X vs P3-5 LIX-X	<0.0001	445.7 ± 22.2 vs 42.7 ± 9.1	59 cells vs 12 cells from 31 mice
		>P60 LIX-X vs P6-11 LIX-X	<0.0001	445.7 ± 22.2 vs 64.1 ± 7.3	59 cells vs 38 cells from 36 mice
		>P60 LIX-X vs P12-17 LIX-X	0.0003	445.7 ± 22.2 vs 291.2 ± 17.1	59 cells vs 14 cells from 29 mice
		>P60 LIX-X vs P18-29 LIX-X	0.0007	445.7 ± 22.2 vs 304.5 ± 31.3	59 cells vs 15 cells from 32 mice
		>P60 LIX-X vs P30-P59 LIX-X	0.002	445.7 ± 22.2 vs 351.6 ± 28.1	59 cells vs 35 cells from 40 mice

Related Figure	**Test applied**	**Groups**	***p*-value**	**Descriptive values**	**Number of cells / mice**
Figure 7	Two-way ANOVA multiple comparisons	P21 Z– vs P10 Z–	0.96	274.2 ± 73.5 vs 233.0 ± 42.4	8 axons vs 7 axons from 41 mice
		P21 Z– vs P14 Z–	>0.99	274.2 ± 73.5 vs 246.3 ± 22.8	8 axons vs 11 axons from 57 mice
		P21 Z+ vs P10 Z+	>0.99	306.6 ± 42.5 vs 273.25 ± 68.5	18 axons vs 8 axons from 41 mice

Axonal intersections (sholl)		P21 Z+ vs P14 Z+	>0.99	306.6 ± 42.5 vs 293.1 ± 24.6	18 axons vs 20 axons from 57 mice
Figure 7 Climbing fiber coverage of molecular layer	Two-way ANOVA multiple comparisons	P60 LI-III vs P7 LI-III	<0.0001	82.7 ± 0.6 % vs 11.1 ± 1.1 %	3 mice vs 3 mice
		P60 LI-III vs P14 LI-III	<0.0001	82.7 ± 0.6 % vs 62.4 ± 1.1 %	3 mice vs 3 mice
		P60 LI-III vs P21 LI-III	0.002	82.7 ± 0.6 % vs 69.1 ± 0.3 %	3 mice vs 3 mice
		P60 LI-III vs P35 LI-III	0.54	82.7 ± 0.6 % vs 85.1 ± 1.0 %	3 mice vs 3 mice
		P60 LIX-X vs P7 LIX-X	0.89	81.0 ± 0.4 % vs 80.5 ± 1.0 %	3 mice vs 3 mice
		P60 LIX-X vs P14 LIX-X	0.002	81.0 ± 0.4 % vs 66.9 ± 7.8 %	3 mice vs 3 mice
		P60 LIX-X vs P21 LIX-X	0.001	81.0 ± 0.4 % vs 66.0 ± 1.7 %	3 mice vs 3 mice
		P60 LIX-X vs P35 LIX-X	0.90	81.0 ± 0.4 % vs 81.5 ± 1.1 %	3 mice vs 3 mice
Figure Supplement 1.1 B_1 Simple spike CV	Kruskal-Wallis test multiple comparisons	P12-P17 Z– vs P12-P17 Z+	>0.99	2.12 ± 0.31 vs 2.10 ± 0.35	20 cells vs 24 cells from 24 mice
		P18-P29 Z– vs P18-P29 Z+	0.79	0.99 ± 0.18 vs 0.99 ± 0.18	17 cells vs 34 cells from 25 mice
		P30-P59 Z– vs P30-P59 Z+	0.27	0.60 ± 0.12 vs 0.51 ± 0.10	43 cells vs 47 cells from 48 mice
		>P60 Z– vs >P60 Z+	<0.0001	0.68 ± 0.03 vs 0.53 ± 0.05	70 cells vs 62 cells from 64 mice
		P12-P17 Z– vs >P60 Z–	<0.0001	2.12 ± 0.31 vs 0.68 ± 0.03	20 cells vs 70 cells from 51 mice
		P12-P17 Z+ vs >P60 Z+	<0.0001	2.10 ± 0.35 vs 0.53 ± 0.05	24 cells vs 62 cells from 59 mice
Figure Supplement 1.1 B_2 Simple spike regularity index	Kruskal-Wallis test multiple comparisons	P12-P17 Z– vs P12-P17 Z+	0.29	0.19 ± 0.03 vs 0.23 ± 0.03	20 cells vs 24 cells from 24 mice
		P18-P29 Z– vs P18-P29 Z+	0.17	0.10 ± 0.02 vs 0.11 ± 0.02	17 cells vs 34 cells from 25 mice
		P30-P59 Z– vs P30-P59 Z+	0.011	0.06 ± 0.01 vs 0.11 ± 0.02	43 cells vs 47 cells from 48 mice
		>P60 Z– vs >P60 Z+	0.24	0.01 ± 0.00 vs 0.01 ± 0.00	70 cells vs 62 cells from 64 mice
		P12-P17 Z– vs >P60 Z–	<0.0001	0.19 ± 0.03 vs 0.01 ± 0.00	20 cells vs 70 cells from 51 mice

		P12-P17 Z+ vs >P60 Z+	<0.0001	0.23 ± 0.03 vs 0.01 ± 0.00	24 cells vs 62 cells from 59 mice
Figure Supplement 1.1 C_1 Complex spike CV2	Two-way ANOVA multiple comparisons	P12-P17 Z– vs P12-P17 Z+	0.015	0.91 ± 0.03 vs 0.85 ± 0.02	20 cells vs 24 cells from 24 mice
		P18-P29 Z– vs P18-P29 Z+	0.86	0.82 ± 0.02 vs 0.82 ± 0.02	17 cells vs 34 cells from 25 mice
		P30-P59 Z– vs P30-P59 Z+	0.22	0.85 ± 0.01 vs 0.82 ± 0.01	43 cells vs 47 cells from 48 mice
		>P60 Z– vs >P60 Z+	0.034	0.84 ± 0.01 vs 0.81 ± 0.01	70 cells vs 62 cells from 64 mice

Related Figure	**Test applied**	**Groups**	***p*-value**	**Descriptive values**	**Number of cells / mice**
Figure Supplement 1.3 A_1 Simple spike rate P>60	One-way ANOVA multiple comparisons	P>60 LI-II vs P>60 LIII	0.44	91.9 ± 5.3 Hz vs 87.0 ± 3.9 Hz	19 cells vs 22 cells from 22 mice
		P>60 LI-II vs P>60 LIV-V	0.009	91.9 ± 5.3 Hz vs 71.3 ± 7.8 Hz	19 cells vs 11 cells from 17 mice
		P>60 LI-II vs P>60 LVI-VII	0.53	91.9 ± 5.3 Hz vs 86.7 ± 8.4 Hz	19 cells vs 9 cells from 17 mice
		P>60 LI-II vs P>60 LIX	0.002	91.9 ± 5.3 Hz vs 72.0 ± 3.1 Hz	19 cells vs 25 cells from 23 mice
		P>60 LI-II vs P>60 LX	<0.0001	91.9 ± 5.3 Hz vs 58.7 ± 3.6 Hz	19 cells vs 28 cells from 33 mice
		P>60 LIII vs P>60 LIV-V	0.037	87.0 ± 3.9 Hz vs 71.3 ± 7.8 Hz	22 cells vs 11 cells from 21 mice
		P>60 LIII vs P>60 LVI-VII	0.97	87.0 ± 3.9 Hz vs 86.7 ± 8.4 Hz	22 cells vs 9 cells from 21 mice
		P>60 LIII vs P>60 LIX	0.013	87.0 ± 3.9 Hz vs 72.0 ± 3.1 Hz	22 cells vs 25 cells from 27 mice
		P>60 LIII vs P>60 LX	<0.0001	87.0 ± 3.9 Hz vs 58.7 ± 3.6 Hz	22 cells vs 28 cells from 37 mice
		P>60 LIV-V vs P>60 LVI-VII	0.09	71.3 ± 7.8 Hz vs 86.7 ± 8.4 Hz	11 cells vs 9 cells from 16 mice
		P>60 LIV-V vs P>60 LIX	0.92	71.3 ± 7.8 Hz vs 72.0 ± 3.1 Hz	11 cells vs 25 cells from 22 mice

		P>60 LIV-V vs P>60 LX	0.08	71.3 ± 7.8 Hz vs 58.7 ± 3.6 Hz	11 cells vs 28 cells from 32 mice
		P>60 LVI-VII vs P>60 LIX	0.06	86.7 ± 8.4 Hz vs 72.0 ± 3.1 Hz	9 cells vs 25 cells from 22 mice
		P>60 LVI-VII vs P>60 LX	0.0005	86.7 ± 8.4 Hz vs 58.7 ± 3.6 Hz	9 cells vs 28 cells from 32 mice
		P>60 LIX vs P>60 LX	0.018	72.0 ± 3.1 Hz vs 58.7 ± 3.6 Hz	25 cells vs 28 cells from 38 mice
Figure Supplement 1.3 A_2 Simple spike rate P30-59	One-way ANOVA multiple comparisons	P30-59 LI-II vs P30-59 LIII	0.83	73.4 ± 5.7 Hz vs 75.7 ± 4.7 Hz	10 cells vs 3 cells from 12 mice
		P30-59 LI-II vs P30-59 LIV-V	0.38	73.4 ± 5.7 Hz vs 79.5 ± 4.1 Hz	10 cells vs 13 cells from 20 mice
		P30-59 LI-II vs P30-59 LVI-VII	0.35	73.4 ± 5.7 Hz vs 80.7 ± 6.7 Hz	10 cells vs 8 cells from 16 mice
		P30-59 LI-II vs P30-59 LVIII	0.52	73.4 ± 5.7 Hz vs 68.3 ± 2.9 Hz	10 cells vs 8 cells from 16 mice
		P30-59 LI-II vs P30-59 LIX	0.024	73.4 ± 5.7 Hz vs 57.9 ± 5.0 Hz	10 cells vs 15 cells from 21 mice
		P30-59 LI-II vs P30-59 LX	0.007	73.4 ± 5.7 Hz vs 55.6 ± 3.7 Hz	10 cells vs 20 cells from 24 mice
		P30-59 LIII vs P30-59 LIV-V	0.72	75.7 ± 4.7 Hz vs 79.5 ± 4.1 Hz	3 cells vs 13 cells from 14 mice
		P30-59 LIII vs P30-59 LVI-VII	0.66	75.7 ± 4.7 Hz vs 80.7 ± 6.7 Hz	3 cells vs 8 cells from 10 mice
		P30-59 LIII vs P30-59 LVIII	0.51	75.7 ± 4.7 Hz vs 68.3 ± 2.9 Hz	3 cells vs 8 cells from 10 mice
		P30-59 LIII vs P30-59 LIX	0.09	75.7 ± 4.7 Hz vs 57.9 ± 5.0 Hz	3 cells vs 15 cells from 15 mice
		P30-59 LIII vs P30-59 LX	0.05	75.7 ± 4.7 Hz vs 55.6 ± 3.7 Hz	3 cells vs 20 cells from 18 mice
		P30-59 LIV-V vs P30-59 LVI-VII	0.87	79.5 ± 4.1 Hz vs 80.7 ± 6.7 Hz	13 cells vs 8 cells from 18 mice
		P30-59 LIV-V vs P30-59 LVIII	0.14	79.5 ± 4.1 Hz vs 68.3 ± 2.9 Hz	13 cells vs 8 cells from 18 mice
		P30-59 LIV-V vs P30-59 LIX	0.0009	79.5 ± 4.1 Hz vs 57.9 ± 5.0 Hz	13 cells vs 15 cells from 23 mice
		P30-59 LIV-V vs P30-59 LX	0.0001	79.5 ± 4.1 Hz vs 55.6 ± 3.7 Hz	13 cells vs 20 cells from 26 mice
		P30-59 LVI-VII vs P30-59 LVIII	0.14	80.7 ± 6.7 Hz vs 68.3 ± 2.9 Hz	8 cells vs 8 cells from 14 mice
		P30-59 LVI-VII vs P30-59 LIX	0.002	80.7 ± 6.7 Hz vs 57.9 ± 5.0 Hz	8 cells vs 15 cells from 19 mice

		P30-59 LVI-VII vs P30-59 LX	0.0005	80.7 ± 6.7 Hz vs 55.6 ± 3.7 Hz	8 cells vs 20 cells from 22 mice
		P30-59 LVIII vs P30-59 LIX	0.15	68.3 ± 2.9 Hz vs 57.9 ± 5.0 Hz	8 cells vs 15 cells from 19 mice
		P30-59 LVIII vs P30-59 LX	0.07	68.3 ± 2.9 Hz vs 55.6 ± 3.7 Hz	8 cells vs 20 cells from 22 mice
		P30-59 LIX vs P30-59 LX	0.68	57.9 ± 5.0 Hz vs 55.6 ± 3.7 Hz	15 cells vs 20 cells from 27 mice
Related Figure	**Test applied**	**Groups**	***p*-value**	**Descriptive values**	**Number of cells / mice**
Figure Supplement 1.3 A_3 Simple spike rate P18-29	One-way ANOVA multiple comparisons	P18-29 LI-II vs P18-29 LIII	0.76	55.4 ± 12.1 Hz vs 59.7 ± 17.0 Hz	3 cells vs 3 cells from 6 mice
		P18-29 LI-II vs P18-29 LIV-V	0.07	55.4 ± 12.1 Hz vs 80.7 ± 13.5 Hz	3 cells vs 4 cells from 6 mice
		P18-29 LI-II vs P18-29 LIX	0.61	55.4 ± 12.1 Hz vs 61.1 ± 3.1 Hz	3 cells vs 13 cells from 12 mice
		P18-29 LI-II vs P18-29 LX	0.84	55.4 ± 12.1 Hz vs 53.0 ± 5.2 Hz	3 cells vs 8 cells from 11 mice
		P18-29 LIII vs P18-29 LIV-V	0.12	59.7 ± 17.0 Hz vs 80.7 ± 13.5 Hz	3 cells vs 4 cells from 6 mice
		P18-29 LIII vs P18-29 LIX	0.90	59.7 ± 17.0 Hz vs 61.1 ± 3.1 Hz	3 cells vs 13 cells from 12 mice
		P18-29 LIII vs P18-29 LX	0.57	59.7 ± 17.0 Hz vs 53.0 ± 5.2 Hz	3 cells vs 8 cells from 11 mice
		P18-29 LIV-V vs P18-29 LIX	0.06	80.7 ± 13.5 Hz vs 61.1 ± 3.1 Hz	4 cells vs 13 cells from 12 mice
		P18-29 LIV-V vs P18-29 LX	0.015	80.7 ± 13.5 Hz vs 53.0 ± 5.2 Hz	4 cells vs 8 cells from 11 mice
		P18-29 LIX vs P18-29 LX	0.30	61.1 ± 3.1 Hz vs 53.0 ± 5.2 Hz	13 cells vs 8 cells from 17 mice
Figure Supplement 1.3 A_4 Simple spike rate P12-17	One-way ANOVA multiple comparisons	P12-17 LIV-V vs P12-17 LVI-VII	0.76	62.2 ± 12.0 Hz vs 67.9 ± 21.3 Hz	7 cells vs 3 cells from 9 mice
		P12-17 LIV-V vs P12-17 LX	0.02	62.2 ± 12.0 Hz vs 24.9 ± 3.8 Hz	7 cells vs 7 cells from 10 mice
		P12-17 LVI-VII vs P12-17 LX	0.03	67.9 ± 21.3 Hz vs 24.9 ± 3.8 Hz	3 cells vs 7 cells from 7 mice

Figure Supplement 1.3 B_1 Simple spike rate ZebrinII- anterior and hemisphere	One-way ANOVA multiple comparisons	>P60 Ant. Z– vs P30-59 Ant. Z–	0.03	87.7 ± 2.9 Hz vs 76.7 ± 3.0 Hz	50 cells vs 26 cells from 53 mice
		>P60 Ant. Z– vs P18-29 Ant. Z–	0.13	87.7 ± 2.9 Hz vs 76.0 ± 6.9 Hz	50 cells vs 8 cells from 37 mice
		>P60 Ant. Z– vs P12-17 Ant. Z–	0.001	87.7 ± 2.9 Hz vs 61.2 ± 10.5 Hz	50 cells vs 8 cells from 37 mice
		>P60 Hem. Z– vs P30-59 Hem. Z–	0.74	91.6 ± 7.7 Hz vs 95.8 ± 19.7 Hz	8 cells vs 4 cells from 11 mice
		>P60 Hem. Z– vs P18-29 Hem. Z–	0.01	91.6 ± 7.7 Hz vs 63.5 ± 6.8 Hz	8 cells vs 6 cells from 13 mice
		>P60 Hem. Z– vs P12-17 Hem. Z–	<0.0001	91.6 ± 7.7 Hz vs 44.5 ± 4.6 Hz	8 cells vs 7 cells from 13 mice
Figure Supplement 1.3 B_2 Simple spike rate ZebrinII+ Nodulus and Flocculus	One-way ANOVA multiple comparisons	>P60 Nod. Z+ vs P30-59 Nod. Z+	0.14	62.2 ± 2.5 Hz vs 56.4 ± 2.8 Hz	48 cells vs 32 cells from 62 mice
		>P60 Nod. Z+ vs P18-29 Nod. Z+	0.40	62.2 ± 2.5 Hz vs 58.4 ± 2.9 Hz	48 cells vs 20 cells from 54 mice
		>P60 Nod. Z+ vs P12-17 Nod. Z+	<0.0001	62.2 ± 2.5 Hz vs 24.9 ± 3.8 Hz	48 cells vs 7 cells from 41 mice
		>P60 Floc. Z+ vs P18-29 Floc. Z+	0.82	67.3 ± 9.8 Hz vs 64.7 ± 14.2 Hz	9 cells vs 3 cells from 11 mice
Figure Supplement 2.1 C_1 Simple spike CV (*in vitro*)	Kruskal-Wallis test multiple comparisons	P3-P5 LIII vs P3-P5 LX	0.13	0.24 ± 0.03 vs 0.44 ± 0.06	23 cells vs 18 cells from 3 mice
		P6-P9 LIII vs P6-P9 LX	0.007	0.43 ± 0.21 vs 0.34 ± 0.08	30 cells vs 25 cells from 6 mice
		P10-P11 LIII vs P10-P11 LX	0.13	0.10 ± 0.01 vs 0.09 ± 0.01	37 cells vs 36 cells from 3 mice
		P12-P17 LIII vs P12-P17 LX	0.10	0.08 ± 0.01 vs 0.09 ± 0.04	23 cells vs 25 cells from 4 mice
		P18-P29 LIII vs P18-P29 LX	0.007	0.14 ± 0.01 vs 0.10 ± 0.01	43 cells vs 73 cells from 9 mice
		P30-P59 LIII vs P30-P59 LX	0.003	0.14 ± 0.04 vs 0.09 ± 0.01	44 cells vs 50 cells from 7 mice
		>P60 LIII vs >P60 LX	<0.0001	0.13 ± 0.01 vs 0.08 ± 0.01	102 cells vs 121 cells from 17 mice

Related Figure	Test applied	Groups	*p*-value	Descriptive values	Number of cells / mice
Figure Supplement 2.1 C_2 Simple spike regularity index (*in vitro*)	Kruskal-Wallis test multiple comparisons	P3-P5 LIII vs P3-P5 LX	0.67	0.006 ± 0.002 vs 0.002 ± 0.001	23 cells vs 18 cells from 3 mice
		P6-P9 LIII vs P6-P9 LX	0.008	0.032 ± 0.005 vs 0.010 ± 0.003	30 cells vs 25 cells from 6 mice
		P10-P11 LIII vs P10-P11 LX	0.33	0.044 ± 0.005 vs 0.055 ± 0.007	37 cells vs 36 cells from 3 mice
		P12-P17 LIII vs P12-P17 LX	0.017	0.037 ± 0.003 vs 0.064 ± 0.006	23 cells vs 25 cells from 4 mice
		P18-P29 LIII vs P18-P29 LX	<0.0001	0.016 ± 0.002 vs 0.060 ± 0.004	43 cells vs 73 cells from 9 mice
		P30-P59 LIII vs P30-P59 LX	<0.0001	0.026 ± 0.004 vs 0.086 ± 0.009	44 cells vs 50 cells from 7 mice
		>P60 LIII vs >P60 LX	<0.0001	0.017 ± 0.001 vs 0.082 ± 0.004	102 cells vs 121 cells from 17 mice
Figure Supplement 2.2 A_1 Simple spike rate *in vivo* and *in vitro*	Kruskal-Wallis test multiple comparisons	P12-P17 LIII vs P12-P17 Z–	0.40	51.7 ± 3.4 Hz vs 57.3 ± 5.3 Hz	23 cells vs 20 cells
		P18-P29 LIII vs P18-P29 Z–	0.034	55.8 ± 5.6 Hz vs 69.0 ± 4.4 Hz	43 cells vs 17 cells
		P30-P59 LIII vs P30-P59 Z–	<0.001	59.1 ± 4.8 Hz vs 78.4 ± 3.2 Hz	44 cells vs 43 cells
		>P60 LIII vs >P60 Z–	<0.0001	61.2 ± 2.5 Hz vs 89.2 ± 2.3 Hz	102 cells vs 70 cells
		P12-P17 LX vs P12-P17 Z+	0.18	34.8 ± 2.0 Hz vs 42.3 ± 5.7 Hz	24 cells vs 25 cells
		P18-P29 LX vs P18-P29 Z+	0.001	42.4 ± 2.9 Hz vs 55.9 ± 3.2 Hz	34 cells vs 73 cells
		P30-P59 LX vs P30-P59 Z+	<0.001	45.6 ± 3.6 Hz vs 56.7 ± 2.2 Hz	47 cells vs 50 cells
		>P60 LX vs >P60 Z+	<0.0001	46.3 ± 1.9 Hz vs 61.5 ± 2.4 Hz	62 cells vs 121 cells
Figure Supplement 6.1 A_1 OKR gain	Mixed-effects repeated measures	Young vs Adult	0.84	0.60 ± 0.09 vs 0.59 ± 0.10	16 mice vs 11 mice

Figure Supplement 6.1 A_2 VOR gain	Mixed-effects repeated measures	Young vs Adult	<0.0001	0.42 ± 0.09 vs 0.61 ± 0.09	16 mice vs 11 mice
Figure Supplement 6.1 A_3 VVOR gain	Mixed-effects repeated measures	Young vs Adult	0.009	0.89 ± 0.01 vs 0.96 ± 0.01	16 mice vs 11 mice
Figure Supplement 6.1 B_1 OKR Phase	Mixed-effects repeated measures	Young vs Adult	0.96	-15.5 ± 6.7 ° vs -15.4 ± 5.0 °	16 mice vs 11 mice
Figure Supplement 6.1 B_2 VOR phase	Mixed-effects repeated measures	Young vs Adult	0.002	29.4 ± 5.8 ° vs 21.4 ± 4.5 °	16 mice vs 11 mice
Figure Supplement 6.1 B_3 VVOR phase	Mixed-effects repeated measures	Young vs Adult	0.97	1.33 ± 0.46 ° vs 1.35 ± 0.13 °	16 mice vs 11 mice

Related Figure	**Test applied**	**Groups**	***p*-value**	**Descriptive values**	**Number of cells / mice**

Figure Supplement 6.2 B VOR phase reversal gain	Mixed-effects repeated measures	Young vs Adult day1 Young vs Adult day2 Young vs Adult day3 Young vs Adult day4 Young vs Adult day5	<0.0001 <0.0001 0.002 0.54 0.38	0.28 ± 0.04 vs 0.52 ± 0.04 0.11 ± 0.01 vs 0.33 ± 0.03 0.15 ± 0.02 vs 0.22 ± 0.02 0.21 ± 0.01 vs 0.20 ± 0.01 0.23 ± 0.007 vs 0.21 ± 0.005	16 mice vs 11 mice
Figure Supplement 6.2 C VOR gain consolidation	One-way ANOVA multiple comparisons	Young vs Adult day1-2 Young vs Adult day2-3 Young vs Adult day3-4	0.0005 0.0006 0.007	101.8 ± 7.0 % vs 62.6 ± 4.6 % 71.7 ± 9.0 % vs 33.0 ± 7.7 % 85.4 ± 5.4 % vs 55.6 ± 9.2 %	16 mice vs 11 mice
Figure Supplement 6.2 D VOR phase reversal gain training	Mixed-effects repeated measures	Young vs Adult day1 Young vs Adult day2 Young vs Adult day3 Young vs Adult day4 Young vs Adult day5	<0.0001 0.01 0.0003 0.26 0.22	0.11 ± 0.02 vs 0.16 ± 0.02 0.81 ± 0.05 vs 0.66 ± 0.06 0.70 ± 0.02 vs 0.59 ± 0.02 0.78 ± 0.01 vs 0.74 ± 0.02 0.82 ± 0.01 vs 0.79 ± 0.01	16 mice vs 11 mice
Figure Supplement 6.2 E VOR phase reversal phase training	Mixed-effects repeated measures	Young vs Adult day1 Young vs Adult day2 Young vs Adult day3 Young vs Adult day4 Young vs Adult day5	0.97 <0.0001 <0.0001 <0.0001 <0.0001	45.8 ± 1.11 ° vs 45.8 ± 1.03 ° 174.8 ± 2.74 ° vs 155.1 ± 3.68 ° 180.3 ± 0.74 ° vs 172.5 ± 1.38 ° 180.7 ± 0.54 ° vs 174.0 ± 0.77 ° 181.1 ± 0.18 ° vs 175.7 ± 0.71 °	16 mice vs 11 mice
Figure Supplement 6.4 B_1	Mixed-effects repeated measures	Young vs Adult	0.41	5.61 ± 0.15 msec vs 6.41 ± 0.10 msec	18 mice vs 13 mice

Unconditioned response onset					
Figure Supplement 6.4 B_2 Unconditioned response peaktime	Mixed-effects repeated measures	Young vs Adult	0.55	67.2 ± 1.0 msec vs 69.0 ± 1.0 msec	18 mice vs 13 mice

References:

Aarts, E., Verhage, M., Veenvliet, J. V., Dolan, C. V., & van der Sluis, S. (2014). A solution to dependency: Using multilevel analysis to accommodate nested data. *Nature Neuroscience*, *17*(4), 491–496. https://doi.org/10.1038/nn.3648

Akil, O., Oursler, A., Fan, K., & Lustig, L. (2016). Mouse Auditory Brainstem Response Testing. *BIO-PROTOCOL*, *6*(6). https://doi.org/10.21769/BioProtoc.1768

Alba, A. (1994). Deficient cerebellar long-term depression and impaired motor learning in mGluR1 mutant mice. *Cell*, *79*(2), 377–388. https://doi.org/10.1016/0092-8674(94)90205-4

Albergaria, C., & Carey, M. R. (2014). All Purkinje cells are not created equal. *ELife*, *3*, e03285. https://doi.org/10.7554/eLife.03285

Albergaria, C., Silva, N. T., Pritchett, D. L., & Carey, M. R. (2018). Locomotor activity modulates associative learning in mouse cerebellum. *Nature Neuroscience*, *21*(5), 725–735. https://doi.org/10.1038/s41593-018-0129-x

Albus, J. S. (1971). A theory of cerebellar function. *Mathematical Biosciences*, *10*(1–2), 25–61. https://doi.org/10.1016/0025-5564(71)90051-4

Altman, J. A., Bechterev, N. N., Radionova, E. A., Shmigidina, G. N., & Syka, J. (1976). Electrical responses of the auditory area of the cerebellar cortex to acoustic stimulation. *Experimental Brain Research*, *26*(3). https://doi.org/10.1007/BF00234933

Alvarado-Mallart, R. M., & Sotelo, C. (1982). Differentiation of cerebellar anlage heterotopically transplanted to adult rat brain: A light and electron microscopic study. *Journal of Comparative Neurology*, *212*(3), 247–267. https://doi.org/10.1002/cne.902120304

Alvina, K., & Khodakhah, K. (2010). KCa Channels as Therapeutic Targets in Episodic Ataxia Type-2. *Journal of Neuroscience*, *30*(21), 7249–7257. https://doi.org/10.1523/JNEUROSCI.6341-09.2010

Ames, L. L., & Yarczower, M. (1965). Some effects of wavelength discrimination on stimulus generalization in the goldfish. *Psychonomic Science*, *3*(1–12), 311–312. https://doi.org/10.3758/BF03343154

Aminov, Y., Donchin, O., Frens, M. A., & Winkelman, B. H. J. (2012). P2s2—"Ping-pong" Spike Sorting: An Interactive Method for Sorting Spikes Based on Their Shape and Inter-Spike Intervals. *Federation of European Neuroscience Societues; University of Barcelona: Barcelona, Spain*.

Anderson, J. R. (2000). *Learning and memory: An integrated approach, 2nd ed* (pp. xviii, 487). John Wiley & Sons Inc.

Andersson, G., & Oscarsson, O. (1978). Climbing fiber microzones in cerebellar vermis and their projection to different groups of cells in the lateral vestibular nucleus. *Experimental Brain Research*, *32*(4). https://doi.org/10.1007/BF00239553

Ansari, M. W., & Nadeem, A. (2016). Anatomy of the Eyelids. In M. W. Ansari & A. Nadeem, *Atlas of Ocular Anatomy* (pp. 53–63). Springer International Publishing. https://doi.org/10.1007/978-3-319-42781-2_5

Apps, R., & Garwicz, M. (2005). Anatomical and physiological foundations of cerebellar information processing. *Nature Reviews Neuroscience*, *6*(4), 297–311. https://doi.org/10.1038/nrn1646

Apps, R., & Hawkes, R. (2009). Cerebellar cortical organization: A one-map hypothesis. *Nature Reviews Neuroscience*, *10*(9), 670–681. https://doi.org/10.1038/nrn2698

Apps, R., Hawkes, R., Aoki, S., Bengtsson, F., Brown, A. M., Chen, G., Ebner, T. J., Isope, P., Jörntell, H., Lackey, E. P., Lawrenson, C., Lumb, B., Schonewille, M., Sillitoe, R. V., Spaeth, L., Sugihara, I., Valera, A., Voogd, J., Wylie, D. R., & Ruigrok, T. J. H. (2018). Cerebellar Modules and Their Role as Operational Cerebellar Processing Units. *The Cerebellum*, *17*(5), 654–682. https://doi.org/10.1007/s12311-018-0952-3

Arancillo, M., White, J. J., Lin, T., Stay, T. L., & Sillitoe, R. V. (2015). In vivo analysis of Purkinje cell firing properties during postnatal mouse development. *Journal of Neurophysiology*, *113*(2), 578–591. https://doi.org/10.1152/jn.00586.2014

Armbrust, K. R., Wang, X., Hathorn, T. J., Cramer, S. W., Chen, G., Zu, T., Kangas, T., Zink, A. N., Oz, G., Ebner, T. J., & Ranum, L. P. W. (2014). Mutant -III Spectrin Causes mGluR1 Mislocalization and Functional Deficits in a Mouse Model of Spinocerebellar Ataxia Type 5. *Journal of Neuroscience*, *34*(30), 9891–9904. https://doi.org/10.1523/JNEUROSCI.0876-14.2014

Armstrong, C. l., Chung, S.-H., Armstrong, J. n., Hochgeschwender, U., Jeong, Y.-G., & Hawkes, R. (2009). A novel somatostatin-immunoreactive mossy fiber pathway asssociated with HSP25-immunoreactive purkinje cell stripes in the mouse cerebellum. *Journal of Comparative Neurology*, *517*(4), 524–538. https://doi.org/10.1002/cne.22167

Armstrong, C. L., & Hawkes, R. (2000). Pattern formation in the cerebellar cortex. *Biochemistry and Cell Biology*, *78*(5), 551–562. https://doi.org/10.1139/o00-071

Armstrong, C. L., Krueger-Naug, A. M., Currie, R. W., & Hawkes, R. (2000). Constitutive expression of the 25-kDa heat shock protein Hsp25 reveals novel parasagittal bands of Purkinje cells in the adult mouse cerebellar cortex. *Journal of Comparative Neurology*, *416*(3), 383–397. https://doi.org/10.1002/(SICI)1096-9861(20000117)416:3<383::AID-CNE9>3.0.CO;2-M

Armstrong, C. L., Krueger-Naug, A. M. R., Currie, R. W., & Hawkes, R. (2001). Expression of heat-shock protein Hsp25 in mouse purkinje cells during development reveals novel features of cerebellar compartmentation. *Journal of Comparative Neurology*, *429*(1), 7–21. https://doi.org/10.1002/1096-9861(20000101)429:1<7::AID-CNE2>3.0.CO;2-Q

Attwell, P. J. E., Rahman, S., & Yeo, C. H. (2001). Acquisition of Eyeblink Conditioning Is Critically Dependent on Normal Function in Cerebellar Cortical Lobule HVI. *The Journal of Neuroscience*, *21*(15), 5715–5722. https://doi.org/10.1523/JNEUROSCI.21-15-05715.2001

Badura, A., Verpeut, J. L., Metzger, J. W., Pereira, T. D., Pisano, T. J., Deverett, B., Bakshinskaya, D. E., & Wang, S. S.-H. (2018). Normal cognitive and social development require posterior cerebellar activity. *ELife*, *7*, e36401. https://doi.org/10.7554/eLife.36401

Bang, S. J., Allen, T. A., Jones, L. K., Boguszewski, P., & Brown, T. H. (2008). Asymmetrical stimulus generalization following differential fear conditioning. *Neurobiology of Learning and Memory*, *90*(1), 200–216. https://doi.org/10.1016/j.nlm.2008.02.009

Bao, S., Chen, L., Kim, J. J., & Thompson, R. F. (2002). Cerebellar cortical inhibition and classical eyeblink conditioning. *Proceedings of the National Academy of Sciences*, *99*(3), 1592–1597. https://doi.org/10.1073/pnas.032655399

Barmack, N. H., Qian, Z., & Yoshimura, J. (2000). Regional and cellular distribution of protein kinase C in rat cerebellar purkinje cells. *Journal of Comparative Neurology*, *427*(2), 235–254. https://doi.org/10.1002/1096-9861(20001113)427:2<235::AID-CNE6>3.0.CO;2-6

Barnes, J. A., Ebner, B. A., Duvick, L. A., Gao, W., Chen, G., Orr, H. T., & Ebner, T. J. (2011). Abnormalities in the Climbing Fiber-Purkinje Cell Circuitry Contribute to Neuronal Dysfunction in ATXN1[82Q] Mice. *Journal of Neuroscience*, *31*(36), 12778–12789. https://doi.org/10.1523/JNEUROSCI.2579-11.2011

Baron, A. (1973). Postdiscrimination gradients of human subjects on a tone continuum. *Journal of Experimental Psychology*, *101*(2), 337–342. https://doi.org/10.1037/h0035206

Bastian, A. J., Martin, T. A., Keating, J. G., & Thach, W. T. (1996). Cerebellar ataxia: Abnormal control of interaction torques across multiple joints. *Journal of Neurophysiology*, *76*(1), 492–509. https://doi.org/10.1152/jn.1996.76.1.492

Becker, E. B. E. (2014). The Moonwalker Mouse: New Insights into TRPC3 Function, Cerebellar Development, and Ataxia. *The Cerebellum*, *13*(5), 628–636. https://doi.org/10.1007/s12311-014-0564-5

Beekhof, G. C., Osório, C., White, J. J., van Zoomeren, S., van der Stok, H., Xiong, B., Nettersheim, I. H., Mak, W. A., Runge, M., Fiocchi, F. R., Boele, H.-J., Hoebeek, F. E., & Schonewille, M. (2021). Differential spatiotemporal development of Purkinje cell populations and cerebellum-dependent sensorimotor behaviors. *ELife*, *10*, e63668. https://doi.org/10.7554/eLife.63668

Belmeguenai, A., Hosy, E., Bengtsson, F., Pedroarena, C. M., Piochon, C., Teuling, E., He, Q., Ohtsuki, G., De Jeu, M. T. G., Elgersma, Y., De Zeeuw, C. I., Jorntell, H., & Hansel, C. (2010). Intrinsic Plasticity Complements Long-Term Potentiation in Parallel Fiber Input Gain Control in Cerebellar Purkinje Cells. *Journal of Neuroscience*, *30*(41), 13630–13643. https://doi.org/10.1523/JNEUROSCI.3226-10.2010

Berridge, M. J., & Irvine, R. F. (1984). Inositol trisphosphate, a novel second messenger in cellular signal transduction. *Nature*, *312*(5992), 315–321. https://doi.org/10.1038/312315a0

Berthier, N. E., & Moore, J. W. (1986). Cerebellar Purkinje cell activity related to the classically conditioned nictitating membrane response. *Experimental Brain Research*, *63*(2), 341–350. https://doi.org/10.1007/BF00236851

Berthier, N. E., & Moore, J. W. (1990). Activity of deep cerebellar nuclear cells during classical conditioning of nictitating membrane extension in rabbits. *Experimental Brain Research*, *83*(1), 44–54. https://doi.org/10.1007/BF00232192

Boele, H.-J., Koekkoek, S. K. E., & De Zeeuw, C. I. (2010). Cerebellar and extracerebellar involvement in mouse eyeblink conditioning: The ACDC model. *Frontiers in Cellular Neuroscience*, *3*. https://doi.org/10.3389/neuro.03.019.2009

Boele, H.-J., Peter, S., Ten Brinke, M. M., Verdonschot, L., IJpelaar, A. C. H., Rizopoulos, D., Gao, Z., Koekkoek, S. K. E., & De Zeeuw, C. I. (2018). Impact of parallel fiber to Purkinje cell long-term depression is unmasked in absence of inhibitory input. *Science Advances*, *4*(10), eaas9426. https://doi.org/10.1126/sciadv.aas9426

Boele, H.-J., ten Brinke, M. M., & De Zeeuw, C. I. (2016). Classical Conditioning of Timed Motor Responses. In *The Neuronal Codes of the Cerebellum* (pp. 53–96). Elsevier. https://doi.org/10.1016/B978-0-12-801386-1.00003-4

Boele, H.-J., Koekkoek, S. K. E., De Zeeuw, C. I., & Ruigrok, T. J. H. (2013). Axonal Sprouting and Formation of Terminals in the Adult Cerebellum during Associative Motor Learning. *Journal of Neuroscience*, *33*(45), 17897–17907. https://doi.org/10.1523/JNEUROSCI.0511-13.2013

Boneau, C. A. (1958). The interstimulus interval and the latency of the conditioned eyelid response. *Journal of Experimental Psychology*, *56*(6), 464–471. https://doi.org/10.1037/h0044940

Boucheny, C., Carrillo, R., Ros, E., & Coenen, O. (2005). Real-Time Spiking Neural Network: An Adaptive Cerebellar Model. In *Lecture Notes in Computer Science* (Vol. 3512, p. 144). https://doi.org/10.1007/11494669_18

Bouton, M. E., & Moody, E. W. (2004). Memory processes in classical conditioning. *Neuroscience & Biobehavioral Reviews*, *28*(7), 663–674. https://doi.org/10.1016/j.neubiorev.2004.09.001

Boyden, E. S. (2015). Optogenetics and the future of neuroscience. *Nature Neuroscience*, *18*(9), 1200–1201. https://doi.org/10.1038/nn.4094

Bracha, V., Webster, M. L., Winters, N. K., Irwin, K. B., & Bloedel, J. R. (1994). *Effects of muscimol inactivation of the cerebellar interposed-dentate nuclear complex on the performance of the nictitating membrane response in the rabbit*. 16.

Bradley, P., & Berry, M. (1979). Effects of Thiophene on the Purkinje Cell Dendritic Tree: A Quantitative Golgi Study. *Neuropathology and Applied Neurobiology*, *5*(1), 9–16. https://doi.org/10.1111/j.1365-2990.1979.tb00609.x

Brochu, G., Maler, L., & Hawkes, R. (1990). Zebrin II: A polypeptide antigen expressed selectively by purkinje cells reveals compartments in rat and fish cerebellum. *The Journal of Comparative Neurology*, *291*(4), 538–552. https://doi.org/10.1002/cne.902910405

Brodal, P., Dietrichs, E., & Walberg, F. (1986). Do pontocerebellar mossy fibres give off collaterals to the cerebellar nuclei? An experimental study in the cat with implantation of crystalline HRP-WGA. *Neuroscience Research Supplements*, *4*(1), 12–24. https://doi.org/10.1016/S0921-8696(86)80058-5

Buchtel, H. A., Iosif, G., Marchesi, G. F., Provini, L., & Strata, P. (1972). Analysis of the activity evoked in the cerebellar cortex by stimulation of the visual pathways. *Experimental Brain Research*, *15*(3). https://doi.org/10.1007/BF00235912

Burright, E. N., Servadio, A., Matilla, I. T., Feddersen, R. M., & Duvick, L. A. (1995). *SCA1 Transgenic Mice: A Model for Neurodegeneration Caused by an Expanded CAG Trinucleotide Repeat*. 12.

Cai, L., Chan, J. S. Y., Yan, J., & Peng, K. (2014). Brain plasticity and motor practice in cognitive aging. *Frontiers in Aging Neuroscience*, *6*. https://www.frontiersin.org/articles/10.3389/fnagi.2014.00031

Campolattaro, M. M., Halverson, H. E., & Freeman, J. H. (2007). Medial auditory thalamic stimulation as a conditioned stimulus for eyeblink conditioning in rats. *Learning & Memory*, *14*(3), 152–159. https://doi.org/10.1101/lm.465507

Cason, H. (1922). The conditioned eyelid reaction. *Journal of Experimental Psychology*, *5*(3), 153–196. https://doi.org/10.1037/h0074822

Cerminara, N. L. (2004). Evidence that Climbing Fibers Control an Intrinsic Spike Generator in Cerebellar Purkinje Cells. *Journal of Neuroscience*, *24*(19), 4510–4517. https://doi.org/10.1523/JNEUROSCI.4530-03.2004

Cerminara, N. L., Aoki, H., Loft, M., Sugihara, I., & Apps, R. (2013). Structural Basis of Cerebellar Microcircuits in the Rat. *Journal of Neuroscience*, *33*(42), 16427–16442. https://doi.org/10.1523/JNEUROSCI.0861-13.2013

Cerminara, N. L., Lang, E. J., Sillitoe, R. V., & Apps, R. (2015). Redefining the cerebellar cortex as an assembly of non-uniform Purkinje cell microcircuits. *Nature Reviews Neuroscience*, *16*(2), 79–93. https://doi.org/10.1038/nrn3886

Chapman, P. F., Kairiss, E. W., Keenan, C. L., & Brown, T. H. (1990). Long-Term synaptic potentiation in the amygdala. *Synapse*, *6*(3), 271–278. https://doi.org/10.1002/syn.890060306

Chédotal, A., Bloch-Gallego, E., & Sotelo, C. (1997). *The embryonic cerebellum contains topographic cues that guide developing inferior olivary axons*. 10.

Cheng, K., Spetch, M. L., & Johnston, M. (1997). Spatial peak shift and generalization in pigeons. *Journal of Experimental Psychology: Animal Behavior Processes*, *23*(4), 469–481. https://doi.org/10.1037/0097-7403.23.4.469

Chettih, S. N., McDougle, S. D., Ruffolo, L. I., & Medina, J. F. (2011). Adaptive Timing of Motor Output in the Mouse: The Role of Movement Oscillations in Eyelid Conditioning. *Frontiers in Integrative Neuroscience*, *5*. https://doi.org/10.3389/fnint.2011.00072

Chopra, R., Bushart, D. D., Cooper, J. P., Yellajoshyula, D., Morrison, L. M., Huang, H., Handler, H. P., Man, L. J., Dansithong, W., Scoles, D. R., Pulst, S. M., Orr, H. T., & Shakkottai, V. G. (2020). Altered Capicua expression drives regional Purkinje neuron vulnerability through ion channel gene dysregulation in spinocerebellar ataxia type 1. *Human Molecular Genetics*, *29*(19), 3249–3265. https://doi.org/10.1093/hmg/ddaa212

Chopra, R., Bushart, D. D., & Shakkottai, V. G. (2018). Dendritic potassium channel dysfunction may contribute to dendrite degeneration in spinocerebellar ataxia type 1. *PLOS ONE*, *13*(5), e0198040. https://doi.org/10.1371/journal.pone.0198040

Chung, S.-H., Marzban, H., Croci, L., Consalez, G. G., & Hawkes, R. (2008). Purkinje cell subtype specification in the cerebellar cortex: Early B-cell factor 2 acts to repress the zebrin II-positive Purkinje cell phenotype. *Neuroscience*, *153*(3), 721–732. https://doi.org/10.1016/j.neuroscience.2008.01.090

Cingolani, L. A., Gymnopoulos, M., Boccaccio, A., Stocker, M., & Pedarzani, P. (2002). Developmental Regulation of Small-Conductance Ca^{2+}-Activated K^{+} Channel Expression and Function in Rat Purkinje Neurons. *The Journal of Neuroscience*, *22*(11), 4456–4467. https://doi.org/10.1523/JNEUROSCI.22-11-04456.2002

Claborn, M. K., Stevens, D. L., Walker, C. K., & Gildon, B. L. (2019). Nusinersen: A Treatment for Spinal Muscular Atrophy. *Annals of Pharmacotherapy*, *53*(1), 61–69. https://doi.org/10.1177/1060028018789956

Clark, H. B., Burright, E. N., Yunis, W. S., Larson, S., Wilcox, C., Hartman, B., Matilla, A., Zoghbi, H. Y., & Orr, H. T. (1997). Purkinje Cell Expression of a Mutant Allele of *SCA1* in Transgenic Mice Leads to Disparate Effects on Motor Behaviors, Followed by a Progressive Cerebellar Dysfunction and Histological Alterations. *The Journal of Neuroscience*, *17*(19), 7385–7395. https://doi.org/10.1523/JNEUROSCI.17-19-07385.1997

Colin, F., Manil, J., & Desclin, J. C. (1980). The olivocerebellar system. I. Delayed and slow inhibitory effects: An overlooked salient feature of cerebellar climbing fibers. *Brain Research*, *187*(1), 3–27. https://doi.org/10.1016/0006-8993(80)90491-6

Collewijn, H. (1977). Eye- and head movements in freely moving rabbits. *The Journal of Physiology*, *266*(2), 471–498. https://doi.org/10.1113/jphysiol.1977.sp011778

Conquet, F., Bashir, Z. I., Davies, C. H., Daniel, H., Ferraguti, F., Bordi, F., Franz-Bacon, K., Reggiani, A., Matarese, V., Condé, F., Collingridge, G. L., & Crépel, F. (1994). Motor deficit and impairment of synaptic plasticity in mice lacking mGluR1. *Nature*, *372*(6503), 237–243. https://doi.org/10.1038/372237a0

Cook, A. A., Fields, E., & Watt, A. J. (2021). Losing the Beat: Contribution of Purkinje Cell Firing Dysfunction to Disease, and Its Reversal. *Neuroscience*, *462*, 247–261. https://doi.org/10.1016/j.neuroscience.2020.06.008

de Hoz, L., & Nelken, I. (2014). Frequency Tuning in the Behaving Mouse: Different Bandwidths for Discrimination and Generalization. *PLoS ONE*, *9*(3), e91676. https://doi.org/10.1371/journal.pone.0091676

de Oude, N. L., Hoebeek, F. E., ten Brinke, M. M., de Zeeuw, C. I., & Boele, H.-J. (2021). Pavlovian eyeblink conditioning is severely impaired in tottering mice. *Journal of Neurophysiology*, *125*(2), 398–407. https://doi.org/10.1152/jn.00578.2020

De Zeeuw, C. I., Hoebeek, F. E., Bosman, L. W. J., Schonewille, M., Witter, L., & Koekkoek, S. K. (2011). Spatiotemporal firing patterns in the cerebellum. *Nature Reviews Neuroscience*, *12*(6), 327–344. https://doi.org/10.1038/nrn3011

De Zeeuw, C. I., Holstege, J. C., Ruigrok, T. J. H., & Voogd, J. (1989). Ultrastructural study of the GABAergic, cerebellar, and mesodiencephalic innervation of the cat medial accessory olive: Anterograde tracing combined with immunocytochemistry. *Journal of Comparative Neurology*, *284*(1), 12–35. https://doi.org/10.1002/cne.902840103

De Zeeuw, C. I., Hoogenraad, C. C., Koekkoek, S. K. E., Ruigrok, T. J. H., Galjart, N., & Simpson, J. I. (1998). Microcircuitry and function of the inferior olive. *Trends in Neurosciences*, *21*(9), 391–400. https://doi.org/10.1016/S0166-2236(98)01310-1

De Zeeuw, C. I., Lisberger, S. G., & Raymond, J. L. (2021a). Diversity and dynamism in the cerebellum. *Nature Neuroscience*, *24*(2), 160–167. https://doi.org/10.1038/s41593-020-00754-9

De Zeeuw, C. I., & Ten Brinke, M. M. (2015a). Motor Learning and the Cerebellum. *Cold Spring Harbor Perspectives in Biology*, *7*(9), a021683. https://doi.org/10.1101/cshperspect.a021683

De Zeeuw, C. I., & Yeo, C. H. (2005). Time and tide in cerebellar memory formation. *Current Opinion in Neurobiology*, *15*(6), 667–674. https://doi.org/10.1016/j.conb.2005.10.008

Dehnes, Y., Chaudhry, F. A., Ullensvang, K., Lehre, K. P., Storm-Mathisen, J., & Danbolt, N. C. (1998). The Glutamate Transporter EAAT4 in Rat Cerebellar Purkinje Cells: A Glutamate-Gated Chloride Channel Concentrated near the Synapse in Parts of the Dendritic Membrane Facing Astroglia. *The Journal of Neuroscience*, *18*(10), 3606–3619. https://doi.org/10.1523/JNEUROSCI.18-10-03606.1998

Deisseroth, K. (2011). Optogenetics. *Nature Methods*, *8*(1), 26–29. https://doi.org/10.1038/nmeth.f.324

Delgado-García, J. M., Gruart, A., & Múnera, A. (2002). Neural organization of eyelid responses. *Movement Disorders*, *17*(S2), S33–S36. https://doi.org/10.1002/mds.10055

Delgado-García, J. M., Gruart, A., & Trigo, J. A. (2003). Physiology of the Eyelid Motor System. *Annals of the New York Academy of Sciences*, *1004*(1), 1–9. https://doi.org/10.1196/annals.1303.001

Dent, M. L., Fay, R. R., & Popper, A. N. (Eds.). (2018). *Rodent Bioacoustics* (Vol. 67). Springer International Publishing. https://doi.org/10.1007/978-3-319-92495-3

Dow, R. S., & Moruzzi, G. (1958). *The Physiology and Pathology of the Cerebellum* (NED-New edition). University of Minnesota Press. https://www.jstor.org/stable/10.5749/j.ctttt76w

Dunsmoor, J. E., Kroes, M. C. W., Braren, S. H., & Phelps, E. A. (2017). Threat intensity widens fear generalization gradients. *Behavioral Neuroscience*, *131*(2), 168–175. https://doi.org/10.1037/bne0000186

Dunsmoor, J. E., & LaBar, K. S. (2013). Effects of discrimination training on fear generalization gradients and perceptual classification in humans. *Behavioral Neuroscience*, *127*(3), 350–356. https://doi.org/10.1037/a0031933

Dunsmoor, J. E., Mitroff, S. R., & LaBar, K. S. (2009). Generalization of conditioned fear along a dimension of increasing fear intensity. *Learning & Memory*, *16*(7), 460–469. https://doi.org/10.1101/lm.1431609

Dunsmoor, J. E., & Paz, R. (2015). Fear Generalization and Anxiety: Behavioral and Neural Mechanisms. *Biological Psychiatry*, *78*(5), 336–343. https://doi.org/10.1016/j.biopsych.2015.04.010

Durr, A. (2010). Autosomal dominant cerebellar ataxias: Polyglutamine expansions and beyond. *The Lancet Neurology*, *9*(9), 885–894. https://doi.org/10.1016/S1474-4422(10)70183-6

Dusart, I., Airaksinen, M. S., & Sotelo, C. (1997). Purkinje Cell Survival and Axonal Regeneration Are Age Dependent: An In Vitro Study. *Journal of Neuroscience*, *17*(10), 3710–3726. https://doi.org/10.1523/JNEUROSCI.17-10-03710.1997

Dusart, I., & FLAMANT, F. (2012). Profound morphological and functional changes of rodent Purkinje cells between the first and the second postnatal weeks: A metamorphosis? *Frontiers in Neuroanatomy*, *6*. https://www.frontiersin.org/articles/10.3389/fnana.2012.00011

Duvick, L., Barnes, J., Ebner, B., Agrawal, S., Andresen, M., & Lim, J. (2010). *SCA1-like disease in mice expressing wild-type Ataxin-1 with a serine to aspartic acid replacement at residue 776. Neuron [Internet]*. Elsevier Inc.

Dymond, S., Dunsmoor, J. E., Vervliet, B., Roche, B., & Hermans, D. (2015). Fear Generalization in Humans: Systematic Review and Implications for Anxiety Disorder Research. *Behavior Therapy*, *46*(5), 561–582. https://doi.org/10.1016/j.beth.2014.10.001

Ebel, H. C., & Prokasy, W. F. (1963). Classical eyelid conditioning as a function of sustained and shifted interstimulus intervals. *Journal of Experimental Psychology*, *65*(1), 52–58. https://doi.org/10.1037/h0048115

Ebner, B. A., Ingram, M. A., Barnes, J. A., Duvick, L. A., Frisch, J. L., Clark, H. B., Zoghbi, H. Y., Ebner, T. J., & Orr, H. T. (2013). Purkinje Cell Ataxin-1 Modulates Climbing Fiber Synaptic Input in Developing and Adult Mouse Cerebellum. *Journal of Neuroscience*, *33*(13), 5806–5820. https://doi.org/10.1523/JNEUROSCI.6311-11.2013

Eccles, J. C. (2013). *The Cerebellum as a Neuronal Machine*. Springer Science & Business Media.

Eisenman, L. M., Schalekamp, M. P. A., & Voogd, J. (1991). Development of the cerebellar cortical efferent projection: An in-vitro anterograde tracing study in rat brain slices. *Developmental Brain Research*, *60*(2), 261–266. https://doi.org/10.1016/0165-3806(91)90055-N

Ekerot, C. F., Garwicz, M., & Schouenborg, J. (1991). Topography and nociceptive receptive fields of climbing fibres projecting to the cerebellar anterior lobe in the cat. *The Journal of Physiology*, *441*(1), 257–274. https://doi.org/10.1113/jphysiol.1991.sp018750

Empson, R. M., Turner, P. R., Nagaraja, R. Y., Beesley, P. W., & Knöpfel, T. (2010). Reduced expression of the Ca2+ transporter protein PMCA2 slows Ca2+ dynamics in mouse cerebellar Purkinje neurones and alters the precision of motor coordination. *The Journal of Physiology*, *588*(6), 907–922. https://doi.org/10.1113/jphysiol.2009.182196

Estes, W. K. (2014). *Handbook of Learning and Cognitive Processes (Volume 2): Conditioning and Behavior Theory*. Psychology Press.

Faulstich, B. M., Onori, K. A., & du Lac, S. (2004). Comparison of plasticity and development of mouse optokinetic and vestibulo-ocular reflexes suggests differential gain control mechanisms. *Vision Research*, *44*(28), 3419–3427. https://doi.org/10.1016/j.visres.2004.09.006

Ferrante, M., Migliore, M., & Ascoli, G. A. (2013). Functional Impact of Dendritic Branch-Point Morphology. *Journal of Neuroscience*, *33*(5), 2156–2165. https://doi.org/10.1523/JNEUROSCI.3495-12.2013

Ferreira, T. A., Blackman, A. V., Oyrer, J., Jayabal, S., Chung, A. J., Watt, A. J., Sjöström, P. J., & van Meyel, D. J. (2014). Neuronal morphometry directly from bitmap images. *Nature Methods*, *11*(10), 982–984. https://doi.org/10.1038/nmeth.3125

Fiocchi, F. R., Dijkhuizen, S., Koekkoek, S. K. E., Zeeuw, C. I. D., & Boele, H. J. (2022). Stimulus Generalization in Mice during Pavlovian Eyeblink Conditioning. *ENeuro*, *9*(2). https://doi.org/10.1523/ENEURO.0400-21.2022

Fleming, J., & Chiang, C. (2015). The Purkinje neuron: A central orchestrator of cerebellar neurogenesis. *Neurogenesis*, *2*(1), e1025940. https://doi.org/10.1080/23262133.2015.1025940

Foy, M. R., Steinmetz, J. E., & Thompson, R. F. (1984). Single unit analysis of the cerebellum during classically conditioned eyelid responses. *Soc. Neurosci. Abstr*, *10*(122), 76.

Foy, M. R., & Thompson, R. F. (1986). Single unit analysis of Purkinje cell discharge in classically conditioned and untrained rabbits. *Soc. Neurosci. Abstr*, *12*, 518.

Fredette, B. J., & Mugnaini, E. (1991). The GABAergic cerebello-olivary projection in the rat. *Anatomy and Embryology*, *184*(3), 225–243. https://doi.org/10.1007/BF01673258

Freeman, J. H. (2015a). Cerebellar learning mechanisms. *Brain Research*, *1621*, 260–269. https://doi.org/10.1016/j.brainres.2014.09.062

Freeman, J. H., & Duffel, J. W. (2008). Eyeblink conditioning using cochlear nucleus stimulation as a conditioned stimulus in developing rats. *Developmental Psychobiology*, *50*(7), 640–646. https://doi.org/10.1002/dev.20331

Freeman, J. H., Halverson, H. E., & Hubbard, E. M. (2007). Inferior colliculus lesions impair eyeblink conditioning in rats. *Learning & Memory*, *14*(12), 842–846. https://doi.org/10.1101/lm.716107

Freeman, J. H., & Nicholson, D. A. (2000). Developmental Changes in Eye-Blink Conditioning and Neuronal Activity in the Cerebellar Interpositus Nucleus. *The Journal of Neuroscience*, *20*(2), 813–819. https://doi.org/10.1523/JNEUROSCI.20-02-00813.2000

Freeman, J. H., & Nicholson, D. A. (2001). Ontogenetic changes in the neural mechanisms of eyeblink conditioning. *Integrative Physiological & Behavioral Science*, *36*(1), 15–35. https://doi.org/10.1007/BF02733945

Freeman, J. H., Rabinak, C. A., & Campolattaro, M. M. (2005). Pontine stimulation overcomes developmental limitations in the neural mechanisms of eyeblink conditioning. *Learning & Memory*, *12*(3), 255–259. https://doi.org/10.1101/lm.91105

Freeman, J. H., Spencer, C. O., & Skelton, R. W. (1993). *Ontogeny of eyeblink conditioning in the rat: Effects of US intensity and interstimulus interval on delay conditioning*. 10.

Freeman, J. H., & Steinmetz, A. B. (2011). Neural circuitry and plasticity mechanisms underlying delay eyeblink conditioning. *Learning & Memory*, *18*(10), 666–677. https://doi.org/10.1101/lm.2023011

Frey, P. W. (1970). Within-subject analysis of the CS-US interval in rabbit eyelid conditioning. *Learning and Motivation*, *1*(4), 337–345. https://doi.org/10.1016/0023-9690(70)90099-8

Fujita, H., Aoki, H., Ajioka, I., Yamazaki, M., Abe, M., Oh-Nishi, A., Sakimura, K., & Sugihara, I. (2014). Detailed Expression Pattern of Aldolase C (Aldoc) in the Cerebellum, Retina and Other Areas of the CNS Studied in Aldoc-Venus Knock-In Mice. *PLOS ONE*, *9*(1), e86679. https://doi.org/10.1371/journal.pone.0086679

Fujita, H., Kodama, T., & du Lac, S. (2020). Modular output circuits of the fastigial nucleus for diverse motor and nonmotor functions of the cerebellar vermis. *ELife*, *9*, e58613. https://doi.org/10.7554/eLife.58613

Fujita, H., Morita, N., Furuichi, T., & Sugihara, I. (2012). Clustered Fine Compartmentalization of the Mouse Embryonic Cerebellar Cortex and Its Rearrangement into the Postnatal Striped Configuration. *Journal of Neuroscience*, *32*(45), 15688–15703. https://doi.org/10.1523/JNEUROSCI.1710-12.2012

Furutama, D., Morita, N., Takano, R., Sekine, Y., Sadakata, T., Shinoda, Y., Hayashi, K., Mishima, Y., Mikoshiba, K., Hawkes, R., & Furuichi, T. (2010). Expression of the IP3R1 promoter-driven nls-lacZ transgene in Purkinje cell parasagittal arrays of developing mouse cerebellum. *Journal of Neuroscience Research*, *88*(13), 2810–2825. https://doi.org/10.1002/jnr.22451

Gao, Z., Proietti-Onori, M., Lin, Z., ten Brinke, M. M., Boele, H.-J., Potters, J.-W., Ruigrok, T. J. H., Hoebeek, F. E., & De Zeeuw, C. I. (2016). Excitatory Cerebellar Nucleocortical Circuit Provides Internal Amplification during Associative Conditioning. *Neuron*, *89*(3), 645–657. https://doi.org/10.1016/j.neuron.2016.01.008

Gao, Z., van Beugen, B. J., & De Zeeuw, C. I. (2012). Distributed synergistic plasticity and cerebellar learning. *Nature Reviews Neuroscience*, *13*(9), 619–635. https://doi.org/10.1038/nrn3312

Garcia, K. S., & Mauk, M. D. (1998). Pharmacological analysis of cerebellar contributions to the timing and expression of conditioned eyelid responses. *Neuropharmacology*, *37*(4), 471–480. https://doi.org/10.1016/S0028-3908(98)00055-0

Garcia, K. S., Mauk, M. D., Weidemann, G., & Kehoe, E. J. (2003). Covariation of alternative measures of responding in rabbit (Oryctolagus cuniculus) eyeblink conditioning during acquisition training and tone generalization. *Behavioral Neuroscience*, *117*(2), 292–303. https://doi.org/10.1037/0735-7044.117.2.292

Garwicz, M., & Ekerot, C. F. (1994). Topographical organization of the cerebellar cortical projection to nucleus interpositus anterior in the cat. *The Journal of Physiology*, *474*(2), 245–260. https://doi.org/10.1113/jphysiol.1994.sp020017

Gauck, V., & Jaeger, D. (2000). The Control of Rate and Timing of Spikes in the Deep Cerebellar Nuclei by Inhibition. *The Journal of Neuroscience*, *20*(8), 3006–3016. https://doi.org/10.1523/JNEUROSCI.20-08-03006.2000

Gerwig, M. (2005). Timing of Conditioned Eyeblink Responses Is Impaired in Cerebellar Patients. *Journal of Neuroscience*, *25*(15), 3919–3931. https://doi.org/10.1523/JNEUROSCI.0266-05.2005

Gerwig, M., Kolb, F. P., & Timmann, D. (2007). The involvement of the human cerebellum in eyeblink conditioning. *The Cerebellum*, *6*(1), 38. https://doi.org/10.1080/14734220701225904

Ghirlanda, S., & Enquist, M. (2003). A century of generalization. *Animal Behavior*, *66*(1), 15–36. https://doi.org/10.1006/anbe.2003.2174

Gincel, D., Regan, M. R., Jin, L., Watkins, A. M., Bergles, D. E., & Rothstein, J. D. (2007). Analysis of cerebellar Purkinje cells using EAAT4 glutamate transporter promoter reporter in mice generated via bacterial artificial chromosome-mediated transgenesis. *Experimental Neurology*, *203*(1), 205–212. https://doi.org/10.1016/j.expneurol.2006.08.016

Gollo, L. L., Kinouchi, O., & Copelli, M. (2013). Single-neuron criticality optimizes analog dendritic computation. *Scientific Reports*, *3*(1), 3222. https://doi.org/10.1038/srep03222

Gong, S., Zheng, C., Doughty, M. L., Losos, K., Didkovsky, N., Schambra, U. B., Nowak, N. J., Joyner, A., Leblanc, G., Hatten, M. E., & Heintz, N. (2003). A gene expression atlas of the central nervous system based on bacterial artificial chromosomes. *Nature*, *425*(6961), 917–925. https://doi.org/10.1038/nature02033

Gormezano, E. E. (1962). Nicitatin membrane: Classical conditioning in the Albino Rabbit. *Science*, *138*(3536), 34–36. https://doi.org/10.1126/science.138.3536.34

Gormezano, I., & Moore, J. W. (1962). Effects of instructional set and UCS intensity on the latency, percentage, and form of the eyelid response. *Journal of Experimental Psychology*, *63*(5), 487–494. https://doi.org/10.1037/h0038848

Graham, D. J., & Wylie, D. R. (2012). Zebrin-immunopositive and -immunonegative stripe pairs represent functional units in the pigeon vestibulocerebellum. *The Journal of Neuroscience: The Official Journal of the Society for Neuroscience*, *32*(37), 12769–12779. https://doi.org/10.1523/JNEUROSCI.0197-12.2012

Grasselli, G., Boele, H.-J., Titley, H. K., Bradford, N., van Beers, L., Jay, L., Beekhof, G. C., Busch, S. E., De Zeeuw, C. I., Schonewille, M., & Hansel, C. (2020). SK2 channels in cerebellar Purkinje cells contribute to excitability modulation in motor-learning–specific memory traces. *PLOS Biology*, *18*(1), e3000596. https://doi.org/10.1371/journal.pbio.3000596

Grasselli, G., & Hansel, C. (2014). Chapter Three - Cerebellar Long-Term Potentiation: Cellular Mechanisms and Role in Learning. In M. D. Mauk (Ed.), *International Review of Neurobiology* (Vol. 117, pp. 39–51). Academic Press. https://doi.org/10.1016/B978-0-12-420247-4.00003-8

Guo, C. C., Ke, M. C., & Raymond, J. L. (2014). Cerebellar Encoding of Multiple Candidate Error Cues in the Service of Motor Learning. *Journal of Neuroscience*, *34*(30), 9880–9890. https://doi.org/10.1523/JNEUROSCI.5114-13.2014

Guttman, N., & Kalish, H. I. (1956). Discriminability and stimulus generalization. *Journal of Experimental Psychology*, *51*(1), 79–88. https://doi.org/10.1037/h0046219

Gynther, M. D. (1957). *DIFFERENTIAL EYELID CONDITIONING AS A FUNCTION OF STIMULUS SIMILARITY AND STRENGTH OF RESPONSE TO THE CS J*. 9.

Halverson, H. E., Khilkevich, A., & Mauk, M. D. (2015). Relating Cerebellar Purkinje Cell Activity to the Timing and Amplitude of Conditioned Eyelid Responses. *Journal of Neuroscience*, *35*(20), 7813–7832. https://doi.org/10.1523/JNEUROSCI.3663-14.2015

Halverson, H. E., Khilkevich, A., & Mauk, M. D. (2018). Cerebellar Processing Common to Delay and Trace Eyelid Conditioning. *The Journal of Neuroscience*, *38*(33), 7221–7236. https://doi.org/10.1523/JNEUROSCI.0430-18.2018

Hansel, C., Linden, D. J., & D'Angelo, E. (2001). Beyond parallel fiber LTD: The diversity of synaptic and non-synaptic plasticity in the cerebellum. *Nature Neuroscience*, *4*(5), 467–475. https://doi.org/10.1038/87419

Hansen, S. T., Meera, P., Otis, T. S., & Pulst, S. M. (2013). Changes in Purkinje cell firing and gene expression precede behavioral pathology in a mouse model of SCA2. *Human Molecular Genetics*, *22*(2), 271–283. https://doi.org/10.1093/hmg/dds427

Hanson, H. M. (1957). Discrimination Training Effect on Stimulus Generalization Gradient for Spectrum Stimuli. *Science*, *125*(3253), 888–889. https://doi.org/10.1126/science.125.3253.888

Hardiman, MervynJ., Ramnani, N., & Yeo, ChristopherH. (1996). Reversible inactivations of the cerebellum with muscimol prevent the acquisition and extinction of conditioned nictitating membrane responses in the rabbit. *Experimental Brain Research*, *110*(2). https://doi.org/10.1007/BF00228555

Harding, A. E. (1983). CLASSIFICATION OF THE HEREDITARY ATAXIAS AND PARAPLEGIAS. *The Lancet*, *321*(8334), 1151–1155. https://doi.org/10.1016/S0140-6736(83)92879-9

Hashimoto, K., Ichikawa, R., Kitamura, K., Watanabe, M., & Kano, M. (2009). Translocation of a "Winner" Climbing Fiber to the Purkinje Cell Dendrite and Subsequent Elimination of "Losers" from the Soma in Developing Cerebellum. *Neuron*, *63*(1), 106–118. https://doi.org/10.1016/j.neuron.2009.06.008

Hashimoto, K., & Kano, M. (2005). Postnatal development and synapse elimination of climbing fiber to Purkinje cell projection in the cerebellum. *Neuroscience Research*, *53*(3), 221–228. https://doi.org/10.1016/j.neures.2005.07.007

Hashimoto, M., & Mikoshiba, K. (2003). Mediolateral Compartmentalization of the Cerebellum Is Determined on the "Birth Date" of Purkinje Cells. *The Journal of Neuroscience*, *23*(36), 11342–11351. https://doi.org/10.1523/JNEUROSCI.23-36-11342.2003

Hauge, S. A., Tracy, J. A., Baudry, M., & Thompson, R. F. (1998). Selective changes in AMPA receptors in rabbit cerebellum following classical conditioning of the eyelid-nictitating membrane response. *Brain Research*, *803*(1), 9–18. https://doi.org/10.1016/S0006-8993(98)00525-3

Hawkes, R., & Eisenman, L. M. (1997). Stripes and zones: The origins of regionalization of the adult cerebellum. *Perspectives on Developmental Neurobiology*, *5*(1), 95–105.

Hawkes, R., & Herrup, K. (1995). Aldolase C/zebrin II and the regionalization of the cerebellum. *Journal of Molecular Neuroscience*, *6*(3), 147–158. https://doi.org/10.1007/BF02736761

Hearst, E., Koresko, M. B., & Poppen', R. (1986). *STIMULUS GENERALIZATION AND THE RESPONSE-REINFORCEMENT CONTINGENCY*. 12.

Heffner, H. E., & Heffner, R. S. (2007). Hearing Ranges of Laboratory Animals. *Journal of the American Association for Laboratory Animal Science*, 3.

Heiney, S. A., Kim, J., Augustine, G. J., & Medina, J. F. (2014). Precise Control of Movement Kinematics by Optogenetic Inhibition of Purkinje Cell Activity. *Journal of Neuroscience*, *34*(6), 2321–2330. https://doi.org/10.1523/JNEUROSCI.4547-13.2014

Heiney, S. A., Wohl, M. P., Chettih, S. N., Ruffolo, L. I., & Medina, J. F. (2014). Cerebellar-Dependent Expression of Motor Learning during Eyeblink Conditioning in Head-Fixed Mice. *The Journal of Neuroscience*, *34*(45), 14845–14853. https://doi.org/10.1523/JNEUROSCI.2820-14.2014

Hekman, K. E., & Gomez, C. M. (2015). The autosomal dominant spinocerebellar ataxias: Emerging mechanistic themes suggest pervasive Purkinje cell vulnerability. *Journal of Neurology, Neurosurgery & Psychiatry*, *86*(5), 554–561. https://doi.org/10.1136/jnnp-2014-308421

Hensch, T. K., & Bilimoria, P. M. (2012). Re-opening Windows: Manipulating Critical Periods for Brain Development. *Cerebrum: The Dana Forum on Brain Science*, *2012*, 11.

Hesslow, G. (1994a). Inhibition of classically conditioned eyeblink responses by stimulation of the cerebellar cortex in the decerebrate cat. *The Journal of Physiology*, *476*(2), 245–256. https://doi.org/10.1113/jphysiol.1994.sp020127

Hesslow, G. (1994b). Correspondence between climbing fibre input and motor output in eyeblink-related areas in cat cerebellar cortex. *The Journal of Physiology*, *476*(2), 229–244. https://doi.org/10.1113/jphysiol.1994.sp020126

Hesslow, G., & Ivarsson, M. (1994). Suppression of cerebellar Purkinje cells during conditioned responses in ferrets: *NeuroReport*, *5*(5), 649–652. https://doi.org/10.1097/00001756-199401000-00030

Hesslow, G., Jirenhed, D.-A., Rasmussen, A., & Johansson, F. (2013). Classical conditioning of motor responses: What is the learning mechanism? *Neural Networks*, *47*, 81–87. https://doi.org/10.1016/j.neunet.2013.03.013

Hilgard, E. R., & Marquis, D. G. (1935). Acquisition, extinction, and retention of conditioned lid responses to light in dogs. *Journal of Comparative Psychology*, *19*(1), 29–58. https://doi.org/10.1037/h0057836

Hirano, T. (1990). Depression and potentiation of the synaptic transmission between a granule cell and a Purkinje cell in rat cerebellar culture. *Neuroscience Letters*, *119*(2), 141–144. https://doi.org/10.1016/0304-3940(90)90818-T

Holland, P. C. (1993). Cognitive aspects of classical conditioning. *Current Opinion in Neurobiology*, *3*(2), 230–236. https://doi.org/10.1016/0959-4388(93)90215-K

Honig, W. K., Thomas, D. R., & Guttman, N. (1959). Differential effects of continuous extinction and discrimination training on the generalization gradient. *Journal of Experimental Psychology*, *58*(2), 145–152. https://doi.org/10.1037/h0048484

Hoppenbrouwers, S. S., Schutter, D. J. L. G., Fitzgerald, P. B., Chen, R., & Daskalakis, Z. J. (2008). The role of the cerebellum in the pathophysiology and treatment of neuropsychiatric disorders: A review. *Brain Research Reviews*, *59*(1), 185–200. https://doi.org/10.1016/j.brainresrev.2008.07.005

Horn, K. M., Pong, M., & Gibson, A. R. (2010). Functional Relations of Cerebellar Modules of the Cat. *Journal of Neuroscience*, *30*(28), 9411–9423. https://doi.org/10.1523/JNEUROSCI.0440-10.2010

Hoshino, M., Nakamura, S., Mori, K., Kawauchi, T., Terao, M., Nishimura, Y. V., Fukuda, A., Fuse, T., Matsuo, N., Sone, M., Watanabe, M., Bito, H., Terashima, T., Wright, C. V. E., Kawaguchi, Y., Nakao, K., & Nabeshima, Y. (2005). Ptf1a, a bHLH Transcriptional Gene, Defines GABAergic Neuronal Fates in Cerebellum. *Neuron*, *47*(2), 201–213. https://doi.org/10.1016/j.neuron.2005.06.007

Hosy, E., Piochon, C., Teuling, E., Rinaldo, L., & Hansel, C. (2011). SK2 channel expression and function in cerebellar Purkinje cells: SK2 channel expression and function in Purkinje cells. *The Journal of Physiology*, *589*(14), 3433–3440. https://doi.org/10.1113/jphysiol.2011.205823

Hourez, R., Servais, L., Orduz, D., Gall, D., Millard, I., de Kerchove d'Exaerde, A., Cheron, G., Orr, H. T., Pandolfo, M., & Schiffmann, S. N. (2011). Aminopyridines Correct Early Dysfunction and Delay Neurodegeneration in a Mouse Model of Spinocerebellar Ataxia Type 1. *Journal of Neuroscience*, *31*(33), 11795–11807. https://doi.org/10.1523/JNEUROSCI.0905-11.2011

Hovland, C. I. (1937). The Generalization of Conditioned Responses: I. The Sensory Generalization of Conditioned Responses with Varying Frequencies of Tone. *The Journal of General Psychology*, *17*(1), 125–148. https://doi.org/10.1080/00221309.1937.9917977

Hoxha, E., Balbo, I., Miniaci, M. C., & Tempia, F. (2018). Purkinje Cell Signaling Deficits in Animal Models of Ataxia. *Frontiers in Synaptic Neuroscience*, *10*. https://www.frontiersin.org/articles/10.3389/fnsyn.2018.00006

Huang, J.-M., Money, M. K., Berlin, C. I., & Keats, B. J. B. (1995). Auditory phenotyping of heterozygous sound-responsive (+/dn) and deafness (dn/dn) mice. *Hearing Research*, *88*(1–2), 61–64. https://doi.org/10.1016/0378-5955(95)00099-P

Hupka, R. B., Liu, S. S., & Moore, J. W. (1969). Auditory differential conditioning of the rabbit nictitating membrane response: V. Stimulus generalization as a function of the position of CS+ and CS on the frequency dimension. *Psychonomic Science*, *15*(3), 129–131. https://doi.org/10.3758/BF03336238

Hyson, R. L., & Rudy, J. W. (1984). Ontogenesis of learning. II. Variation in the rat's reflexive and learned responses to acoustic stimulation. *Developmental Psychobiology*, *17*(3), 263–283. https://doi.org/10.1002/dev.420170307

Ichikawa, R., Hashimoto, K., Miyazaki, T., Uchigashima, M., Yamasaki, M., Aiba, A., Kano, M., & Watanabe, M. (2016). Territories of heterologous inputs onto Purkinje cell dendrites are segregated by mGluR1-dependent parallel fiber synapse elimination. *Proceedings of the National Academy of Sciences*, *113*(8), 2282–2287. https://doi.org/10.1073/pnas.1511513113

Ichise, T., Kano, M., Hashimoto, K., Yanagihara, D., Nakao, K., Shigemoto, R., Katsuki, M., & Aiba, A. (2000). MGluR1 in Cerebellar Purkinje Cells Essential for Long-Term Depression, Synapse

Elimination, and Motor Coordination. *Science*, *288*(5472), 1832–1835. https://doi.org/10.1126/science.288.5472.1832

Ingham, N. J., Pearson, S., & Steel, K. P. (2011). Using the Auditory Brainstem Response (ABR) to Determine Sensitivity of Hearing in Mutant Mice. *Current Protocols in Mouse Biology*, *1*(2), 279–287. https://doi.org/10.1002/9780470942390.mo110059

Ison, J. R., Allen, P. D., & O'Neill, W. E. (2007). Age-Related Hearing Loss in C57BL/6J Mice has both Frequency-Specific and Non-Frequency-Specific Components that Produce a Hyperacusis-Like Exaggeration of the Acoustic Startle Reflex. *JARO: Journal of the Association for Research in Otolaryngology*, *8*(4), 539–550. https://doi.org/10.1007/s10162-007-0098-3

Isope, P., & Barbour, B. (2002). Properties of Unitary Granule Cell→Purkinje Cell Synapses in Adult Rat Cerebellar Slices. *The Journal of Neuroscience*, *22*(22), 9668–9678. https://doi.org/10.1523/JNEUROSCI.22-22-09668.2002

Ito, M. (1982). Cerebellar Control of the Vestibulo-Ocular Reflex–Around the Flocculus Hypothesis. *Annual Review of Neuroscience*, *5*(1), 275–297. https://doi.org/10.1146/annurev.ne.05.030182.001423

Ito, M. (1986). Long-term depression as a memory process in the cerebellum. *Neuroscience Research*, *3*(6), 531–539. https://doi.org/10.1016/0168-0102(86)90052-0

Ito, M. (2000). Mechanisms of motor learning in the cerebellum11Published on the World Wide Web on 24 November 2000. *Brain Research*, *886*(1), 237–245. https://doi.org/10.1016/S0006-8993(00)03142-5

Ito, M. (2002). Historical Review of the Significance of the Cerebellum and the Role of Purkinje Cells in Motor Learning. *Annals of the New York Academy of Sciences*, *978*(1 THE CEREBELLU), 273–288. https://doi.org/10.1111/j.1749-6632.2002.tb07574.x

Ito, M. (2008). Control of mental activities by internal models in the cerebellum. *Nature Reviews Neuroscience*, *9*(4), 304–313. https://doi.org/10.1038/nrn2332

Ito, M. (2014). Cerebellar Microcircuitry☆. In *Reference Module in Biomedical Sciences* (p. B978012801238304544X). Elsevier. https://doi.org/10.1016/B978-0-12-801238-3.04544-X

Ito, M., & Itō, M. (1984). *The cerebellum and neural control*. Raven press.

Ito, M., & Kano, M. (1982). Long-lasting depression of parallel fiber-Purkinje cell transmission induced by conjunctive stimulation of parallel fibers and climbing fibers in the cerebellar cortex. *Neuroscience Letters*, *33*(3), 253–258. https://doi.org/10.1016/0304-3940(82)90380-9

Jacobi, H., Reetz, K., Tezenas du Montcel, S., Bauer, P., Mariotti, C., Nanetti, L., Rakowicz, M., Sulek, A., Durr, A., Charles, P., Filla, A., Antenora, A., Schöls, L., Schicks, J., Infante, J., Kang, J.-S., Timmann, D., Fabio, R., Masciullo, M., & Klockgether, T. (2013). Biological and clinical characteristics of individuals at risk for spinocerebellar ataxia types 1, 2, 3, and 6 in the longitudinal RISCA study: Analysis of baseline data. *Lancet Neurology*, *12*. https://doi.org/10.1016/S1474-4422(13)70104-2

Jelitai, M., Puggioni, P., Ishikawa, T., Rinaldi, A., & Duguid, I. (2016). Dendritic excitation–inhibition balance shapes cerebellar output during motor behavior. *Nature Communications*, *7*(1), 13722. https://doi.org/10.1038/ncomms13722

Ji, Z., & Hawkes, R. (1995). Developing mossy fiber terminal fields in the rat cerebellar cortex may segregate because of Purkinje cell compartmentation and not competition. *Journal of Comparative Neurology*, *359*(2), 197–212. https://doi.org/10.1002/cne.903590202

Jirenhed, D.-A., Bengtsson, F., & Hesslow, G. (2007). Acquisition, Extinction, and Reacquisition of a Cerebellar Cortical Memory Trace. *Journal of Neuroscience*, *27*(10), 2493–2502. https://doi.org/10.1523/JNEUROSCI.4202-06.2007

Jirenhed, D.-A., & Hesslow, G. (2011). Time Course of Classically Conditioned Purkinje Cell Response Is Determined by Initial Part of Conditioned Stimulus. *Journal of Neuroscience*, *31*(25), 9070–9074. https://doi.org/10.1523/JNEUROSCI.1653-11.2011

Jirenhed, D.-A., Rasmussen, A., Johansson, F., & Hesslow, G. (2017). Learned response sequences in cerebellar Purkinje cells. *Proceedings of the National Academy of Sciences*, *114*(23), 6127–6132. https://doi.org/10.1073/pnas.1621132114

Johannson, K. A., Vittinghoff, E., Lee, K., Balmes, J. R., Ji, W., Kaplan, G. G., Kim, D. S., & Collard, H. R. (2014). Acute exacerbation of idiopathic pulmonary fibrosis associated with air pollution exposure. *European Respiratory Journal*, *43*(4), 1124–1131. https://doi.org/10.1183/09031936.00122213

Johansson, F., Hesslow, G., & Medina, J. F. (2016). Mechanisms for motor timing in the cerebellar cortex. *Current Opinion in Behavioral Sciences*, *8*, 53–59. https://doi.org/10.1016/j.cobeha.2016.01.013

Jörntell, H., & Ekerot, C.-F. (2002). Reciprocal Bidirectional Plasticity of Parallel Fiber Receptive Fields in Cerebellar Purkinje Cells and Their Afferent Interneurons. *Neuron*, *34*(5), 797–806. https://doi.org/10.1016/S0896-6273(02)00713-4

Kano, M., Hashimoto, K., Chen, C., Abeliovich, A., Aiba, A., Kurihara, H., Watanabe, M., Inoue, Y., & Tonegawa, S. (1995). Impaired synapse elimination during cerebellar development in PKCγ mutant mice. *Cell*, *83*(7), 1223–1231.

Kano, M., Hashimoto, K., Kurihara, H., Watanabe, M., Inoue, Y., Aiba, A., & Tonegawa, S. (1997). Persistent Multiple Climbing Fiber Innervationof Cerebellar Purkinje Cellsin Mice Lacking mGluR1. *Neuron*, *18*(1), 71–79. https://doi.org/10.1016/S0896-6273(01)80047-7

Kano, M., Watanabe, T., Uesaka, N., & Watanabe, M. (2018). Multiple Phases of Climbing Fiber Synapse Elimination in the Developing Cerebellum. *The Cerebellum*, *17*(6), 722–734. https://doi.org/10.1007/s12311-018-0964-z

Kashiwabuchi, N., Ikeda, K., Araki, K., Hirano, T., Shibuki, K., Takayama, C., Inoue, Y., Kutsuwada, T., Yagi, T., Kang, Y., Aizawa, S., & Mishina'e, M. (1995). *Impairment of Motor Coordination, Purkinje Cell Synapse Formation, and Cerebellar Long-Term Depression in GluR ;2 Mutant Mice*. 8.

Kasumu, A., & Bezprozvanny, I. (2012). Deranged Calcium Signaling in Purkinje Cells and Pathogenesis in Spinocerebellar Ataxia 2 (SCA2) and Other Ataxias. *The Cerebellum*, *11*(3), 630–639. https://doi.org/10.1007/s12311-010-0182-9

Kawamura, Y., Nakayama, H., Hashimoto, K., Sakimura, K., Kitamura, K., & Kano, M. (2013). Spike timing-dependent selective strengthening of single climbing fibre inputs to Purkinje cells during cerebellar development. *Nature Communications*, *4*(1), 2732. https://doi.org/10.1038/ncomms3732

Kehoe, E. J. (1982). Overshadowing and summation in compound stimulus conditioning of the rabbit's nictitating membrane response. *Journal of Experimental Psychology: Animal Behavior Processes*, *8*(4), 313–328. https://doi.org/10.1037/0097-7403.8.4.313

Kehoe, E. J., Horne, A. J., & Macrae, M. (1995). Learning to Learn: Real-Time Features and a Connectionist Model. *Adaptive Behavior*, *3*(3), 235–271. https://doi.org/10.1177/105971239500300301

Kehoe, E. J., & Joscelyne, A. (2005). Temporally specific extinction of conditioned responses in the rabbit (Oryctolagus cuniculus) nictitating membrane preparation. *Behavioral Neuroscience*, *119*(4), 1011–1022. https://doi.org/10.1037/0735-7044.119.4.1011

Kehoe, E. J., Ludvig, E. A., Dudeney, J. E., Neufeld, J., & Sutton, R. S. (2008). Magnitude and timing of nictitating membrane movements during classical conditioning of the rabbit (Oryctolagus cuniculus). *Behavioral Neuroscience*, *122*(2), 471–476. https://doi.org/10.1037/0735-7044.122.2.471

Kehoe, E. J., & white, N. E. (2002). Extinction revisited: Similarities between extinction and reductions in US intensity in classical conditioning of the rabbit's nictitating membrane response. *Animal Learning & Behavior*, *30*(2), 96–111. https://doi.org/10.3758/BF03192912

Kern, J. K. (2002). The possible role of the cerebellum in autism/PDD: Disruption of a multisensory feedback loop. *Medical Hypotheses*, *59*(3), 255–260. https://doi.org/10.1016/S0306-9877(02)00212-8

Khilkevich, A., Canton-Josh, J., DeLord, E., & Mauk, M. D. (2018). A cerebellar adaptation to uncertain inputs. *Science Advances*, *4*(5), eaap9660. https://doi.org/10.1126/sciadv.aap9660

Kim, C.-H., Oh, S.-H., Lee, J. H., Chang, S. O., Kim, J., & Kim, S. J. (2012). Lobule-specific membrane excitability of cerebellar Purkinje cells. *The Journal of Physiology*, *590*(2), 273–288. https://doi.org/10.1113/jphysiol.2011.221846

Kim, E. J., Horovitz, O., Pellman, B. A., Tan, L. M., Li, Q., Richter-Levin, G., & Kim, J. J. (2013). Dorsal periaqueductal gray-amygdala pathway conveys both innate and learned fear responses in rats. *Proceedings of the National Academy of Sciences*, *110*(36), 14795–14800. https://doi.org/10.1073/pnas.1310845110

Kim, J. J., & Thompson, R. E. (1997). Cerebellar circuits and synaptic mechanisms involved in classical eyeblink conditioning. *Trends in Neurosciences*, *20*(4), 177–181. https://doi.org/10.1016/S0166-2236(96)10081-3

Kim, S. J. (2013). TRPC3 Channel Underlies Cerebellar Long-Term Depression. *The Cerebellum*, *12*(3), 334–337. https://doi.org/10.1007/s12311-013-0455-1

Kimura, K., Hirano, M., Kobayashi, R., & Hirano, T. (1998). Phosphorylation and Activation of 13 *S* Condensin by Cdc2 in Vitro. *Science*, *282*(5388), 487–490. https://doi.org/10.1126/science.282.5388.487

King, J., Insanally, M., Jin, M., Martins, A. R. O., D'amour, J. A., & Froemke, R. C. (2015). Rodent auditory perception: Critical band limitations and plasticity. *Neuroscience*, *296*, 55–65. https://doi.org/10.1016/j.neuroscience.2015.03.053

Klockgether, T., Mariotti, C., & Paulson, H. L. (2019). Spinocerebellar ataxia. *Nature Reviews Disease Primers*, *5*(1), 1–21. https://doi.org/10.1038/s41572-019-0074-3

Kloth, A. D., Badura, A., Li, A., Cherskov, A., Connolly, S. G., Giovannucci, A., Bangash, M. A., Grasselli, G., Peñagarikano, O., Piochon, C., Tsai, P. T., Geschwind, D. H., Hansel, C., Sahin, M., Takumi, T., Worley, P. F., & Wang, S. S.-H. (2015). Cerebellar associative sensory learning defects in five mouse autism models. *ELife*, *4*, e06085. https://doi.org/10.7554/eLife.06085

Koekkoek, S. K. E. (2003). Cerebellar LTD and Learning-Dependent Timing of Conditioned Eyelid Responses. *Science*, *301*(5640), 1736–1739. https://doi.org/10.1126/science.1088383

Koekkoek, S. K. E., Den Ouden, W. L., Perry, G., Highstein, S. M., & De Zeeuw, C. I. (2002). Monitoring Kinetic and Frequency-Domain Properties of Eyelid Responses in Mice With Magnetic Distance Measurement Technique. *Journal of Neurophysiology*, *88*(4), 2124–2133. https://doi.org/10.1152/jn.2002.88.4.2124

Konno, A., Shuvaev, A., Miyake, N., Miyake, K., Iizuka, A., Matsuura, S., Huda, F., Nakamura, K., Yanagi, S., Shimada, T., & Hirai, H. (2013). Mutant Ataxin-3 with an Abnormally Expanded Polyglutamine Chain Disrupts Dendritic Development and Metabotropic Glutamate Receptor Signaling in Mouse Cerebellar Purkinje Cells. *Cerebellum (London, England)*, *13*. https://doi.org/10.1007/s12311-013-0516-5

Koo, T., & Wood, M. J. (2013). Clinical Trials Using Antisense Oligonucleotides in Duchenne Muscular Dystrophy. *Human Gene Therapy*, *24*(5), 479–488. https://doi.org/10.1089/hum.2012.234

Korn, H., & Axelrad, H. (1980). Electrical inhibition of Purkinje cells in the cerebellum of the rat. *Proceedings of the National Academy of Sciences*, *77*(10), 6244–6247. https://doi.org/10.1073/pnas.77.10.6244

Kronenbuerger, M., Gerwig, M., Brol, B., Block, F., & Timmann, D. (2007). Eyeblink conditioning is impaired in subjects with essential tremor. *Brain*, *130*(6), 1538–1551. https://doi.org/10.1093/brain/awm081

Krupa, D. J., Thompson, J. K., & Thompson, R. F. (1993). Localization of a Memory Trace in the Mammalian Brain. *Science*, *260*(5110), 989–991.

Krupa, D. J., Weiss, C., Tracy, J., & Thompson, R. F. (1990). Single unit responses from the cerebellar cortex of naive rabbits. *Society for Neuroscience Abstracts*, *16*, 762.

Kuo, P.-H., Gan, S.-R., Wang, J., Lo, R. Y., Figueroa, K. P., Tomishon, D., Pulst, S. M., Perlman, S., Wilmot, G., Gomez, C. M., Schmahmann, J. D., Paulson, H., Shakkottai, V. G., Ying, S. H., Zesiewicz, T., Bushara, K., Geschwind, M. D., Xia, G., Subramony, S. H., … Kuo, S.-H. (2017). Dystonia and ataxia progression in spinocerebellar ataxias. *Parkinsonism & Related Disorders*, *45*, 75–80. https://doi.org/10.1016/j.parkreldis.2017.10.007

Kuo, S.-H., Lin, C.-Y., Wang, J., Sims, P. A., Pan, M.-K., Liou, J., Lee, D., Tate, W. J., Kelly, G. C., Louis, E. D., & Faust, P. L. (2017). Climbing fiber-Purkinje cell synaptic pathology in tremor and cerebellar degenerative diseases. *Acta Neuropathologica*, *133*(1), 121–138. https://doi.org/10.1007/s00401-016-1626-1

Lam, Y. C., Bowman, A. B., Jafar-Nejad, P., Lim, J., Richman, R., Fryer, J. D., Hyun, E. D., Duvick, L. A., Orr, H. T., Botas, J., & Zoghbi, H. Y. (2006). ATAXIN-1 Interacts with the Repressor Capicua in Its Native Complex to Cause SCA1 Neuropathology. *Cell*, *127*(7), 1335–1347. https://doi.org/10.1016/j.cell.2006.11.038

Lange, I., Kasanova, Z., Goossens, L., Leibold, N., De Zeeuw, C. I., van Amelsvoort, T., & Schruers, K. (2015). The anatomy of fear learning in the cerebellum: A systematic meta-analysis. *Neuroscience & Biobehavioral Reviews*, *59*, 83–91. https://doi.org/10.1016/j.neubiorev.2015.09.019

Lannoo, M. J., Ross, L., Maler, L., & Hawkes, R. (1991). Development of the cerebellum and its extracerebellar purkinje cell projection in teleost fishes as determined by zebrin II immunocytochemistry. *Progress in Neurobiology*, *37*(4), 329–363. https://doi.org/10.1016/0301-0082(91)90022-S

Larouche, M., Che, P. M., & Hawkes, R. (2006). Neurogranin expression identifies a novel array of Purkinje cell parasagittal stripes during mouse cerebellar development. *Journal of Comparative Neurology*, *494*(2), 215–227. https://doi.org/10.1002/cne.20791

Larouche, M., & Hawkes, R. (2006). From clusters to stripes: The developmental origins of adult cerebellar compartmentation. *The Cerebellum*, *5*(2), 77–88. https://doi.org/10.1080/14734220600804668

Lashley, K. S., & Wade, M. (1946). The Pavlovian theory of generalization. *Psychological Review*, *53*(2), 72–87. https://doi.org/10.1037/h0059999

Laufer, O., Israeli, D., & Paz, R. (2016). Behavioral and Neural Mechanisms of Overgeneralization in Anxiety. *Current Biology*, *26*(6), 713–722. https://doi.org/10.1016/j.cub.2016.01.023

Laxmi, T. R., Stork, O., & Pape, H.-C. (2003). Generalisation of conditioned fear and its behavioral expression in mice. *Behavioral Brain Research*, *145*(1–2), 89–98. https://doi.org/10.1016/S0166-4328(03)00101-3

Leclerc, N., Dore´, L., Parent, A., & Hawkes, R. (1990). The compartmentalization of the monkey and rat cerebellar cortex: Zebrin I and cytochrome oxidase. *Brain Research*, *506*(1), 70–78. https://doi.org/10.1016/0006-8993(90)91200-Z

Leergaard, T., & Bjaalie, J. (2007). Topography of the complete corticopontine projection: From experiments to principal maps. *Frontiers in Neuroscience*, *1*. https://www.frontiersin.org/articles/10.3389/neuro.01.1.1.016.2007

Lepora, N., Porrill, J., Yeo, C., & Dean, P. (2010). Sensory Prediction or Motor Control? Application of Marr–Albus Type Models of Cerebellar Function to Classical Conditioning. *Frontiers in Computational Neuroscience*, *4*. https://www.frontiersin.org/articles/10.3389/fncom.2010.00140

Lewis, J. L., Loturco, J. J., & Solomon, P. R. (1987). Lesions of the middle cerebellar peduncle disrupt acquisition and retention of the rabbit's classically conditioned nicititating membrane response. *Behav. Neurosci*, 101–151.

Lewis, P. M., Gritli-Linde, A., Smeyne, R., Kottmann, A., & McMahon, A. P. (2004). Sonic hedgehog signaling is required for expansion of granule neuron precursors and patterning of the mouse cerebellum. *Developmental Biology*, *270*(2), 393–410. https://doi.org/10.1016/j.ydbio.2004.03.007

Lin, X., Antalffy, B., Kang, D., Orr, H. T., & Zoghbi, H. Y. (2000). Polyglutamine expansion down-regulates specific neuronal genes before pathologic changes in SCA1. *Nature Neuroscience*, *3*(2), 157–163. https://doi.org/10.1038/72101

Linden, D. J., & Ahn, S. (1999). Activation of Presynaptic cAMP-Dependent Protein Kinase Is Required for Induction of Cerebellar Long-Term Potentiation. *The Journal of Neuroscience*, *19*(23), 10221–10227. https://doi.org/10.1523/JNEUROSCI.19-23-10221.1999

Lisberger, S. G. (1988). The Neural Basis for Learning of Simple Motor Skills. *Science*, *242*(4879), 728–735.

Lissek, S., Biggs, A. L., Rabin, S. J., Cornwell, B. R., Alvarez, R. P., Pine, D. S., & Grillon, C. (2008). Generalization of conditioned fear-potentiated startle in humans: Experimental validation and clinical relevance. *Behavior Research and Therapy*, *46*(5), 678–687. https://doi.org/10.1016/j.brat.2008.02.005

Liu, S. S. (1971). Differential conditioning and stimulus generalization of the rabbit's nictitating membrane response. *Journal of Comparative and Physiological Psychology*, *77*(1), 136–142. https://doi.org/10.1037/h0031587

Llinás, R., & Welsh, J. P. (1993). On the cerebellum and motor learning. *Current Opinion in Neurobiology*, *3*(6), 958–965. https://doi.org/10.1016/0959-4388(93)90168-X

Louis, E. D., Kerridge, C. A., Chatterjee, D., Martuscello, R. T., Diaz, D. T., Koeppen, A. H., Kuo, S.-H., Vonsattel, J.-P. G., Sims, P. A., & Faust, P. L. (2019). Contextualizing the pathology in the essential tremor cerebellar cortex: A patholog-omics approach. *Acta Neuropathologica*, *138*(5), 859–876. https://doi.org/10.1007/s00401-019-02043-7

Lubow, R. (1973). Latent inhibition. *Psychological Bulletin*, *79*(6), 398–407. https://doi.org/10.1037/h0034425

Lubow, R., & Moore, A. (1959). Latent inhibition: The effect of nonreinforced pre-exposure to the conditional stimulus. *Journal of Comparative and Physiological Psychology*, *52*, 415–419. https://doi.org/10.1037/h0046700

de Luca, A. de, Vassallo, S., Benitez-Temino, B., Menichetti, G., Rossi, F., & Buffo, A. (2009). Distinct Modes of Neuritic Growth in Purkinje Neurons at Different Developmental Stages: Axonal Morphogenesis and Cellular Regulatory Mechanisms. *PLOS ONE*, *4*(8), e6848. https://doi.org/10.1371/journal.pone.0006848

Mackintosh, N. J. (1974). *The psychology of animal learning* (pp. xiv, 730). Academic Press.

Mainen, Z. F., & Sejnowski, T. J. (1996). Influence of dendritic structure on firing pattern in model neocortical neurons. *Nature*, *382*(6589), 363–366. https://doi.org/10.1038/382363a0

Manto, M., Bower, J. M., Conforto, A. B., Delgado-García, J. M., da Guarda, S. N. F., Gerwig, M., Habas, C., Hagura, N., Ivry, R. B., Mariën, P., Molinari, M., Naito, E., Nowak, D. A., Oulad Ben Taib, N., Pelisson, D., Tesche, C. D., Tilikete, C., & Timmann, D. (2012). Consensus Paper: Roles of the Cerebellum in Motor Control—The Diversity of Ideas on Cerebellar Involvement in Movement. *The Cerebellum*, *11*(2), 457–487. https://doi.org/10.1007/s12311-011-0331-9

Marr, D. (1969). *A THEORY OF CEREBELLAR CORTEX*. 35.

Martin, P., & Albers, M. (1995). Cerebellum and Schizophrenia: A Selective Review. *Schizophrenia Bulletin*, *21*(2), 241–250. https://doi.org/10.1093/schbul/21.2.241

Martin, S. J., Grimwood, P. D., & Morris, R. G. M. (2000). Synaptic Plasticity and Memory: An Evaluation of the Hypothesis. *Annual Review of Neuroscience*, *23*(1), 649–711. https://doi.org/10.1146/annurev.neuro.23.1.649

Marzban, H., Chung, S., Watanabe, M., & Hawkes, R. (2007). Phospholipase cβ4 expression reveals the continuity of cerebellar topography through development. *Journal of Comparative Neurology*, *502*(5), 857–871. https://doi.org/10.1002/cne.21352

Maschke, M., Erichsen, M., Drepper, J., Jentzen, W., Müller, S. P., Kolb, F. P., Diener, H.-C., & Timmann, D. (2003). Cerebellar representation of the eyeblink response as revealed by PET. *NeuroReport*, *14*(10), 1371–1374. https://doi.org/10.1097/01.wnr.0000078540.07662.d9

Mateos, J. M., Benítez, R., Elezgarai, I., Azkue, J. J., Lázaro, E., Osorio, A., Bilbao, A., Doñate, F., Sarría, R., Conquet, F., Ferraguti, F., Kuhn, R., Knöpfel, T., & Grandes, P. (2000). Immunolocalization of the mGluR1b Splice Variant of the Metabotropic Glutamate Receptor 1 at Parallel Fiber-Purkinje Cell Synapses in the Rat Cerebellar Cortex. *Journal of Neurochemistry*, *74*(3), 1301–1309. https://doi.org/10.1046/j.1471-4159.2000.741301.x

Mauk, M. D., & Buonomano, D. V. (2004). THE NEURAL BASIS OF TEMPORAL PROCESSING. *Annual Review of Neuroscience*, *27*(1), 307–340. https://doi.org/10.1146/annurev.neuro.27.070203.144247

Mauk, M. D., & Donegan, N. H. (1997). A model of Pavlovian eyelid conditioning based on the synaptic organization of the cerebellum. *Learning & Memory*, *4*(1), 130–158. https://doi.org/10.1101/lm.4.1.130

Mauk, M. D., & Ruiz, B. P. (1992). *Learning-Dependent Timing of Pavlovian Eyelid Responses: Differential Conditioning Using Multiple Interstimulus Intervals*. 16.

Mauk, M. D., Steinmetz, J. E., & Thompson, R. F. (1986). Classical conditioning using stimulation of the inferior olive as the unconditioned stimulus. *Proceedings of the National Academy of Sciences*, *83*(14), 5349–5353. https://doi.org/10.1073/pnas.83.14.5349

McCormick, D. A., Clark, G. A., Lavond, D. G., & Thompson, R. F. (1982). Initial localization of the memory trace for a basic form of learning. *Proceedings of the National Academy of Sciences*, *79*(8), 2731–2735. https://doi.org/10.1073/pnas.79.8.2731

Mccormick, D. A., Lavond, D. G., Clark, G. A., Kettner, R. E., Rising, C. E., & Thompson, R. F. (1981). The engram found? Role of the cerebellum in classical conditioning of nictitating membrane and eyelid responses. *Bulletin of the Psychonomic Society*, *18*(3), 103–105. https://doi.org/10.3758/BF03333573

McCormick, D. A., Lavond, D. G., & Thompson, R. F. (1982). Concomitant classical conditioning of the rabbit nictitating membrane and eyelid responses: Correlations and implications. *Physiology & Behavior*, *28*(5), 769–775. https://doi.org/10.1016/0031-9384(82)90192-5

McCormick, D. A., Steinmetz, J. E., & Thompson, R. F. (1985). Lesions of the inferior olivary complex cause extinction of the classically conditioned eyeblink response. *Brain Research*, *359*(1), 120–130. https://doi.org/10.1016/0006-8993(85)91419-2

McCormick, D. A., & Thompson, R. F. (1984). Cerebellum: Essential Involvement in the Classically Conditioned Eyelid Response. *Science*, *223*(4633), 296–299.

McKay, B. E., & Turner, R. W. (2005). Physiological and morphological development of the rat cerebellar Purkinje cell. *The Journal of Physiology*, *567*(Pt 3), 829–850. https://doi.org/10.1113/jphysiol.2005.089383

Medina, J. F., & Lisberger, S. G. (2007). Variation, Signal, and Noise in Cerebellar Sensory-Motor Processing for Smooth-Pursuit Eye Movements. *Journal of Neuroscience*, *27*(25), 6832–6842. https://doi.org/10.1523/JNEUROSCI.1323-07.2007

Medina, J. F., & Mauk, M. D. (2000). Computer simulation of cerebellar information processing. *Nature Neuroscience*, *3*(S11), 1205–1211. https://doi.org/10.1038/81486

Meulders, A., & Vlaeyen, J. W. S. (2013). The acquisition and generalization of cued and contextual pain-related fear: An experimental study using a voluntary movement paradigm: *Pain*, *154*(2), 272–282. https://doi.org/10.1016/j.pain.2012.10.025

Miles, F. A. (1981). Lisberger SG Plasticity in the vestibulo-ocular reflex: A new hypothesis. *Annu Rev Neurosci*, *4*, 273–299.

Miquel, M., Toledo, R., Garcia, L., Coria-Avila, G., & Manzo, J. (2009). Why Should We Keep the Cerebellum in Mind When Thinking About Addiction? *Current Drug Abuse Reviewse*, *2*(1), 26–40. https://doi.org/10.2174/1874473710902010026

Mittman, E. (2005). Fashioning the Socialist Nation: The Gender of Consumption in Slatan Dudow's 'Destinies of Women'. *German Politics & Society*, *23*(4 (77)), 28–44.

Mittmann, W., Koch, U., & Häusser, M. (2005). Feed-forward inhibition shapes the spike output of cerebellar Purkinje cells: Feed-forward inhibition in the cerebellar cortex. *The Journal of Physiology*, *563*(2), 369–378. https://doi.org/10.1113/jphysiol.2004.075028

Montarolo, P. G., Palestini, M., & Strata, P. (1982). The inhibitory effect of the olivocerebellar input on the cerebellar Purkinje cells in the rat†. *The Journal of Physiology*, *332*(1), 187–202. https://doi.org/10.1113/jphysiol.1982.sp014409

Moore, J. W. (1964). Differential eyelid conditioning as a function of the frequency and intensity of auditory CSs. *Journal of Experimental Psychology*, *68*(3), 250–259. https://doi.org/10.1037/h0040807

Moore, J. W. (1972). Stimulus control: Studies of auditory generalization in rabbits. *Classical Conditioning II: Current Research and Theory*, 206–230.

Moore, J. W., & Mis, F. W. (1973). Differential conditioning along two dimensions and stimulus generalization of the rabbit's nictitating membrane response. *Bulletin of the Psychonomic Society*, *1*(2), 123–125. https://doi.org/10.3758/BF03334316

Morales, D., & Hatten, M. E. (2006). Molecular Markers of Neuronal Progenitors in the Embryonic Cerebellar Anlage. *Journal of Neuroscience*, *26*(47), 12226–12236. https://doi.org/10.1523/JNEUROSCI.3493-06.2006

Mostofi, A., Holtzman, T., Grout, A. S., Yeo, C. H., & Edgley, S. A. (2010). Electrophysiological Localization of Eyeblink-Related Microzones in Rabbit Cerebellar Cortex. *Journal of Neuroscience*, *30*(26), 8920–8934. https://doi.org/10.1523/JNEUROSCI.6117-09.2010

Moulton, E. A., Elman, I., Becerra, L. R., Goldstein, R. Z., & Borsook, D. (2014). The cerebellum and addiction: Insights gained from neuroimaging research: Cerebellum and addiction. *Addiction Biology*, *19*(3), 317–331. https://doi.org/10.1111/adb.12101

Moye, T. B., & Rudy, J. W. (1985). Ontogenesis of learning: VI. Learned and unlearned responses to visual stimulation in the infant hooded rat. *Developmental Psychobiology*, *18*(5), 395–409. https://doi.org/10.1002/dev.420180505

Nagao, S. (1989). Role of cerebellar flocculus in adaptive interaction between optokinetic eye movement response and vestibulo-ocular reflex in pigmented rabbits. *Experimental Brain Research*, *77*(3), 541–551. https://doi.org/10.1007/BF00249607

Najafi, F., & Medina, J. F. (2020). Bidirectional short-term plasticity during single-trial learning of cerebellar-driven eyelid movements in mice. *Neurobiology of Learning and Memory*, *170*, 107097. https://doi.org/10.1016/j.nlm.2019.107097

Namba, K., Sugihara, I., & Hashimoto, M. (2011). Close correlation between the birth date of purkinje cells and the longitudinal compartmentalization of the mouse adult cerebellum. *Journal of Comparative Neurology*, *519*(13), 2594–2614. https://doi.org/10.1002/cne.22640

Narain, D., Remington, E. D., Zeeuw, C. I. D., & Jazayeri, M. (2018). A cerebellar mechanism for learning prior distributions of time intervals. *Nature Communications*, *9*(1), 469. https://doi.org/10.1038/s41467-017-02516-x

Navabpour, S., Kwapis, J. L., & Jarome, T. J. (2020). A neuroscientist's guide to transgenic mice and other genetic tools. *Neuroscience & Biobehavioral Reviews*, *108*, 732–748. https://doi.org/10.1016/j.neubiorev.2019.12.013

Nedelescu, H., & Abdelhack, M. (2013). Comparative Morphology of Dendritic Arbors in Populations of Purkinje Cells in Mouse Sulcus and Apex. *Neural Plasticity*, *2013*, e948587. https://doi.org/10.1155/2013/948587

Nedelescu, H., Abdelhack, M., & Pritchard, A. T. (2018). Regional differences in Purkinje cell morphology in the cerebellar vermis of male mice. *Journal of Neuroscience Research*, *96*(9), 1476–1489. https://doi.org/10.1002/jnr.24206

Nguyen-Vu, T. D. B., Kimpo, R. R., Rinaldi, J. M., Kohli, A., Zeng, H., Deisseroth, K., & Raymond, J. L. (2013). Cerebellar Purkinje cell activity drives motor learning. *Nature Neuroscience*, *16*(12), 1734–1736. https://doi.org/10.1038/nn.3576

Nicholson, D. A., & Freeman, J. H. (2000). Developmental Changes in Eye-Blink Conditioning and Neuronal Activity in the Inferior Olive. *Journal of Neuroscience*, *20*(21), 8218–8226. https://doi.org/10.1523/JNEUROSCI.20-21-08218.2000

Nicholson, D. A., & Freeman, J. H. (2003). Developmental Changes in Evoked Purkinje Cell Complex Spike Responses. *Journal of Neurophysiology*, *90*(4), 2349–2357. https://doi.org/10.1152/jn.00481.2003

Nicholson, D. A., & Freeman, J. H. (2004). Developmental changes in eyeblink conditioning and simple spike activity in the cerebellar cortex. *Developmental Psychobiology*, *44*(1), 45–57. https://doi.org/10.1002/dev.10149

Nordholm, A., Thompson, J., Dersarkissian, C., & Thompson, R. (1993). Lidocaine Infusion in a Critical Region of Cerebellum Completely Prevents Learning of the Conditioned Eyeblink Response. *Behavioral Neuroscience*, *107*, 882–886. https://doi.org/10.1037//0735-7044.107.5.882

Notartomaso, S., Zappulla, C., Biagioni, F., Cannella, M., Bucci, D., Mascio, G., Scarselli, P., Fazio, F., Weisz, F., Lionetto, L., Simmaco, M., Gradini, R., Battaglia, G., Signore, M., Puliti, A., & Nicoletti, F. (2013). Pharmacological enhancement of mGlu1 metabotropic glutamate receptors causes a prolonged symptomatic benefit in a mouse model of spinocerebellar ataxia type 1. *Molecular Brain*, *6*(1), 48. https://doi.org/10.1186/1756-6606-6-48

Nunes, M. L. A., Sotelo, C., & Wehrlé, R. (1988). Organization of spinocerebellar projection map in three types of agranular cerebellum: Purkinje cells vs. granule cells as organizer element. *Journal of Comparative Neurology*, *273*(1), 120–136. https://doi.org/10.1002/cne.902730110

Oh, A. K., Jacobson, K. M., Jen, J. C., & Baloh, R. W. (2001). Slowing of voluntary and involuntary saccades: An early sign in spinocerebellar ataxia type 7. *Annals of Neurology*, *49*(6), 801–804. https://doi.org/10.1002/ana.1059

Ohinata, S. (1978). *SHIFT OF THE AURATUS) ON A CONTINUUM*. 10.

Ohmae, S., Kunimatsu, J., & Tanaka, M. (2017). Cerebellar Roles in Self-Timing for Sub- and Supra-Second Intervals. *The Journal of Neuroscience*, *37*(13), 3511–3522. https://doi.org/10.1523/JNEUROSCI.2221-16.2017

Ohmae, S., & Medina, J. F. (2015). Climbing fibers encode a temporal-difference prediction error during cerebellar learning in mice. *Nature Neuroscience*, *18*(12), 1798–1803. https://doi.org/10.1038/nn.4167

Ohyama, T. (2003). Stimulus Generalization of Conditioned Eyelid Responses Produced Without Cerebellar Cortex: Implications for Plasticity in the Cerebellar Nuclei. *Learning & Memory*, *10*(5), 346–354. https://doi.org/10.1101/lm.67103

Oswald, B. B., Knuckley, B., Mahan, K., Sanders, C., & Powell, D. A. (2009). Prefrontal control of trace eyeblink conditioning in rabbits (Oryctolagus cuniculus) II: Effects of type of unconditioned stimulus (air puff vs. periorbital shock) and unconditioned stimulus intensity. *Physiology & Behavior*, *96*(1), 67–72. https://doi.org/10.1016/j.physbeh.2008.08.013

Ozol, K., Hayden, J. M., Oberdick, J., & Hawkes, R. (1999). Transverse zones in the vermis of the mouse cerebellum. *Journal of Comparative Neurology*, *412*(1), 95–111. https://doi.org/10.1002/(SICI)1096-9861(19990913)412:1<95::AID-CNE7>3.0.CO;2-Y

Pantoni, M. M., Herrera, G. M., Van Alstyne, K. R., & Anagnostaras, S. G. (2020). Quantifying the Acoustic Startle Response in Mice Using Standard Digital Video. *Frontiers in Behavioral Neuroscience*, *14*. https://doi.org/10.3389/fnbeh.2020.00083

Parvizi, J., Joseph, J., Press, D. Z., & Schmahmann, J. D. (2007). Pathological laughter and crying in patients with multiple system atrophy-cerebellar type. *Movement Disorders*, *22*(6), 798–803. https://doi.org/10.1002/mds.21348

Passey, G. E. (1948). The influence of intensity of unconditioned stimulus upon acquisition of a conditioned response. *Journal of Experimental Psychology*, *38*(4), 420–428. https://doi.org/10.1037/h0059569

Paukert, M., Huang, Y. H., Tanaka, K., Rothstein, J. D., & Bergles, D. E. (2010). Zones of Enhanced Glutamate Release from Climbing Fibers in the Mammalian Cerebellum. *Journal of Neuroscience*, *30*(21), 7290–7299. https://doi.org/10.1523/JNEUROSCI.5118-09.2010

Paulson, H. L., Shakkottai, V. G., Brent Clark, H., & Orr, H. T. (2017). Polyglutamine spinocerebellar ataxias—From genes to potential treatments. *Nature Reviews. Neuroscience*, *18*(10), 613–626. https://doi.org/10.1038/nrn.2017.92

Pavlov, P. I. (1927). Conditioned reflexes: An investigation of the physiological activity of the cerebral cortex. *Annals of Neurosciences*, *17*(3), 136–141. https://doi.org/10.5214/ans.0972-7531.1017309

Pijpers, A., Apps, R., Pardoe, J., Voogd, J., & Ruigrok, T. J. H. (2006). Precise Spatial Relationships between Mossy Fibers and Climbing Fibers in Rat Cerebellar Cortical Zones. *Journal of Neuroscience*, *26*(46), 12067–12080. https://doi.org/10.1523/JNEUROSCI.2905-06.2006

Pijpers, A., & Ruigrok, T. J. H. (2006). Organization of pontocerebellar projections to identified climbing fiber zones in the rat. *Journal of Comparative Neurology*, *496*(4), 513–528. https://doi.org/10.1002/cne.20940

Piochon, C., Levenes, C., Ohtsuki, G., & Hansel, C. (2010). Purkinje Cell NMDA Receptors Assume a Key Role in Synaptic Gain Control in the Mature Cerebellum. *Journal of Neuroscience*, *30*(45), 15330–15335. https://doi.org/10.1523/JNEUROSCI.4344-10.2010

Power, E. M., Morales, A., & Empson, R. M. (2016). Prolonged Type 1 Metabotropic Glutamate Receptor Dependent Synaptic Signaling Contributes to Spino-Cerebellar Ataxia Type 1. *The Journal of Neuroscience*, *36*(18), 4910–4916. https://doi.org/10.1523/JNEUROSCI.3953-15.2016

Purtle, R. B. (1973). Peak shift: A review. *Psychological Bulletin*, *80*(5), 408–421. https://doi.org/10.1037/h0035233

Raman, I. M., & Bean, B. P. (1999). Ionic Currents Underlying Spontaneous Action Potentials in Isolated Cerebellar Purkinje Neurons. *The Journal of Neuroscience*, *19*(5), 1663–1674. https://doi.org/10.1523/JNEUROSCI.19-05-01663.1999

Ramnani, N. (2006). The primate cortico-cerebellar system: Anatomy and function. *Nature Reviews Neuroscience*, *7*(7), 511–522. https://doi.org/10.1038/nrn1953

Raposo, M., Vasconcelos, J., Bettencourt, C., Kay, T., Coutinho, P., & Lima, M. (2014). Nystagmus as an early ocular alteration in Machado-Joseph disease (MJD/SCA3). *BMC Neurology*, *14*(1), 17. https://doi.org/10.1186/1471-2377-14-17

Raymond, J. L., Lisberger, S. G., & Mauk, M. D. (1996). The Cerebellum: A Neuronal Learning Machine? *Science*, *272*(5265), 1126–1131. https://doi.org/10.1126/science.272.5265.1126

Razran, G. (1949). Stimulus generalization of conditioned responses. *Psychological Bulletin*, *46*(5), 337–365. https://doi.org/10.1037/h0060507

Reetz, K., Rodríguez-Labrada, R., Dogan, I., Mirzazade, S., Romanzetti, S., Schulz, J. B., Cruz-Rivas, E. M., Alvarez-Cuesta, J. A., Aguilera Rodríguez, R., Gonzalez Zaldivar, Y., Auburger, G., & Velázquez-Pérez, L. (2018). Brain atrophy measures in preclinical and manifest spinocerebellar ataxia type 2. *Annals of Clinical and Translational Neurology*, *5*(2), 128–137. https://doi.org/10.1002/acn3.504

Rehman, I., Mahabadi, N., Sanvictores, T., & Rehman, C. I. (2021). Classical Conditioning. In *StatPearls [Internet]*. StatPearls Publishing. https://www.ncbi.nlm.nih.gov/books/NBK470326/

Reynolds, R. P., Kinard, W. L., Degraff, J. J., Leverage, N., & Norton, J. N. (2010). Noise in a Laboratory Animal Facility from the Human and Mouse Perspectives. *Journal of the American Association for Laboratory Animal Science : JAALAS*, *49*(5), 592–597.

Rigo, F., Hua, Y., Krainer, A. R., & Bennett, C. F. (2012). Antisense-based therapy for the treatment of spinal muscular atrophy. *Journal of Cell Biology*, *199*(1), 21–25. https://doi.org/10.1083/jcb.201207087

Rilling, M. (1977). Stimulus Control and Inhibitory Processes*. In *Handbook of Operant Behavior*. Routledge.

Robinson, K. J., Watchon, M., & Laird, A. S. (2020). Aberrant Cerebellar Circuitry in the Spinocerebellar Ataxias. *Frontiers in Neuroscience*, *14*. https://www.frontiersin.org/articles/10.3389/fnins.2020.00707

Rodriques, S. G., Stickels, R. R., Goeva, A., Martin, C. A., Murray, E., Vanderburg, C. R., Welch, J., Chen, L. M., Chen, F., & Macosko, E. Z. (2019). Slide-seq: A scalable technology for measuring genome-wide expression at high spatial resolution. *Science*, *363*(6434), 1463–1467. https://doi.org/10.1126/science.aaw1219

Ross, M. E., Fletcher, C., Mason, C. A., Hatten, M. E., & Heintz, N. (1990). Meander tail reveals a discrete developmental unit in the mouse cerebellum. *Proceedings of the National Academy of Sciences*, *87*(11), 4189–4192. https://doi.org/10.1073/pnas.87.11.4189

Rousseaux, M. W. C., Tschumperlin, T., Lu, H.-C., Lackey, E. P., Bondar, V. V., Wan, Y.-W., Tan, Q., Adamski, C. J., Friedrich, J., Twaroski, K., Chen, W., Tolar, J., Henzler, C., Sharma, A., Bajić, A., Lin, T., Duvick, L., Liu, Z., Sillitoe, R. V., … Orr, H. T. (2018). ATXN1-CIC Complex Is the Primary Driver of Cerebellar Pathology in Spinocerebellar Ataxia Type 1 through a Gain-of-Function Mechanism. *Neuron*, *97*(6), 1235-1243.e5. https://doi.org/10.1016/j.neuron.2018.02.013

Ruegsegger, C., Stucki, D. M., Steiner, S., Angliker, N., Radecke, J., Keller, E., Zuber, B., Rüegg, M. A., & Saxena, S. (2016). Impaired mTORC1-Dependent Expression of Homer-3 Influences SCA1 Pathophysiology. *Neuron*, *89*(1), 129–146. https://doi.org/10.1016/j.neuron.2015.11.033

Ruigrok, T. J. H. (2011). Ins and Outs of Cerebellar Modules. *The Cerebellum*, *10*(3), 464–474. https://doi.org/10.1007/s12311-010-0164-y

Ruigrok, T. J. H., Pijpers, A., Goedknegt-Sabel, E., & Coulon, P. (2008). Multiple cerebellar zones are involved in the control of individual muscles: A retrograde transneuronal tracing study with rabies virus in the rat. *European Journal of Neuroscience*, *28*(1), 181–200. https://doi.org/10.1111/j.1460-9568.2008.06294.x

Ruigrok, T. J. H., & Voogd, J. (1990). Cerebellar nucleo-olivary projections in the rat: An anterograde tracing study withPhaseolus vulgaris-leucoagglutinin (PHA-L). *The Journal of Comparative Neurology*, *298*(3), 315–333. https://doi.org/10.1002/cne.902980305

Ruigrok, T. J. H., & Voogd, J. (2000). *Organization of projections from the inferior olive to the cerebellar nuclei in the rat*. 20.

Salin, P. A., Scanziani, M., Malenka, R. C., & Nicoll, R. A. (1996). Distinct short-term plasticity at two excitatory synapses in the hippocampus. *Proceedings of the National Academy of Sciences*, *93*(23), 13304–13309. https://doi.org/10.1073/pnas.93.23.13304

Sanchez, M., Sillitoe, R. V., Attwell, P. J. E., Ivarsson, M., Rahman, S., Yeo, C. H., & Hawkes, R. (2002). Compartmentation of the rabbit cerebellar cortex. *The Journal of Comparative Neurology*, *444*(2), 159–173. https://doi.org/10.1002/cne.10144

Sánchez-Campusano, R., Gruart, A., & Delgado-García, J. (2011). Timing and causality in the generation of learned eyelid responses. *Frontiers in Integrative Neuroscience*, *5*. https://www.frontiersin.org/articles/10.3389/fnint.2011.00039

Sarna, J. R., & Hawkes, R. (2003). Patterned Purkinje cell death in the cerebellum. *Progress in Neurobiology*, *70*(6), 473–507. https://doi.org/10.1016/S0301-0082(03)00114-X

Sarna, J. R., Marzban, H., Watanabe, M., & Hawkes, R. (2006). Complementary stripes of phospholipase Cβ3 and Cβ4 expression by Purkinje cell subsets in the mouse cerebellum. *Journal of Comparative Neurology*, *496*(3), 303–313. https://doi.org/10.1002/cne.20912

Scaglioni, D., Catapano, F., Ellis, M., Torelli, S., Chambers, D., Feng, L., Beck, M., Sewry, C., Monforte, M., Harriman, S., Koenig, E., Malhotra, J., Popplewell, L., Guglieri, M., Straub, V., Mercuri, E., Servais, L., Phadke, R., Morgan, J., & Muntoni, F. (2021). The administration of antisense oligonucleotide golodirsen reduces pathological regeneration in patients with Duchenne muscular dystrophy. *Acta Neuropathologica Communications*, *9*(1), 7. https://doi.org/10.1186/s40478-020-01106-1

Schielzeth, H., Dingemanse, N. J., Nakagawa, S., Westneat, D. F., Allegue, H., Teplitsky, C., Réale, D., Dochtermann, N. A., Garamszegi, L. Z., & Araya-Ajoy, Y. G. (2020). Robustness of linear mixed-effects models to violations of distributional assumptions. *Methods in Ecology and Evolution*, *11*(9), 1141–1152. https://doi.org/10.1111/2041-210X.13434

Schmahmann, J. D., & Caplan, D. (2006). Cognition, emotion and the cerebellum. *Brain*, *129*(2), 290–292. https://doi.org/10.1093/brain/awh729

Schmahmann, J. D., & Sherman, J. C. (1998). *The cerebellar cognitive affective syndrome*. 19.

Schneiderman, N. (1966). Interstimulus interval function of the nictitating membrane response of the rabbit under delay versus trace conditioning. *Journal of Comparative and Physiological Psychology*, *62*(3), 397–402. https://doi.org/10.1037/h0023946

Schneiderman, N., & Gormezano, I. (1964). *Conditioning of the nictitating membrane of the rabbit as a function of CS-US interval.* 8.

Schonewille, M., Belmeguenai, A., Koekkoek, S. K., Houtman, S. H., Boele, H. J., van Beugen, B. J., Gao, Z., Badura, A., Ohtsuki, G., Amerika, W. E., Hosy, E., Hoebeek, F. E., Elgersma, Y., Hansel, C., & De Zeeuw, C. I. (2010). Purkinje Cell-Specific Knockout of the Protein Phosphatase PP2B Impairs Potentiation and Cerebellar Motor Learning. *Neuron*, *67*(4), 618–628. https://doi.org/10.1016/j.neuron.2010.07.009

Schonewille, M., Gao, Z., Boele, H.-J., Vinueza Veloz, M. F., Amerika, W. E., Šimek, A. A. M., De Jeu, M. T., Steinberg, J. P., Takamiya, K., Hoebeek, F. E., Linden, D. J., Huganir, R. L., & De Zeeuw, C. I. (2011). Reevaluating the Role of LTD in Cerebellar Motor Learning. *Neuron*, *70*(1), 43–50. https://doi.org/10.1016/j.neuron.2011.02.044

Schreurs, B. G. (2019). Changes in cerebellar intrinsic neuronal excitability and synaptic plasticity result from eyeblink conditioning. *Neurobiology of Learning and Memory*, *166*, 107094. https://doi.org/10.1016/j.nlm.2019.107094

Schreurs, B. G., Gusev, P. A., Tomsic, D., Alkon, D. L., & Shi, T. (1998). Intracellular Correlates of Acquisition and Long-Term Memory of Classical Conditioning in Purkinje Cell Dendrites in Slices of Rabbit Cerebellar Lobule HVI. *The Journal of Neuroscience*, *18*(14), 5498–5507. https://doi.org/10.1523/JNEUROSCI.18-14-05498.1998

Schreurs, B. G., Tomsic, D., Gusev, P. A., & Alkon, D. L. (1997). Dendritic Excitability Microzones and Occluded Long-Term Depression After Classical Conditioning of the Rabbit's Nictitating

Membrane Response. *Journal of Neurophysiology*, *77*(1), 86–92. https://doi.org/10.1152/jn.1997.77.1.86

Scoles, D. R., Meera, P., Schneider, M. D., Paul, S., Dansithong, W., Figueroa, K. P., Hung, G., Rigo, F., Bennett, C. F., Otis, T. S., & Pulst, S. M. (2017). Antisense oligonucleotide therapy for spinocerebellar ataxia type 2. *Nature*, *544*(7650), 362–366. https://doi.org/10.1038/nature22044

Serra, H. G., Byam, C. E., Lande, J. D., Tousey, S. K., Zoghbi, H. Y., & Orr, H. T. (2004). Gene profiling links SCA1 pathophysiology to glutamate signaling in Purkinje cells of transgenic mice. *Human Molecular Genetics*, *13*(20), 2535–2543. https://doi.org/10.1093/hmg/ddh268

Serra, H. G., Duvick, L., Zu, T., Carlson, K., Stevens, S., Jorgensen, N., Lysholm, A., Burright, E., Zoghbi, H. Y., Clark, H. B., Andresen, J. M., & Orr, H. T. (2006). RORα-Mediated Purkinje Cell Development Determines Disease Severity in Adult SCA1 Mice. *Cell*, *127*(4), 697–708. https://doi.org/10.1016/j.cell.2006.09.036

Shaban, H., Humeau, Y., Herry, C., Cassasus, G., Shigemoto, R., Ciocchi, S., Barbieri, S., van der Putten, H., Kaupmann, K., Bettler, B., & Lüthi, A. (2006). Generalization of amygdala LTP and conditioned fear in the absence of presynaptic inhibition. *Nature Neuroscience*, *9*(8), 1028–1035. https://doi.org/10.1038/nn1732

Shepard, R. N. (1987). Toward a Universal Law of Generalization for Psychological Science. *Science*, *237*(4820), 1317–1323. https://doi.org/10.1126/science.3629243

Shin, M., Moghadam, S. H., Sekirnjak, C., Bagnall, M. W., Kolkman, K. E., Jacobs, R., Faulstich, M., & Lac, S. du. (2011). Multiple Types of Cerebellar Target Neurons and Their Circuitry in the Vestibulo-ocular Reflex. *Journal of Neuroscience*, *31*(30), 10776–10786. https://doi.org/10.1523/JNEUROSCI.0768-11.2011

Shin, S.-L., Hoebeek, F. E., Schonewille, M., Zeeuw, C. I. D., Aertsen, A., & Schutter, E. D. (2007). Regular Patterns in Cerebellar Purkinje Cell Simple Spike Trains. *PLOS ONE*, *2*(5), e485. https://doi.org/10.1371/journal.pone.0000485

Shin, S.-L., Zhao, G. Q., & Raymond, J. L. (2014). Signals and Learning Rules Guiding Oculomotor Plasticity. *Journal of Neuroscience*, *34*(32), 10635–10644. https://doi.org/10.1523/JNEUROSCI.4510-12.2014

Shuvaev, A. N., Horiuchi, H., Seki, T., Goenawan, H., Irie, T., Iizuka, A., Sakai, N., & Hirai, H. (2011). Mutant PKC in Spinocerebellar Ataxia Type 14 Disrupts Synapse Elimination and Long-Term Depression in Purkinje Cells In Vivo. *Journal of Neuroscience*, *31*(40), 14324–14334. https://doi.org/10.1523/JNEUROSCI.5530-10.2011

Siegel, S., Hearst, E., & George, N. (1968). Generalization gradients obtained from individual subjects following classical conditioning. *Journal of Experimental Psychology*, *78*(1), 171–174. https://doi.org/10.1037/h0026178

Sillitoe, R. V., Chung, S.-H., Fritschy, J.-M., Hoy, M., & Hawkes, R. (2008). Golgi Cell Dendrites Are Restricted by Purkinje Cell Stripe Boundaries in the Adult Mouse Cerebellar Cortex. *Journal of Neuroscience*, *28*(11), 2820–2826. https://doi.org/10.1523/JNEUROSCI.4145-07.2008

Sillitoe, R. V., Gopal, N., & Joyner, A. L. (2009). Embryonic origins of ZebrinII parasagittal stripes and establishment of topographic Purkinje cell projections. *Neuroscience*, *162*(3), 574–588. https://doi.org/10.1016/j.neuroscience.2008.12.025

Sillitoe, R. V., & Hawkes, R. (2002). Whole-mount Immunohistochemistry: A High-throughput Screen for Patterning Defects in the Mouse Cerebellum. *Journal of Histochemistry & Cytochemistry*, *50*(2), 235–244. https://doi.org/10.1177/002215540205000211

Smeets, C. J. L. M., & Verbeek, D. S. (2016). Climbing fibers in spinocerebellar ataxia: A mechanism for the loss of motor control. *Neurobiology of Disease*, *88*, 96–106. https://doi.org/10.1016/j.nbd.2016.01.009

Smith, D. R., Gallagher, M., & Stanton, M. E. (2007). Genetic background differences and nonassociative effects in mouse trace fear conditioning. *Learning & Memory*, *14*(9), 597–605. https://doi.org/10.1101/lm.614807

Smith, M. C. (1968). CS-US interval and US intensity in classical conditioning of the rabbit's nictitating membrane response. *Journal of Comparative and Physiological Psychology*, *66*(3, Pt.1), 679–687. https://doi.org/10.1037/h0026550

Sokoloff, G., Plumeau, A. M., Mukherjee, D., & Blumberg, M. S. (2015). Twitch-related and rhythmic activation of the developing cerebellar cortex. *Journal of Neurophysiology*, *114*(3), 1746–1756. https://doi.org/10.1152/jn.00284.2015

Solomon, P. R., & Moore, J. W. (1975). *Latent Inhibition and Stimulus Generalization of the Classically Conditioned Nictitating Membrane Response in Rabbits (Oryctolagus cuniculus) Following Dorsal Hippocampal Ablation*. 12.

Sotelo, C. (2004). Cellular and genetic regulation of the development of the cerebellar system. *Progress in Neurobiology*, *72*(5), 295–339. https://doi.org/10.1016/j.pneurobio.2004.03.004

Sotelo, C., & Arsenio-Nunes, M. L. (1976). Development of Purkinje cells in absence of climbing fibers. *Brain Research*, *111*(2), 389–395. https://doi.org/10.1016/0006-8993(76)90782-4

Sotelo, C., & Chédotal, A. (2005). Development of the olivocerebellar system: Migration and formation of cerebellar maps. In *Progress in Brain Research* (Vol. 148, pp. 1–20). Elsevier. https://doi.org/10.1016/S0079-6123(04)48001-7

Sotelo, C., & Wassef, M. (1991). Cerebellar Development: Afferent Organization and Purkinje Cell Heterogeneity. *Philosophical Transactions: Biological Sciences*, *331*(1261), 307–313.

Spence, K. W. (1937). *THE DIFFERENTIAL RESPONSE IN ANIMALS TO STIMULI VARYING WITHIN A SINGLE DIMENSIONl*. 15.

Spence, K. W., Swisher, D., & Taylor, J. (1953). *LEARNING AND PERFORMANCE IN EYELID CONDITIONING AS A FUNCTION OF INTENSITY OF THE UCS*. 7.

Spencer, R. M. C., Zelaznik, H. N., Diedrichsen, J., & Ivry, R. B. (2003). Disrupted Timing of Discontinuous But Not Continuous Movements by Cerebellar Lesions. *Science*, *300*(5624), 1437–1439. https://doi.org/10.1126/science.1083661

Stanton, M. E., Fox, G. D., & Carter, C. S. (1998). Ontogeny of the conditioned eyeblink response in rats: Acquisition or expression? *Neuropharmacology*, *37*(4), 623–632. https://doi.org/10.1016/S0028-3908(98)00072-0

Stanton, M. E., Freeman, J. H., & Skelton, R. W. (1992). Eyeblink conditioning in the developing rat. *Behavioral Neuroscience*, *106*(4), 657–665. https://doi.org/10.1037/0735-7044.106.4.657

Steinmetz, J. E., Lavond, D. G., & Thompson, R. F. (1989). Classical conditioning in rabbits using pontine nucleus stimulation as a conditioned stimulus and inferior olive stimulation as an unconditioned stimulus. *Synapse*, *3*(3), 225–233. https://doi.org/10.1002/syn.890030308

Steinmetz, J. E., Logan, C. G., Rosen, D. J., Thompson, J. K., Lavond, D. G., & Thompson, R. F. (1987). Initial localization of the acoustic conditioned stimulus projection system to the cerebellum essential for classical eyelid conditioning. *Proceedings of the National Academy of Sciences*, *84*(10), 3531–3535. https://doi.org/10.1073/pnas.84.10.3531

Steinmetz, J. E., Rosen, D. J., Chapman, P. F., Lavond, D. G., & Thompson, R. F. (1986). Classical conditioning of the rabbit eyelid response with a mossy-fiber stimulation CS: I. Pontine nuclei

and middle cerebellar peduncle stimulation. *Behavioral Neuroscience*, *100*(6), 878–887. https://doi.org/10.1037/0735-7044.100.6.878

Steinmetz, J. E., & Sengelaub, D. R. (1992). Possible conditioned stimulus pathway for classical eyelid conditioning in rabbits. I. Anatomical evidence for direct projections from the pontine nuclei to the cerebellar interpositus nucleus. *Behavioral and Neural Biology*, *57*(2), 103–115. https://doi.org/10.1016/0163-1047(92)90593-S

Storm, G., & Crommelin, D. J. A. (1998). Liposomes: Quo vadis? *Pharmaceutical Science & Technology Today*, *1*(1), 19–31. https://doi.org/10.1016/S1461-5347(98)00007-8

Sudarov, A., & Joyner, A. L. (2007). Cerebellum morphogenesis: The foliation pattern is orchestrated by multi-cellular anchoring centers. *Neural Development*, *2*(1), 26. https://doi.org/10.1186/1749-8104-2-26

Sugihara, I. (2004). Molecular, Topographic, and Functional Organization of the Cerebellar Cortex: A Study with Combined Aldolase C and Olivocerebellar Labeling. *Journal of Neuroscience*, *24*(40), 8771–8785. https://doi.org/10.1523/JNEUROSCI.1961-04.2004

Sugihara, I. (2011). Compartmentalization of the Deep Cerebellar Nuclei Based on Afferent Projections and Aldolase C Expression. *The Cerebellum*, *10*(3), 449–463. https://doi.org/10.1007/s12311-010-0226-1

Sugihara, I., Fujita, H., Na, J., Quy, P. N., Li, B.-Y., & Ikeda, D. (2009). Projection of reconstructed single purkinje cell axons in relation to the cortical and nuclear aldolase C compartments of the rat cerebellum. *Journal of Comparative Neurology*, *512*(2), 282–304. https://doi.org/10.1002/cne.21889

Sugihara, I., Marshall, S. P., & Lang, E. J. (2007). Relationship of complex spike synchrony bands and climbing fiber projection determined by reference to aldolase C compartments in crus IIa of the rat cerebellar cortex. *Journal of Comparative Neurology*, *501*(1), 13–29. https://doi.org/10.1002/cne.21223

Sugihara, I., & Quy, P. N. (2007). Identification of aldolase C compartments in the mouse cerebellar cortex by olivocerebellar labeling. *Journal of Comparative Neurology*, *500*(6), 1076–1092. https://doi.org/10.1002/cne.21219

Sugihara, I., & Shinoda, Y. (2004). Molecular, Topographic, and Functional Organization of the Cerebellar Cortex: A Study with Combined Aldolase C and Olivocerebellar Labeling. *Journal of Neuroscience*, *24*(40), 8771–8785. https://doi.org/10.1523/JNEUROSCI.1961-04.2004

Sugihara, I., & Shinoda, Y. (2007). Molecular, Topographic, and Functional Organization of the Cerebellar Nuclei: Analysis by Three-Dimensional Mapping of the Olivonuclear Projection and Aldolase C Labeling. *Journal of Neuroscience*, *27*(36), 9696–9710. https://doi.org/10.1523/JNEUROSCI.1579-07.2007

Suvrathan, A., & Raymond, J. L. (2018). Depressed by learning – heterogeneity of the plasticity rules at parallel fiber synapses onto Purkinje cells. *Cerebellum (London, England)*, *17*(6), 747–755. https://doi.org/10.1007/s12311-018-0968-8

Svensson, P., & Ivarsson, M. (1999). Short-lasting conditioned stimulus applied to the middle cerebellar peduncle elicits delayed conditioned eye blink responses in the decerebrate ferret: Short CS to the middle cerebellar peduncle. *European Journal of Neuroscience*, *11*(12), 4333–4340. https://doi.org/10.1046/j.1460-9568.1999.00862.x

Svensson, P., Ivarsson, M., & Hesslow, G. (1997). Effect of varying the intensity and train frequency of forelimb and cerebellar mossy fiber conditioned stimuli on the latency of conditioned eye-

blink responses in decerebrate ferrets. *Learning & Memory*, *4*(1), 105–115. https://doi.org/10.1101/lm.4.1.105

Svensson, P., Jirenhed, D.-A., Bengtsson, F., & Hesslow, G. (2010). Effect of Conditioned Stimulus Parameters on Timing of Conditioned Purkinje Cell Responses. *Journal of Neurophysiology*, *103*(3), 1329–1336. https://doi.org/10.1152/jn.00524.2009

Tano, D., Napieralski, J. A., Eisenman, L. M., Messer, A., Plummer, J., & Hawkes, R. (1992). Novel developmental boundary in the cerebellum revealed by zebrin expression in the Lurcher (Lc/+) mutant mouse. *Journal of Comparative Neurology*, *323*(1), 128–136. https://doi.org/10.1002/cne.903230111

Taroni, F., & DiDonato, S. (2004). Pathways to motor incoordination: The inherited ataxias. *Nature Reviews Neuroscience*, *5*(8), 641–655. https://doi.org/10.1038/nrn1474

ten Brinke, M. M., Heiney, S. A., Wang, X., Proietti-Onori, M., Boele, H.-J., Bakermans, J., Medina, J. F., Gao, Z., & De Zeeuw, C. I. (2017a). Dynamic modulation of activity in cerebellar nuclei neurons during pavlovian eyeblink conditioning in mice. *ELife*, *6*, e28132. https://doi.org/10.7554/eLife.28132

ten Brinke, M. M., Boele, H.-J., Spanke, J. K., Potters, J.-W., Kornysheva, K., Wulff, P., IJpelaar, A. C. H. G., Koekkoek, S. K. E., & De Zeeuw, C. I. (2015a). Evolving Models of Pavlovian Conditioning: Cerebellar Cortical Dynamics in Awake Behaving Mice. *Cell Reports*, *13*(9), 1977–1988. https://doi.org/10.1016/j.celrep.2015.10.057

Terrace, H. S. (1964). Wavelength Generalization after Discrimination Learning with and without Errors. *Science*, *144*(3614), 78–80.

Terrace, H. S. (1966a). Discrimination Learning and Inhibition. *Science*, *154*(3757), 1677–1680.

Terrace, H. S. (1966b). Behavioral contrast and the peak shift: Effects of extended discrimination training. *Journal of the Experimental Analysis of Behavior*, *9*(6), 613–617. https://doi.org/10.1901/jeab.1966.9-613

Thoma, P., Bellebaum, C., Koch, B., Schwarz, M., & Daum, I. (2008). The Cerebellum Is Involved in Reward-based Reversal Learning. *The Cerebellum*, *7*(3), 433–443. https://doi.org/10.1007/s12311-008-0046-8

Thomas, D. R., & Mitchell, K. (1962). Instructions and stimulus categorizing in a measure of stimulus generalization. *Journal of the Experimental Analysis of Behavior*, *5*(3), 375–381. https://doi.org/10.1901/jeab.1962.5-375

Thompson, L. (1990). Negotiation behavior and outcomes: Empirical evidence and theoretical issues. *Psychological Bulletin*, *108*(3), 515–532. https://doi.org/10.1037/0033-2909.108.3.515

Thompson, R. F. (1983). Neuronal substrates of simple associative learning: Classical conditioning. *Trends in Neurosciences*, *6*, 270–275. https://doi.org/10.1016/0166-2236(83)90117-0

Thompson, R. F. (1990). Neural Mechanisms of Classical Conditioning in Mammals. *Philosophical Transactions: Biological Sciences*, *329*(1253), 161–170.

Thompson, R. F., & Steinmetz, J. E. (2009). The role of the cerebellum in classical conditioning of discrete behavioral responses. *Neuroscience*, *162*(3), 732–755. https://doi.org/10.1016/j.neuroscience.2009.01.041

Thurling, M., Kahl, F., Maderwald, S., Stefanescu, R. M., Schlamann, M., Boele, H.-J., De Zeeuw, C. I., Diedrichsen, J., Ladd, M. E., Koekkoek, S. K. E., & Timmann, D. (2015). Cerebellar Cortex and Cerebellar Nuclei Are Concomitantly Activated during Eyeblink Conditioning: A 7T fMRI Study in Humans. *Journal of Neuroscience*, *35*(3), 1228–1239. https://doi.org/10.1523/JNEUROSCI.2492-14.2015

Timmann, D., & Daum, I. (2007). Cerebellar contributions to cognitive functions: A progress report after two decades of research. *The Cerebellum*, *6*(3), 159, 14734220701496448. https://doi.org/10.1080/14734220701496448

Titley, H. K., Brunel, N., & Hansel, C. (2017). Toward a Neurocentric View of Learning. *Neuron*, *95*(1), 19–32. https://doi.org/10.1016/j.neuron.2017.05.021

Titley, H. K., Watkins, G. V., Lin, C., Weiss, C., McCarthy, M., Disterhoft, J. F., & Hansel, C. (2020). Intrinsic Excitability Increase in Cerebellar Purkinje Cells after Delay Eye-Blink Conditioning in Mice. *The Journal of Neuroscience*, *40*(10), 2038–2046. https://doi.org/10.1523/JNEUROSCI.2259-19.2019

Tracy, J. A. (1995). *Brain and behavior correlates in classical conditioning of the rabbit eyeblink response* [PhD Thesis]. University of Southern California.

Tracy, J. A., Britton, G. B., & Steinmetz, J. E. (2001). Comparison of Single Unit Responses to Tone, Light, and Compound Conditioned Stimuli during Rabbit Classical Eyeblink Conditioning. *Neurobiology of Learning and Memory*, *76*(3), 253–267. https://doi.org/10.1006/nlme.2001.4024

Tracy, J. A., & Steinmetz, J. E. (1998). Purkinje cell responses to pontine stimulation CS during rabbit eyeblink conditioning. *Physiology & Behavior*, *65*(2), 381–386. https://doi.org/10.1016/S0031-9384(98)00217-0

Turner, J. G., Parrish, J. L., Hughes, L. F., Toth, L. A., & Caspary, D. M. (2005). Hearing in Laboratory Animals: Strain Differences and Nonauditory Effects of Noise. *Comparative Medicine*, *55*(1), 12.

Uusisaari, M., & Knöpfel, T. (2011). Functional Classification of Neurons in the Mouse Lateral Cerebellar Nuclei. *The Cerebellum*, *10*(4), 637–646. https://doi.org/10.1007/s12311-010-0240-3

Valera, A. M., Doussau, F., Poulain, B., Barbour, B., & Isope, P. (2012). Adaptation of Granule Cell to Purkinje Cell Synapses to High-Frequency Transmission. *Journal of Neuroscience*, *32*(9), 3267–3280. https://doi.org/10.1523/JNEUROSCI.3175-11.2012

Van Alphen, A. M., & De Zeeuw, C. I. (2002). Cerebellar LTD facilitates but is not essential for long-term adaptation of the vestibulo-ocular reflex. *European Journal of Neuroscience*, *16*(3), 486–490. https://doi.org/10.1046/j.1460-9568.2002.02094.x

van Beugen, B. J., Gao, Z., Boele, H.-J., Hoebeek, F., & De Zeeuw, C. I. (2013). High Frequency Burst Firing of Granule Cells Ensures Transmission at the Parallel Fiber to Purkinje Cell Synapse at the Cost of Temporal Coding. *Frontiers in Neural Circuits*, *7*. https://doi.org/10.3389/fncir.2013.00095

Van Der Giessen, R. S., Koekkoek, S. K., van Dorp, S., De Gruijl, J. R., Cupido, A., Khosrovani, S., Dortland, B., Wellershaus, K., Degen, J., Deuchars, J., Fuchs, E. C., Monyer, H., Willecke, K., De Jeu, M. T. G., & De Zeeuw, C. I. (2008). Role of Olivary Electrical Coupling in Cerebellar Motor Learning. *Neuron*, *58*(4), 599–612. https://doi.org/10.1016/j.neuron.2008.03.016

van Gaalen, J., Maas, R. P. P. W. M., Ippel, E. F., Elting, M. W., van Spaendonck-Zwarts, K. Y., Vermeer, S., Verschuuren-Bemelmans, C., Timmann, D., & van de Warrenburg, B. P. (2019). Abnormal eyeblink conditioning is an early marker of cerebellar dysfunction in preclinical SCA3 mutation carriers. *Experimental Brain Research*, *237*(2), 427–433. https://doi.org/10.1007/s00221-018-5424-y

van Ham, J. J., & Yeo, C. H. (1996). The Central Distribution of Primary Afferents from the External Eyelids, Conjunctiva, and Cornea in the Rabbit, Studied Using WGA-HRP and B-HRP as

Transganglionic Tracers. *Experimental Neurology*, *142*(2), 217–225. https://doi.org/10.1006/exnr.1996.0193

van Looij, M. A. J., Liem, S.-S., van der Burg, H., van der Wees, J., De Zeeuw, C. I., & van Zanten, B. G. A. (2004). Impact of conventional anesthesia on auditory brainstem responses in mice. *Hearing Research*, *193*(1–2), 75–82. https://doi.org/10.1016/j.heares.2004.02.009

Van Overwalle, F., D'aes, T., & Mariën, P. (2015). Social cognition and the cerebellum: A meta-analytic connectivity analysis. *Human Brain Mapping*, *36*(12), 5137–5154. https://doi.org/10.1002/hbm.23002

van Welie, I., Smith, I. T., & Watt, A. J. (2011). The metamorphosis of the developing cerebellar microcircuit. *Current Opinion in Neurobiology*, *21*(2), 245–253. https://doi.org/10.1016/j.conb.2011.01.009

Velázquez-Pérez, L., Rodríguez-Labrada, R., Canales-Ochoa, N., Montero, J. M., Sánchez-Cruz, G., Aguilera-Rodríguez, R., Almaguer-Mederos, L. E., & Laffita-Mesa, J. M. (2014). Progression of early features of spinocerebellar ataxia type 2 in individuals at risk: A longitudinal study. *The Lancet Neurology*, *13*(5), 482–489. https://doi.org/10.1016/S1474-4422(14)70027-4

Vetter, P., Roth, A., & Häusser, M. (2001). Propagation of Action Potentials in Dendrites Depends on Dendritic Morphology. *Journal of Neurophysiology*, *85*(2), 926–937. https://doi.org/10.1152/jn.2001.85.2.926

Volkow, N. D., Wang, G.-J., Ma, Y., Fowler, J. S., Zhu, W., Maynard, L., Telang, F., Vaska, P., Ding, Y.-S., Wong, C., & Swanson, J. M. (2003). Expectation Enhances the Regional Brain Metabolic and the Reinforcing Effects of Stimulants in Cocaine Abusers. *The Journal of Neuroscience*, *23*(36), 11461–11468. https://doi.org/10.1523/JNEUROSCI.23-36-11461.2003

Voogd, J. (1964). *The cerebellum of the cat: Structure and fibre connexions*. Van Gorcum Assen.

Voogd, J. (2003). The human cerebellum. *Journal of Chemical Neuroanatomy*, *26*(4), 243–252. https://doi.org/10.1016/j.jchemneu.2003.07.005

Voogd, J., Broere, G., & van, R. J. (1969). The medio-lateral distribution of the spinocerebellar projection in the anterior lobe and the simple lobule in the cat and a comparison with some other afferent fibre systems. *Psychiatria, Neurologia, Neurochirurgia*, *72*(1), 137–151.

Voogd, J., & Glickstein, M. (1998). The anatomy of the cerebellum. *Trends in Cognitive Sciences*, *2*(9), 307–313. https://doi.org/10.1016/S1364-6613(98)01210-8

Voogd, J., & Ruigrok, T. J. H. (1997). Chapter 2 Transverse and longitudinal patterns in the mammalian cerebellum. In C. I. De Zeeuw, P. Strata, & J. Voogd (Eds.), *Progress in Brain Research* (Vol. 114, pp. 21–37). Elsevier. https://doi.org/10.1016/S0079-6123(08)63356-7

Voogd, J., & Ruigrok, T. J. H. (2004). The organization of the corticonuclear and olivocerebellar climbing fiber projections to the rat cerebellar vermis: The congruence of projection zones and the zebrin pattern. *Journal of Neurocytology*, *33*(1), 5–21. https://doi.org/10.1023/B:NEUR.0000029645.72074.2b

Voogd, J., Schraa-Tam, C. K. L., van der Geest, J. N., & De Zeeuw, C. I. (2012). Visuomotor Cerebellum in Human and Nonhuman Primates. *The Cerebellum*, *11*(2), 392–410. https://doi.org/10.1007/s12311-010-0204-7

Wadiche, J. I., & Jahr, C. E. (2005). Patterned expression of Purkinje cell glutamate transporters controls synaptic plasticity. *Nature Neuroscience*, *8*(10), 1329–1334. https://doi.org/10.1038/nn1539

Walter, J. T., Alviña, K., Womack, M. D., Chevez, C., & Khodakhah, K. (2006). Decreases in the precision of Purkinje cell pacemaking cause cerebellar dysfunction and ataxia. *Nature Neuroscience*, *9*(3), 389–397. https://doi.org/10.1038/nn1648

Wang, S. S.-H., Kloth, A. D., & Badura, A. (2014). The Cerebellum, Sensitive Periods, and Autism. *Neuron*, *83*(3), 518–532. https://doi.org/10.1016/j.neuron.2014.07.016

Wang, X., Chen, G., Gao, W., & Ebner, T. J. (2011). Parasagittally aligned, mGluR $_1$ -dependent patches are evoked at long latencies by parallel fiber stimulation in the mouse cerebellar cortex in vivo. *Journal of Neurophysiology*, *105*(4), 1732–1746. https://doi.org/10.1152/jn.00717.2010

Wang, Y. T., & Linden, D. J. (2000). Expression of Cerebellar Long-Term Depression Requires Postsynaptic Clathrin-Mediated Endocytosis. *Neuron*, *25*(3), 635–647. https://doi.org/10.1016/S0896-6273(00)81066-1

Watanabe, M., & Kano, M. (2011). Climbing fiber synapse elimination in cerebellar Purkinje cells. *European Journal of Neuroscience*, *34*(10), 1697–1710. https://doi.org/10.1111/j.1460-9568.2011.07894.x

Waters, M. F., Minassian, N. A., Stevanin, G., Figueroa, K. P., Bannister, J. P. A., Nolte, D., Mock, A. F., Evidente, V. G. H., Fee, D. B., Müller, U., Dürr, A., Brice, A., Papazian, D. M., & Pulst, S. M. (2006). Mutations in voltage-gated potassium channel KCNC3 cause degenerative and developmental central nervous system phenotypes. *Nature Genetics*, *38*(4), 447–451. https://doi.org/10.1038/ng1758

Wells, G. R., Hardiman, M. J., & Yeo, C. H. (1989). Visual projections to the pontine nuclei in the rabbit: Orthograde and retrograde tracing studies with WGA-HRP. *The Journal of Comparative Neurology*, *279*(4), 629–652. https://doi.org/10.1002/cne.902790410

Welsh, J. P. (1992). Changes in the motor pattern of learned and unlearned responses following cerebellar lesions: A kinematic analysis of the nictitating membrane reflex. *Neuroscience*, *47*(1), 1–19. https://doi.org/10.1016/0306-4522(92)90116-J

Welsh, J. P., & Harvey, J. A. (1991). Pavlovian conditioning in the rabbit during inactivation of the interpositus nucleus. *The Journal of Physiology*, *444*(1), 459–480. https://doi.org/10.1113/jphysiol.1991.sp018888

Welsh, J. P., & Harvey, J. A. (1998). Acute inactivation of the inferior olive blocks associative learning. *European Journal of Neuroscience*, *10*(11), 3321–3332. https://doi.org/10.1046/j.1460-9568.1998.00400.x

Welsh, J. P., Yamaguchi, H., Zeng, X.-H., Kojo, M., Nakada, Y., Takagi, A., Sugimori, M., & Llinás, R. R. (2005). Normal motor learning during pharmacological prevention of Purkinje cell long-term depression. *Proceedings of the National Academy of Sciences*, *102*(47), 17166–17171. https://doi.org/10.1073/pnas.0508191102

White, J. J., Bosman, L. W. J., Blot, F. G. C., Osório, C., Kuppens, B. W., Krijnen, W. H. J. J., Andriessen, C., De Zeeuw, C. I., Jaarsma, D., & Schonewille, M. (2021). Region-specific preservation of Purkinje cell morphology and motor behavior in the ATXN1[82Q] mouse model of spinocerebellar ataxia 1. *Brain Pathology*, *31*(5), e12946. https://doi.org/10.1111/bpa.12946

White, J. J., & Sillitoe, R. V. (2013). Development of the cerebellum: From gene expression patterns to circuit maps. *WIREs Developmental Biology*, *2*(1), 149–164. https://doi.org/10.1002/wdev.65

Wiesel, T. N., & Hubel, D. H. (1965). Extent of recovery from the effects of visual deprivation in kittens. *Journal of Neurophysiology*, *28*(6), 1060–1072. https://doi.org/10.1152/jn.1965.28.6.1060

Willott, J. F. (2006). Measurement of the Auditory Brainstem Response (ABR) to Study Auditory Sensitivity in Mice. *Current Protocols in Neuroscience*, *34*(1), 8.21B.1-8.21B.12. https://doi.org/10.1002/0471142301.ns0821bs34

Witter, L., Canto, C., Hoogland, T., De Gruijl, J., & De Zeeuw, C. (2013). Strength and timing of motor responses mediated by rebound firing in the cerebellar nuclei after Purkinje cell activation. *Frontiers in Neural Circuits*, *7*. https://www.frontiersin.org/articles/10.3389/fncir.2013.00133

Womack, M., & Khodakhah, K. (2002). Active Contribution of Dendrites to the Tonic and Trimodal Patterns of Activity in Cerebellar Purkinje Neurons. *The Journal of Neuroscience*, *22*(24), 10603–10612. https://doi.org/10.1523/JNEUROSCI.22-24-10603.2002

Wood, M. J. A., Talbot, K., & Bowerman, M. (2017). Spinal muscular atrophy: Antisense oligonucleotide therapy opens the door to an integrated therapeutic landscape. *Human Molecular Genetics*, *26*(R2), R151–R159. https://doi.org/10.1093/hmg/ddx215

Wu, B., Blot, F. G., Wong, A. B., Osório, C., Adolfs, Y., Pasterkamp, R. J., Hartmann, J., Becker, E. B., Boele, H.-J., De Zeeuw, C. I., & Schonewille, M. (2019). TRPC3 is a major contributor to functional heterogeneity of cerebellar Purkinje cells. *ELife*, *8*, e45590. https://doi.org/10.7554/eLife.45590

Wulff, P., Schonewille, M., Renzi, M., Viltono, L., Sassoè-Pognetto, M., Badura, A., Gao, Z., Hoebeek, F. E., van Dorp, S., Wisden, W., Farrant, M., & De Zeeuw, C. I. (2009). Synaptic inhibition of Purkinje cells mediates consolidation of vestibulo-cerebellar motor learning. *Nature Neuroscience*, *12*(8), 1042–1049. https://doi.org/10.1038/nn.2348

Xia, J., Chung, H. J., Wihler, C., Huganir, R. L., & Linden, D. J. (2000). Cerebellar Long-Term Depression Requires PKC-Regulated Interactions between GluR2/3 and PDZ Domain–Containing Proteins. *Neuron*, *28*(2), 499–510. https://doi.org/10.1016/S0896-6273(00)00128-8

Xiao, J., Cerminara, N. L., Kotsurovskyy, Y., Aoki, H., Burroughs, A., Wise, A. K., Luo, Y., Marshall, S. P., Sugihara, I., Apps, R., & Lang, E. J. (2014). Systematic Regional Variations in Purkinje Cell Spiking Patterns. *PLoS ONE*, *9*(8), e105633. https://doi.org/10.1371/journal.pone.0105633

Yamada, M., Seto, Y., Taya, S., Owa, T., Inoue, Y. U., Inoue, T., Kawaguchi, Y., Nabeshima, Y., & Hoshino, M. (2014). Specification of Spatial Identities of Cerebellar Neuron Progenitors by Ptf1a and Atoh1 for Proper Production of GABAergic and Glutamatergic Neurons. *Journal of Neuroscience*, *34*(14), 4786–4800. https://doi.org/10.1523/JNEUROSCI.2722-13.2014

Yamazaki, T., & Tanaka, S. (2009). Computational Models of Timing Mechanisms in the Cerebellar Granular Layer. *The Cerebellum*, *8*(4), 423–432. https://doi.org/10.1007/s12311-009-0115-7

Yeo, C. H., Hardiman, M. J., & Glickstein, M. (1985). *Classical conditioning of the nictitating membrane response of the rabbit*. 13.

Yeo, C. H., & Hesslow, G. (1998). Cerebellum and conditioned reflexes. *Trends in Cognitive Sciences*, *2*(9), 322–330. https://doi.org/10.1016/S1364-6613(98)01219-4

Yeo, C. H., Lobo, D. H., & Baum, A. (1997). Acquisition of a new-latency conditioned nictitating membrane response—Major, but not complete, dependence on the ipsilateral cerebellum. *Learning & Memory*, *3*(6), 557–577. https://doi.org/10.1101/lm.3.6.557

Yeo, Christopher H., & Hardiman, Mervyn J. (1992). Cerebellar cortex and eyeblink conditioning: A reexamination. *Experimental Brain Research*, *88*(3). https://doi.org/10.1007/BF00228191

Zagon, I. S., McLaughlin, P. J., & Smith, S. (1977). Neural populations in the human cerebellum: Estimations from isolated cell nuclei. *Brain Research*, *127*(2), 279–282. https://doi.org/10.1016/0006-8993(77)90541-8

Zbarska, S., Bloedel, J. R., & Bracha, V. (2008). Cerebellar Dysfunction Explains the Extinction-Like Abolition of Conditioned Eyeblinks After NBQX Injections in the Inferior Olive. *Journal of Neuroscience*, *28*(1), 10–20. https://doi.org/10.1523/JNEUROSCI.3403-07.2008

Zbarska, S., Holland, E. A., Bloedel, J. R., & Bracha, V. (2007). Inferior olivary inactivation abolishes conditioned eyeblinks: Extinction or cerebellar malfunction? *Behavioral Brain Research*, *178*(1), 128–138. https://doi.org/10.1016/j.bbr.2006.12.012

Zhang, J., Zhang, K.-Y., Zhang, L.-B., Zhang, W.-W., Feng, H., Yao, Z.-X., Hu, B., & Chen, H. (2019). A method for combining multiple-units readout of optogenetic control with natural stimulation-evoked eyeblink conditioning in freely-moving mice. *Scientific Reports*, *9*(1), 1857. https://doi.org/10.1038/s41598-018-37885-w

Zheng, Q. Y., Johnson, K. R., & Erway, L. C. (1999). Assessment of hearing in 80 inbred strains of mice by ABR threshold analyses. *Hearing Research*, *130*(1–2), 94–107.

Zhou, H., Lin, Z., Voges, K., Ju, C., Gao, Z., Bosman, L. W., Ruigrok, T. J., Hoebeek, F. E., De Zeeuw, C. I., & Schonewille, M. (2014). Cerebellar modules operate at different frequencies. *ELife*, *3*, e02536. https://doi.org/10.7554/eLife.02536

Zu, T. (2004). Recovery from Polyglutamine-Induced Neurodegeneration in Conditional SCA1 Transgenic Mice. *Journal of Neuroscience*, *24*(40), 8853–8861. https://doi.org/10.1523/JNEUROSCI.2978-04.2004

Appendices

Summary ENG

This thesis represents a further elucidation towards the definition of the role of cerebellar-related plasticity mechanisms that are driving procedural and associative learning. One of the most widely used experimental paradigm to study mechanisms of learning and memory is Pavlovian eyeblink conditioning.

The neural circuitry involved in this experimental paradigm, which probes cerebellar functions, is described in **Chapter 1** of this thesis. Converging lines of evidence show that the specific eyeblink controlling microzones within the cerebellar cortex are driving the conditioned eyelid response (CRs). More specifically, the Purkinje cell simple spike suppression and the consequent disinhibition of the cerebellar nuclei drives this precisely timed motor behavior on a trial-by-trial basis. Classical conditioning techniques and specifically Pavlovian eyeblink conditioning have been used for more than three decades in humans and mice to investigate the circuitry underlying learning and memory formation.

One fundamental feature of conditioned learning is that it can be generalized to different context and stimuli. This is the reason why stimulus generalization has been a topic of interest for the field of psychology and ethology, as it is essential for survival. For this reason, in **Chapter 2** we investigated what is the probability for mice to generalize eyelid conditioned responses. Together with probability of eyelid responses we also looked at amplitude and timing and we show that testing different sound frequencies produced a gaussian-shaped generalization gradient of eyelid responses for the measure of amplitude and probability but not for the timing of the onset.

We studied the effect of unexpected stimuli on the level of stimulus generalization during Pavlovian eyeblink conditioning in **Chapter 3** of this thesis. We trained mice using a procedure called differential training, which included both one reinforced CS (CS+) always paired with an air puff and one non-reinforced CS (CS-). We found that the bigger the spacing distance between the CS+ and the CS- the steeper the learning curve of the animals in response to the CS+ during differential training. When testing generalization, we found that this spacing distance between CS+ and CS- also influenced the probability of eyelid conditioned responses. At the same time, the amplitude of the eyelid CR would also change based on the generalization CS tested, while no effect was found on timing of the peak or the onset.

Complementary to the abovementioned work related predominantly to behavioral sensorimotor learning, in **Chapter 4** we investigated the differential spatiotemporal pattern of development within the so called, Purkinje cells in specific zebrin-negative microzones. The convoluted structure of the cerebellum can be divided through parasagittal zones which are characterized by the presence or absence of specific proteins, among which also the Zebrin II protein. The absence or presence of the Zebrin II protein and others also has an impact on the physiological properties of Purkinje cells. As we have demonstrated, these neurons in the cerebellar cortex show differentiation patterns which reflect in the behavioral phenotype when sensorimotor learning of young and adult mice is compared.

In **Chapter 5** another important question is raised: What are the pathological events driving Purkinje cell dysfunction? Spinocerebellar ataxia (SCA) is a class of cerebellar neurodegenerative diseases of which the most evident hallmark are cerebellar-related symptoms. One imperative step in order to correctly interpret the functional and behavioral consequences of this type of cerebellar-related disorder is understanding what causes Purkinje cells dysfunction. For this reason, we used a mouse

model of spinocerebellar ataxia 1 (ATXN1[82Q] SCA1) which revealed high levels of the mutant ATXN1[82Q] gene already before the onset of ataxia. Since our SCA1 mouse model show already impairment in eyeblink conditioning before the onset of the ataxic phenotype, this classical conditioning paradigm can be potentially used as a sensitive tool to detect early cerebellar dysfunction.

Samenvatting NL

Dit proefschrift vertegenwoordigt een verdere opheldering over de rol van cerebellair gerelateerde plasticiteitsmechanismen die procedureel en associatief leren aansturen. Een van de meest gebruikte experimentele leermodellen om mechanismen van leren en geheugenvorming te bestuderen is Pavloviaans ooglid conditioneren.

In **hoofdstuk 1** worden de neuronale circuits beschreven welke betrokken zijn binnen dit leermodel. Steeds meer data toont aan dat specifieke ooglid conditionering microzones, welke gelegen zijn in de cerebellaire cortex, de geconditioneerde response (CRs) aansturen. Specifieker, de suppressie van de actiepotentialen door de Purkinjecel en de disinhibitie van de cerebellaire kernen leidt tot nauwkeurig getimede motorische responsen. Al meer dan drie decennia wordt bij mensen en muizen gebruik gemaakt van klassieke conditioneringstechnieken, specifiek Pavloviaans ooglidconditioneren, om de connecties te onderzoeken die ten grondslag liggen aan leren en geheugenvorming.

Een fundamenteel kenmerk van geconditioneerd leren is dat het kan worden gegeneraliseerd naar verschillende contexten en stimuli. Dit is de reden dat stimulusgeneralisatie een onderwerp van interesse is geweest voor het gebied van psychologie en ethologie, omdat het essentieel is om te overleven. In **hoofdstuk 2** hebben we daarom onderzocht wat de kans in muizen is om ooglid geconditioneerde reacties te generaliseren. Naast de waarschijnlijkheid van oogknipperresponsen hebben we ook gekeken naar de amplitude en timing, en laten we zien dat het testen van verschillende geluidsfrequenties een Gaussiaans-vormige generalisatiegradiënt van oogknipperresponsen vormen. Dit was alleen het geval voor de amplitude en de waarschijnlijkheid, maar niet voor de timing van de oogknipperrespons.

In **hoofdstuk 3** van dit proefschrift hebben we het effect bestudeerd van onverwachte stimuli op het niveau van stimulusgeneralisatie tijdens Pavloviaans ooglid conditioneren. We hebben muizen getraind met behulp van een procedure die differentiële training wordt genoemd, welke altijd een versterkte CS (CS +) gepaard met een lucht puf als een niet-versterkte CS (CS-) omvat. We ontdekten dat hoe groter de afstand tussen de CS+ en de CS- is, des te steiler de leercurve van de dieren is in reactie op de CS+ tijdens differentiële training. Bij het testen van stimulusgeneralisatie ontdekten we dat deze afstand, tussen CS+ en CS-, ook de kans op geconditioneerde oogknipperresponsen beïnvloedde. Tegelijkertijd veranderde ook de amplitude van de ooglid CR, maar werd er geen effect gevonden op de timing en start van de oogknipper.

Als aanvulling op het bovengenoemde werk dat voornamelijk betrekking heeft op gedrags-sensomotorisch leren, hebben we in **hoofdstuk 4** het differentiële spatiotemporele ontwikkelingspatroon binnen de zogenaamde Purkinje-cellen in specifieke Zebrin-negatieve microzones onderzocht. De ingewikkelde structuur van het cerebellum kan worden verdeeld in parasagittale zones die worden gekenmerkt door de aan- of afwezigheid van specifieke eiwitten, waaronder ook het Zebrin II-eiwit. De aanwezigheid of afwezigheid van het Zebrin II-eiwit, en eventuele andere eiwitten, hebben impact op de fysiologische eigenschappen van Purkinje-cellen. Zoals we hebben aangetoond, vertonen deze neuronen in de cerebellaire cortex differentiatiepatronen die het gedragsfenotype weerspiegelen wanneer sensomotorisch leren van jonge en volwassen muizen wordt vergeleken.

In **hoofdstuk 5** wordt een andere belangrijke vraag gesteld: Wat zijn de pathologische gebeurtenissen die Purkinjecel disfunctie veroorzaken? Spinocerebellaire ataxie (SCA) is een klasse van cerebellaire neurodegeneratieve ziekten, waarvan het duidelijkste kenmerk cerebellaire symptomen zijn. Een noodzakelijke stap om de functionele- en gedragsconsequenties van dit type cerebellaire gerelateerde

stoornis correct te interpreteren, is begrijpen wat de oorzaak is van het disfunctioneren van Purkinje-cellen. Om deze reden hebben we gebruik gemaakt van het spinocerebellaire ataxie 1 (ATXN1[82Q] SCA1) muismodel, dat al vóór het begin van ataxie hoge niveaus van het ATXN1[82Q]-gen onthulde. Aangezien ons SCA1-muismodel al een verslechtering in ooglid conditionering vertoonde vóór de start van het ataxische fenotype, kan dit klassieke conditioneringsleermodel mogelijk worden gebruikt als een hulpmiddel om vroege cerebellaire disfunctie te detecteren.

Curriculum Vitae

Personal details

Name:	Francesca Romana Fiocchi
Birthdate:	October 11, 1991
Birthplace:	Rome
Nationality:	Italian

Education & experience

2022-2017 PhD student at Erasmus MC, Dept. of Neuroscience, Rotterdam

2017-2016 Internship student at European Center for Brain Research (CERC) Santa Lucia Foundation, Rome

2016-2014 MSc Cognitive Neuroscience and Psychological Rehabilitation, Excellence Program (magna cum laude) at La Sapienza University, Rome

2011-2014 BSc Medicine and Psychology at La Sapienza University, Rome

PhD Portfolio

Fiocchi, F.R., van Dorp, N., Dijkhuizen, S., van den Berg, M., Wong, A., De Zeeuw, C.I., Boele, H.J. (In preparation). Discrimination training affects stimulus generalization in mice during Pavlovian eyeblink conditioning.

Osório, C., White, J.J., Lu, H., Beekhof, G.C., **Fiocchi, F.R**., Andriessen, C.A., Dijkhuizen, S., Post, L., and Schonewille, S. (Submitted). Pre-ataxic loss of intrinsic plasticity and motor learning in a mouse model of SCA1.

Fiocchi, F.R., Dijkhuizen, S., Koekkoek, S.S.K., De Zeeuw, C.I., and Boele, H.J. (2022). Stimulus generalization in mice during Pavlovian eyeblink conditioning, *eNeuro*, 0400-21.2022.

Beekhof, G.C., Osório, C., White, J.J., van Zoomeren, S., van der Stok, H., Xiong, B., Nettersheim, I. H.M.S., Mak, W.A., Runge, M., **Fiocchi, F.R**., Boele, H.J., Hoebeek, F.E., Schonewille, M. (2021). Differential spatiotemporal development of Purkinje cell populations and cerebellum-dependent sensorimotor behaviors, *eLife*, 10: e63668.

Acknowledgements

I'm done! Although, as I have been saying to everyone asking me how I feel about finishing up: "I will not believe it until it happens". Still now, while writing these lines I still cannot realize that this part of the journey has arrived, the part where I thank all the people who have been part of it and helped me along the way.

To my Promotor, Prof. Dr. **Chris De Zeeuw**, for all the support and motivation he has given to me during these years. I am grateful for all of the scientific knowledge and inspiration you could transmit since the first day I started, how you always had time for me and took initiative to help me survive throughout this long and incredible journey.

A special note of gratitude to my co-promotor **Henk-Jan Boele**. From helping me to finalize my first-author paper to the patience of introducing me to the fascinating cerebellar-related world, you have continuously accompanied me with stimulating scientific conversations throughout the course of my PhD (either during the day or later at night on the US time-zone!). Thank you for being a patient teacher and an understanding supervisor.

To my co-promotor **Devika Narain**, thank you for being the scaffolding supervisor I needed during these years. I have extreme admiration and respect for the quality of your scientific work, and I am extremely grateful I had the chance to learn from you (even though with a lot of pain, I have to say!), not only the basics of coding, but also how to implement curiosity as a tool in order to produce quality science. You pushed me to overcome limits I did not even know I had. Thank you for being a capable motivator and a truthful mentor and for all the help in this last part of my PhD trajectory, for anticipating my needs and for always being there at the end of the hallway or just one email away.

I am very grateful to all the member of the Reading and Opposition committee who have accepted to read my PhD thesis and contributed to it with useful comments and suggestions.

Prof. Dr **Gerard Borst**, thank you for making the LISTEN project real and giving me and all the other members the chance to interact with top-notch scientists and research creating this collective formidable experience which I believe has been deeply empowering for the most of us.

Prof. Dr **Simon Rumpel** for accepting of being part of my PhD committee and kindly hosting me in your lab at the University of Mainz. Thank you for your scientific contribution and time invested into my little project since the very beginning. You are of inspiration and a good-hearted mentor to any person who is passing by your laboratory as you have been to me for the little time I spent there.

Dr. **Aleksandra Badura**, thank you for being the Secretary of my reading committee and for helping me improving the final version of my thesis with your helpful comments and suggestions. I deeply admire your scientific knowledge and the dedication you have for all your students, not to mention the quality of your work.

Prof. Dr. **Bas Koekkoek**, for taking everything was said in the eyeblink lab not entirely serious and be able to make people laugh about it. Thank you for being the smart and helpful engineer always ready to fix anything broken or to explain a concept to the brain of a non-engineer without making us feel entirely unintelligent!

Dr. **Catarina Osorio**, I extremely admire your dedication and the passion you have for your work. I thank you for all the little chats we casually had in random corners of the Department during long working weekends and for all the empathy you showed to me when I was in my complaining mood.

Dear **Heiling**, thank you for proof-reading my thesis for being encouraging and positive with me all the time. You still have some way to go, and I can see you have the determination and stubbornness to go until the end. Your kindness and your organization skills – always noticed how clean and tidy your desk is – will help you along the way and I am sure there is an easier part of this journey waiting for you soon!

Dr. **Aaron Wong** and **Mauritz Van Den Berg**, you were both fundamental for a lot of the work which is included in this thesis. Starting with the ABR recordings, the infinite days when we recorded no-stop starting very early in the morning and finishing at an indefinite time of the afternoon completely brain-fried but successful. Thank you Mauritz very much for the time spent complaining and complaining more in every part of Europe we could be either Spain, France or the Netherlands in any type of situation without feeling bad about it. Sometimes you were able to give the voice to something that many people were thinking but no one was saying. There is still some hard time for you to go through, but I believe that as long as your motivation in finding a very remunerative job very far away from Academia stays as I know it, you will get also this last part of your PhD done and move on with your life and all your cats!

Dear Dr**. Anna Vavakou**, my anchor, my sweet, smart, dedicated neuroscientist friend. There are still so many things of the Organ of Corti which will never entirely be clear to me, but your excitement and dedication in research for subjects which many of us can barely grasp are admirable. I am so proud of you for all that you have achieved so far. I still have a clear picture in my mind of that first day we met in front of the Pantheon in Paris in October 2017. You were my anchor there and for all the four years we spent trying to be scientists together. Thank you for making me feel rescued and taken care of and loved and full (of food!) during my darkest times. Only the sky is the limit.

Dear **Marit**, you are always so quiet and at the same time full of surprises! Thank you for all the support and the help during these years. You are sweet, kind and dedicated and I am happy I could share the office with you and thank you for making it always "Christmassy" already around the end of October and sharing a good Gin Tonic on a Friday already at 16pm without making any of it look weird. If Marit does it, it's fine!

Dear **Nikki**, thank you for being extremely passionate and precise in everything you were doing. You and your cucumbers became a fundamental asset in our eyeblink routine so soon that now we still talk about them! I wish you had a blast during these years in Princeton and I am sure you are being an amazing technician, smiling and with your radio on all the time. Thank you for all the work you helped me with which is a very important part of this thesis and especially when I could not be there do to it with you.

I am also grateful I have gotten to know **Hary Siridoupulis**, **Jan de Jong** and **Renee Miedema** thank you for being great engineers and co-workers but also (and most importantly!) always up for a nice chit-chat break. Also thank to **George Smaragdos** who is not always around but when he is, he is always ready to help and fix any computer-related problems. **Elias**, thank you for all the colorful post it and the laughs, you are the person I have met more recently that is the best at doing your job without doing much. You can survive this, hang in there and see you in Buenos Aires! **Xiao Lu**, thank you for the quickest but most helpful advice of all! Thank you, **Erika** for the loud laughs that transmit happiness and your boldness in saying anything you think and **Elize** for always knowing where everything is.

Dear Dr. **Michiel Ten Brinke**, thank you for being impressively resourceful and attentive with me at the very (scary!) beginning and for not laughing to my naive approach to data analysis.

Cara **Roberta**, grazie mille per essere stata di ascolto e di supporto in questi anni, per aver mangiato infiniti piatti di pasta a pranzo con fierezza e senza esitazione e per esserti fatta conoscere (anche se un po' all'ultimo) con tutta te stessa!

Grazie **Manuele** per non aver mai smesso di offrire datteri e per essere sempre la persona più sobria di tutti i week-end (e nonostante tutto ci sopporti spesso!). In bocca al lupo in Norvegia!

Silvia, cucchiaio del mio cuore. Grazie perché sia in Olanda che in Francia con i tuoi poster con le piante, le rape rosse e le grappe, sei stata e sei sempre un punto di riferimento internazionale che scalda il cuore. Sei dolce come una forma di Camabert sciolta nel forno e non esiste cucchiaio piú tenero che con te, anche quando devi innaffiarti l'orecchio prima di andare a dormire! (Io ho il pane, tu hai la nutella, tu hai il formaggio: non ci dividiamo!).

Camilla, cucciolona. Grazie con tutti i cuori di essermi stata vicino durante tanti momenti difficili. Alla fine, ci bastano solo sei ore di treno da Parigi a Milano per raccontarci (quasi) tutto! Evviva il tuo entusiasmo quando parli di costruire elettrodi, la gioia dello yogurt della mattina, gli Aperol Spritz al sole nel cercare di sentirsi un per un secondo a casa e le cene lunghissime piene di chiacchiere. Grazie di tutto sziona, sei stata fondamentale.

Dr. **Francois Blot**, my dearest french person in the entire group of french people I know (two or three max). You have been a real friend, a colleague, a mentor and an advisor and I could feel your affection no matter where in the Netherlands or from France. Thank you for being so supportive and for just speaking up your mind regardless, in any way ending up saying the right things at the right time. I value so much your friendship and the amount of bull you are able to say with a straight face. Thank you for teaching me one of the most important lesson I have ever learned during these years: "People that make it through are not the good ones or the smartest ones, but the ones that struggle but do not give up."

Emanuello! Grazie perché dalla Cambogia ad Ascoli Piceno a Panarea a Roma, tra Almondestraat e Koh Rong Samloem, rendi tutto sempre più divertente e alla fine ci fai stare bene tutti insieme. Quando torniamo da Jacopo a bere vino biologico e a farci il bagno in piscina appena svegli? So che dietro quel tuo sarcasmo e disorganizzazione cronica, si nasconde un cuore tenero. Ci manchi in Europa, torna presto!

Luca (Sparapuzzolo!), ti conosco da tanto poco ma sei un asset fantastico nel laboratorio e in qualunque bar di Rotterdam. Grazie per ridere a tutte le cose stupide che dico ogni giorno e per essere così entusiasta delle cose che ti sono intorno. Trasmetti tante cose belle con i tuoi profondi occhi blu, non smettere!

Caro **Vincenzo**, Principessa del laboratorio dei whisker. I quattro anni di convivenza con te sono stati tra le esperienze più divertenti che mi potessero capitare in Olanda. Grazie per essere stato un collega, amico, compagno di caffè, chiacchiere, mattine in balcone, pomeriggi, pranzi al sole, pizze da Stalles, serate al Perron, presentazioni in power point, serate lunghissime in laboratorio, e tantissimo altro (…!). Sono molto fiera di te e sono contenta di vederti realizzato, felice e finalmente con Daria!

Lorenzo Bina, non sapevo che le persone potessero essere stili di vita. Tutto quello che fai sul lavoro ispira serenità e precisione, in tutto quello che fai fuori da lavoro è unico e speciale come le tue pizze. Non saprei da dove cominciare nel dirti grazie e qualsiasi lista sarebbe riduttiva. Grazie per essere stato tutto te stesso in questi anni e per averlo condiviso con me, per aver reso tutti i venerdì divertenti e spensierati in ogni stagione ed in ogni contesto. Vicino a te ogni piccola cosa diventa bella e si

illumina. Sei una esplosione di naturale bellezza per tutto ciò che ti circonda e trasmetti questo senso di meraviglia e di scoperta alle persone che ti sono intorno.

Almost at the very end of these acknowledgements, but only because I still am not able to find all the right words for it, I want to thank the amazing expat inter-European family that I found here in Rotterdam. Everyone of you is special, unique, and irreplaceable. I am leaving this country but every single one of you contributed to me being the person that I am today. These years have been rough, but you were all there to make me feel the warmth that only a family can give you. To my dear **Geoffrey**, **Matteo**, **Carlos**, **Livia**, **Joana**, **Cristina**, **Elena**, **Thomas**, **Federico**, **Tobia**, **Xavier**. I could never be more grateful.

Dolcissime Cauli! **Marta**, **Agnese** e **Mariagiulia**, che tristezza lasciarvi! Mi sembra che quando siamo tutte insieme possiamo affrontare qualunque cosa. Grazie per avermi ascoltata, supportata e aiutata a crescere come *bilancia.* Siete preziose.

Nina De Oude and Stephanie Dijkhuizen, my paranymphs, my angels during this incredibly challenging but also fun PhD journey. Thank you for standing beside me during my defense and for standing next to me during this amazing adventure. It's been a rollercoaster and I am not sure I could have done it without both of you.

Dearest sweet **Nina**, I believe there is no stronger bond when two people share a coding MatLab course together every day very early in the morning. You made me feel fine and not ashamed even after the biggest mistakes and failures, thank you for sharing the frustration both in the office and out of the office. On scary rollerblades, vary late in a bar, at your place, eating sushi (a lot of sushi!), kapsalon from Jaffa at 4am, going dancing wherever we could hear music, in the Netherlands or in Italy (even when drinking your cappuccino Bayles!) wherever or whatever we did together I always felt home.

Stephanie (Amore!), I sat by your side by chance on the very first day I arrived in the Department, and I could have never found a better spot. I am so glad I had you by my side for all these years. We shared the pain, the frustration, the challenges, the tears, the pain again but also the joy, the Gin Tonics, the stairs all the way downstairs to get zuikerwafles, the zuikerwafles, the kruidnotens and the happiness that comes from all of these. I was amazed from the way you can make everything shine! You were always there for me to make me see the little things I should be proud of when I could not see them. Every end is a new beginning, this is what you said! Let's just cry of happiness for this new beginning that is standing right in front of us.

Alla mia adorata famiglia. Grazie a mio fratello **Alessandro** e alla mia **Mamma** perché dovunque io sia mi fanno sentire sostenuta e amata e sono sempre pronti ad assecondare la mia ricerca di avventure in giro per il mondo. Non importa quanto siamo distanti, perché quando poi siamo insieme, dovunque sia, siamo a casa! Cara Mamma, questo traguardo non è solo mio, ma è anche tuo, ed è fatto di tutto l'amore e la fiducia che mi hai sempre saputo trasmettere. Alessandro, sono la sorella più orgogliosa e fortunata, spero che tu sappia sempre quanto mi scalda il cuore averti accanto. Grazie alla mia **Nonna** (Ni!) e al mio **Papà** che mi hanno trasmesso il valore inestimabile di credere che posso amare quello che faccio e che questo possa essere il mio lavoro. "Non importa cosa e non importa dove, purché tu sia felice!". A loro, che vorrei abbracciare più di ogni altra cosa in questo giorno speciale, dedico il lavoro di questa tesi.